Solar Thermal Power Plants -

Modelling of Parabolic Trough Collector Concepts

Diploma Thesis
of
Fritz Zaversky

Institute for Thermal Turbomachinery and Machine Dynamics
Graz University of Technology

Head of the Institute:
Univ.-Prof. Dr.-Ing. Franz Heitmeir

Supervisor:
A.o.Univ.-Prof. Dipl.-Ing. Dr.techn. Wolfgang Sanz

Graz, 2010

Preface & Acknowledgement

In 2005 I chose “transportation technology” as my main field of study at Graz University of Technology. Therefore most of my lectures dealt with internal combustion engines, as they are the state-of-the-art power source for individual transport. During the last century, the internal combustion engine has been developed to a high technology product that enabled high standards of living and mobilisation, but only available for a minor percentage of the world´s population. Of course the number of people aspiring this way of life is on the rise and unfortunately it is impossible to increase mobility without harming the environment, if we stick to today´s technology.

The more I learned about the laws of thermodynamics and how they limit the energy conversion in internal combustion engines, the more I had doubts about its future applications. Especially concerning the rising awareness of CO_2 – emission and its effects on the world´s climate.

Of course, due to missing alternatives, internal combustion engines will not be replaced in certain applications for a long time, but I think that the major number of tomorrow´s cars will be driven electrically.

As a consequence, to actually satisfy the increasing demand of electric power, power plants have to be improved and renewable energy sources have to be used in large scale.

Knowing that the sun provides a multiple of the world´s energy consumption, I always wondered why the use of solar power is still that low although first research work started in the 1970´s. Hence, I would love to make a contribution to an improvement of solar power usage. It could be one of several steps to improve the standards of living for a reasonable amount of people, without damaging the environment more than it has already happened anyway.

I would like to thank my supervisor a.o.Univ.-Prof. Dipl.-Ing. Dr.techn. Wolfgang Sanz for thoroughly reading the final version of this work and for offering help during the past few months.

Furthermore, special thanks go to the staff at the company SimTech GmbH for the cooperation and the agreeable time. Thank you Stefan for being patient and ready for questions at any time.

Last but not least, I would like to thank my family, especially my parents for supporting me during my years at the university.

Fritz Zaversky Graz, March 2010

Deutsche Fassung:

Beschluss der Curricula-Kommission für Bachelor-, Master- und Diplomstudien vom 10.11.2008
Genehmigung des Senates am 1.12.2008

EIDESSTATTLICHE ERKLÄRUNG

Ich erkläre an Eides statt, dass ich die vorliegende Arbeit selbstständig verfasst, andere als die angegebenen Quellen/Hilfsmittel nicht benutzt, und die den benutzten Quellen wörtlich und inhaltlich entnommene Stellen als solche kenntlich gemacht habe.

Graz, am …… ……..
(Unterschrift)

Englische Fassung:

STATUTORY DECLARATION

I declare that I have authored this thesis independently, that I have not used other than the declared sources / resources, and that I have explicitly marked all material which has been quoted either literally or by content from the used sources.

…… ……..
date (signature)

Abstract

The basic concern of this work is the use of renewable solar thermal energy in conventional steam cycles, in order to provide electric power.

As there is an increasing awareness concerning the bad effects of vast CO_2 emission, the use of solar thermal energy can be one of several ways to provide clean electric energy.

Possible concepts of the solar power´s transformation into usable electricity are discussed. The specific advantages, disadvantages and efficiencies are outlined.

Generally speaking, the incoming solar radiation is received by a certain aperture area, reflected and concentrated onto an absorber surface. The absorbers usually are arrangements of tubes through that special heat transfer fluids flow.

Since the actual position and radiant power of the sun is crucial for the collector´s performance, a solar radiation model has been created, too.

Then, the today´s most used concentrating collector type, the parabolic trough collector, is described in detail. The attenuation of the incoming solar radiation is modelled, as well as the heat transfer and the heat loss of the absorber tube. Concerning the heat transfer within the absorber tube, distinctions had to be made, as the heat transfer coefficient depends on the fluid flowing inside. As fluid, high temperature oil or water, that is directly evaporated within the absorber tubes, can be used. The latter concept is called direct steam generation (DSG).

As the topic of this diploma thesis was defined by the company SimTech GmbH, which offers a design software for the modelling of thermal power plants, all required relationships have then been implemented in this simulation software IPSEpro, in order to calculate the performance and efficiency of whole solar power plants.

To verify the models, one existing and successfully operated solar collector field has been calculated using IPSEpro. Finally two parabolic trough solar thermal power plant concepts were simulated with models developed in this work.

Kurzfassung

Diese Arbeit befasst sich grundsätzlich mit der Umwandlung von solarer Einstrahlung in elektrische Energie. Dabei wird die von der Sonne gebotene thermische Energie mit Hilfe von herkömmlichen Dampfkreisläufen in elektrischen Strom umgewandelt.
Da in letzter Zeit Maßnahmen zur CO_2 Einsparung immer mehr in den Vordergrund rücken, ist die Umwandlung von solarer Energie eine von mehreren nachhaltigen und zukunftsweisenden Technologien.

Mögliche Konzepte werden betreffend ihrer Vor- und Nachteile, sowie ihrer Wirkungsgrade diskutiert. Generell wird bei all diesen Konzepten die solare Einstrahlung von bestimmten Kollektorflächen aufgefangen und auf Absorberoberflächen reflektiert beziehungsweise konzentriert. Die thermischen Absorber sind dabei in der Regel Rohrleitungen, die von wärmeaufnehmenden Fluiden durchflossen werden.

Da für die Bestimmung der Kollektorleistung die aktuelle Position und Einstrahlungsleistung der Sonne von essenzieller Bedeutung ist, wurde auch ein Modell der verfügbaren solaren Einstrahlung entworfen.

Der heute meistverwendete Kollektortyp ist der Parabolrinnenkollektor. Dieser wird in weiterer Folge detailliert beschrieben. Sämtliche Abschwächungen der eintreffenden solaren Strahlung, bis sie auf die Absorberoberfläche trifft, werden behandelt. Um den Anteil der solaren Energie zu bestimmen, der schlussendlich das wärmeaufnehmende Fluid aufheizt, ist es auch von Bedeutung den Wärmeübergang sowie die Wärmeverluste zu beschreiben. Bei der Ermittlung des Wärmeübergangskoeffizienten der Absorberrohrinnenseite musste zwischen den möglichen Fluiden unterschieden werden. Grundsätzlich werden Hochtemperaturöle als wärmeaufnehmende Fluide verwendet. Ein neueres Konzept verdampft das für den Dampfkreislauf nötige Wasser gleich in den Absorberrohren (DSG – Direct Steam Generation).

Das Thema dieser Diplomarbeit wurde von der Software-Firma SimTech GmbH ausgeschrieben, welche das thermodynamische Simulationsprogramm IPSEpro anbietet. Darum wurden sämtliche Gleichungen in dieses Programm implementiert, um Parabolrinnenkraftwerke simulieren zu können.

Um die entworfenen Kollektormodelle zu verifizieren, wurde ein bestehendes und erfolgreich arbeitendes Kollektorfeld mit IPSEpro modelliert. Schlussendlich wurden zwei Kraftwerkskonzepte in IPSEpro erstellt und gerechnet.

Table of Contents

Nomenclature

A	altitude of the location in question	[km]
A_a	area of aperture	[m²]
$A_{absorber}$	surface of the absorber tube	[m²]
A_c	cross sectional area of the pipe	[m²]
A_L	cross sectional area of liquid phase in a pipe	[m²]
A_{mirror}	total mirror area	[m²]
A_r	area of the receiver or absorber	[m²]
A_{se}	surface of a fictitious, to the sun concentric, sphere	[m²]
A_{sun}	the sun´s surface	[m²]
A_{st}	cross sectional area of steam phase in a pipe	[m²]
A_{tube}	surface of the surrounding glass tube	[m²]
AM	air mass	[-]
ARR	air return ratio	[-]
B	variable necessary for calculating the solar irradiation	[°]
C	area concentration ratio	[-]
c_{dp}	collector parallel distance	[m]
$c_{dp\ min}$	minimum collector parallel distance	[m]
c_w	collector width	[m]
c_p	specific heat capacity	[J/kgK]
$c_{p\ L}$	heat capacity of the liquid phase	[J/kgK]
$c_{p\ St}$	heat capacity of the steam phase	[J/kgK]
CSP	concentrating solar power	
D	outer diameter of glass tube	[m]
d_o	outer absorber tube diameter	[m]
d_i	inner absorber tube diameter	[m]
DNI	direct normal irradiance	[W/m²]
DSG	direct steam generation	
E	difference between actual solar time and mean solar time	[min]
f	friction factor	[-]
f_L	friction factor liquid phase	[-]
f_{St}	friction factor steam phase	[-]
G	extraterrestrial radiation incident on the plane normal to radiation	[W/m²]
G_{cd}	clear-sky diffuse radiation	[W/m²]
G_{cnb}	clear-sky normal beam radiation	[W/m²]
G_{ct}	total clear-sky radiation incident on a horizontal plane	[W/m²]
G_h	extraterrestrial radiation received on a horizontal plane in space	[W/m²]
G_s	radiant flux density per area	[W/m²]
G_{sc}	solar constant	[W/m²]
g	acceleration due to gravity	[m/s²]
h'	enthalpy of the water at saturated liquid conditions	[J/kg]
h''	enthalpy of the dry saturated steam	[J/kg]
h_v	latent heat of evaporation – enthalpy of evaporation	[J/kg]
IDR	incident direct radiation	[W/m²]

L_c	absorber tube length (parabolic trough collector length)	[m]
L_{loc}	longitude for location in question	[°]
L_{st}	standard meridian for local time zone	[°]
M_{sun}	the sun´s flux density	[W/m²]
$\dot{m}_{St}$	mass flow of steam phase	[kg/s]
$\dot{m}_L$	mass flow of liquid phase	[kg/s]
$\dot{m}$	total mass flow within the tube	[kg/s]
m''	mass of the saturated steam	[kg]
m'	mass of the boiling liquid	[kg]
$\dot{m}_0$	mass flow at reference conditions	[kg/s]
n	n[th] day of the year	[-]
$P_{receiver}$	total power received by the absorber	[W]
P_{total}	total power received by the absorber tube	[W]
p	pressure	[bar]
p_{cr}	critical pressure	[bar]
p_{α}	pressure at turbine entry	[bar]
$p_{\alpha 0}$	pressure at turbine entry at reference conditions	[bar]
p_{ω}	pressure at turbine outlet	[bar]
$p_{\omega 0}$	pressure at turbine outlet at reference conditions	[bar]
Q_C	losses by convection	[W]
Q_{loss}	total absorber heat loss	[W]
Q_R	losses by radiation	[W]
Q_{trans}	power gained by the thermal fluid	[W]
q	heat flow per area	[W/m²]
$q_{critical}$	critical heat flow per area	[W/m²]
q_{fc}	forced convection heat flow	[W/m²]
q_{nb}	nucleate boiling heat flow	[W/m²]
R	distance from the sun´s centre to the earth´s surface	[m]
R_p	pressure loss ratio	[-]
r	radius of the sun	[m]
S	collector shading length	[m]
s	slip between phases	[-]
SEGS	solar electric generating stations	
T	temperature	[°C],[K]
t_s	solar time	[h]
u_{St}	velocity of the steam phase	[m/s]
u_L	velocity of the liquid phase	[m/s]
V_L	volume of liquid phase	[m³]
V_{st}	volume of steam phase	[m³]
V_t	total volume	[m³]
$\dot{V}_{St}$	volume flow of steam phase	[m³/s]
$\dot{V}_t$	total volume flow (steam + liquid phase)	[m³/s]
v	mean velocity of the heat transfer fluid	[m/s]

v_f	velocity of the fictive single phase flow	[m/s]
v_{wind}	mean wind speed	[m/s]
v_L	flow velocity of the liquid phase	[m/s]
v_{St}	velocity of the steam phase	[m/s]
w_{St}	apparent velocity of the gas or steam phase	[m/s]
w_L	apparent velocity of the liquid phase	[m/s]
X	Lockhart-Martinelli parameter	[-]
$\dot{x}$	steam mass fraction of the flow (flow steam quality)	[-]
α	absorptivity of the absorber surface	[-]
α_C	heat transfer coefficient (dependent on the wind-speed)	[W/m²K]
α_{DB}	Dittus-Boelter heat transfer coefficient for properties of the liquid phase	[W/m²K]
α_s	solar altitude angle	[°]
α_{tube}	heat transfer coefficient between the fluid and the inner absorber tube wall	[W/m²K]
α_{fc}	heat transfer coefficient for forced convective heat flow	[W/m²K]
α_{nb}	heat transfer coefficient for nucleate boiling heat flow	[W/m²K]
α_{2Ph}	heat transfer coefficient of the two phase flow	[W/m²K]
β	slope angle	[°]
β_{max}	maximum acceptable slope angle	[°]
β_{tilt}	tilt angle of the pipe	[°]
γ	surface azimuth angle	[°]
γ_s	solar azimuth angle	[°]
δ	angle of declination	[°]
ε	emittance of the absorber tube	[-]
ε_r	mean roughness height	[m]
ε_v	void fraction (volumetric steam quality)	[-]
$\dot{\varepsilon}_v$	volumetric flow steam quality	[-]
ζ_{cos}	cosine loss attenuation factor	[-]
ζ_{IAM}	incidence angle modifier	[-]
$\zeta_{shading}$	shading attenuation factor	[-]
η_{Carnot}	Carnot efficiency	[-]
η_{opt}	optical efficiency of the parabolic trough collector	[-]
$\eta_{optical}$	optical efficiency of the heliostat collector field	[-]
$\eta_{opt,0°}$	peak optical efficiency	[-]
$\eta_{receiver}$	solar receiver efficiency	[-]
η_{total}	ideal conversion efficiency	[-]
η_{St}	dynamic viscosity of the gas or steam phase	[kg/ms]
η_L	dynamic viscosity of the liquid phase	[kg/ms]
λ	wavelength	[µm]
λ	thermal conductivity of the ambient air	[W/m]
λ_L	thermal conductivity of the liquid phase	[W/m]
λ_{St}	thermal conductivity of the steam phase	[W/mK]
λ_{fluid}	thermal conductivity of the fluid in the absorber tube	[W/m]
$\lambda_{absorber}$	thermal conductivity of the absorber tube	[W/m]
υ	kinematic viscosity of the ambient air	[m²/s]

υ_L	kinematic viscosity of the liquid phase		[m²/s]
υ_{St}	kinematic viscosity of the steam phase		[m²/s]
ρ	density of the fluid		[kg/m³]
ρ_L	density of the liquid phase [kg/m³]		[kg/m³]
ρ_r	reflectivity		[-]
ρ_{St}	density of the gas or steam phase [kg/m³]		[kg/m³]
ρ'	density of the water at saturated liquid conditions		[kg/m³]
ρ''	density of the dry saturated steam		[kg/m³]
σ	Stefan-Boltzmann constant	5.67	[W/m²K⁴]
σ_s	surface tension		[N/m]
τ	atmospheric transmittance		[-]
τ_b	atmospheric transmittance for beam radiation		[-]
τ_d	atmospheric transmittance for diffuse radiation		[-]
τ_g	transmissivity of the glass tube		[-]
φ	latitude of the location in question		[°]
χ	intercept factor		[-]
ω	solar hour angle		[°]
Θ	angle of incidence		[°]
Θ_s	apex angle of the sun		[°]
Θ_z	zenith angle		[°]

Bo	Boiling number	[-]
Fr	Froude number	[-]
Nu	Nusselt number	[-]
Pr	Prandtl number	[-]
Re	Reynolds number	[-]
We	Weber number	[-]

1 Introduction

In most of the conventional power plants, thermal energy, produced by combustion of fossil fuels or nuclear reaction, is converted into electric energy. This conversion is usually done by the Rankine steam cycle process (steam turbines) or Brayton cycle process (gas turbines).
Due to the laws of thermodynamics this conversion process has a limited efficiency. The theoretical value of efficiency that can be reached under ideal conditions is defined by the Carnot process. Unfortunately, these ideal conditions cannot be reached in reality and efficiencies stay below this limit. Nuclear power plants reach efficiencies about 30 – 32%, coal fired ones about 40%. Although modern combined cycle power plants reach efficiencies just below 60% and new technologies will further improve the other plants, the future use of renewable energy is crucial; especially if considering the consequences of vast CO_2 emission and the still not available final storage for nuclear waste.

One of the possible solutions is the use of thermal energy provided by the sun. Thus, conventional thermodynamic processes can be used to convert this renewable thermal energy in electric energy, without the emission of CO_2 and other pollutants, that may harm the environment.

This is done by solar thermal power plants.

1.1 The Basic Idea of Solar Thermal Power Plants

As briefly outlined above, the sun´s thermal energy is collected and converted into electric energy.

More precisely, the radiation provided by the sun is used to increase the working fluid´s enthalpy, which finally expands in a turbine that is connected to a generator.

For the most part water/steam is used as the working fluid. Thus, the solar energy evaporates water, which finally expands in a turbine.

Some concepts that are still under research use air as working fluid, which expands in a gas turbine and can even run an attached steam cycle, using heat recovery boilers (solar thermal combined cycle plants).

In some applications, also Sterling engines can be used to convert solar thermal energy.

There are several concepts of collecting solar energy in order to generate steam or heat other fluids. As the efficiency of the connected thermodynamic processes depends on the working fluid´s temperature level, which should usually be as high as possible, concentration of the incoming solar radiation is crucial. According to Duffie & Beckman (2006), the maximum temperature of non-concentrating flat-plate collectors is limited to 100°C above ambient temperature. Since higher temperatures are necessary, concentration is either reached by parabolic structures which concentrate the radiation at a focal point/line, or by many slightly curved mirror elements that concentrate radiation onto a certain area. The maximum working fluid temperatures that are reached with concentration range from 400°C up to 1500°C.

The today´s most used concept is the parabolic trough collector plant.
There the working fluid is heated within the focal line of the parabolic troughs directly or indirectly, using a heat transfer fluid. Due to increasing thermal losses the temperatures reached are limited to about 500°C.

Another concept that has been tested and operated successfully, is the solar power tower concept. There, solar radiation is concentrated onto a certain receiver area, using many mirror elements. After having collected the solar energy, it is transferred to the working fluid. Due to the high concentration ratio, temperatures up to 1500°C can be reached. This concept promises high efficiencies if used with gas turbines and air as working fluid, as it can be extended to combined cycle plants.

Additional concepts are the linear Fresnel collectors and parabolic dish collectors.

The linear Fresnel concept is similar to the parabolic trough systems, but is still under research. There, many longish mirror elements concentrate solar radiation onto a horizontal tube.

Parabolic dish collectors reach high temperatures and concentration ratios. They run Sterling engines that provide good efficiencies in small power classes, ideal for remote off-grid applications.

Generally speaking, solar thermal power plants provide clean electric energy, and have therefore great potential for being an important part of the future´s sustainable power supply.

1.2 The Task

The topic of this diploma thesis was defined by the software company SimTech GmbH. SimTech provides state of the art modelling tools for the power and process industries. The software with the name IPSEpro is able to simulate power plant concepts from conceptual design to on-line plant performance monitoring and optimization.
Due to the increasing interest in solar thermal power applications, SimTech plans to provide customers with ready-to-calculate solar thermal power plant module libraries. Today, the two main technologies for solar thermal power production are the parabolic trough concept and the central receiver (power tower) concept. Several plants have been built in the USA (California) and Europe (Spain), which successfully deliver power to the grid.
Hence, this work´s aim is as follows:

As a first step, the possible solar thermal power plant configurations should be described in general, giving an overview of the actual state of the art. Specific design issues that influence the selection of solar power plant types should be identified.

Then, an already partially existing IPSEpro solar model library should be extended, focusing on a certain selected power plant concept.
Furthermore, an IPSEpro-PSE (Process Simulation Environment) simulation of this selected power plant concept should be performed, using the developed solar modules.

1.3 Overview of Method

First, I wrote a general overview of possible solar power plant concepts, giving an idea of potentials, configurations and specific design issues.

Before I actually started the modelling of solar power plant receivers, I wanted to describe the availability of solar radiation on the earth. I started with the solar radiation provided by the sun, how its magnitude depends on the distance in outer space, and which fraction finally hits the earth´s surface as a function of date and atmospheric conditions.

After having determined the extraterrestrial radiation available and atmospheric attenuation, which depends on the radiation´s path through the atmosphere, the actual position of the sun relative to a certain location on the earth´s surface has to be calculated. This position is defined by the solar azimuth and solar altitude angle. Its calculation requires functions of latitude, longitude, date and time.

As any kind of solar collector is - generally speaking - a plane at a certain angle to the incoming radiation,which may differ from 90° (radiation normal to the plane), only a fraction of the radiation´s flux can be received. For this reason, the position of a plane and its angles to the incoming radiation have to be defined.

I have discussed these necessary relationships mentioned above in theory and made them available in the IPSEpro solar model library.

After the incoming solar radiation was fully defined, I started the modelling of the parabolic trough collector, as it is the most common one in today´s commercial solar power plants.
In order to determine the amount of solar energy which is finally able to drive the steam cycle, I discussed attenuation factors and thermal efficiency, depending on possible collector orientations and locations.
As pumping power in collector fields has an influence on the plant´s total efficiency, it was necessary to discuss suitable pressure loss correlations.

In order to describe the energy transfer within the absorber tubes, also suitable correlations for heat transfer coefficients were necessary.

All these relationships were implemented in several parabolic trough collector models.
As direct steam generation (DSG) promises higher efficiencies, I created one model for heat transfer fluids (oil – without phase change) and one for direct steam generation (evaporation, preheating and super heating of water within the absorber tubes).

Finally, having modelled the parabolic trough collector, I built a model of a complete solar thermal power plant within IPSEpro-PSE.

2 Solar Thermal Power Plant Concepts

In principle, the solar energy (radiation) is collected and concentrated onto a receiver. In today´s successfully operated plants, this receiver absorbs the solar energy and evaporates water directly or via a heat transfer fluid (heat exchangers necessary). Next, the produced steam expands in a turbine and drives a generator in order to produce electric power. After this expansion in the turbine, the steam condenses and is recirculated. The condenser is either water- or air-cooled, depending on the water resources.

In the following there will be described why concentration of the incoming radiation is necessary, how concentration is defined and whether there are limits. Furthermore the issue of absorber efficiency in general will be addressed.

Thereafter possible plant configurations are outlined.

2.1 Why Concentrated Solar Power ?

“Sunlight can be concentrated with mirrors or lenses to such an extent that it is theoretically possible to achieve temperatures approaching those of the sun´s surface. In ancient Syracuse, Archimedes is said to have employed a large number of burnished shields as reflectors to ignite the sails of attacking Roman ships.” [Johansson et al. 1992]

“Energy delivery temperatures can be increased by decreasing the area from which heat losses occur. This is done by interposing an optical device between the source of radiation and the energy-absorbing surface. The small absorber will have smaller heat losses compared to a flat-plate collector at the same absorber temperature.” [Duffie & Beckman 2006]

As there are limits for non-concentrating solar collectors concerning the maximum temperature rise that determine the possible efficiency and use in conventional power cycles, it is necessary to concentrate solar beam radiation. This is done by optical concentrators that can be separated into **imaging** and **non-imaging** ones. Whereas the maximum concentration of imaging concentrators is limited due to aberrations, non-imaging concentrators can be designed to meet or approach the theoretical limit. [Winston 2005]
“Non-imaging concentrators, as the name implies, do not produce clearly defined images of the sun on the absorber but rather distribute radiation from all parts of the solar disc onto all parts of the absorber.” [Duffie & Beckman 2006]
“...consider an imaging problem taking the simplest example of points on a line. An imaging system is required to map those points on another line, called the image, without scrambling the points – that is, to focus the rays issuing from every object point into their corresponding image points....But suppose we consider only the boundary or edge of all the rays. Then all we require is that the boundary be transported from the source to the target. The interior rays will come along....To carry the analogy a bit further, suppose one were faced with the task of transporting a vessel filled with alphabet blocks spelling out a message. Then one would have to take care not to shake the container and thereby scramble the blocks. But if one merely needs to transport the blocks without regard to the message, the task is much easier. This is the key idea of non-imaging optics.” [Winston 2005]

Concentrators can be, amongst other things, defined by the **area concentration ratio C**, the ratio of the area of aperture $\mathbf{A_a}$ to the area of the receiver $\mathbf{A_r}$ or absorber.

$$C = \frac{A_a}{A_r}$$

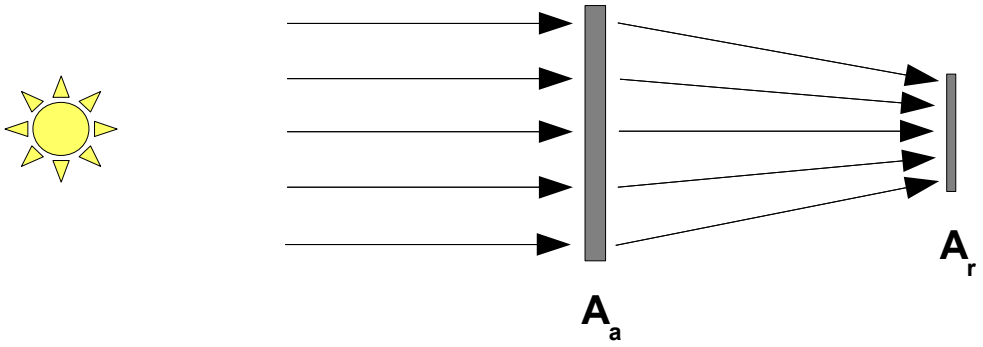

Figure 1: Concentration of Solar Radiation [Quaschning 2007]

2.1.1 The Theoretical Possible Value of the Concentration Ratio

Each square meter of the sun´s surface $\mathbf{A_{sun}}$ emits 63.11 MW of radiant power, which is described by the flux density $\mathbf{M_{sun}}$ with the unit W/m². [Quaschning 2007]

Let´s continue with a thermodynamic argument concerning solar energy concentration. If the sun is assumed as a spherical symmetric source of radiant energy, the radiant flux density per area **G** falls off as the inverse square of the distance **R** from the sun´s centre. That is due to the conservation of power through successive spheres of the area $\mathbf{4\pi R^2}$. If a fictitious concentric sphere with the radius **R**, the distance between the sun´s centre and the earth`s surface, is placed in reference to the sun, the total radiant power penetrating that surface $\mathbf{A_{se}}$ has to be equal to the total emitted power of the sun.

$$M_{sun} \cdot A_{sun} = G \cdot A_{se} = M_{sun} \cdot 4\pi r^2 = G \cdot 4\pi R^2$$

$$G = M_{sun} \cdot \left(\frac{r}{R}\right)^2$$

The sun´s flux density $\mathbf{M_{sun}}$ is reduced by the factor (r/R)² when received on the earth´s surface. By simple geometry (intercept theorems), the ratio r/R is equal to ***sin*** Θ_s. [Winston 2005]

$$\frac{r}{R} = \sin\Theta_s \qquad \rightarrow \qquad \left(\frac{r}{R}\right)^2 = \sin^2\Theta_s$$

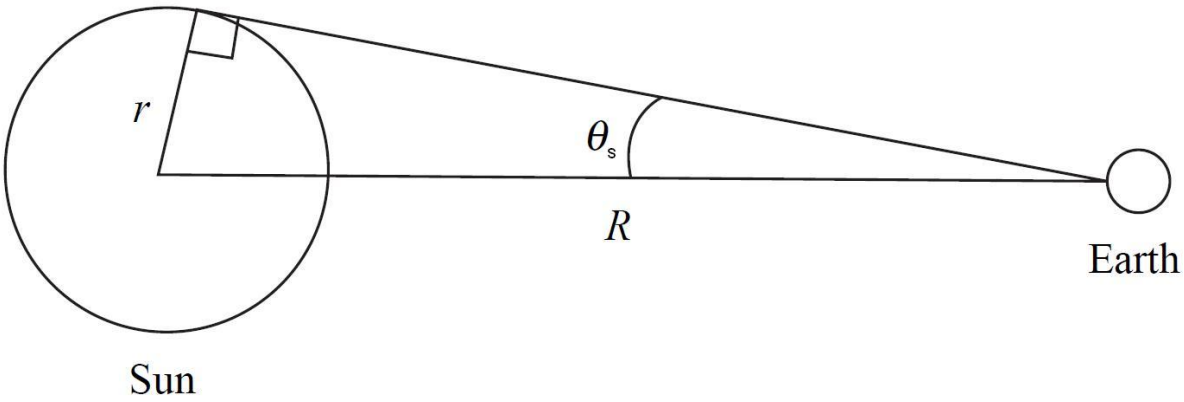

Figure 2: Sun-Earth Geometry

As the sun does not appear as a point at infinity, it is observed as a circle with an apex angle Θ_s, measured between the connecting line - centre of sun to the observers point of view - and the tangent to the sun´s surface through the observers point of view.

$$\Theta_s = \arcsin\left(\frac{radius\ of\ the\ sun}{distance\ sun-earth}\right) = \arcsin\left(\frac{6.963\cdot10^8\,m}{1.496\cdot10^{11}\,m}\right) = 0.27\,°$$

As neither the sun´s radius nor the sun-earth distance is a constant, the above defined apex angle Θ_s varies throughout the year. [Quaschning 2007]

"If we accept the premise that no terrestrial device can boost the flux above its solar surface value (which would lead to a variety of perpetual motion machines), then the limit to concentration is just $\frac{1}{\sin^2\Theta_s}$. We call this limit the sine law of concentration." [Winston 2005]

That limit mentioned above, is for concentration in both transverse dimensions, which is also known as 3-dimensional concentration (or 3D concentration for short). For concentration in one transverse dimension, which is called 2-dimensional (2D) concentration, the limit is $\frac{1}{\sin\Theta_s}$. [Winston 2005]

With Θ_s = 0.27°, the maximum possible concentration ratio for 3D concentrators is **45 000**, and for 2D concentrators the maximum is **212**.
"The higher the temperature at which energy is to be delivered, the higher must be the concentration ratio and the more precise must be the optics of the concentrator and the orientation system." [Duffie & Beckman 2006]

2.1.2 Dependence of Efficiency on the Concentration Ratio and Absorber Surface Temperature

Due to concentration of the incident sun light, higher-quality energy at higher temperatures can be collected. According to the fundamental law of thermodynamics, the higher the temperature at heat input, and the lower the temperature at heat output, the better is the efficiency of the heat engine that is connected to the solar receivers. This heat engine´s operating temperature is directly dependent on the solar receiver, or absorber outlet temperature.
If a simplified model of a solar thermal power plant is assumed, that has an ideal optical concentrator, a solar receiver performing as a black body (therefore having only emission losses) and a turbine or heat engine with Carnot ideal efficiency, system efficiency will depend on the balance of radiative and convective losses in the solar receiver.
The concentrated solar flux raises the absorber´s temperature and simultaneously radiation losses from the absorber surface to the ambient increase. Convective losses are at this point neglected. Thus, if a heat transfer fluid cools the absorber, the solar radiation´s energy equals the sum of the radiative losses and the energy gained by the fluid, if steady state conditions are reached. [Romero-Alvarez et al. 2007]

$$\frac{Q_{trans}}{A_r} = \alpha \cdot C \cdot IDR - \sigma \cdot 10^{-8} \cdot \varepsilon \cdot \left(T^4_{absorber} - T^4_{ambient} \right)$$

IDR ….. incident direct radiation (solar energy that reaches the ideal collector) [W/m²]
Q_{trans} …. power gained by the thermal fluid [W]
A_r …..... absorber area [m²]
C …..... area concentration ratio
α …..... absorptivity of the absorber surface
σ …..... Stefan-Boltzmann constant [5.67 W/m²K⁴]
ε …..... emittance of the absorber tube

The solar receiver efficiency $\eta_{receiver}$ can now be given as the ratio of power gain flux to concentrated solar radiation flux incident on the absorber.

$$\eta_{receiver} = \frac{Q_{trans} / A_r}{C \cdot IDR}$$

$$\rightarrow \qquad \eta_{receiver} = \alpha - \frac{\sigma \cdot 10^{-8} \cdot \varepsilon \cdot \left(T^4_{absorber} - T^4_{ambient} \right)}{C \cdot IDR} \qquad \text{[Romero-Alvarez et al. 2007]}$$

This leads to the following conclusions [Romero-Alvarez et al. 2007]:

- The maximum theoretical efficiency is the effective receiver´s absorptivity **α**.
- The higher the incident direct radiation, the better the efficiency.
- The higher the absorber temperature, the higher is the radiative loss and the lower the efficiency.

- The higher the effective emittance ε, the lower the efficiency.

As the solar receiver is followed by a heat engine, the Carnot cycle efficiency has to be taken into account too. The absorber temperature is assumed to be equal the temperature of heat input, and the ambient temperature corresponds to the temperature at heat output.

$$\eta_{Carnot} = 1 - \frac{T_{ambient}}{T_{absorber}}$$

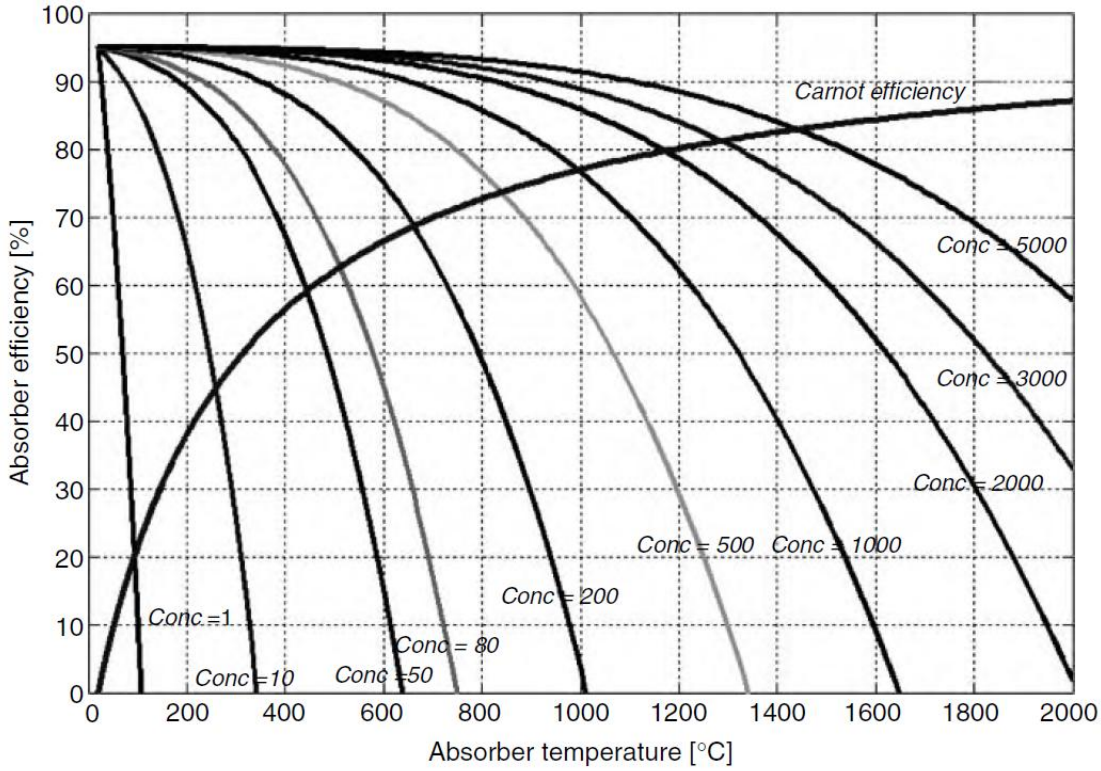

Figure 3: Efficiency of the Receiver and Carnot Efficiency, Assuming $T_{ambient}$ = 20°C, IDR = 770 W/m² and α = ε = 0.95 [Romero-Alvarez et al. 2007]

For a given area concentration ratio **C** there is an absorber threshold temperature at which radiation losses increase dramatically. However, the efficiency of the heat engine increases with higher absorber temperatures. Thus, the two efficiencies have to be multiplied to get the ideal conversion efficiency η_{total} from solar radiation to mechanical work. [Romero-Alvarez et al. 2007]

$$\eta_{total} = \eta_{receiver} \cdot \eta_{Carnot}$$

For each area concentration ratio **C** the efficiency increases with temperature up to a maximum (Carnot efficiency prevails). Once this peak is reached, a rise of absorber temperature correlates with a decrease in efficiency (radiative losses at receiver prevail).

Concentration is necessary to convert solar energy into mechanical work and for each area concentration ratio there is a theoretical optimum absorber operating temperature. [Romero-Alvarez et al. 2007]

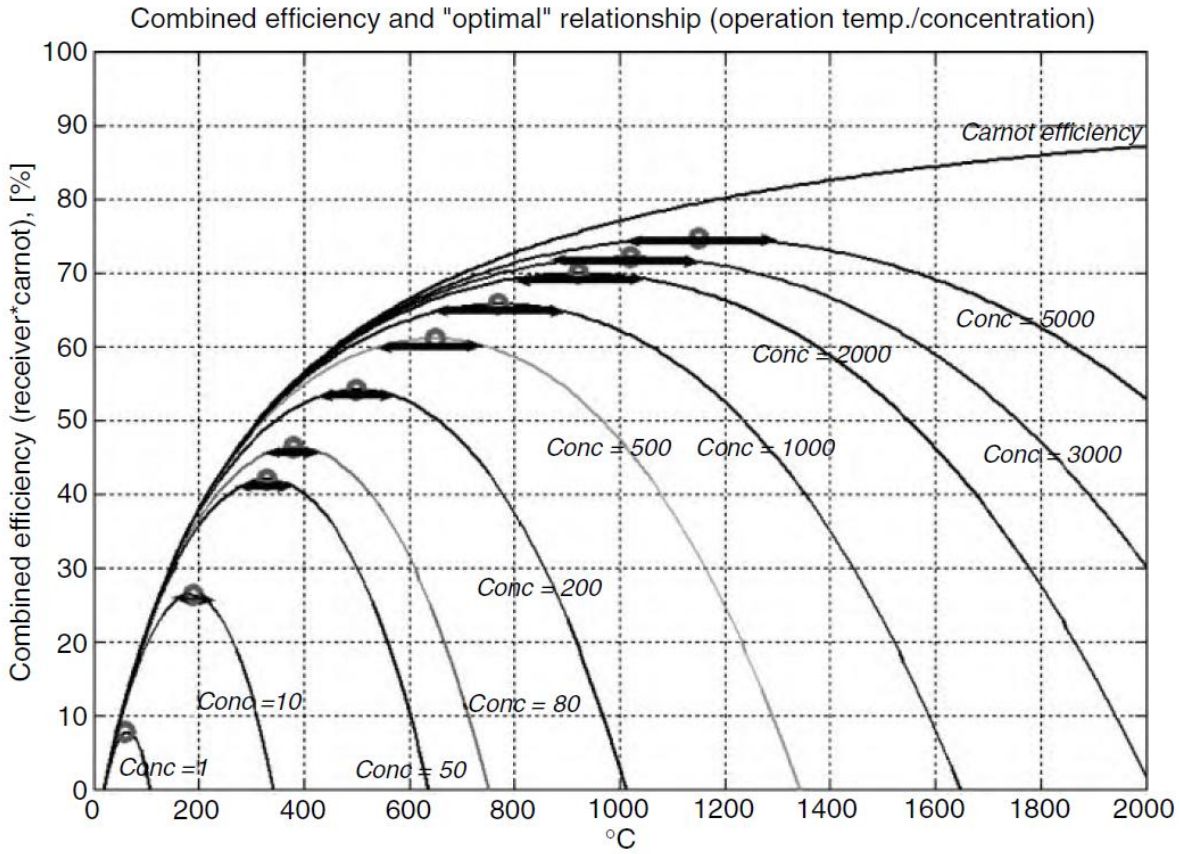

Figure 4: Combined Efficiency of an Ideal Solar Receiver - Heat Engine System, IDR= 770 W/m², $T_{ambient}$ = 20°C, α = ε = 1 [Romero-Alvarez et al. 2007]

2.2 The Parabolic Trough Collector Concept

Let´s imagine a parabola sketched on a piece of paper. If it is further assumed that this parabola has a reflective surface (like a mirror), rays of light that are parallel to its axis would be concentrated at the focal point. If this sketch is now assumed to be 3-dimensional, thus the parabola is extruded to a trough of a certain length, the focal point becomes a focal line.
That fact is used at parabolic trough collectors. More precisely, a tube is placed concentric to the focal line and all the received solar radiation is concentrated onto this tube, which absorbs the energy in order to heat a fluid. Furthermore, the parabolic trough collectors track the sun via one axis which is parallel to the focal line. Parabolic trough collectors are 2D concentrating devices, and the concentration ratio varies between 30 and 80. Depending on the time used (summer, winter or whole year) they are either placed best in a north-south direction or east-west direction, which will be described thoroughly in following chapters.

In parabolic trough collector plants many of these parabolic collectors are connected in series and parallel in order to raise the heat transfer fluid´s temperature to a certain value, that is necessary for the following Rankine steam cycle.

Basically, there are two possible setups.
Parabolic trough power plants can either directly evaporate water or use a heat transfer fluid (oil) that evaporates the water for the steam cycle later on via a heat exchanger.

The direct steam generation (DSG) promises higher conversion efficiencies, due to higher live steam temperatures and less pumping losses within the field, but is so far not commercially available, as controllability and design are still under research.

Parabolic trough power plants using heat transfer fluid are commercially available and state of the art.

Figure 5: EuroTrough at Plataforma Solar de Almeria [Lüpfert et al. 2001]

Figure 6: SEGS III-VII at Mojave Desert, California [Radecki 2007]

In order to receive an impression of the size and layout of a parabolic trough collector field the picture above is shown (figure 6). There the Solar Electric Generation Stations (SEGS) III to VII are pictured. They are located at Kramer Junction, Mojave Desert, California, USA and started the operation between 1986 and 1988. They use synthetic oil as heat transfer fluid and have supplementary natural gas boilers to cope with variations in solar irradiation. An interesting fact is that the power conversion system is rather small when compared to the solar field. The buildings in the centre of each field represent the power conversion system, which includes the steam cycle with steam generator, turbine, condenser and cooling tower. At a closer look one can even see that some parabolic trough collectors are defocused; maybe due to cleaning or maintenance.

2.2.1 Parabolic Trough Plants Using Heat Transfer Fluid

Basically, a thermal solar power plant using parabolic troughs with heat transfer fluid consists of the solar system, the steam generator and the power conversion system. Oil, either mineral oil or synthetic oil, is commonly used as heat transfer fluid. Most of the systems use VP-1 (73.5% diphenyl oxide and 26.5% diphenyl), which can be used up to 395°C. Flowing through the collector loops, the heat transfer fluid´s temperature is raised about 100°C. It enters with a temperature of about 295°C and leaves the field at 390°C. [Romero-Alvarez et al. 2007]

In the steam generator, that is an oil-water heat exchanger, the fluid´s energy is used to produce superheated steam that is required by the turbine. Thus the steam generator is the interface between the solar system and the power conversion system. As usual, the steam generator consists of the preheating section (where water is preheated to a temperature close to evaporation), the evaporating section (where the preheated water is evaporated and converted into saturated steam) and the superheating section (where the saturated steam is heated up to the temperature required by the turbine). The steam turbine is usually composed of a high pressure and a low pressure turbine. Steam leaving the high pressure turbine is usually reheated before entering the low pressure turbine. After that, the steam is condensed and the condensate goes to a water deaerator to remove air and gases dissolved in the water. The selection of the best cooling system depends on the available water resources. Cooling of the condenser can either be achieved through evaporative (wet) cooling, where water is available, or through dry cooling (with air) - both conventional technologies [Richter et al. 2009]. From the deaerator, the water is pumped back to the steam generator, reaching the required pressure level and starting the Rankine thermodynamic cycle again. [Romero-Alvarez et al. 2007]

Typical solar-to-electric efficiencies of a large (> 30 MW_e) solar thermal power plant with parabolic trough collectors range between 15 and 22%. [Romero-Alvarez et al. 2007]

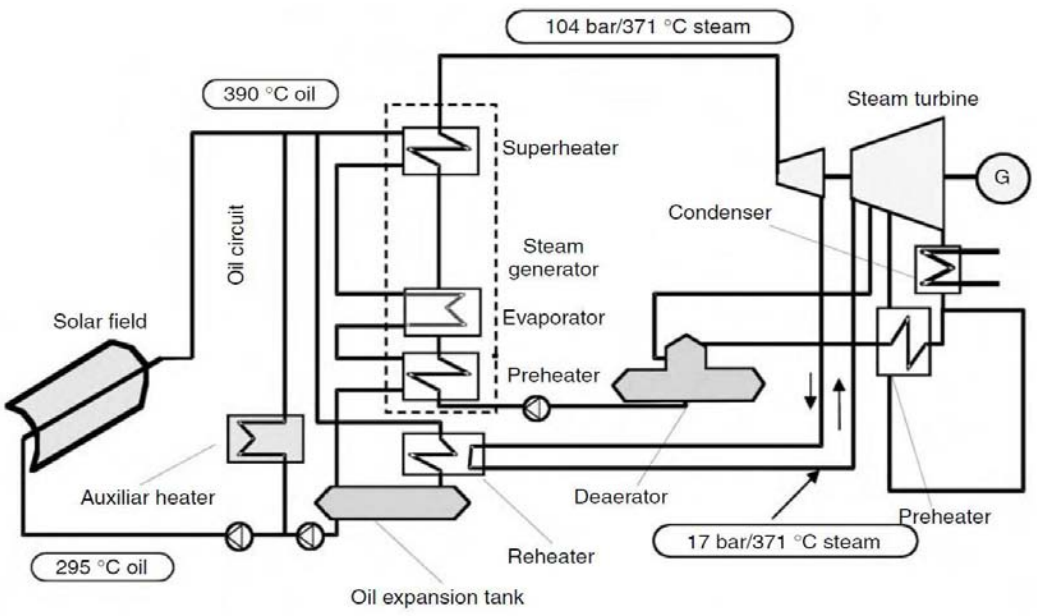

Figure 7: Simplified Parabolic Trough Plant [Romero-Alvarez et al. 2007]

2.2.1.1 Basic Layout of the Collector Field

Basically the piping system of a parabolic trough solar power plant consists of header pipes, pipe segments and fittings (such as reducers, elbows, valves, ball joints or flex hoses). The header pipes can be divided into the cold (leading to the parabolic trough receivers) and hot unit (leading from the parabolic trough receivers to the heat exchanger / steam generator). Header pipe sizes change along the flow path to approximately maintain the design velocity, as for instance, the flow in the cold header is incrementally drawn off through a collector loop and passed to the hot header. The cold header piping diameters are reduced along header length to maintain the appropriate velocity. This design velocity is chosen to approximately optimize the solar field´s piping costs. It is necessary to find the velocity that optimizes the trade off between piping size and parasitic pumping power. Generally, values in the range of 2-3 m/s have been assumed, based on the past experience or results of optimization. Basically, small header pipes reduce piping and fitting costs, but increase pumping parasitics; larger header pipes have the opposite effect. [Kelly & Kearney 2006]

Three basic layouts of piping are used in solar fields with parabolic trough collectors. These are the direct-return concept, the reverse-return concept and the centre-feed concept. To minimize thermal losses the hot header piping should be shorter than the cold. [Romero-Alvarez et al. 2007]

The **direct-return** piping configuration is the simplest and probably the most extensively used in small solar fields. Its main disadvantage is that there is a much greater pressure difference between the inlets of parallel collector rows, so that balancing valves must be used to keep flow rates equal. These valves cause a significant pressure drop at the beginning of the array, and thus have a quite high impact on the system´s total pressure loss.
The **reverse-return** layout, where the fluid leaves the collector array at the opposite end has a lower parasitic energy consumption. Header pipes with different diameters are used in this configuration to balance the array flow. While balancing valves may still be required, the additional system pressure loss is much lower than in a direct-return configuration.
In large solar fields though, the most widely used configuration is the **centre-feed** layout. This layout minimizes the total amount of piping because there is no pipe running along the collector row length. There is also direct access to each collector row without buried pipes.
[Romero-Alvarez et al. 2007]

The pressure loss in the flow to the outermost loop of a centre-feed layout defines the pressure loss through all loops. The pressure loss in the inner loops is set equal to the pressure loss in the outermost loop by throttling action of either orifices or valves. The diameter of the cold header steps down as the distance from the power block increases to provide a roughly constant fluid velocity. Thus, the diameter of the hot header increases as the distance to the power block decreases. [Kelly & Kearney 2006]

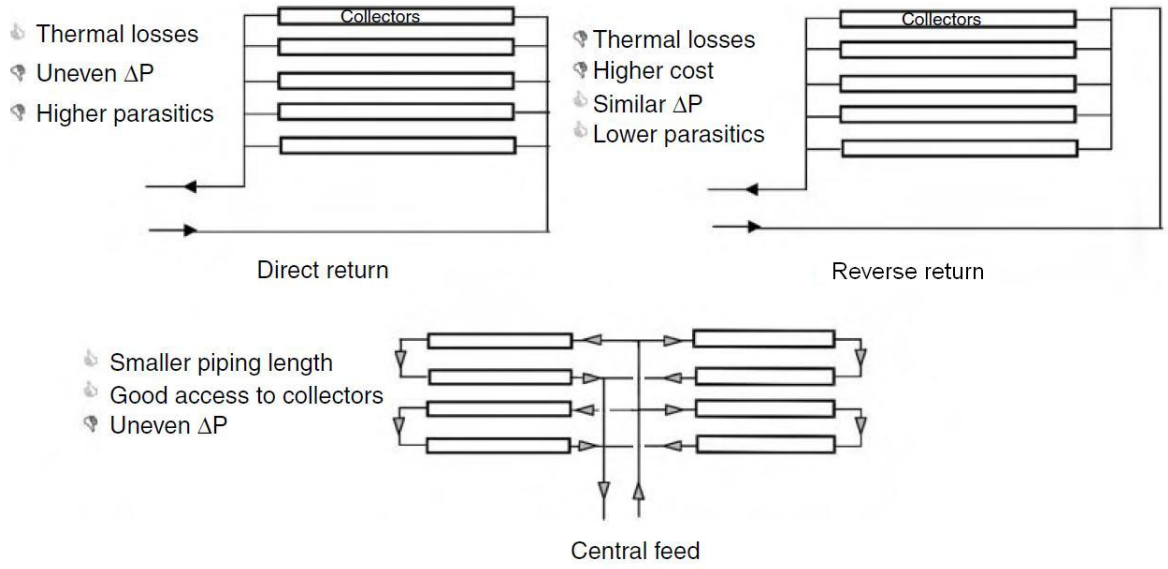

Figure 8: Piping Layouts for Parabolic Trough Power Plants [Romero-Alvarez et al. 2007]

2.2.1.2 Thermal Storage Systems

To allow operation of thermal solar power plants when solar radiation is not available any more, storage systems can be added. In this case, the solar field has to be oversized in order to charge the thermal storage system while the power conversion system is working too. This stored energy is then used to keep the plant running after sunset or during cloudy periods. Yearly hours can be significantly increased, thus shortening the time necessary for amortization.
On the one hand thermal energy can be supplied during hours when direct solar radiation is not available, so that solar energy collection and supply of electricity do not have to be simultaneous; on the other hand the power conversion unit can be fed with constant thermal power as the storage system filters variations in the solar field outlet-temperature. [Romero-Alvarez et al. 2007]

As the necessary pressure in a hot water storage system would make the system too expensive, different storage mediums are required for parabolic trough power plants. Depending on the medium, there are two types of systems that are used; the single medium storage system and the dual medium storage system. [Romero-Alvarez et al. 2007]

In **single medium storage systems** the same fluid that is flowing through the collectors is also used for storage. The most common fluid used is thermal oil and the efficiency that can be reached is over 90%. For low-capacity storage systems, thermal energy can be stored in a single tank, in which the oil is stratified by temperature. As the density of the oil changes with temperature the hottest remains at the top of the tank. The cold oil leaves the tank at the bottom and is pumped through the collector field to be heated up and fed back at the top of the storage tank. If there is additional need of thermal energy hot oil is taken from the top and mixed with the hot oil coming from the solar field to maintain a certain temperature level. For high-capacity systems, two oil tanks are needed; one for hot oil and one for cold oil. The steam generator is fed from the hot tank and once the oil has transferred the heat to the water it is pumped to the cold tank. The cold tank feeds the solar field, returning hot oil to the storage or power conversion unit. Thermal oil has to be kept

pressurized above the vapour pressure corresponding to the maximum temperature in the oil circuit. For the temperature range between 100 – 400°C the pressure required is low and can be easily maintained by injecting argon or nitrogen. This inert atmosphere is anyway necessary to avoid explosions as the mixture of oil with air is dangerous. Thus appropriate fire fighting systems have to be added. [Romero-Alvarez et al. 2007]

In **dual medium storage systems** the heat is stored in a medium different from the working fluid which is pumped through the solar field. Iron plates, ceramic materials, molten salt or concrete can be used as storage medium. Molten salts are an eutectic mixture of sodium and potassium nitrates. Once again, one tank is needed for the hot and one for the cold salt, where the lowest temperature possible is always above the melting point that is approximately 250°C. As a matter of fact there is an additional heat exchanger necessary, between the molten salt and the thermal oil. [Romero-Alvarez et al. 2007]

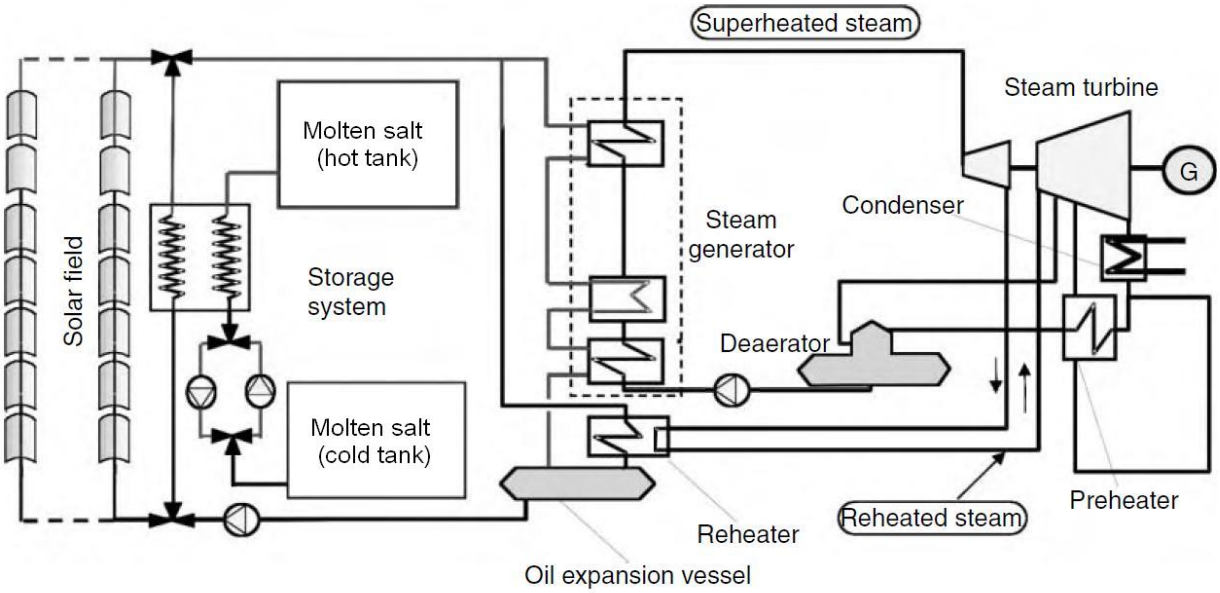

Figure 9: Molten Salt Heat Storage With Oil as Working Fluid [Romero-Alvarez et al. 2007]

2.2.1.3 Parabolic Trough Plants Built and Operated

The first major commercial parabolic trough power plants were built by Luz International Limited in California, USA. These power plants are called Solar Electric Generating Stations (SEGS).

The operation of SEGS I started in 1984. It has a rated power output of 13.8 MW, producing steam at 35.3 bar and 415°C. However, the solar field only produces saturated steam, which is then superheated by a natural gas fired boiler. The Rankine-cycle efficiency achieved is 31.5%. Mineral oil is used as heat transfer fluid within the collector tubes.
SEGS II went on-line in 1985. Its rated power output is 30 MW. It has a natural gas fired boiler too, in order to match the demand curve more easily. [Johansson et al. 1992]

Due to the now gained experience, several components were improved and led to higher

efficiencies of subsequently built plants. The rise of collector operating temperatures from 321°C to 390°C and the introduction of steam reheat enabled steam cycle efficiencies of 37.5%. Thus, projected annual solar-to-electric efficiencies were 11.5% for SEGS III – IV and 14.5% for SEGS VI – VIII. Design point efficiencies were 23 and 26%, respectively. [Johansson et al. 1992]

SEGS III and IV started operation in 1986 with solar mode steam conditions of 43.5 bar and 327°C and 30 MW output.
SEGS V followed in 1987, which has the same design as III and IV. [Johansson et al. 1992]

SEGS VI and VII started operation in 1988. Due to a higher live steam temperature and additional reheat, steam cycle efficiency was increased by 7 percentage points. The solar field outlet temperature of 390°C enabled live steam conditions of 100 bar and 371°C (and again 371°C after reheat). [Johansson et al. 1992]

SEGS VIII and IX entered service in1989 and 1990, respectively. The rated output power was increased to 80 MW, thus improving economies of scale. LS-3 collectors, the third generation of Luz parabolic trough collectors, were used for the entire field. Live steam conditions are 104 bar and 371°C (and again 371°C after reheat). [Johansson et al. 1992]

All SEGS plants have auxiliary natural gas boilers, in order to cope with variations in solar irradiation and extend operation after sunset. In natural gas fired mode, SEGS II, III and IV have live steam conditions of 104 bar and 510°C. SEGS V, VI and VII reach 100 bar and 510°C. SEGS VIII and IX have the same conditions as in solar mode. [Romero-Alvarez et al. 2007]

Unfortunately, Luz International Limited filed for bankruptcy in 1991, after failing to finance SEGS X [Johansson et al. 1992]. The significant reduction in both, fossil fuel prices and tax exemptions, made it impossible for the SEGS plants to maintain the profit margin they had had at the beginning. Luz International Limited developed three generations of parabolic trough collectors, called LS-1, LS-2 and LS-3. Whereas LS-1 and LS-2 are conceptual very similar and only differ in overall dimensions, the LS-3 collector represents a change in design. It has a lighter and stiffer structure, with highly accurate operation in high winds. Furthermore, it is twice as long as the LS-2 collector and 14% wider [Romero-Alvarez et al. 2007]. After 1991 the company Solel Solar Systems continued providing parabolic trough collectors based on the LS-3 design. Since then several more companies started to develop commercial parabolic trough designs. At present, the list appears to be: Flagsol (part of Solar Millennium), Solel Solar Systems (now part of Siemens Concentrated Solar Power, Ltd), Acciona Solar Power (was Solargenix), Sener / ACS Cobra, Solucar R&D (part of Abengoa), IST Solucar (part of Abengoa) [Kearney 2007].

“The electricity produced by the SEGS plants is sold to the local utility, Southern California Edison, under individual 30-year contracts for every plant.” [Romero-Alvarez et al. 2007]

At Plataforma Solar de Almeria (PSA) in Spain, which belongs to the Center for Energy, Environment and Technological Research (CIEMAT), several parabolic trough test facilities have been built since 1997. Some of them were even pioneers in Europe. Besides test loops for different heat transfer fluids (oil or molten salt) one parabolic trough facility has been built in order to study the direct steam generation (DSG). This experimental plant (DISS project) is the only facility in the world where the two-phase-flow water/steam process in parabolic trough collectors can be studied under real conditions. [PSA 2010]

In 2008, Andasol 1, Europe´s first parabolic trough power plant, built by the Solar Millennium AG, started its operation. It is the first of three (Andasol 1, 2 and 3) solar power plants (50 MW each),

located 10 km east of Guadix, Granada, Spain. Their peak solar-to-electric efficiency is about 28%; the annual average is about 15%. Oil is used as heat transfer fluid and a molten salt storage concept allows a plant operation for about 7.5 hours, after sunset. [Solar Millennium AG 2008]

In 2007, the company Abengoa Solar started the construction of two 50 MW parabolic trough plants in Spain (Solnova 1 and Solnova 3). They are located at the Solucar Platform, close to Sanlucar la Mayor, Sevilla. Solnova 1 produces steam at 100 bar and 390°C. Oil is used as heat transfer fluid, which leaves the steam generator at 302°C and enters it at 395°C. After the high pressure turbine section, the steam is reheated again to about 390°C. A natural gas boiler enables the plant operation at night and during low solar radiation. [Abengoa Solar 2008]

In 2008 the construction of Solnova 4 began, which will have the same design as the previous two. Two more similar plants, Solnova 2 and Solnova 5, with a rated power output of 50 MW each, are still under development. They will be located at the Solucar Platform too. [Abengoa Solar 2008]

Furthermore, a 280 MW parabolic trough power plant “Solana” is under development in Arizona, USA. It will be located at Gila Bend, near Phoenix. Its operating concept will be similar to those at the Solucar Platform, but with additional molten salt storage concept. [Abengoa Solar 2008]

An additional 250 MW parabolic trough project will start its operation in 2013. It will be located near Harper Dry Lake in the Mojave desert, 100 miles north east of Los Angeles. [Abengoa Solar 2008]

2.2.2 Direct Steam Generation (DSG)

Direct-steam generation is a concept to generate steam in the solar field itself. Thus, there is no need for the heat-transfer fluid and centralized oil-heated steam generators. For this reason significant cost savings can be achieved. In addition to this, there is a reduced environmental risk and fire hazard in case of leaks, without the use of oil. Furthermore, performance gains due to the following mechanisms are possible:
First, by eliminating the heat-transfer fluid, the solar field´s operating temperature can be lowered without affecting the temperature of the steam entering the turbine. This will slightly reduce thermal losses, by omitting the oil-water/steam heat exchanger. Although, if direct steam generation is used, one´s ambitions are more towards higher turbine entry temperatures, as there is no temperature limit given by the oil.
Another reason is that there is by far less pumping power required because the system will only operate boiler feed water pumps. The high pressure drop due to the thermal oil can be avoided. However, a sophisticated control has to facilitate the two-phase flow of water and steam. [Johansson et al. 1992]
Due to the maximum oil-temperature allowed the steam temperature is limited to 380°C in conventional parabolic trough power plants. In direct steam generation plants, steam temperatures up to 550°C at pressure levels of 100 bar are possible. [Zarza 2007]
The steam turbine inlet temperature approaches the optimum for operation at 550°C and total energy conversion efficiencies of 23% can be reached. Thus the efficiency of solar thermal parabolic trough power plants can be significantly improved if a direct steam generating solar field is used to deliver steam at 550°C/100 bar. [Zarza et al. 2001]
Using direct steam generation, a reduction in operation and maintenance costs can be achieved, as a certain amount of oil has to be changed every year. [Odeh et al. 1998]

Unfortunately direct-steam generation technology involves certain technical risks. Tube overheating in the boiling region and flow instabilities in parallel arrays may occur. The major problem facing that technology is stratification of the flow in the absorber tube that causes

temperature gradients and tube failure. [Odeh et al. 1998a]
Among other things, following topics have to be investigated before commercial plants can be designed:

The operation of single and parallel absorber rows under steady-state and transient conditions have to be defined.
The start-up and shut-down procedures have to be established (solar field control).
Furthermore, absorber-tubes have to endure strain due to transients, and the best operation mode has to be investigated.

Basically, there are three process options of solar direct steam generation for electrical power supply. The once-through concept, the recirculation concept and the injection concept.

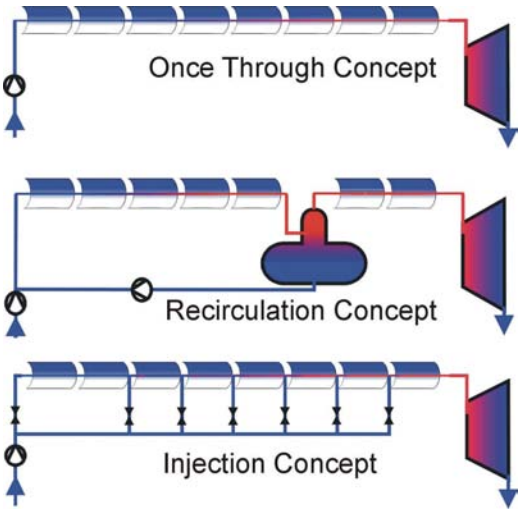

Figure 10: Direct Steam Generation Concepts [Eck 2001]

Flash steam generation is suitable, if steam at low pressures for industrial processes is needed.

2.2.2.1 The Once-Through Concept

In the **once-through concept** the water enters the absorber tube, is preheated, evaporated and finally superheated before it leaves the tube, flowing to the turbine. Indeed it is the most simple and cheapest setup but hard to control. Due to the constant mass-flow at the inlet the outlet temperature is dependent on the incident direct solar radiation. Furthermore, one specific problem of the once-through concept is the local variation of the end of the evaporation section, that is the cause of high temperature gradients in the absorber tube that may lead to failure. [Eck 2001]
During a sudden decrease of solar radiation, the start of the super-heating section is set further downstream. Thus on the one hand the steam temperature at the turbine entry is reduced, and on the other hand water with boiling temperature reaches regions of the absorber tube where the tube walls have already reached much higher temperature levels. That may disturb the turbine´s operation and may lead to thermo-shock loading of the absorber tube. [Goebel 1998]

2.2.2.2 The Recirculation Concept

The **recirculation concept** is equivalent to a conventional recirculation boiler. Although it is the most secure one, it is more expensive due to the required separator and recirculation-pump. A certain number of absorber tubes are responsible for preheating and evaporation. Then the steam and remaining water are separated in the separator and the steam is superheated in a following sequence of absorber tubes before it enters the turbine. The remaining water that could not be evaporated is pumped back to the preheating and evaporating part.
Another possibility would be that the water leaving the separator is pumped directly back to the beginning of the evaporating part. This would require a separate preheating section and thus a more complex tube assembly. [Goebel 1998]
The recirculation is defined by the recirculation-rate, which is the ratio of mass-flow recirculated to mass-flow entering the super-heating section, flowing to the turbine. Practical values for the recirculation-rate would range between 3 and 5. [Goebel 1998]
High recirculation-rates cause a high mass flow within the evaporation section, which guarantees a good cooling of the absorber tube and thus a safe operation. However, high mass flows cause high pressure drops and thus increase parasitic power consumption. For this reason, it is important to identify a minimum recirculation-rate, that still guarantees the required cooling. [Eck et al. 2003]
As separators, there are mainly large separator vessels used (similar to steam drums in conventional steam generators), that have a wall-thickness of several centimetres (depending on the volume) due to the high working pressure (100 bar). Thus, they represent a high thermal inertia that causes a longer start-up time. If the recirculation-rate can be kept small, it is possible to use cyclone separators as they have a lower thermal inertia and are cheaper. Another possibility would be T-junctions that separate the two phases after the evaporation section. [Eck 2001]

2.2.2.2.1 Compact Field Separators for Direct Steam Generation

Field steam separators are located at the inlet of the super-heating collectors. It should guarantee constant steam parameters despite a varying solar irradiation. For first field designs for the recirculation concept, conventional vessel-type separator drums are used, that are bulky, expensive and do not offer a perfect separation when operated at high gas velocities. Therefore, alternative separators are thought after. [Malayeri et al. 2004]

Apart from cost considerations, the separator also influences the behaviour of the collector field. Its thermal inertia increases the field´s dynamic losses, as it increases for instance the start-up time of the system. In order to achieve a good system performance, a fast and compact separator is therefore desirable. [Malayeri et al. 2004]

“Due to the time-varying nature of the solar DSG process the separator has to cope with a broad range of operating conditions: mass flux, steam quality and operation pressure vary during the day. The mass flux is determined by the actual irradiance. The steam quality and the operation pressure are determined by the operation strategy and can vary throughout the day too.” [Malayeri et al. 2004]

Basically, there are several design options possible. Commonly used separators are hydrocyclone separators, baffle type separators and T-junctions. Hydrocyclones are a more compact option, but are usually designed for a narrow range of operating conditions, which could make additional control equipment necessary. Baffle type separators consist of several sinusoidal curved deflectors that require a minimum flow velocity for a satisfying phase separation, which limits the work capability. The most simple design is the T-junction separator. It offers a partial to perfect phase

separation for horizontal two-phase flows. [Malayeri et al. 2004]

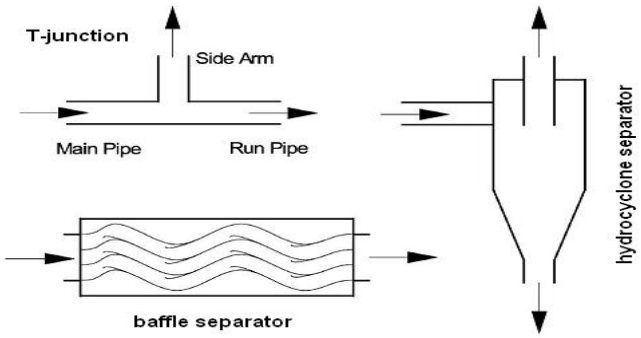

Figure 11: Phase Separator Types [Malayeri et al. 2004]

The phase separation in a T-junction can be attributed to inertia forces and gravity forces. The phase with the higher momentum tends to flow in the axial direction and enters the run pipe, whereas the phase with lower momentum preferentially enters the side arm. Furthermore, gravity forces tend to keep the liquid phase at the bottom of the pipe, thus avoiding the entering of the side arm. At higher gas velocities the change in flow-pattern influences the separation. With an increasing steam velocity annular flow becomes more likely. Thus, water is flowing as a liquid film at the tube walls with a relatively low momentum and therefore might enter the side arm too.
As there is a sudden change in direction of the gas flow, the pressure in the main pipe increases (centripetal effect), which weakens the momentum of the liquid film too. [Malayeri et al. 2004]

2.2.2.3 The Injection Concept

In the **injection concept** water is injected along the solar absorber tube to control stratification while generating steam. The collector loop is subdivided into units that are connected in series. Each unit consists of an absorber tube (certain length), injection and gauging equipment. The controllability of this process is expected to be better. [Eck 2001]
However a disadvantage of the injection-concept is the requirement of additional components like tubes, valves and wires for the measurement and control tasks. [Goebel 1998]

Experimental results showed that the recirculation concept is the most feasible option for commercial applications. There is a good stability of the recirculation process, even with a low recirculation-rate, thus making possible the use of small and cheap separators in the solar field. [Romero-Alvarez et al. 2007]

2.2.2.4 Flash Steam Systems

In flash steam systems water is circulated through the collector field. To avoid boiling and a two phase flow inside the absorber tubes the pressure is kept high enough. After leaving the absorber tubes the hot water is led through a throttling valve into a separator. This constant enthalpy process converts water into a two phase mixture at a defined pressure in the separator. But due to thermodynamic constraints only 10% of the total flow are converted into steam, that can be used in

the following industrial process. The remaining water is recirculated to the solar collector field. One disadvantage of the flash steam system is that freezing, due to low ambient temperatures, has to be avoided. Furthermore, the collector temperature must be significantly higher than the steam delivery temperature, to obtain reasonable steam qualities with a limited water recirculation rate. Pressure levels that can be achieved by this method are approximately at 20 bar, by keeping the electrical power necessary for pumping within acceptable limits. [Romero-Alvarez et al. 2007]

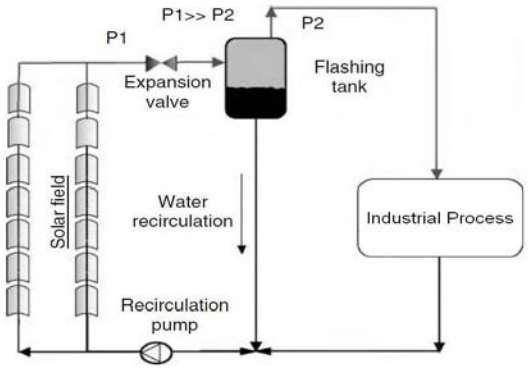

Figure 12: Flash Steam Generation [Romero-Alvarez et al. 2007]

2.2.2.5 Storage Concepts for Direct Steam Generation

Due to the water´s phase change a sensible heat storage system only as used in oil-cycle parabolic trough power plants is not the best option. More suitable is a three component storage system that is adapted to the three sections for preheating, evaporation and super-heating. Whereas preheating and super-heating is made by a sensible heat storage system, the energy required for the evaporation is provided by a latent heat storage system that makes use of the fact that the temperature stays constant during phase change. In such systems salt is melted or frozen while the necessary heat flow is used to condense or evaporate steam.
A salt that might be used in DSG power plants is $NaNO_3$, which has its melting point at 306°C. Thus, assuming a temperature difference of 10°C in the heat exchanger, while charging, the steam has to be condensed at 316°C and while discharging, the water is evaporated at 296°C. Hence, there are two different pressure levels required, namely the saturation pressures of 316°C (107 bar) and 269°C (81 bar). Another salt suitable for a charging pressure of 156 bar (345.3°C) and a discharging pressure of 116 bar (322°C) is KNO_3. [Birnbaum et al. 2008]
The need for these two pressure levels has a significant impact on the design of the plant. As steam that comes from the collector field has a different pressure than the steam provided by the storage loop, a throttle is necessary in order to mix these flows before entering the turbine. To be able to mix these two streams without throttling it is possible to operate the plant in sliding pressure mode. This is done by reducing the pressure at the feed water pump until both streams have the same pressure. [Birnbaum et al. 2008]
A possibility to operate a DSG power plant with storage at a combined (steam from collector field and from storage enters the turbine) operation mode is to feed steam from the storage into a later stage of the high-pressure turbine where the pressure level is adequate. [Birnbaum et al. 2008]

In order to compensate fast transients in solar irradiation, which are usually not predictable, buffer storage systems can be integrated. These systems should have short reaction times, high discharge rates and a thermal capacity in the range of 5-10 minutes. In this way it is possible to protect the power plant´s components from high thermal transients. Steam accumulators meet these requirements, providing saturated steam at pressures up to 100 bar. As the direct storage of saturated or superheated steam in pressure vessels is not economic due to the low volumetric energy density, steam accumulators use sensible heat storage in pressurized saturated liquid water. Thus, steam is produced by lowering the pressure of the saturated liquid during discharge. During the charging process either the temperature of the liquid inside the vessel is increased by condensation of superheated steam, or saturated water is fed directly into the system. [Steinmann & Eck 2006]

In case the steam production of the collector field exceeds the demand of the turbine, the surplus steam is condensed in the accumulator. And vice versa, during reduced irradiation, steam is taken from the accumulator. Again, the recirculation DSG concept works best, as it is a cost effective approach to combine storage and phase separation in a single component. There, wet steam from the evaporation section of the collector field enters a combined separator-accumulator. During the charging process, the mass flow entering the vessel through the wet steam feed line exceeds the total drain mass flow. [Steinmann & Eck 2006]

Investment costs for these steam accumulators are dominated by the pressure vessel. Thus, the use of components like steam drums, feed water tanks or deaerators as storage vessels, offers an interesting option for the limitation of additional costs for steam accumulator systems. [Steinmann & Eck 2006]

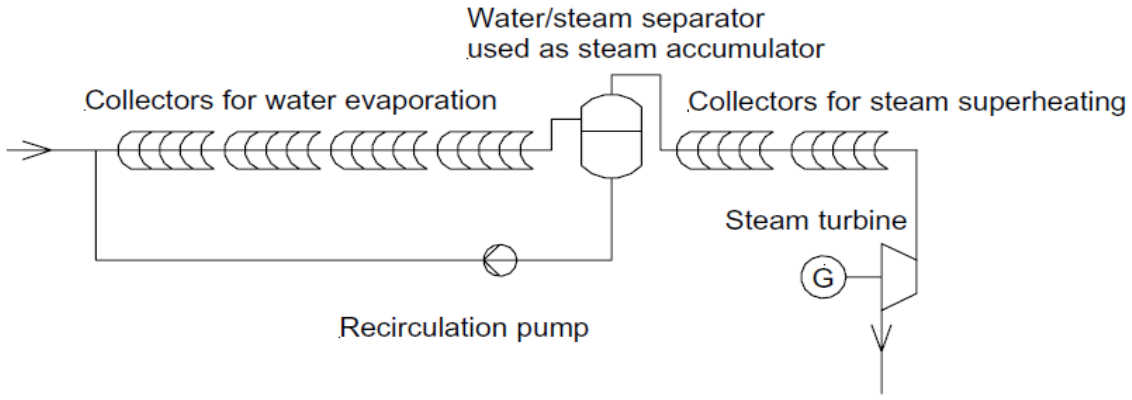

Figure 13: Water - Steam Separator Used as Steam Accumulator [Steinmann & Eck 2006]

2.3 The Linear Fresnel Collector Concept

The linear Fresnel concept is another line focusing method, that is similar to the parabolic trough technology which is described in the previous chapters.

The basic idea of this concept is to replace large continuous reflectors, which are for the most part quite complex and therefore expensive to manufacture, by small elements distributed over a certain area. [Mills & Morrison 2000]
“Flat or elastically curved glass reflectors mounted close to the ground are used to minimise structural costs.” [Mills & Morrison 2000]
It even offers the potential of greater concentration ratios than those achievable with parabolic trough collectors, as the size of single-piece reflectors is limited. [Reynolds et al. 2002]

A classic linear Fresnel collector consists of one linear absorber that is placed several meters above a bank of parallel mirror rows. Each mirror row (primary mirror) has to be aligned in a certain angle to reflect the incident solar radiation on the absorber´s surface.
However, it is difficult to avoid shading of the incident solar radiation and blocking of reflected solar radiation by adjacent mirror rows. This problem can either be solved by using higher absorber towers or by increasing the spacing between mirror rows. Both possibilities will lead to higher costs and are therefore not suitable improvements. [Mills & Morrison 2000]

A much more promising method is provided by the compact linear Fresnel reflector (CLFR) concept, which will be described in the following chapter.

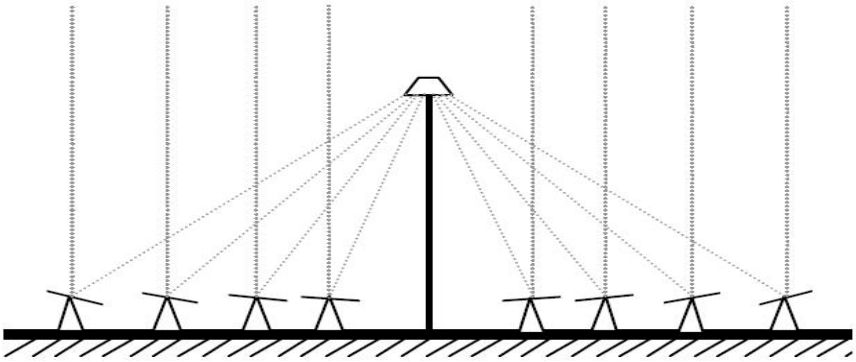

Figure 14: Classic Linear Fresnel Collector [Reynolds et al. 2002]

Unlike the parabolic trough concept, the heat transfer loop is separated from the reflector field and fixed in space. High costs of flexible high pressure lines or especially high pressure rotating joints can be avoided. [Mills & Morrison 2000]

Furthermore, wind loads are substantially reduced due to the reflector array´s planarity and low height. Thus, the reflector area for one absorber can easily be three times the area of comparable parabolic troughs. [Bockamp et al. 2003]

These advantages can lead to a substantial cost reduction for the solar field compared to parabolic trough technologies, and besides lower investment costs, there is potential for reasonable savings offered by lower operation and maintenance costs. [Bockamp et al. 2003]

Linear Fresnel collectors can be used for direct steam generation as well as for power generation with heat transfer fluids.

The orientation of linear Fresnel collectors can either be north-south or east-west, depending on the site´s latitude and required annual performance. In order to improve performance during winter, the collector arrays can be tilted towards the equator (the higher the site´s latitude the higher is the required tilt angle, in order to limit the maximum angle of incidence). Although this tilted configuration has in principle a high efficiency, it uses by far more ground than the horizontal mirror field collectors, as spaces have to be left between rows to avoid shading. [Mills & Morrison 2000]

2.3.1 Primary Mirror Curvature

The necessary mirror curvature is small but crucial. The focal length (~ 30 m) is mainly determined by the absorber distance of the outer field mirrors, as these mirror elements produce most of the beam spread. The closer a mirror is moved towards the absorber the fewer rays are “spilled”, even if the focal length of the mirror is incorrect. Thus, results gained from experiments with variable curvature do not differ much from those of constant curvature. The optimised constant curvature has a reduction in performance of about 0.5 – 0.6%. The performance of flat mirrors is reduced by about 13%. A constant curvature system with elastically formed mirrors represents a very low cost and practical option, as moulding or sagging of glass is not required. [Mills & Morrison 2000]

2.3.2 The Compact Linear Fresnel Reflector (CLFR) Concept

As the classic linear Fresnel collector has only one linear absorber, each mirror´s alignment is determined. Adjacent mirrors are tilted towards the same direction, but at different angles.

“However, if one assumes that the size of the field will be large, as it must be in technology supplying electricity in the multi-MW class, it is reasonable to assume that there will be many linear absorbers in the system. If they are close enough, then individual reflectors will have the option of directing reflected solar radiation to at least two absorbers.”[Mills & Morrison 2000]
Thus it is possible to pack the mirror arrays much more densely when alternating the inclination, as shading and blocking can be avoided then. This concept allows higher reflector densities and lower absorber tower heights to be used. [Mills & Morrison 2000]

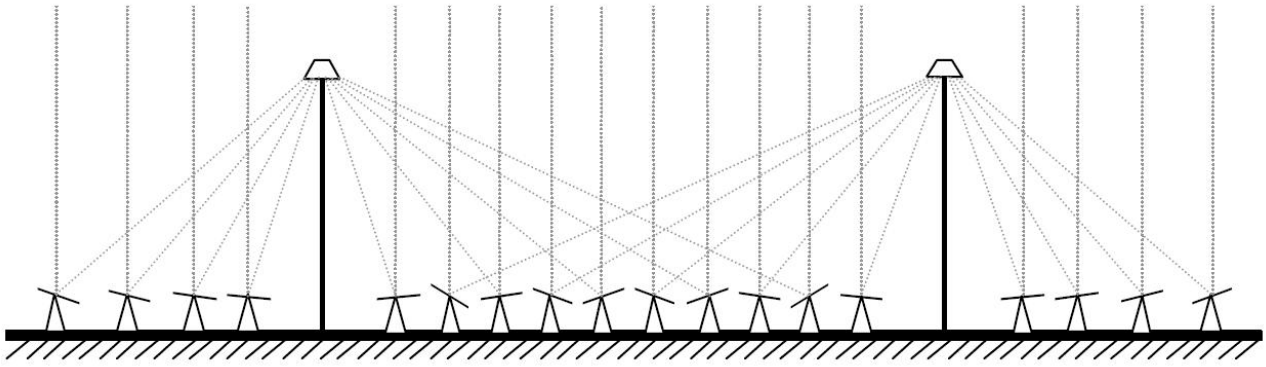

Figure 15: Compact Linear Fresnel Concept [Reynolds et al. 2002]

2.3.2.1 Field Raytrace

Regarding the optimal mirror tilt angles it is necessary to consider two possible positions for each solar radiation incident angle, as there are two possible absorber targets. So, at the beginning, modelling processes involve raytracing with an arbitrary starting configuration of the mirror field. Then the first mirror is flipped and the whole field is raytraced again. After having determined the first mirror´s best position, the same procedure is made for the entire field and for all incidence angles. Thus, the resulting raytrace computations are quite large.
A compact linear Fresnel collector reaches its optimum performance when each mirror strip reflects the incoming ray to the best receiver for the time of the day. As a matter of principle, each mirror row must have an independent tracking then.
However, the simplest and cheapest setup would be a combined tracking system, that is run from a single motor. For this reason it is important to consider performance penalties when several mirror rows have a common tracking system. This combination of rows is usually called “mirror row ganging”. [Mills & Morrison 2000]

2.3.2.2 Mirror Row Ganging

Since mirrors, that reflect solar radiation to the same absorber, move together through the same tracking angle, they can have a linked tracking system with one single motor, although the absolute angle of each mirror is different. The cost of the tracking system may be reduced then. However, performance is reduced, too, due to shading, as the optimal orientation (two collector targets are possible) of certain mirror rows changes throughout the year. This cost-performance trade off has to be considered. Although the annual energy delivery of the ganged field is only 0.2% less than that of the independently row-tracked case, the independently row-tracked arrangement should be preferred as is it has several advantages. Focusing can be finely tuned; all mirrors can be aligned vertically in hailstorms, or horizontally in high winds; single mirror lines can be aligned or inverted for cleaning; during absorber maintenance, mirrors can be realigned to adjacent absorbers. [Mills & Morrison 2000]

2.3.3 Receiver Types of Linear Fresnel Collectors

There are three different kinds of absorber types proposed. Cavity-type, single tube-type and Dewar tube-type absorbers.

2.3.3.1 Cavity-Type Absorbers

This type of absorber concept has the advantage of cheaper components and manufacturing costs over Dewar tube-type arrangements. [Reynolds et al. 2002]
It consists of a certain number of closely-packed pipes mounted at the top of a downward-facing trapezoidal cavity, which is insulated at the top and covered with a glass window at the bottom. [Pye et al. 2006]

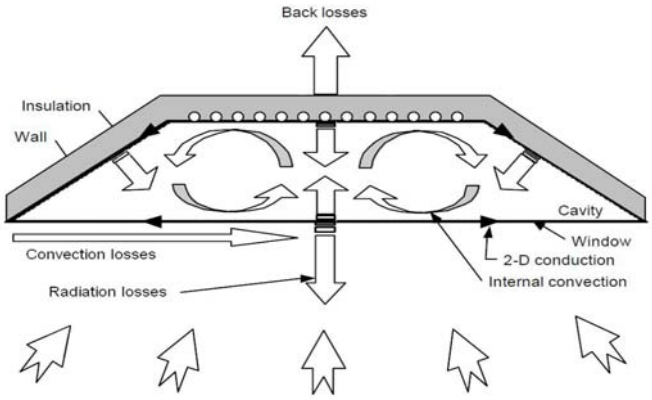

Figure 16: Cross Section of a Linear Fresnel Cavity Absorber [Reynolds et al. 2002]

2.3.3.2 Dewar Tube-Type Absorbers

These Absorbers are named after the Scottish physicist Sir James Dewar, who invented a vessel designed to provide very good thermal insulation by using a vacuum layer.

Basically a Dewar tube-type absorber consists of one main pipe (header pipe), which ranges from the beginning to the end of one absorber tower, and many branch pipes that are connected to the header pipe. Each of the branch pipes is surrounded by an additional glass tube in order to provide an evacuated layer to minimize thermal losses. This evacuated tube receiver rack can either be placed vertically (illuminated from both sides), or horizontally (mainly illuminated from underneath).

Performance investigations have shown that the horizontally mounted version slightly exceeds the vertically mounted one in power. Best results are reached with a north-south-oriented primary collector field which is inclined at the latitude angle facing the equator. [Mills & Morrison 2000]

2.3.3.2.1 Vertically Mounted Receiver Rack

Mills & Morrison (2000) considered the following dimensions for a vertical mounted receiver rack design. Each branch pipe (absorber tube), that is 1.2 m long and has a diameter of 37 mm, is surrounded by an additional glass tube (for the vacuum layer), which has an outer diameter of 45 mm and a wall thickness of 1.5 mm. The absorber tube surface is coated with a selective layer to keep the radiation losses low. Due to the use of single ended absorber tubes (branch pipes), this design can only operate as boiler (direct steam generation). It cannot generate superheated steam. The feed water enters the branch tubes through the header pipe, boiling occurs in the branch tube and the saturated steam leaves via the header again. An additional disadvantage of that arrangement is that the evacuated spaces between the adjacent absorber tubes allow radiation to pass through the absorber rack. This loss can be significant, as the gaps between the tubes amount to around 18% of the face area of the absorber. [Mills & Morrison 2000]

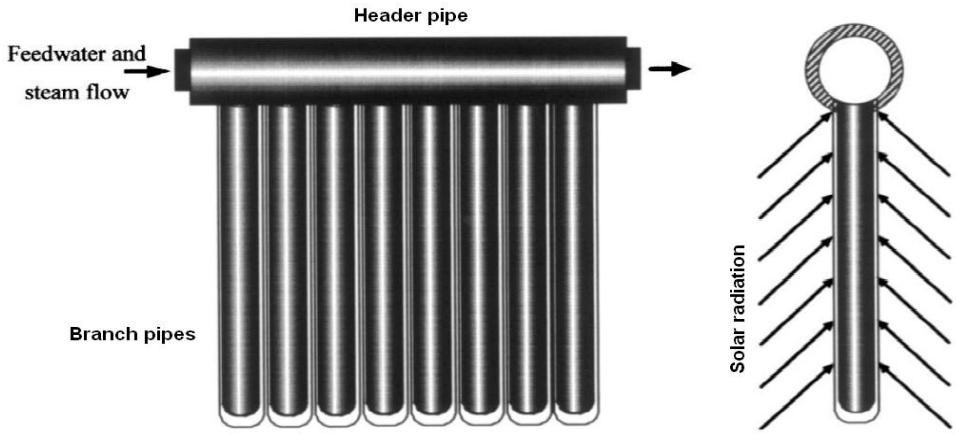

Figure 17: Vertical Mounted Receiver Rack [Mills & Morrison 2000]

In order to avoid these gap losses, it is possible to use a “zig-zag” double row of absorber tubes. In the following figure a closely packed absorber tube arrangement (a) and one with larger distances (b) is shown.
[Mills & Morrison 2000]

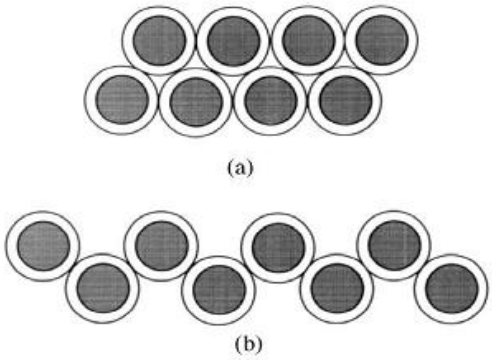

Figure 18: "zig-zag" Absorber Tube Arrangement [Mills & Morrison 2000]

2.3.3.2.2 The Horizontally Mounted Receiver Rack

At this configuration the absorber tubes are only illuminated by one side. For this reason it would be a quite expensive solution to use “zig-zag” arrangements again. A better possibility is to place a reflector above the horizontal absorber tubes to illuminate, with passing rays, the top of the tubes. Furthermore, an additional secondary reflector can be used underneath the absorber tubes to enhance optical collection and increase concentration. However only rays on the periphery of the reflected beam (coming from mirrors on the ground) use the secondary reflector. Otherwise rays coming from mirrors close to the absorber would be influenced too much or deflected.
[Mills & Morrison 2000]

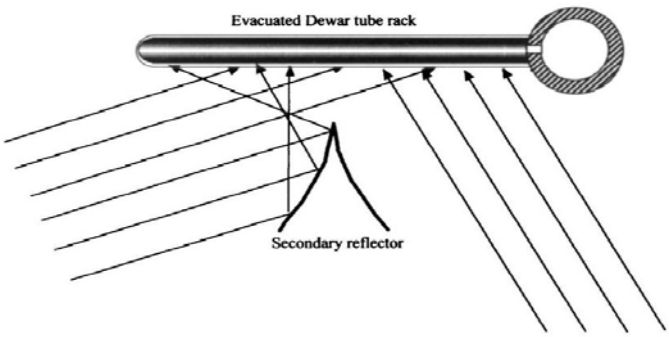

Figure 19: Horizontal Mounted Absorber Rack with Secondary Reflector[Mills & Morrison 2000]

In order to reach a suitable liquid flow within the absorber tubes the whole collector tube assembly has to be slightly inclined from the horizontal. [Mills & Morrison 2000]

2.3.3.3 Single Tube-Type Absorbers

These absorbers consist of one single absorber tube, a secondary reflector at the top and a glass plate at the bottom (figure 20). The secondary reflector enlarges the target for the primary mirrors and provides insulation for the hot absorber tube. In order to reduce convective heat losses at the bottom, the glass tube is used. Due to that configuration there is no need for vacuum technology to reduce heat losses as it is used at parabolic trough concepts. This setup can reduce solar field costs up to 50%, compared to parabolic trough fields. [Häberle et al. 2002]

This type of absorbers has the potential to capture 10% more thermal energy than comparable multi-tube-receivers. [Morin et al. 2006]
However, it reaches only 70% of the parabolic trough´s thermal performance. But, taking into account the significant lower investment costs, single tube linear Fresnel power plants could reduce electricity costs by 10%, compared to trough systems. [Häberle et al. 2002]

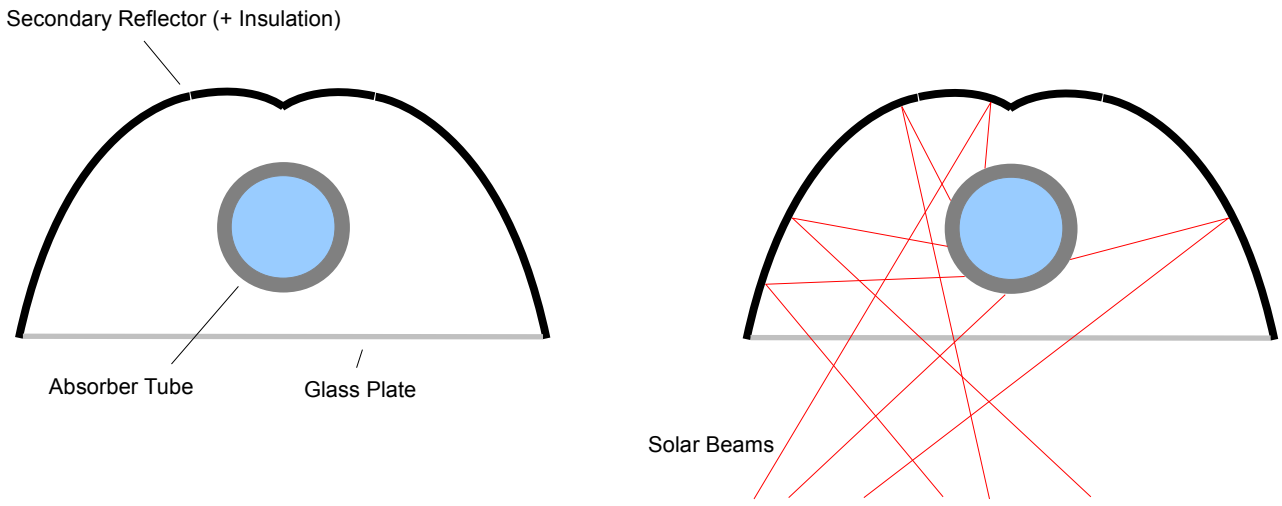

Figure 20: Single Tube Fresnel Collector Operated by Solarmundo [Häberle et al. 2002]

2.3.4 Secondary Reflectors

Secondary reflectors can redirect solar radiation onto the receiver tubes that otherwise would have missed them. They can either be placed below and above receivers or just at the top. The secondary reflector at the top enables mirror rows to be put closer towards the absorber tower, in order to improve spacing. [Mills & Morrison 2000]

2.4 The Central Receiver Concept (Solar Power Tower)

Unlike the other solar collector field concepts, where the solar energy is collected by several absorber devices equally distributed over the field, central receiver configurations have one single tower with the solar field´s only absorber at the top of it. This tower is surrounded by a field of sun-tracking mirrors (heliostats), that reflect the solar radiation towards the absorber. There the solar energy is transferred to a fluid, which is then used to produce steam for a following conventional steam cycle. Another possibility is to directly expand the heated fluid in a gas turbine (Brayton Cycle). Even combined cycle configurations are possible that promise high efficiencies. Solar power towers achieve concentration ratios of 300 to 1500 and thus can operate at temperatures from 500 to 1500°C. The heliostat field can either be placed just north of the tower (northern hemisphere), or surround it. In the first case the receiver faces northward. The second case requires a cylindrical receiver surface, facing in all directions. [Johansson et al.1992]

Today, the central receiver technology is on the verge of commercialization, as several 0.5 to 10 MW pilot plants were operated in the early 1980s. These pilot projects proved the technical feasibility and furthermore showed that central receiver plants can be equipped with large heat storage systems. Design point efficiencies of 23% and annual efficiencies of 20% are predicted. [Romero-Alvarez et al. 2007]

2.4.1 The Heliostat-Field

As the absorber has a fixed position, the normal vector of the heliostat´s mirror plane always has to coincide with the bisecting line of the angle subtended by the sun and the receiver. Thus, each heliostat has to track the sun and its actual orientation is a function of the sun´s altitude angle, azimuth angle, the absorbers hight and the heliostat´s position in the field. [Romero-Alvarez et al. 2007]

The field´s performance is determined by the optical efficiency $\eta_{optical}$, that includes the cosine attenuation, blocking and shading, mirror reflectivity, atmospheric attenuation and receiver spillage.

$$\eta_{optical} = \frac{P_{receiver}}{DNI \cdot A_{mirror}}$$ [Falcone 1986, as cited by Romero-Alvarez et al. 2007]

$\eta_{optical}$..... optical efficiency of the heliostat collector field
$P_{receiver}$... total power received by the absorber [W]
DNI..... direct normal irradiance [W/m²]
A_{mirror}..... total mirror area

In order to place the heliostats as close as possible, complex optimization algorithms are used to improve the annual energy produced per unit of land area. The annual average cosine attenuation factor depends on the site´s latitude. Therefore, at locations close to the equator surrounding heliostat fields are best, whereas north fields (northern hemisphere) gain performance as latitude increases. The blocking of reflected rays and shading is an important limitation concerning the best spacing between heliostats. For the most part it occurs at low sun altitude angles. As shadows

move during the day and additionally depend on the time of year, there does not exist a simple rule how heliostats should be placed best. [Romero-Alvarez et al. 2007]

Usually a heliostat consists of several mirror facets with high reflectivity. Each facet has a slight curvature in order to give the whole heliostat a spherical shape, as the reflected solar radiation should be focused at the receiver´s surface. [PS10 Report 2006]

Figure 21: Heliostat of the PS10 Central Receiver Power Plant [PS10 Report 2006]

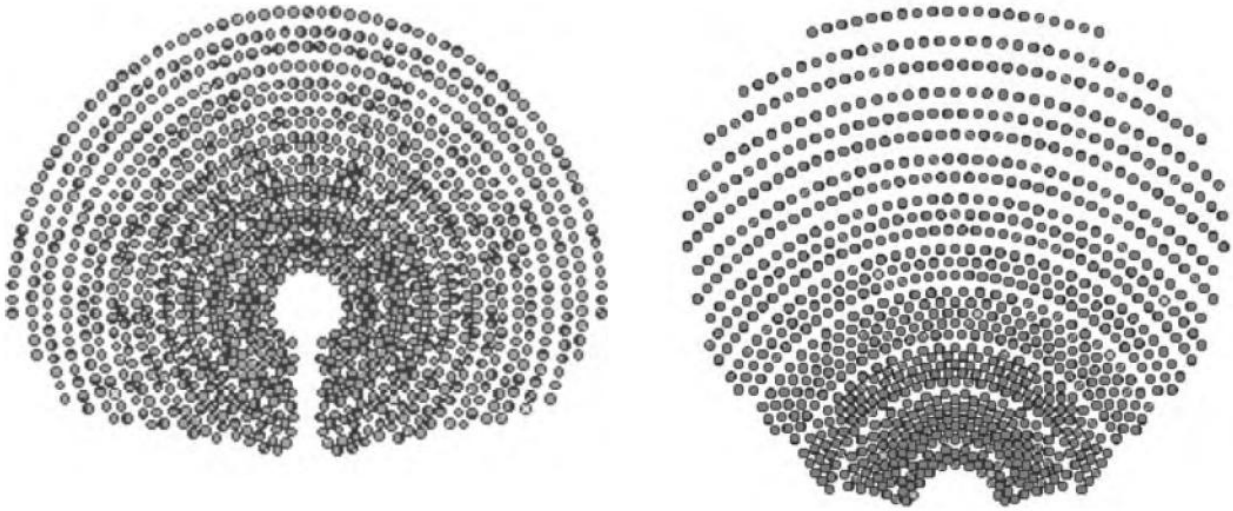

Figure 22: Surrounding and Northern Heliostat Field [Romero-Alvarez et al.2007]

2.4.2 The Receiver

The temperatures reached at central receiver systems are by far higher than at parabolic trough plants. Therefore high performance materials have to be chosen to withstand the temperatures. Typical absorber operating temperatures are between 500 and 1200°C.

There are different receiver configurations possible. Geometrically, there can be distinguished between external and cavity-type receivers. At cavity-type receivers the incident radiation enters a box-like structure before it hits the absorber`s surface. This kind of receivers is used at north-

(northern hemisphere) and south-field layouts (southern hemisphere). External receivers can either be flat-plate or cylindrically shaped tubular panels. The cylindrically shaped ones are typically used for surrounding heliostat fields. Furthermore, there can be distinguished between directly or indirectly irradiated receivers. This depends on the maximum heat flux possible and the materials used to transfer the energy to the working fluid. “In general, tubular technologies allow either high temperatures (up to 1000°C) or high pressures (up to 120 bar). Directly irradiated or volumetric receivers allow even higher temperatures but limit pressures to below 15 bar.” [Romero-Alvarez et al. 2007]

2.4.2.1 Directly Heated Receivers

Directly irradiated receivers do not need heat exchanger tubes, that usually limit the maximum temperature. At this type of receiver a film of heat transfer fluid (molten salt), that flows down a nearly vertical panel, absorbs the concentrated solar radiation. The heat transfer fluid has to be blackened with a dopant to increase absorptivity. Due to the absence of tubes between the incoming radiation and the heat transfer fluid, this receiver type withstands significant higher solar fluxes. Also particle streams can be used as heat transfer fluid. Particle receivers use an air stream that is darkened with small particles, close to the wavelength of visible light. In theory, such a particle receiver can cope with temperatures as high as 2000°C. The required mass of particles can kept below 0.2 weight percent. The hot particle stream produces then steam (Rankine cylce) or hot air (Brayton cycle) via a ceramic/metal heat exchanger. [Johansson et al. 1992]

In order to avoid leaking to the atmosphere, direct receivers should have a transparent window. [Romero-Alvarez et al. 2007]

2.4.2.2 Indirectly Heated Receivers

Indirectly heated receivers use tubular panels or volumetric surfaces. Tubular panels are configurations with many parallel tubes that have a selective black coating on the outer surface. Within the tubes the heat is transferred to the heat transfer fluid by convection. As the heat is transferred through the tube wall the heat flux is limited to 600 kW/m². Especially air cooled tubular receivers are limited in heat flux as heat transfer coefficients are too low. The highest values can be reached with liquid sodium cooled receivers. In volumetric receivers high porous structures absorb the concentrated solar radiation and transfer the energy to the heat transfer fluid via convection. As the name already implies, the solar radiation is absorbed within the structure “volume”. Mainly air is used as heat transfer fluid, which is heated up while flowing through the structure. These receivers are usually made of heat-resistant layered grids of wires or ceramic/metal foam structures. The temperature of heat transfer fluid leaving a good volumetric receiver, can be even higher than the irradiated side of the absorber (“volumetric effect”). [Romero-Alvarez et al. 2007]

2.4.2.2.1 Tubular Receivers

“The most common systems used in the past have been tubular receivers where concentrated radiation is transferred to the cooling fluid through a metal or ceramic wall. Conventional panels with darkened metal tubes have been used with steam, sodium and molten salts for temperatures up to 500-600°C.”[Romero-Alvarez et al. 2007]

Due to the single sided heating of the tubes and many variations in temperature (daily start-up, shut-down, clouds) the receiver tubes have to withstand great stress that causes thermal fatigue. Thus, the receiver represents the key risk element and is a real design challenge. [Johansson et al. 1992]

2.4.2.2.1.1 Cavity Tubular Receivers

The CESA-1 plant was operated between 1983 and 1986 in Almeria, Spain. It had a north facing water/steam tube cavity receiver producing superheated steam at 525°C.
[Romero-Alvarez et al.2007]

The Themis central receiver pilot plant was operated between 1983 and 1986 in Targasonne, France. It used molten salt as heat transfer fluid in the receiver and for thermal storage. It mainly demonstrated the advantages of decoupling solar-energy collection from power generation, using thermal storage. [Johansson et al. 1992]

The recently built central receiver power plant PS10 in Sanlucar la Mayor near Seville, Spain, works with a saturated steam receiver concept, at relative low values of temperature and pressure (250°C and 40 bar). The receiver represents a forced circulation boiler with a low steam fraction at the outlet to ensure wetted inner tube walls. In that way large temperature gradients due to variations of the heat transfer coefficient can be avoided. Thus, deformation and fatigue problems that occurred in super heating receivers, are eliminated. Radiant flux peaks of 650 kW/m² are reached. The saturated steam coming from the receiver either loads the storage tank or expands in the turbine, producing electricity. [PS10 Report 2006]

At rated conditions the PS10 power plant reaches a total solar-to-electric efficiency of 21.7%. The total annual solar-to-electric efficiency amounts to 15.4%. [Fernandez]

In the immediate vicinity of PS10 the power tower plant PS20 started its operation in 2009. The design is similar to that of PS10, but it has twice the capacity (20 MW). Experiences with the previous built PS10 plant led to certain improvements (for instance, higher efficiency for the storage system and the receiver). [Abengoa Solar 2008]

The most recently built solar power tower plant is the Solar Tres project in Spain. It is located near the city Ecija in Andalusia. The design concept is based on the Solar One and Solar Two demonstration projects. Molten salt is used as heat transfer fluid and for storage. Its rated power output is 17 MW and the thermal storage system enables an additional plant operation of 15 hours. [Sener 2007]

2.4.2.2.1.2 External Tubular Receivers

This type of receiver was used in the Solar One power plant, California, USA (1984 – 1988). It was an external cylindrical receiver, with the feed water preheat tubes facing southward and the once through evaporator and super heater tubes facing northward. Live steam pressure and temperature designed were 100 bar and 516°C. Due to solar transients and poor heat transfer overheating and deformation occurred in the super heating section. [Romero-Alvarez et al. 2007]

The Solar Two plant was a redesigned version of Solar One and was operated until 1999. It was

run with molten salt as heat transfer fluid and is still the technical reference for molten salt tubular receivers. The peak flux at the receiver was 800 kW/m² with a reported thermal efficiency of around 86% at low winds. The molten salt entered the receiver tubes at about 290°C and left at 565°C. As there phase change did not occur, problems of water/steam receivers were no concern. Although, molten nitrate salt (60% sodium nitrate, 40% potassium nitrate) provided good thermal conductivity and heat capacity at low prices, the freezing point at 220°C could be troublesome. [Romero-Alvarez et al. 2007]

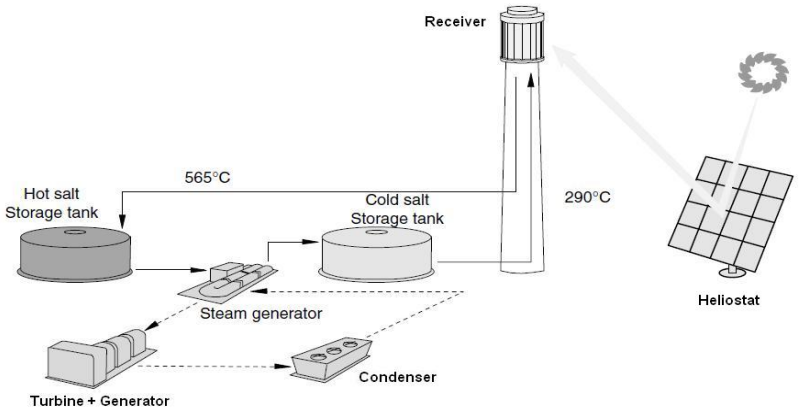

Figure 23: Schematic of a Molten Salt Central Receiver System (Cylindrical Tubular Receiver) [Romero-Alvarez et al. 2007]

2.4.2.2.2 Volumetric Receivers

Due to the possible high heat fluxes (up to 1 MW/m²) and low cost absorber material the volumetric receiver is a very attractive concept. However, the high energy flux and aperture surface areas of 30 to 50 m² were a limit for the heat transfer fluid´s pressure, as window materials needed were not available. Therefore, first concepts only operated at atmospheric pressure, reaching air temperatures of 700 to 800°C for generating steam. [Johansson et al. 1992]

Today, volumetric receivers can either be run open at atmospheric conditions or enclosed by a transparent window. Metal wire absorbers reach outlet temperatures up to 850°C. Using ceramic foam or monolith structures as absorber material, outlet temperatures can exceed 1000°C. The thermal efficiencies reached with open volumetric receivers range between 60 and 75%. “Although simplicity and operating results are satisfactory, it is obvious that open volumetric receiver thermal efficiencies must be improved to achieve cost-effective plant designs able to replace tubular receivers.” Furthermore the air return ratio (ARR) should be increased in open volumetric receiver designs. The air return ratio is defined as the ratio of air recirculated to fresh ambient air. Thus, a certain amount of the air coming from the steam generator mixes with fresh ambient air and enters again the open volumetric receiver. Especially mixing losses at the receiver inlet are disadvantages of this concept. As the Rankine power cycle forces the air to return at temperatures between 110-170°C, plant performance analysis suggest air return ratios of 70%, in order to keep air-cooled solar power plants in the same efficiency range as plants cooled with molten salt or water/steam. [Romero-Alvarez et al.2007]

Using enclosed (window) volumetric receivers makes it possible to pressurize the cooling air (up to 15 bar). Thus, another attractive application is to expand the hot pressurized air in a gas turbine. Even a final Rankine steam cycle can be connected to the gas turbine exhaust stream,

representing a solar powered combined cycle process (promising high efficiencies). [Romero-Alvarez et al.2007]

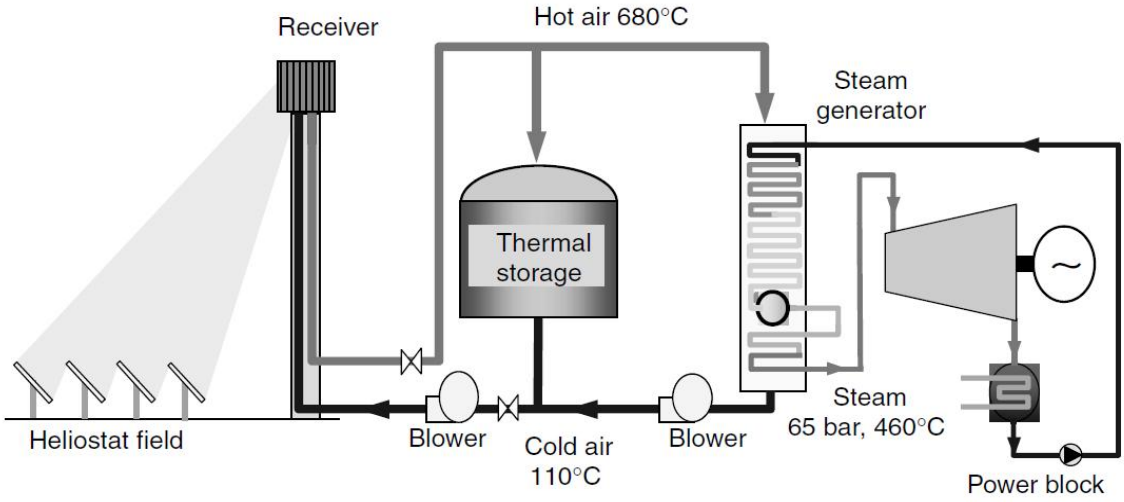

Figure 24: Schematic of an Open Volumetric Receiver Plant [Romero-Alvarez et al. 2007]

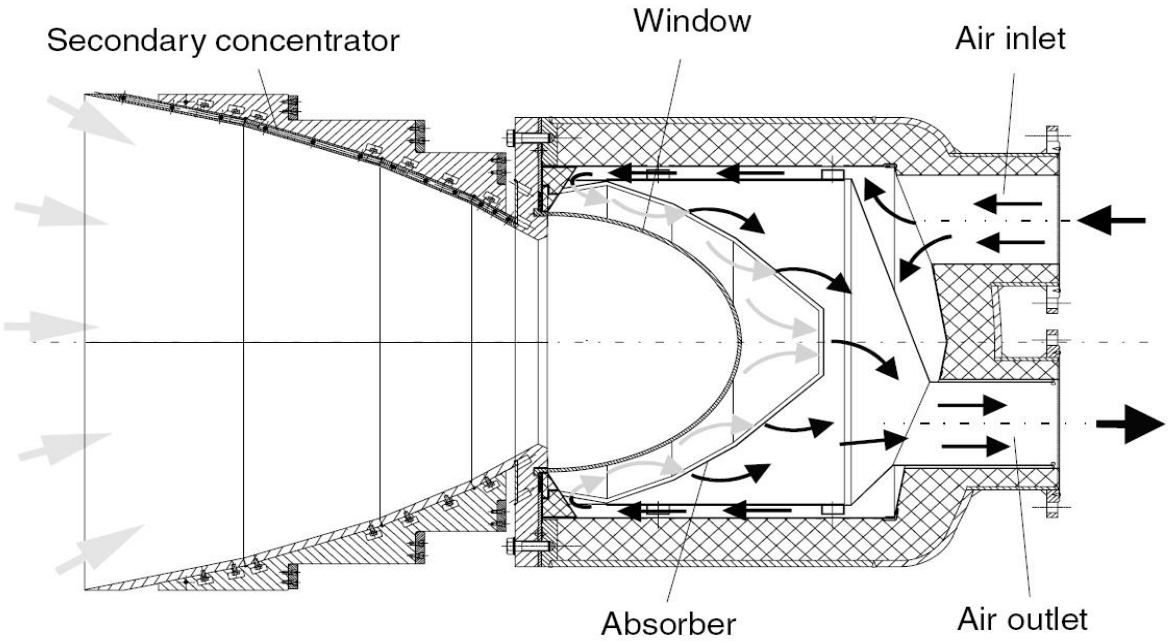

Figure 25: Pressurized Volumetric Receiver [Romero-Alvarez et al. 2007]

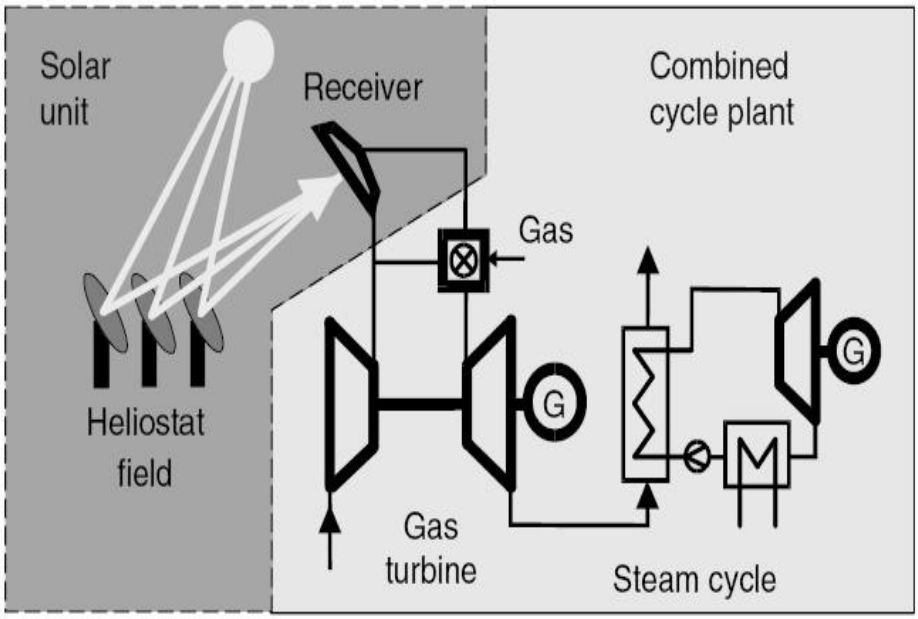

Figure 26: Solar - Natural Gas - Combined Cycle Plant [Romero-Alvarez et al. 2007]

Project	Country	Power (MW)	Heat Transfer Fluid	Storage Media	Start of Operation
SSPS	Spain	0.5	Liquid sodium	Sodium	1981
Eurelios	Italy	1	Steam	Nitrate salt/water	1981
Sunshine	Japan	1	Steam	Nitrate salt/water	1981
Solar One	USA	10	Steam	Oil/rock	1982
CESA-1	Spain	1	Steam	Nitrate salt	1982
MSEE/Cat B	USA	1	Nitrate salt	Nitrate salt	1983
Themis	France	2.5	Hitec salt	Hitec salt	1984
SPP-5	Russia	5	Steam	Water/steam	1986
TSA	Spain	1	Air	Ceramic	1993
Solar Two	USA	10	Nitrate salt	Nitrate salt	1996
Solgate	Spain	0.3	Pressurized Air	Fossil hybrid	2002
PS10	Spain	11	Saturated steam	Steam/Water	2006
PS20	Spain	20	Saturated steam	Steam/Water	2009
Solar Tres	Spain	17	Nitrate salt	Nitrate salt	2009

Table 1: Table of Central Receiver Plants Built [Romero-Alvarez et al. 2007]

2.5 The Parabolic Dish Collector Concept

Like the parabolic trough collector, also the parabolic dish collector concept uses the parabola´s focal point. But instead of a linear extrusion, the parabolic dish collector´s shape is formed by rotation. Thus, parabolic dish collectors are three dimensional concentration devices that reach high concentration ratios between 1000 and 4000. They are small units with integrated power conversion units like Sterling engines or small Brayton mini-turbines. They can be connected to the grid, but usually are used for remote off-grid applications. Due to their high concentration ratios and high temperatures, parabolic dish concepts reach high solar-to-electric efficiencies of about 30% and more. These collectors have to be tracked via two axis, in order to follow the daily path of the sun. With a dish diameter of 5.5 m they reach about 5 kW electric, equipped with a Sterling engine as power conversion unit. [Romero-Alvarez et al. 2007]

The typical power provided ranges between 5 and 50 kW, and thus, parabolic dish collector units are suitable to replace diesel power sets. [Laing et al. 2002]

Due to the low number of dish-Sterling systems produced, the costs per kWh are still relative high, compared to parabolic trough or central receiver systems. [Quaschning 2007]

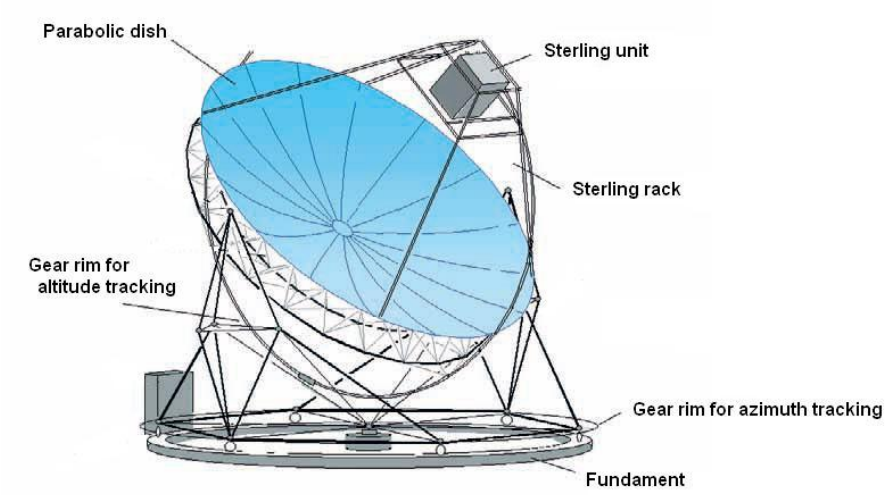

Figure 27: Parabolic Dish Concept [Laing et al. 2002]

The parabolic dishes itself are either faceted or full-surface paraboloids. Faceted concentrators consist of a mounting structure equipped with several mirror segments, which are oriented individually. These mirrors are usually certain materials covered with reflecting foil. Full-surface concentrators are shaped by a special forming process. For instance, this structure can be stabilised via vacuum. [Kaltschmitt et al. 2007]

2.5.1 The Receiver

As working fluid temperatures reach from 650 to 750°C, a cavity design is the optimum solution, regarding heat losses. Working fluids in the Sterling engines are usually helium or hydrogen. They are either heated directly by the solar radiation, flowing through a pipe bundle in the receiver, or via

an additional heat transfer fluid. The latter method uses liquid metal as heat transfer fluid, that evaporates in the receiver and heats the working gas while it condenses. This phase change provides a constant temperature, which is very suitable for the heating of Sterling engines. [Romero-Alvarez et al. 2007]

The directly heated pipe bundle receiver is the simplest configuration, as the heating tubes of the Sterling engine, represent the absorber´s surface. The second kind of receiver types use sodium as heat transfer fluid. The liquid metal is evaporated within a capillary structure in the receiver and then condenses, while transferring the heat to the Sterling engine´s working fluid. Although this concept requires high efforts in terms of production engineering, it offers the advantage of homogeneous heat transfer. The actual absorbing surface of both concepts, is not exactly positioned at the focal spot. It´s distance from the parabolic dish exceeds the focal length by a certain fraction. Therefore the aperture of the cavity can be smaller than the absorber´s surface itself and the solar flux as well as the thermal losses are reduced. [Kaltschmitt et al. 2007]

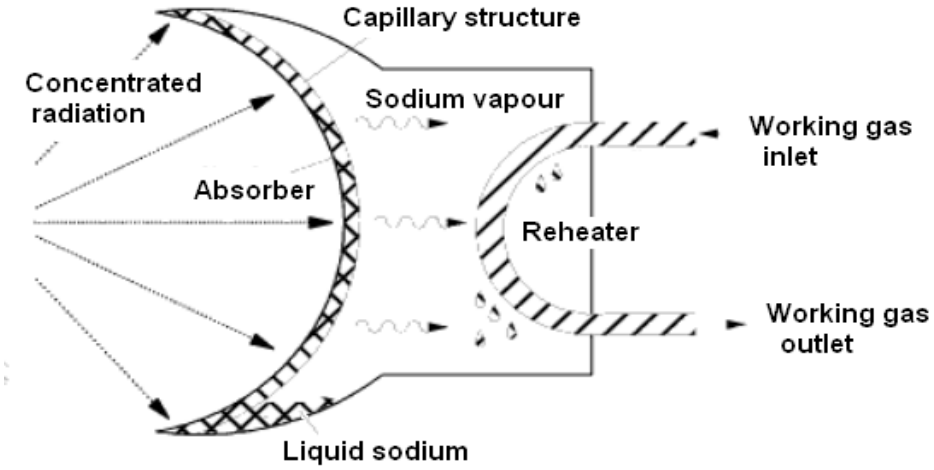

Figure 28: Liquid Metal Receiver [Kaltschmitt et al. 2007]

2.6 Power Generation Costs

In order to calculate the generation costs of solar power several parameters have to be taken into account. Most important are the costs of capital and the expected electricity production. The electricity production depends on the solar conditions at a given site. Therefore, the selection of an appropriate location is crucial for the economic viability. Furthermore, the lifetime of the steam turbine as well as operation and maintenance costs have to be considered.
Currently, the concentrated solar power generation costs range from 0.15 €/kWh, at high solar irradiation sites, up to approximately 0.23 €/kWh, at sites with lower solar irradiation. By 2020, costs are expected to fall, ranging from 0.1 to 0.14€/kWh, due to increased plant sizes and improved component production. [Richter et al. 2009]

The power generation costs of real parabolic trough collector plant projects vary between 0.15 and 0.20 €/kWh. [Platzer 2009]

3 Solar Power Plant Modelling

In this chapter I would like to give a short basic overview of the plant modelling concept used in this work and how the IPSEpro modelling concept works.

The first step of solar power plant modelling would be the calculation of a certain operating point at steady-state conditions. Thus, for a given constant input of solar radiation the steady-state plant output is calculated. Since the input of solar radiation varies with the time of the day and furthermore with the season, also the power plant performance over a certain period would be a matter of interest, as a next step. This performance over certain periods can be obtained by steady-state simulations too. Therefore a suitable number of operating points has to be chosen, that represent the real continuous operating behaviour well enough. Then, having calculated the steady-state results of all these operating points, the performance over the chosen period can be determined.

In this work the steady-state modelling, as mentioned above, has been used. For a given solar radiation the power output of solar power plant models is calculated within IPSEpro. Furthermore, the solar thermal power plant operating behaviour over the course of a day is determined by calculating many representing operating points. Another important fact that has to be mentioned is, that thermal storage systems have not been taken into account in this work. Thus, the part load behaviour of the turbine sections is crucial and has been modelled too.
Additionally, the created models do not feature differential equations. Therefore, calculation results are not functions of time, that would be convenient for the detailed information of process dynamics, like peak temperatures of certain components during variations in load.

3.1 The IPSEpro Modelling Concept

In order to make the understanding of the modelling process easier, one should be familiar with the basic concept of the IPSEpro program environment. Thus, the following sections describe the general application of IPSEpro.

“The IPSEpro Design Suite is a highly flexible software environment for calculating heat balances and simulating processes. It is used in various fields of application like power plant engineering, chemical engineering and other related areas.

Using the IPSEpro Design Suite, you create your process model graphically by appropriately connecting component models from a library. IPSEpro provides efficient data management, powerful mathematical methods and an intuitive graphic user interface, so that you can fully concentrate on the technical aspects of your models.

IPSEpro offers virtually unlimited flexibility: It allows you to modify existing component models or to create your own ones in order to meet exactly your modelling requirements.” [SimTech 2002]

“For a growing number of fields of application, ready-to-use standard model libraries are available. This includes libraries for thermal power processes, refrigeration processes and desalination processes” [SimTech 2002]

“At the core of the software package is the capability to build process models from components, typically representing individual pieces of equipment, like heat exchangers, pumps, etc.

IPSEpro is a software framework. It strictly distinguishes between the actual program and the application-specific component models. The user is not limited by built-in component models: The component models are organized in model libraries, which contain all component specific information, from graphical appearance to the equations that describe the behaviour of the components. The user can modify existing model libraries and create new ones. This makes it possible to adjust IPSEpro to new fields of application without modifying the program itself.” [Perz & Bergmann 2006]

The Process Simulation Environment (PSE) is used to model and solve thermodynamic processes based on components from a library. PSE provides a graphic flow-sheet editor for setting up process models. The user selects the required components from the library menu and arranges them appropriately. All process data is entered directly in the flow-sheet. PSE generates output protocols automatically and displays the results in the flow-sheet, at the end of a simulation run. [Perz & Bergmann 2006]

“MDK, IPSEpro's Model Development Kit, provides the capabilities that are required to define new models and to translate them into a form that can be used by PSE. MDK consists out of two functional units:

- Model editor
- Model compiler

The model editor allows the user to design icons that represent the models and to describe the model behaviour mathematically in the form of model equations.” [Perz & Bergmann 2006]

After compiling the new models are loaded into the Process Simulation Environment and a certain process can be modelled and calculated.

The figure below shows the basic architecture of the program IPSEpro.

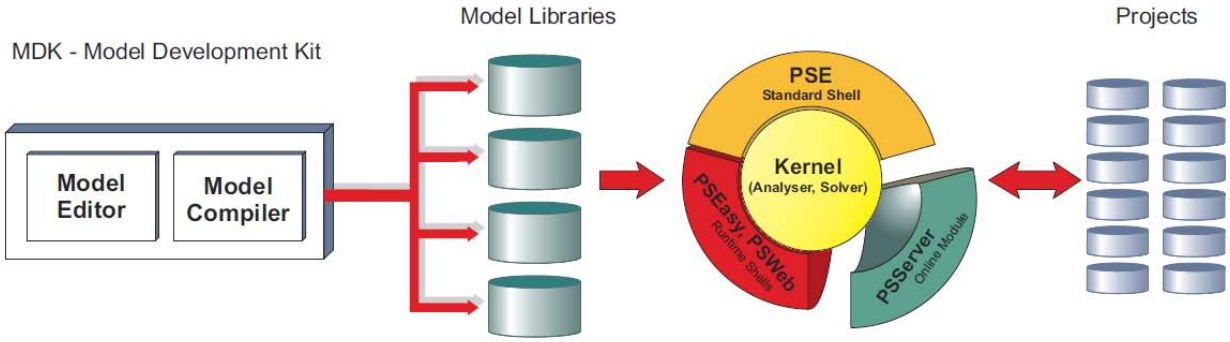

Figure 29: IPSEpro Architecture [SimTech 2002]

The program modules “PSEasy” , “PSWeb” and “PSServer” (shown in the figure above) are not explained, as they are not used in this work.

4 The Solar Irradiation Model

Before I actually start the modelling of solar power plant receivers, I want to describe the availability of solar radiation on the earth. First of all, I start with the solar radiation provided by the sun, how its magnitude depends on the distance in outer space, and which fraction finally hits the earth´s surface as a function of date and atmospheric conditions.

Of course the question arises, up to which extent a model of atmospheric attenuation correlates with real radiation data.
As the condition of the atmosphere, regarding the attenuation of solar radiation, is not at all constant and does not obey certain rules, only empirically established correlations based on measured data can be used.
In addition to this, certain assumptions of a cloud-free atmosphere have to be made.

Hottel (1976) established a model for clear standard atmosphere, which of course can only give an estimation of the available radiation, but can give accurate enough values when parameters are adjusted with local measurements. [Silva et al. 2002]

4.1 The Sun

The sun is the world´s largest and most important source of regenerative energy. The sun´s radiation can be either used directly via solar thermal and photovoltaic power plants, or indirectly via hydro power and wind energy.
Basically the sun consists of 80% hydrogen and 20% helium and its radiant power is the result of nuclear fusion processes. Each square meter of the sun´s surface $\mathbf{A_{sun}}$ emits 63.11 MW of radiant power, which is described by the flux density $\mathbf{M_{sun}}$ with the unit W/m^2. Due to that fact, a fifth of a square kilometre would satisfy the world´s demand of primary energy. [Quaschning 2007]

4.2 Extraterrestrial Radiation

However, only a fraction of that radiant power is received by the earth´s surface. To get the radiant power received by the earth, the distance between sun and earth has to be taken into account. If a fictitious concentric sphere with the radius **R**, the distance between the sun´s centre and the earth`s surface, is placed in reference to the sun, the total radiant power penetrating that surface $\mathbf{A_{se}}$ has to be equal the sun´s total emitted power.

$$M_{sun} \cdot A_{sun} = G \cdot A_{se}$$

$$A_{sun} = 4 \cdot \pi \cdot r^2$$

$$A_{se} = 4 \cdot \pi \cdot R^2$$

Where **r** is the radius of the sun and **R** is the distance between the sun´s centre and the earth´s surface.

The fact that the sun-earth distance varies between 1.47 * 10^8 and 1.52 * 10^8 km, depending on the time of year, leads to a variation of the extraterrestrial solar radiation in the range of ± 3.3%. The mean value is the so called **solar constant G_{sc}** and constitutes 1367 W/m². [Quaschning 2007]
"The solar constant G_{sc} is the energy from the sun per unit time received on a unit area of surface perpendicular to the direction of propagation of the radiation at mean earth-sun distance outside the atmosphere." [Duffie & Beckman 2006]

The dependence of extraterrestrial radiation on time of year is given by following equations, where **G** is the extraterrestrial radiation incident on the plane normal to radiation on the **n**th day of the year starting at January 1st.

$$G = G_{sc} \cdot \left(1 + 0.033 \cdot \cos\left(\frac{360 \cdot n}{365}\right)\right)$$ [Duffie & Beckman 2006]

A more accurate equation (± 0.01%): [Duffie & Beckman 2006]

$$G = G_{sc} \cdot (1.00011 + 0.034221 \cdot \cos(B) + 0.00128 \cdot \sin(B) + 0.000719 \cdot \cos(2 \cdot B) + 0.000077 \cdot \sin(2 \cdot B))$$

$$\text{with} \quad B = \frac{(n-1) \cdot 360}{365}$$

In addition to the total energy in the solar spectrum (i.e., the solar constant), it is useful to know the spectral distribution of the extraterrestrial radiation, that ranges from 0.25 to 3.0 μm wavelength λ. [Duffie & Beckman 2006]

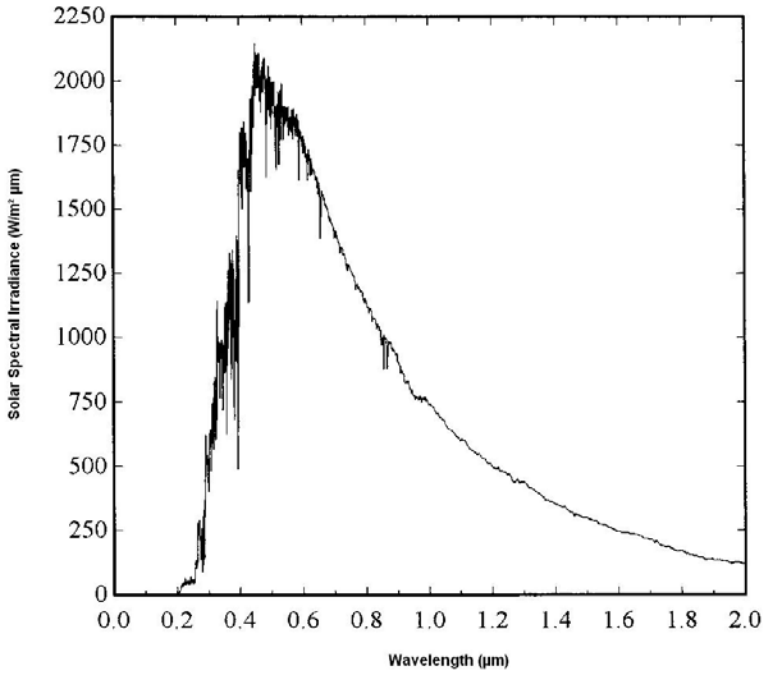

Figure 30: Extraterrestrial Spectral Irradiance Curve at Mean Earth-Sun Distance [Duffie & Beckman 2006]

4.3 Terrestrial Solar Radiation

On the earth´s surface, measurements of the solar radiation show values that are by far smaller than the solar constant. Locally, on a clear and sunny day the radiation received on earth can reach or even exceed 1000 W/m^2, which is about 73% of G_{sc}. As the radiation penetrates the atmosphere it is attenuated by

- reflection at the entry,
- absorption (O_3, H_2O, O_2 and CO_2),
- Rayleigh-scattering,
- and Mie-scattering.

Absorption of radiation is due to gas molecules in the atmosphere. [Quaschning 2007]

“There is almost complete absorption of short-wave radiation by ozone in the upper atmosphere at wavelengths below 0.29 μm. Ozone absorption decreases as λ increases above 0.29 μm, until at 0.35 μm there is no absorption. There is also a weak ozone absorption band near λ = 0.6 μm. Water vapour absorbs strongly in bands in the infrared part of the solar spectrum, with strong absorption bands centred at 1.0, 1.4 and 1.8 μm. Beyond 2.5 μm, the transmission of the atmosphere is very low due to absorption by H_2O and CO_2. The energy in the extraterrestrial spectrum at λ > 2.5 μm is less than 5% of total solar spectrum, and energy received at the ground at λ > 2.5 μm is very small.” [Duffie & Beckman 2006]

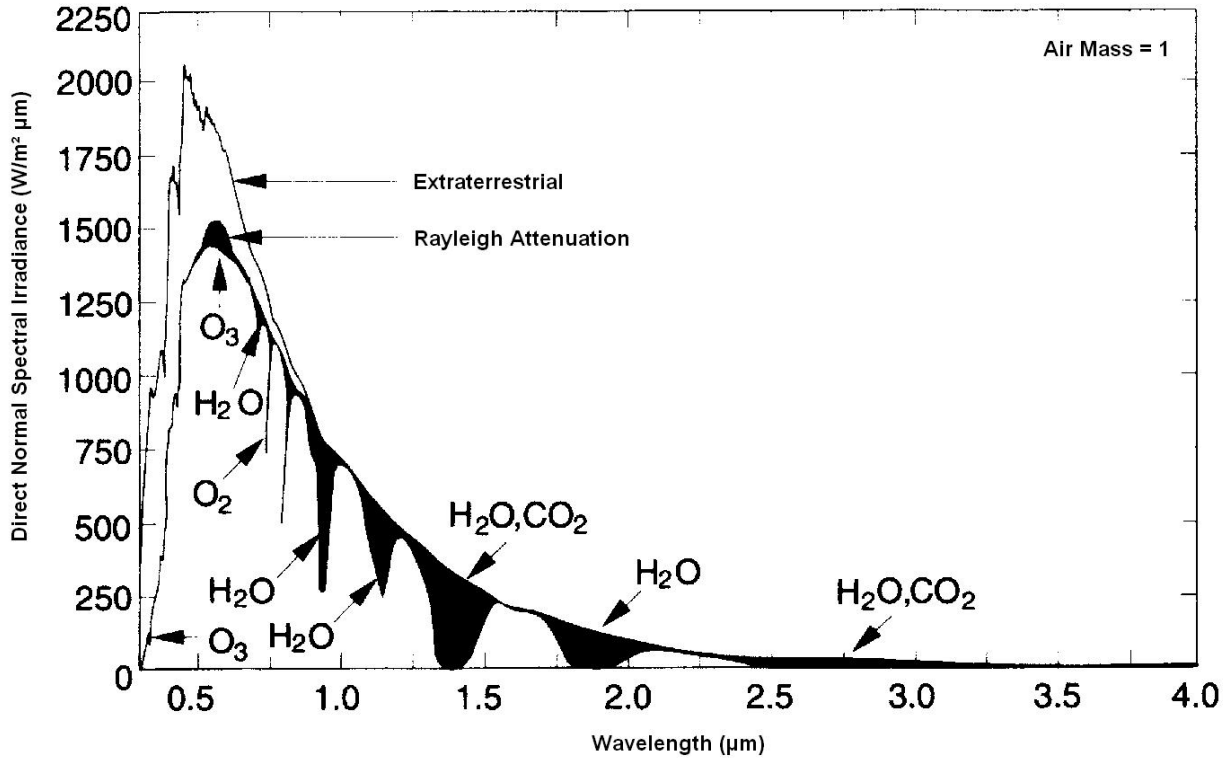

Figure 31:Effects of Rayleigh Scattering and Atmospheric Absorption on the Spectral Distribution of Beam Irradiance [Duffie & Beckman 2006]

Attenuation by Rayleigh-scattering is done by molecular parts of the air that are smaller than the solar radiation´s wavelength. This effect is only significant at short wavelength and becomes less important above λ = 0.6 µm.
Mie-scattering is done by dust particles or air pollution. The diameter of those particles is larger than the solar radiation´s wavelength. The influence of Mie-scattering is strongly dependent on the location. It is low in the mountains but very high in industrial areas with polluted air. [Quaschning 2007]

Furthermore the attenuation of solar radiation depends on the length of the way through the atmosphere. That effect is taken into account by the term **air mass AM**.
The air mass is the ratio of the mass of the atmosphere through which radiation passes to the mass it would pass if the sun was at the zenith. The position of the sun is defined by the zenith angle Θ_z, which is zero when the sun is at the zenith and 90° at sunset.
However, if the zenith angle is above 70°, the effect of earth´s curvature becomes significant and must be taken into account. [Duffie & Beckman 2006]

$$AM = \frac{1}{\cos \Theta z}$$

For Θ_z is above 70° and approaching 90°, following formula can be used (A is the site`s altitude in km): [Duffie & Beckman 2006]

$$AM = \frac{\exp(-0.0001184 \cdot A \cdot 1000)}{\cos \Theta z + 0.5057 \cdot (96.080 - \Theta z)^{-1.634}}$$

Due to the atmosphere´s scattering influence, the solar radiation is made up of **beam radiation** (beam radiation is also referred to as **direct radiation**) and **diffuse radiation**.
Beam radiation is that part of solar radiation that is received without having been scattered by the atmosphere.
Diffuse radiation is solar radiation whose direction has been changed by scattering by the atmosphere.
The sum of beam and diffuse solar radiation is called **total solar radiation** or **global radiation**.

Especially during days with low total solar radiation the diffuse part is rather high and may reach 100%. On the other hand, during days with high total solar radiation the diffuse part is less than 20%. The table below shows, that the annual sum of diffuse radiation varies only slightly if measurements of different locations on earth are compared, whereas beam radiation can vary largely. [Quaschning 2007]

kWh/(m² d)	Stockholm	Berlin	London	Vienna	Rome	Lisbon	Athens
beam	1.41	1.2	0.99	1.4	2.41	3.06	2.67
diffuse	1.42	1.61	1.47	1.63	1.78	1.67	1.66

Table 2: Annual Average of Daily Beam and Diffuse Solar Radiation [Palz & Greif 1996]

Due to the fact that only beam solar radiation can be used in concentrating solar power plants, locations must be chosen to maximise the solar input.

4.3.1 Estimation of Clear-Sky Normal Beam Radiation

The influence of the atmosphere on absorbing and scattering solar radiation is variable with time as atmospheric conditions and the air mass ratio change. This influence can be described by the **atmospheric transmittance** τ. It varies with location and elevation between 0 and 1.
It is useful to define a standard atmosphere “clear sky” and calculate solar radiation that would be received on the earth´s surface under these standard conditions. [Sen 2008]

A method to estimate the beam radiation transmitted through clear standard atmosphere, which takes into account zenith angle, the site´s altitude and four climate types, can be defined as follows [Duffie & Beckman 2006]:

The **clear-sky normal beam radiation** G_{cnb} is the solar beam radiation that reaches the earth´s surface and is measured in a plane normal to the incident radiation. Often this type of radiation is also referred to as **direct normal irradiance DNI**.
G is the extraterrestrial radiation incident on the plane normal to radiation; τ_b the **atmospheric transmittance for beam radiation only**.

$$G_{cnb} = G \cdot \tau_b$$

$$\tau_b = a_0 + a_1 \cdot \exp\left(\frac{-k}{\cos\Theta_z}\right)$$

The constants a_0, a_1 and **k** are valid for standard atmosphere with 23 km visibility and are derived from following equations by applying correction factors r_0, r_1 and r_k, to allow for changes in climate types. **A** is the altitude in kilometres of the location in question.

$$a_0^{\bullet} = 0.4237 - 0.00821 \cdot (6 - A)^2$$

$$a_1^{\bullet} = 0.5055 + 0.00595 \cdot (6.5 - A)^2$$

$$k^{\bullet} = 0.2711 + 0.01858 \cdot (2.5 - A)^2$$

$$r_0 = \frac{a_0}{a_0^{\bullet}} \qquad r_1 = \frac{a_1}{a_1^{\bullet}} \qquad r_k = \frac{k}{k^{\bullet}}$$

The values of the correction factors r_0, r_1 and r_k are given for four climate types in the table below.

Climate Type	r_0	r_1	r_k
Tropical φ < 30°	0.95	0.98	1.02
Mid-latitude summer 30° < φ < 60°	0.97	0.99	1.02
Mid-latitude winter 30° < φ < 60°	1.03	1.01	1
Subarctic summer 60° > φ	0.99	0.99	1.01

Table 3: Correction Factors for Climate Type; φ = Latitude of the Location [Hottel 1976]

4.3.2 Estimation of Clear-Sky Diffuse Radiation

To be able to calculate the total radiation received on the earth´s surface, the clear-sky diffuse radiation has to be known too.
The relationship between the atmospheric transmittance for beam radiation τ_b and the atmospheric transmittance for diffuse radiation τ_d can be described empirically as follows:
[Duffie & Beckman 2006]

G_{cd} is the clear-sky diffuse radiation incident on a horizontal plane on the earth´s surface.
G is the extraterrestrial radiation incident on the plane normal to radiation.
G_h is the extraterrestrial radiation received on a horizontal plane (outside the earth´s atmosphere).

$$G_h = G \cdot \cos(\Theta_z)$$

$$\tau_d = \frac{G_{cd}}{G_h} = 0.271 - 0.2939 \cdot \tau_b$$

Note:

In order to get the **total clear-sky solar radiation G_{ct}** (clear-sky global radiation) incident on a **horizontal** plane on the earth´s surface, the clear-sky normal beam radiation G_{cnb} has to be multiplied by the cosine of the zenith angle.

$$G_{ct} = G_{cnb} \cdot \cos(\Theta_z) + G_{cd}$$

4.3.3 Measured Solar Radiation Data

Although in this work only the clear-sky irradiation model by Hottel (1976) is used, I would like to mention some aspects concerning measured solar radiation data.

There are two types of radiation data that are widely available. The first is the monthly average daily total radiation on a horizontal surface $\overline{H}$. The unit of $\overline{H}$ is energy received per day and square meter and is mainly given in megajoules (MJ) per square meter and day. The second is the hourly total radiation on a horizontal surface **I** (for extended periods, such as one or more years). The unit of I is energy received per hour and square meter and is mainly given in kilojoules (kJ) per square meter and hour. These data are available from weather services and literature.
Furthermore, typical meteorological year (TMY) data sets for specific locations have been produced by national weather services. These represent the average weather conditions over time periods such as 30 years, providing hourly values of solar radiation, ambient temperature, humidity, wind speed, wind direction and other weather data. [Duffie & Beckman 2006]

To obtain reliable radiation data at ground level systematic measurements are required. However, in most countries the spatial density of stations, that measure solar radiation data, is insufficient. For example, the ratio of weather stations collecting solar radiation data to those collecting temperature data is approximately 1:100 in the USA and 1:500 worldwide. Inaccuracies of practically available solar beam radiation data vary in a range of 3%. [Badescu 2008]

4.4 Calculation of the Sun´s Position

After having determined the extraterrestrial radiation available and atmospheric attenuation, which depends on the radiation´s path through the atmosphere, the actual position of the sun relative to a certain location on the earth´s surface has to be determined.
This position is defined by the solar azimuth, solar altitude and the zenith angle. Its calculation requires functions of latitude, longitude, date and time. These functions will be described in the following section.

The current position of the sun is at every location on earth defined by following angles:

The **zenith angle** Θ_z is the angle between the vertical and the line to the sun.
The **solar altitude angle** α_s is the angle between the horizontal and the line to the sun. It is the complement of the zenith angle.
The **solar azimuth angle** γ_s is the angle between the projection of beam radiation on the horizontal plane and the direction southward. Displacements east of south are negative and west of south are positive (northern hemisphere). Sometimes the solar azimuth angle is measured between the projection of beam radiation on the horizontal plane and the direction northward, with displacements east of north positive and west of north negative. Thus, one has to make sure which convention is valid in order to interpret the values of angles correctly.
Furthermore the definition of the solar azimuth angle depends on whether the location in question is in the **northern** or **southern hemisphere**.
In the southern hemisphere the definitions for the solar azimuth angle have to be adapted, as the sun´s way leads through the northern part of the sky. As the solar azimuth angle should be zero at noon too, in this work following definition is used:
The solar azimuth angle γ_s is the angle between the projection of beam radiation on the horizontal plane and the direction northward. Displacements east of north are negative and west of north are positive.

Within a year the latitude where the sun reaches the zenith at solar noon varies between 23°27' north (positive), the tropic of Cancer, and 23°27' south (negative), the tropic of Capricorn. This variation is called **declination of the sun** and is described by the **declination angle** δ ($-23.45 \leq \delta \leq +23.45$).

Thus the declination δ depends on the date and can be described by following equation:
[Duffie & Beckman 2006]

$$\delta = 23.45 \cdot \sin\left(\frac{360 \cdot (284 + n)}{365}\right)$$

n..... n^{th} day of the year, starting at January 1^{st}

Due to the fact that the latitude where the sun is at the zenith varies, one special case in each hemisphere has to be considered:
If the location in question is in the northern hemisphere but the declination (dependent on the time of year) exceeds its latitude (possible if the location´s latitude is smaller than 23°27' north), then the southern hemisphere´s angle definitions are valid.
On the other hand, if the location in question is in the southern hemisphere, but its latitude is within the tropic of Capricorn (23°27' south) and exceeds the declination, the angle definitions of the northern hemisphere are valid.

Solar altitude and solar azimuth are dependent on the location on earth, date and time.

For the calculation of the sun´s position the **solar time t_s** is necessary. “The solar time is the time used in all of the sun-angle relationships; it does not coincide with local clock time. It is necessary to convert local standard time to solar time by applying two corrections. First, there is a constant correction for the difference in longitude between the observer´s meridian (longitude) and the meridian on which the local standard time is based.” [Duffie & Beckman 2006]
To find the local standard meridian, multiply the time difference (in hours) between local standard time and UTC (universal time coordinated) by 15°. (Note that with daylight saving time, 1 hour must be subtracted from local clock time to get local standard time.) Within 1 hour the earth rotates through 15°. Thus the sun takes 4 minutes to transverse 1° of longitude.
The second correction takes into account the difference between mean solar time and actual solar time. “Mean solar time is a convention based on a fictitious sun which is assumed to proceed with constant angular velocity in a circular orbit. Actual solar time is related to the real motion of the earth around the sun.” [Winter 1991]
The time equation E takes into account that due to Kepler´s laws the earth´s apparent velocity around the sun is not constant. [Crastan 2009]

This difference **E** between actual solar time and mean solar time, that varies roughly from -15 to +15 minutes, is described by following equation

$$E = 229.2 \cdot (0.000075 + 0.001868 \cdot \cos(B) - 0.032077 \cdot \sin(B) - 0.014615 \cdot \cos(2B) - 0.04089 \cdot \sin(2B))$$

with $B = \frac{(n-1) \cdot 360}{365}$ and the result in minutes. [Duffie & Beckman 2006]

n..... n^{th} day of the year, starting at January 1^{st}

Month	***n*** for the i^{th} day of each month:
January	i
February	31 + i
March	59 + i
April	90 + i
May	120 + i
June	151 + i
July	181 + i
August	212 + i
September	243 + i
October	273 + i
November	304 + i
December	334 + i

Table 4: Values for the Day of the Year Number n

With the standard meridian L_{st} for local time zone and the longitude L_{loc} of the location in question (**longitudes are in degrees west**, 0°< L < 360°), the difference in minutes between solar time and standard local time is [Duffie & Beckman 2006]:

$$solar\ time\ t_s - local\ standard\ time = 4 \cdot (L_{st} - L_{loc}) + E$$

With longitudes in **degrees east**, 0° < L < 360°, the difference in minutes between solar time and standard local time is [Crastan 2009]:

$$solar\ time\ t_s - local\ standard\ time = 4 \cdot (L_{loc} - L_{st}) + E$$

Furthermore the **hour angle ω** is important to finally calculate the solar altitude and solar azimuth. The hour angle is the angular displacement of the sun east or west of the local meridian due to rotation of the earth on its axis at 15° per hour. From sunrise to solar noon it is negative, at solar noon zero and in the afternoon positive till sunset. This definition is valid for northern and southern hemisphere. [Quaschning 2007]

$$\omega = (solar\ time\ t_s - 12) \cdot 15\,°$$

In the equation above the solar time t_s has to be inserted in hours.

Solar altitude angle α_s with **φ** as latitude of the location in question and declination **δ** (valid for northern and southern hemisphere): [Quaschning 2007]

$$\sin(\alpha_s) = \cos(\Theta_z) = \cos(\omega) \cdot \cos(\varphi) \cdot \cos(\delta) + \sin(\varphi) \cdot \sin(\delta)$$

$$\alpha_s = \arcsin(\cos(\omega) \cdot \cos(\varphi) \cdot \cos(\delta) + \sin(\varphi) \cdot \sin(\delta))$$

Solar azimuth angle γ_s with **φ** as latitude of the location in question and declination **δ** : [Quaschning 2007]

northern hemisphere:
$$\gamma_s = sign(\omega) \cdot \arccos\left(\frac{\sin\alpha_s \cdot \sin\varphi - \sin\delta}{\cos\alpha_s \cdot \cos\varphi}\right)$$

southern hemisphere:
$$\gamma_s = \arccos\left(\frac{\sin\alpha_s \cdot \sin\varphi - \sin\delta}{\cos\alpha_s \cdot \cos\varphi}\right) - 180 \quad \text{for } \omega < 0$$

$$\gamma_s = 180 - \arccos\left(\frac{\sin\alpha_s \cdot \sin\varphi - \sin\delta}{\cos\alpha_s \cdot \cos\varphi}\right) \quad \text{for } \omega > 0$$

4.4.1 Angle of Incidence on a Plane of Any Particular Orientation Relative to the Earth

As any kind of solar collector is generally speaking a plane at a certain angle to the incoming radiation,which may differ from 90° (radiation normal to the plane), only a fraction of the radiation´s flux can be received. For this reason, the position of a plane and its angles to the incoming radiation have to be defined.

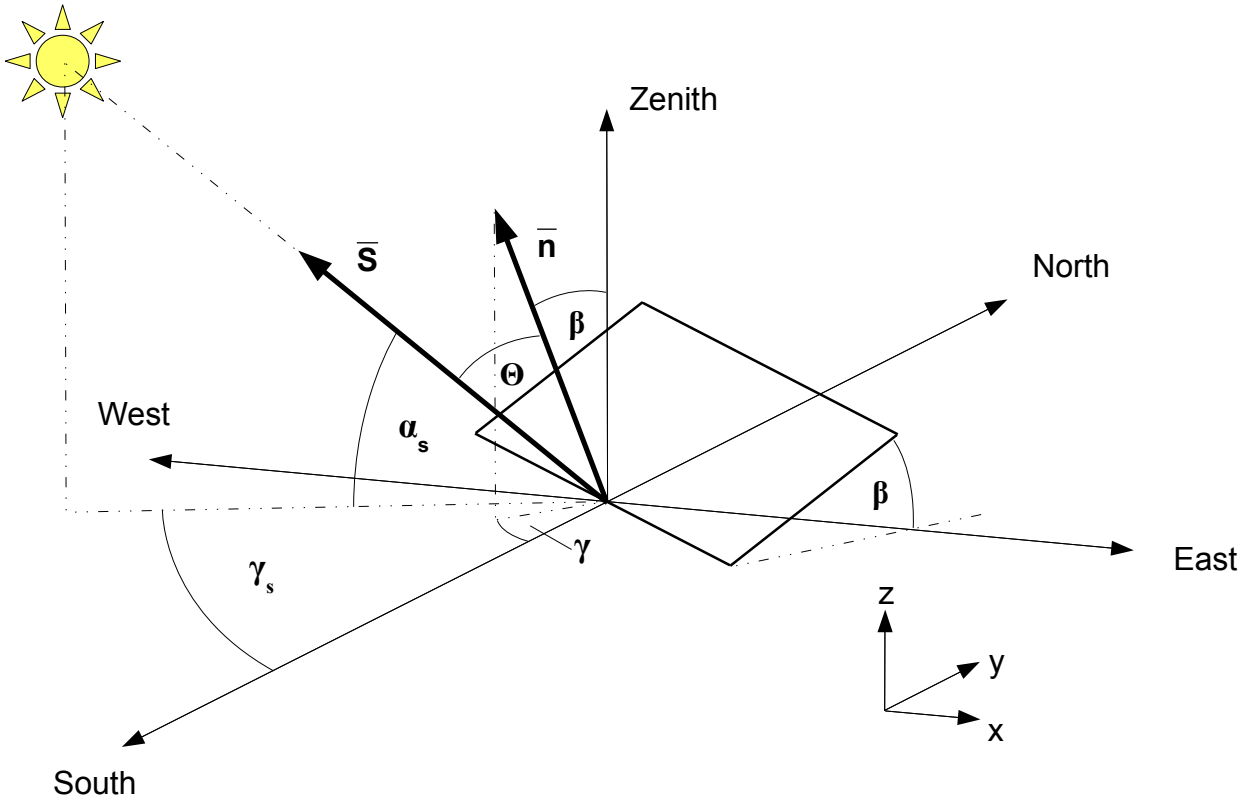

Figure 32: Sketch for the Angle of Incidence on a Plane (Northern Hemisphere)

The **angle of incidence Θ** is the angle between the beam radiation on a surface and the normal to that surface.
To get the angle of incidence on a **horizontal** plane at a certain location on earth, just the zenith angle has to be calculated. Thus in case of a horizontal plane the angle of incidence constitutes:

$$\Theta = \Theta_z = 90° - \alpha_s$$

To calculate the angle of incidence on a plane of any particular orientation relative to the earth, two more angles have to be defined.

The **slope β** is the angle between the plane of the surface in question and the horizontal. If that angle exceeds 90° the surface has a downward-facing component.

Again we have to distinguish between northern and southern hemisphere. In the **northern hemisphere** following definitions are valid:

The **surface azimuth angle** γ is the angle between the projection of the plane´s normal on the horizontal plane and the direction southward. Displacements east of south are negative and west of south are positive.

Furthermore the unit normal vector $\vec{n}$ of the plane and the unit vector of the beam radiation direction $\vec{s}$ have to be determined. The coordinate system used has the x-axis towards east, y-axis towards north and the z-axis towards the zenith.

$$\vec{n} = \begin{bmatrix} -\sin\beta \cdot \sin\gamma \\ -\sin\beta \cdot \cos\gamma \\ \cos\beta \end{bmatrix} \qquad \vec{s} = \begin{bmatrix} -\cos\alpha_s \cdot \sin\gamma_s \\ -\cos\alpha_s \cdot \cos\gamma_s \\ \sin\alpha_s \end{bmatrix}$$

Analogue in the **southern hemisphere:**

The **surface azimuth angle** γ is the angle between the projection of the plane´s normal on the horizontal plane and the direction northward. Displacements east of north are negative and west of north are positive.

The coordinate system used has the x-axis towards west, y-axis towards south and the z-axis towards the zenith.

$$\vec{n} = \begin{bmatrix} \sin\beta \cdot \sin\gamma \\ -\sin\beta \cdot \cos\gamma \\ \cos\beta \end{bmatrix} \qquad \vec{s} = \begin{bmatrix} \cos\alpha_s \cdot \sin\gamma_s \\ -\cos\alpha_s \cdot \cos\gamma_s \\ \sin\alpha_s \end{bmatrix}$$

When the unit normal vector $\vec{n}$ of the plane and the unit vector of the beam radiation direction $\vec{s}$ are determined, the **angle of incidence** Θ is calculated as follows (valid in northern and southern hemisphere):

$$\cos\Theta = \vec{n} \cdot \vec{s} \qquad \Theta = \arccos(\vec{n} \cdot \vec{s})$$

$$\Theta = \arccos(\sin\beta \cdot \sin\gamma \cdot \cos\alpha_s \cdot \sin\gamma_s + \sin\beta \cdot \cos\gamma \cdot \cos\alpha_s \cdot \cos\gamma_s + \cos\beta \cdot \sin\alpha_s)$$

At solar thermal power plants, concentrating devices “track” the sun by moving in prescribed ways to minimize the angle of incidence Θ of beam radiation on their surfaces and therefore maximize the received energy. This “tracking” can either be realized by single axis or two axis movement.

4.5 Solar Irradiation in IPSEpro

Before I start describing the implementation, I have to explain an important feature of IPSEpro. This feature is called “global”.
“Globals” are program components that can be loaded into the code of all units. Thus, it is possible to calculate certain variables, that are needed in many units, just in one “global”. Then, after having defined this certain “global”, the calculation results can be loaded into all units, where they are required.

Since the solar data is the same for all collector units, it is appropriate to use a global in this case. Therefore, all the radiation data needed for simulation of thermal solar power plants, is calculated and defined in a global of the type “location_and_solar_parameters”. There the sun´s position and irradiation at any location on the earth´s surface can be calculated.

The necessary equations and empirical correlations have been inserted using the IPSE-Pro Model Developing Kit (MDK). All necessary variables, parameters and switches, have been defined and edited in the MDK.

In case a new collector unit is placed in an IPSEpro project file, all the necessary solar data is accessed via the global “location_and_solar_parameters”. After having defined a new global of this type it can be selected in an adequate unit.

In order to define a new global of the type “location_and_solar_parameters” the following inputs are necessary. Therefore, the upper part of the corresponding dialogue window is shown below. The remaining variables that are not shown in this figure do not have to be defined by the user. These are calculation results. All variables are explained in the appendix.

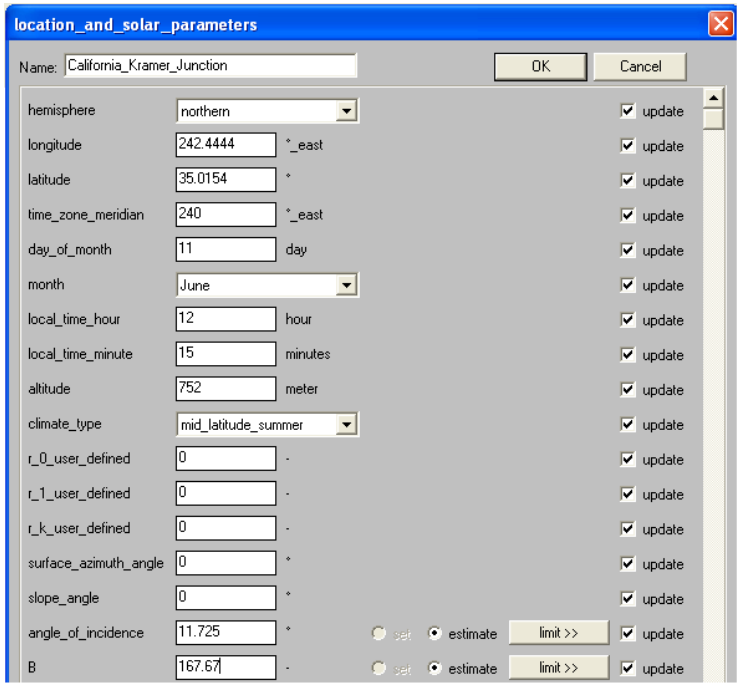

Figure 33: The Upper Part of the IPSEpro Dialogue Window "location_and_solar_parameters"

At first there has to be distinguished between southern and northern hemisphere. This is done by the switch “hemisphere”.

The month is defined by the switch “month”.

The following parameters are necessary, too, and have been created in the MDK: time_zone_meridian, day_of_month, local_time_hour, local_time_minute, latitude, longitude and altitude.

The “time_zone_meridian” is the meridian in degrees east on which the local standard time is based. For instance, for "Central European Time" the standard meridian in degrees east is 15.

For the local standard time 10:30, the “local_time_hour” is 10. Note: If daylight saving time is valid one hour has to be subtracted. The local time hour would be 9 then. The time format is 24 hours, beginning with hour 0 up to hour 23

For the local standard time 10:30, the “local_time_minute” is 30. Values range from 0 up to 59 minutes.

The parameter “latitude” is the latitude north or south. It is zero at the equator, north positive and south negative.

The parameter “longitude” is the longitude of the location in question in degrees east of Greenwich.

The parameter “altitude” is the site´s elevation above sea level in meters.

Next, for the atmospheric attenuation model by Hottel (1976), a switch “climate_typ” is used to distinguish between the four different climate types, that are shown in table 3 on page 45.
In case the climate type “user_defined” is selected, the parameters “r_0_user_defined”, “r_1_user_defined” and “r_k_user_defined” have to be set by the user. These values have to be determined by local measurements.
If an available climate type is selected, the values can be set to zero, as shown in figure 33.

The last parameters that can be set by the user is the slope angle, and the azimuth angle of any particular plane (figure 32 on page 50). As a result, the variable “angle_of_incidence” gives the angle of incidence according to that plane. Note: These two parameters do not influence the angle of incidence of other units. It just offers the possibility of an independent calculation. If not needed, values can be set to zero. The result can be displayed by the unit “solar_properties” (figure 34).

Having defined all the parameters above, the solar model can be used.

In order to access the solar data calculated, in the process simulation environment PSE, the global can either be selected in the unit “sun_properties” or in the collector units (“T_Solar_collector”, “W_Solar_collector”). In the unit “sun_properties” (figure 34) all the calculated solar data can be accessed and displayed without the definition of a certain thermodynamic circuit or loop.

All used variables and parameters are explained within the appendix.

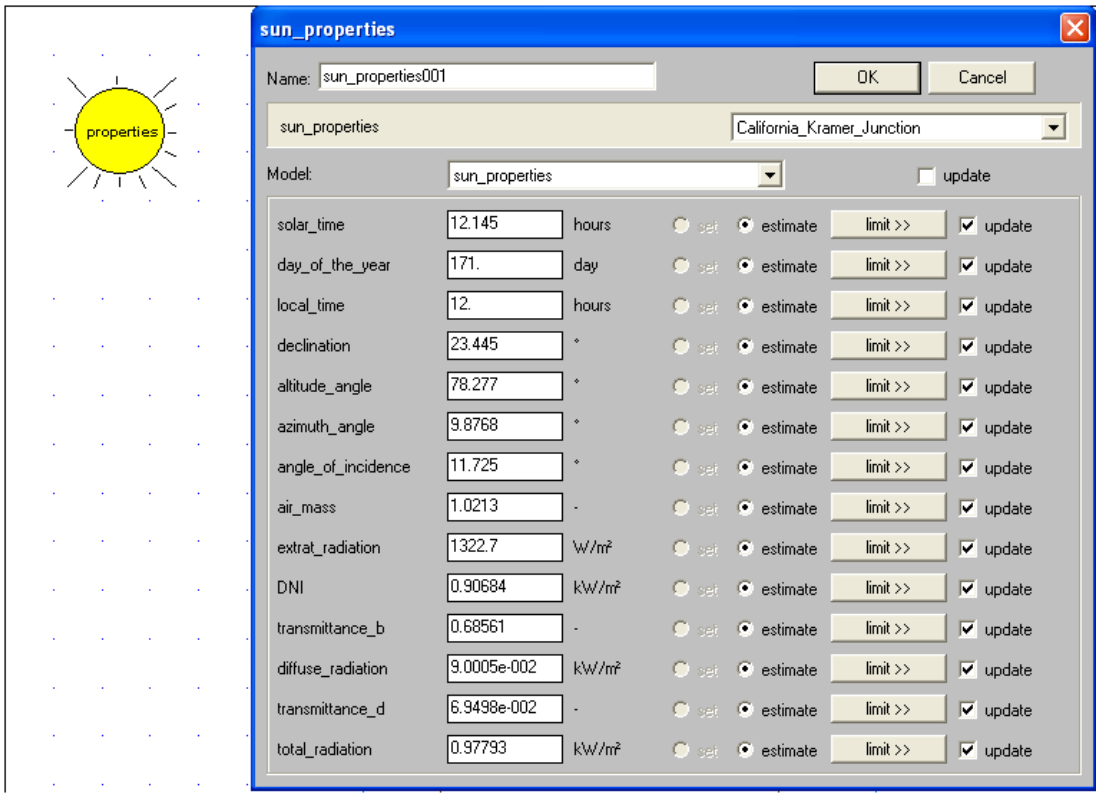

Figure 34: IPSEpro Unit "sun_properties"

Important for the further calculation of collector specific attenuation factors and power available, are the variables "DNI" (direct normal irradiance), "altitude_angle" (the sun´s altitude angle) and "azimuth_angle" (the sun´s azimuth angle).

5 The Parabolic Trough Collector Model – Attenuation Factors and Losses (Oil & DSG)

After having defined the incoming solar radiation and its angles, depending on time and location, I started with the modelling of the parabolic trough collector, as it is the most common one in today´s commercial solar power plants.

Step by step I discuss all factors that attenuate the incoming solar radiation before it hits the absorber tube.

Then the thermal losses due to radiation and convection are examined. There I propose empirically established models, based on measurements, and in addition a pure physical model, which of course needs more input data by the user.
Furthermore, a chapter deals with the properties and composition of selective surfaces, as this is an important topic concerning thermal losses.

In order to calculate the enthalpy rise of the fluid within the absorber tube the general equations of heat transfer for a cylindrical tube are necessary. The basic equations are valid for all kinds of parabolic trough collectors. Only concerning the correlations for the heat transfer coefficient within the tube α_{tube}, a distinction has to be made between the fluids used in different applications.

Therefore, there has to be distinguished between the parabolic troughs using oil as heat transfer fluid and those for direct steam generation (DSG).

From now on, the two collector concepts are dealt with separately in own chapters (chapter 6 and 7). There, I propose suitable correlations for pressure loss and especially discuss empirical models for the two phase flow heat transfer coefficient, including general information and definitions. All this information is necessary to finally find correlations that are suitable for modelling.

At the end of each chapter the implementation in IPSEpro is described.

Finally, when all necessary correlations were found and implemented in the IPSEpro collector models, I modelled different plants with IPSEpro-PSE. These are described in chapter 8.

After having given a general overview of this modelling method, I would like to start with the actual matter of this chapter, thus describing the attenuation of the incoming solar radiation until it hits the absorber tube´s outer surface.

As described in previous chapters the properties of the solar beam radiation incident on the earth´s surface can be calculated. It would be convenient if the solar beam radiation´s energy was directly assigned to the heat transfer fluid or water (in case of direct steam generation). In reality, also this kind of energy transfer does not happen without losses.
The maximum of energy that can be received by these collectors is defined by the clear-sky normal beam radiation $\mathbf{G_{cnb}}$, with its altitude angle α_s, azimuth angle γ_s and angle of incidence Θ.

To get the solar beam radiation that can be received by a parabolic trough receiver, the clear-sky normal beam radiation $\mathbf{G_{cnb}}$ has to be multiplied by two factors. The cosine-loss attenuation factor ζ_{cos} and the shading attenuation factor $\zeta_{shading}$.

For the sake of completeness, a third factor would be the end-loss attenuation factor ζ_{end}, which can be neglected. [Quaschning 2007]

5.1 The Cosine-Loss Attenuation Factor

As parabolic trough collectors are placed horizontally either along the north-south axis or east-west axis and can only rotate about that axis, there is always a certain angle of incidence Θ remaining (exceptions: north-south orientation: sun is at the zenith or near the horizon; east-west orientation: at solar noon) that is the cause for **cosine losses**. The angle of incidence Θ is the angle between the normal to the aperture plane of the collector $\vec{R}$ and the vector to the sun $\vec{s}$ (figure 37).
As described before, the angle of incidence Θ on a certain plane can be calculated if the plane´s azimuth angle γ and slope β are known.

The following figures show typical angle of incidence variations during one day in summer and one in winter. The red line represents the east-west orientation, the blue line the north-south orientation.

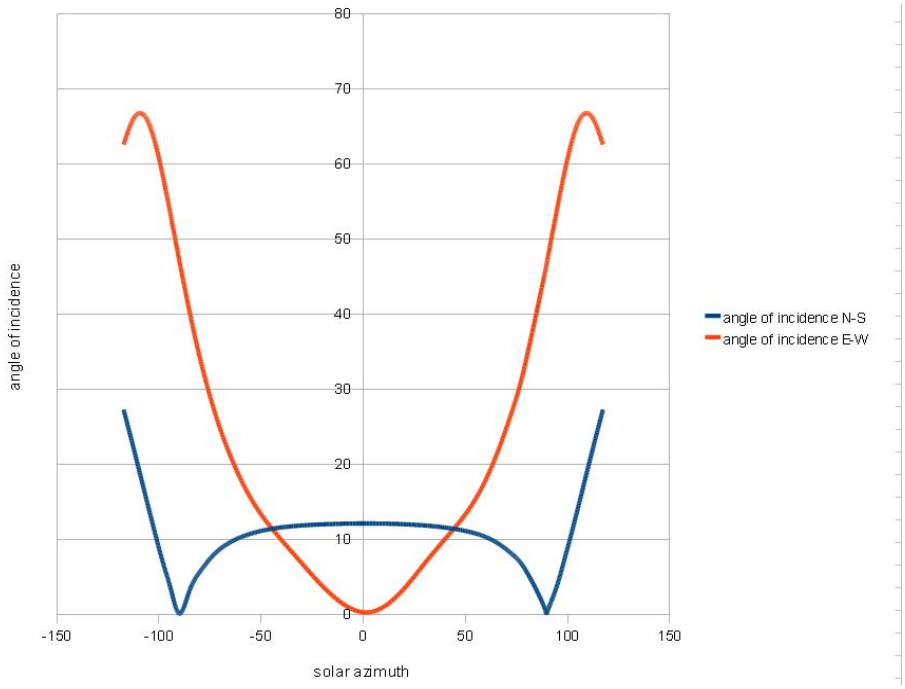

Figure 35: Angle of Incidence Variation in Summer (35.33°N)

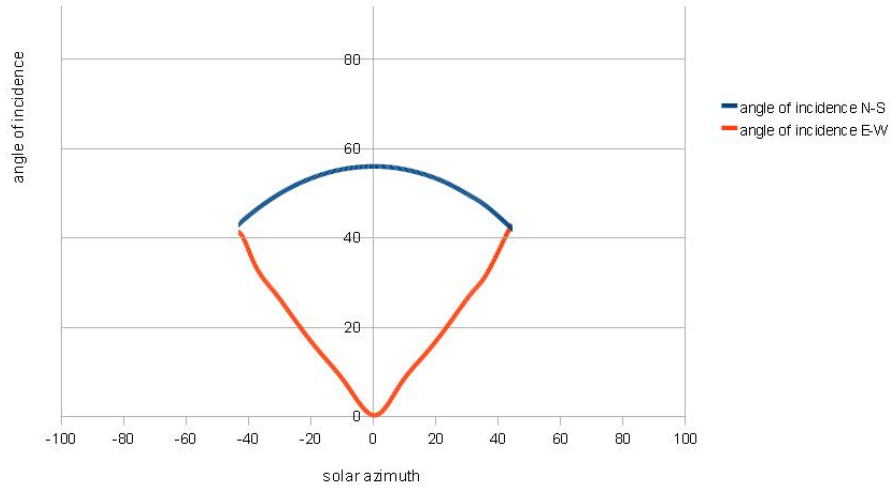

Figure 36: Angle of Incidence Variation in Winter (35.33°N)

"Seasonal variations in energy delivery are much smaller for an east-west orientation, usually less than 50%. Nevertheless, a north-south sun-tracking axis orientation provides more energy on a yearly basis." [Romero-Alvarez et al. 2007]

The following chapters deal with the calculation of the parabolic trough collector´s actual slope angle β and azimuth angle γ, as they depend on the actual position of the sun.

5.1.1 North-South Orientation of the Parabolic Trough Receiver

The slope β of the receiver in question is determined by the solar altitude and azimuth angle. In fact, the straight line Γ imagined from the receiver to the sun has to be element of the trough receiver´s plane of symmetry Ω.
If furthermore a plane Λ is imagined, that is normal to the receiver´s plane of symmetry Ω and parallel to the receiver´s axis (north-south axis), the slope β and azimuth angle γ of that plane Λ are equivalent to the receiver´s slope and azimuth. With these two angles the required angle of incidence Θ can be calculated. If Γ is element of the plane Ω , the angle of incidence Θ is in between the two vectors $\overline{\mathbf{R}}$ and $\overline{\mathbf{S}}$. Where $\overline{\mathbf{S}}$ is the vector pointing to the sun, and $\overline{\mathbf{R}}$ is the unit normal vector of the plane Λ.

5.1.1.1 Northern Hemisphere

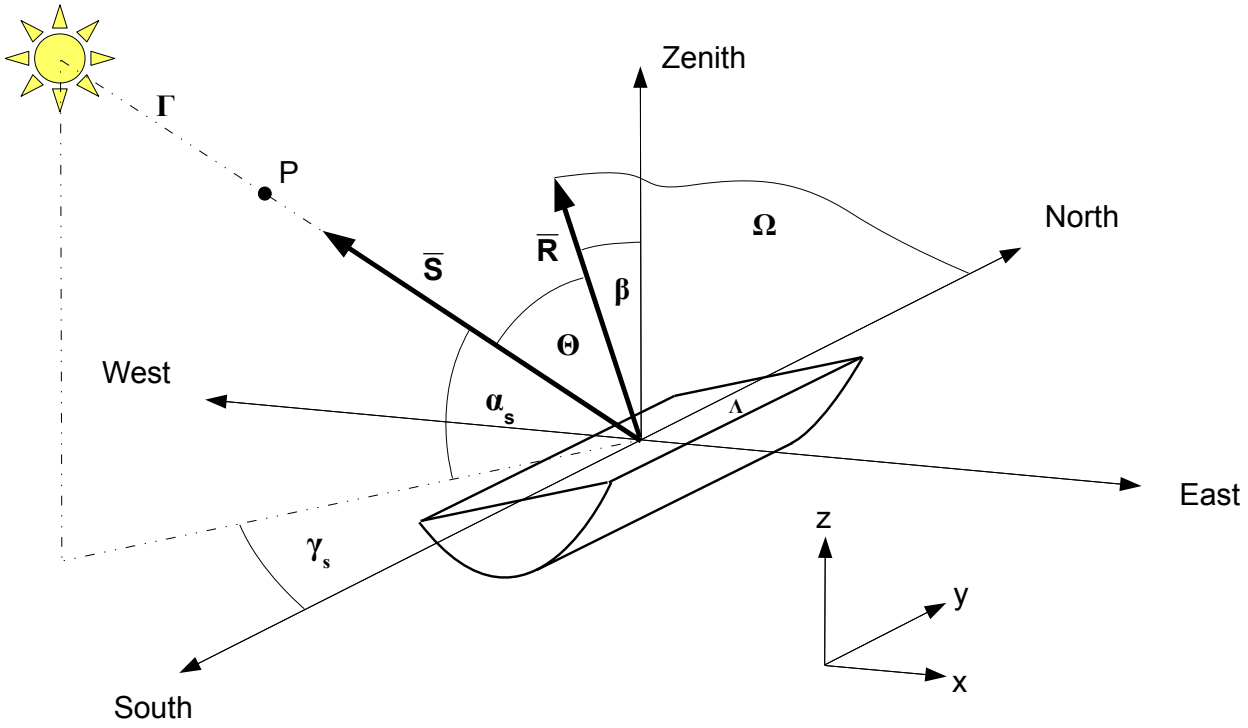

Figure 37: Sketch for the Cosine-Loss Calculation (Northern Hemisphere, N-S Orientation)

The receiver´s azimuth angle γ is 90° if the solar azimuth angle γ_s is positive and it is -90° if γ_s is negative.

The receiver´s slope β can be calculated in the following way:

In the calculations the coordinate system´s origin coincides with the receiver´s plane of symmetry Ω and is element of the plane Λ. The x-axis points towards east, y-axis towards north and the z-axis towards the zenith.

The vector pointing to the sun $\vec{s} = \begin{bmatrix} -\cos\alpha_s \cdot \sin\gamma_s \\ -\cos\alpha_s \cdot \cos\gamma_s \\ \sin\alpha_s \end{bmatrix}$.

With the slope **β** the receiver´s plane of symmetry **Ω** in parametric representation (**a** and **b** as parameters) is

$$\vec{\Omega} = \begin{bmatrix} 0 \\ 0 \\ 0 \end{bmatrix} + a \cdot \begin{bmatrix} -\sin\beta \\ 0 \\ \cos\beta \end{bmatrix} + b \cdot \begin{bmatrix} 0 \\ 1 \\ 0 \end{bmatrix} .$$

The cross product yields the normal vector $\vec{n}_\Omega$ of the plane **Ω**: $\vec{n}_\Omega = \begin{bmatrix} \cos\beta \\ 0 \\ \sin\beta \end{bmatrix}$

Thus the equation of plane **Ω** is: $x \cdot \cos\beta + z \cdot \sin\beta = 0$

As mentioned above, the straight line **Γ** imagined from the receiver to the sun has to be element of the trough receiver´s plane of symmetry **Ω**.

The straight line **Γ** through the origin and the sun in parametric representation (parameter **b**):

$$\vec{\Gamma} = \begin{bmatrix} 0 \\ 0 \\ 0 \end{bmatrix} + b \cdot \begin{bmatrix} -\cos\alpha_s \cdot \sin\gamma_s \\ -\cos\alpha_s \cdot \cos\gamma_s \\ \sin\alpha_s \end{bmatrix}$$

To make sure that the straight line **Γ** is element of the plane **Ω**, two points of that straight line have to satisfy the equation of plane **Ω** too. As both **Γ** and **Ω** go through the origin there is one more point required. With the parameter **b** assumed equal to 1 the second point **P** is:

$$\vec{P} = \begin{bmatrix} -\cos\alpha_s \cdot \sin\gamma_s \\ -\cos\alpha_s \cdot \cos\gamma_s \\ \sin\alpha_s \end{bmatrix}$$

To determine now the slope **β** of the parabolic trough receiver the **x** and **z** values of the vector **P** have to be inserted in the equation of plane **Ω**. That yields the one necessary equation for the unknown variable **β**. As defined in a previous chapter **β** is always positive under this terms.

$$\tan\beta = \frac{\cos\alpha_s \cdot \sin\gamma_s}{\sin\alpha_s} \qquad \beta = \left| \arctan\left(\frac{\cos\alpha_s \cdot \sin\gamma_s}{\sin\alpha_s} \right) \right|$$

$$\Theta = \arccos(\sin\beta \cdot \sin\gamma \cdot \cos\alpha_s \cdot \sin\gamma_s + \sin\beta \cdot \cos\gamma \cdot \cos\alpha_s \cdot \cos\gamma_s + \cos\beta \cdot \sin\alpha_s)$$

With the definition of the angle of incidence **Θ** the **cosine loss attenuation factor** ζ_{cos} is given by the **cosine** of that angle **Θ**.

$$\zeta_{\cos} = \cos\Theta$$

5.1.1.2 Southern Hemisphere

In the calculations the coordinate system´s origin coincides with the receiver´s plane of symmetry **Ω** and is element of the plane **Λ**. The x-axis points towards west, y-axis towards south and the z-axis towards the zenith.

The receiver´s azimuth angle **γ** is 90° if the solar azimuth angle γ_s is positive and it is -90° if γ_s is negative.

The receiver´s slope **β** can be calculated in the following way:

The vector pointing to the sun $\vec{s} = \begin{bmatrix} \cos\ \alpha_s \cdot \sin\gamma_s \\ -\cos\alpha_s \cdot \cos\gamma_s \\ \sin\alpha_s \end{bmatrix}$.

With the slope **β** the receiver´s plane of symmetry **Ω** in parametric representation (**a** and **b** as parameters) is

$$\vec{\Omega} = \begin{bmatrix} 0 \\ 0 \\ 0 \end{bmatrix} + a \cdot \begin{bmatrix} \sin\ \beta \\ 0 \\ \cos\ \beta \end{bmatrix} + b \cdot \begin{bmatrix} 0 \\ 1 \\ 0 \end{bmatrix} \quad .$$

The cross product yields the normal vector $\vec{n}_\Omega$ of the plane **Ω**: $\vec{n}_\Omega = \begin{bmatrix} -\cos\ \beta \\ 0 \\ \sin\ \beta \end{bmatrix}$

Thus the equation of plane **Ω** is: $-x \cdot \cos\ \beta + z \cdot \sin\ \beta = 0$

As mentioned above, the straight line **Γ** imagined from the receiver to the sun has to be element of the trough receiver´s plane of symmetry **Ω**.

The straight line **Γ** through the origin and the sun in parametric representation (parameter **b**):

$$\vec{\Gamma} = \begin{bmatrix} 0 \\ 0 \\ 0 \end{bmatrix} + b \cdot \begin{bmatrix} \cos\ \alpha_s \cdot \sin\gamma_s \\ -\cos\alpha_s \cdot \cos\gamma_s \\ \sin\alpha_s \end{bmatrix}$$

To make sure that the straight line **Γ** is element of the plane **Ω**, two points of that straight line have to satisfy the equation of plane **Ω** too. As both **Γ** and **Ω** go through the origin there is one more point required. With the parameter **b** assumed equal to 1 the second point **P** is:

$$\vec{P} = \begin{bmatrix} \cos\ \alpha_s \cdot \sin\gamma_s \\ -\cos\alpha_s \cdot \cos\gamma_s \\ \sin\alpha_s \end{bmatrix}$$

To determine now the slope **β** of the parabolic trough receiver the **x** and **z** values of the vector **P** have to be inserted in the equation of plane **Ω**. That yields the one necessary equation for the unknown variable **β**. As defined in a previous chapter **β** is always positive under this terms.

$$\tan\ \beta = \frac{\cos\ \alpha_s \cdot \sin\ \gamma_s}{\sin\ \alpha_s} \qquad \beta = \left| \arctan\left(\frac{\cos\ \alpha_s \cdot \sin\ \gamma_s}{\sin\ \alpha_s} \right) \right|$$

$$\Theta = \arccos(\sin\beta \cdot \sin\gamma \cdot \cos\alpha_s \cdot \sin\gamma_s + \sin\beta \cdot \cos\gamma \cdot \cos\alpha_s \cdot \cos\gamma_s + \cos\beta \cdot \sin\alpha_s)$$

With the definition of the angle of incidence **Θ** the **cosine loss attenuation factor** ζ_{cos} is given by the **cosine** of that angle **Θ**.

$$\zeta_{\cos} = \cos\ \Theta$$

5.1.2 East-West Orientation of the Parabolic Trough Receiver

5.1.2.1 Northern Hemisphere

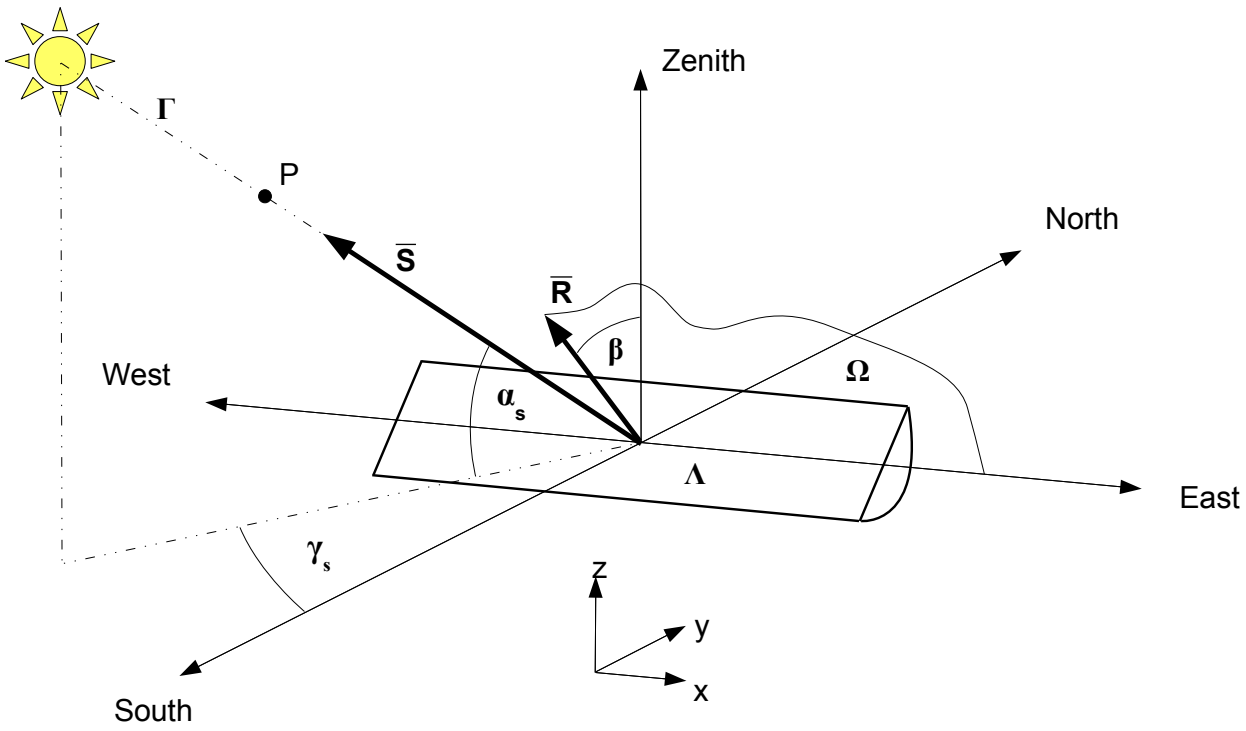

Figure 38: Sketch for the Cosine-Loss Calculation (Northern Hemisphere, E-W Orientation)

The slope **β** of the receiver in question is determined by the solar altitude and azimuth angle. In fact, the straight line **Γ** imagined from the receiver to the sun has to be element of the trough receiver´s plane of symmetry **Ω**.
If furthermore a plane **Λ** is imagined, that is normal to the receiver´s plane of symmetry **Ω** and parallel to the receiver´s axis (east-west axis), the slope **β** and azimuth angle **γ** of that plane **Λ** are equivalent to the receiver´s slope and azimuth. With these two angles the required angle of incidence **Θ** can be calculated.

In the calculations the coordinate system´s origin coincides with the receiver´s plane of symmetry **Ω** and is element of the plane **Λ**. The x-axis points towards east, y-axis towards north and the z-axis towards the zenith.

The receiver´s azimuth angle **γ** is zero if the solar azimuth angle γ_s is between -90° and 90° ($-90° < \gamma_s < 90°$). It is 180° if the solar azimuth angle γ_s is smaller than -90° or exceeds 90° ($-90° > \gamma_s \;||\; \gamma_s > 90°$).

The receiver´s slope **β** can be calculated in the following way:

The vector pointing to the sun $\vec{s} = \begin{bmatrix} -\cos\alpha_s \cdot \sin\gamma_s \\ -\cos\alpha_s \cdot \cos\gamma_s \\ \sin\alpha_s \end{bmatrix}$.

With the slope **β** the receiver´s plane of symmetry **Ω** in parametric representation (**a** and **b** as parameters) is

$$\vec{\Omega} = \begin{bmatrix} 0 \\ 0 \\ 0 \end{bmatrix} + a \cdot \begin{bmatrix} 0 \\ -\sin\beta \\ \cos\beta \end{bmatrix} + b \cdot \begin{bmatrix} 1 \\ 0 \\ 0 \end{bmatrix} .$$

The cross product yields the normal vector $\vec{n}_\Omega$ of the plane **Ω**: $\vec{n}_\Omega = \begin{bmatrix} 0 \\ \cos\beta \\ \sin\beta \end{bmatrix}$

Thus the equation of plane **Ω** is: $y \cdot \cos\beta + z \cdot \sin\beta = 0$

As mentioned above, the straight line **Γ** imagined from the receiver to the sun has to be element of the trough receiver´s plane of symmetry **Ω**.

The straight line **Γ** through the origin and the sun in parametric representation (parameter **b**):

$$\vec{\Gamma} = \begin{bmatrix} 0 \\ 0 \\ 0 \end{bmatrix} + b \cdot \begin{bmatrix} -\cos\alpha_s \cdot \sin\gamma_s \\ -\cos\alpha_s \cdot \cos\gamma_s \\ \sin\alpha_s \end{bmatrix}$$

To make sure that the straight line **Γ** is element of the plane **Ω**, two points of that straight line have to satisfy the equation of plane **Ω** too. As both **Γ** and **Ω** go through the origin there is one more point required. With the parameter **b** assumed equal to 1 the second point **P** is:

$$\vec{P} = \begin{bmatrix} -\cos\alpha_s \cdot \sin\gamma_s \\ -\cos\alpha_s \cdot \cos\gamma_s \\ \sin\alpha_s \end{bmatrix}$$

To determine now the slope **β** of the parabolic trough receiver the **y** and **z** values of the vector **P** have to be inserted in the equation of plane **Ω**. That yields the one necessary equation for the unknown variable **β**. As defined in a previous chapter **β** is always positive under this terms.

$$\tan \beta = \frac{\cos \alpha_s \cdot \cos \gamma_s}{\sin \alpha_s} \qquad \beta = \left| \arctan \left(\frac{\cos \alpha_s \cdot \cos \gamma_s}{\sin \alpha_s} \right) \right|$$

$$\Theta = \arccos(\sin\beta \cdot \sin\gamma \cdot \cos\alpha_s \cdot \sin\gamma_s + \sin\beta \cdot \cos\gamma \cdot \cos\alpha_s \cdot \cos\gamma_s + \cos\beta \cdot \sin\alpha_s)$$

With the definition of the angle of incidence **Θ** the **cosine loss attenuation factor** ζ_{cos} is given by the **cosine** of that angle **Θ**.

$$\zeta_{\cos} = \cos \Theta$$

5.1.2.2 Southern Hemisphere

In the calculations the coordinate system´s origin coincides with the receiver´s plane of symmetry **Ω** and is element of the plane **Λ**. The x-axis points towards west, y-axis towards south and the z-axis towards the zenith.

The receiver´s azimuth angle **γ** is zero if the solar azimuth angle γ_s is between -90° and 90° ($-90° < \gamma_s < 90°$). It is 180° if the solar azimuth angle γ_s is smaller than -90° or exceeds 90° ($-90° > \gamma_s \ || \ \gamma_s > 90°$).

The receiver´s slope **β** can be calculated in the same way as done above. The vector pointing to the sun $\vec{s}$ changes, but the result stays the same.

$$\tan \beta = \frac{\cos \alpha_s \cdot \cos \gamma_s}{\sin \alpha_s} \qquad \beta = \left| \arctan \left(\frac{\cos \alpha_s \cdot \cos \gamma_s}{\sin \alpha_s} \right) \right|$$

$$\Theta = \arccos(\sin\beta \cdot \sin\gamma \cdot \cos\alpha_s \cdot \sin\gamma_s + \sin\beta \cdot \cos\gamma \cdot \cos\alpha_s \cdot \cos\gamma_s + \cos\beta \cdot \sin\alpha_s)$$

With the definition of the angle of incidence **Θ** the **cosine loss attenuation factor** ζ_{cos} is given by the **cosine** of that angle **Θ**.

$$\zeta_{\cos} = \cos \Theta$$

5.2 The Shading Attenuation Factor

As solar power plants have huge collector fields that consist of several rows of parabolic trough receivers that are placed parallel with certain distances between them, mutual shading cannot be neglected in early morning and late afternoon hours (north-south-orientation).
Of course, that fact depends on the collector parallel distance $\mathbf{c_{dp}}$. If the collector parallel distance $\mathbf{c_{dp}}$ exceeds a certain value that is determined by the collector width $\mathbf{c_w}$ and the maximum acceptable slope angle $\boldsymbol{\beta_{max}}$, shading does not matter. Following formula gives the relationship between the minimum collector parallel distance $\mathbf{c_{dp\,min}}$ for a given $\boldsymbol{\beta_{max}}$, at which shading does not have to be taken into account.

$$c_{dp\,min} = \frac{c_w}{\cos\beta_{max}}$$

If north-south-orientation is valid, $\boldsymbol{\beta_{max}}$ is calculated for a solar altitude angle $\boldsymbol{\alpha_s}$ where the incident radiation due to atmospheric attenuation is not sufficient any more (morning and evening).
If east-west-orientation is valid, $\boldsymbol{\beta_{max}}$ is calculated for the lowest value of the solar altitude angle $\boldsymbol{\alpha_s}$ at noon, where the solar power plant can still be run.
For both cases the formula for $\boldsymbol{\beta_{max}}$ is described in the previous chapter ($\boldsymbol{\beta}$ is replaced by $\boldsymbol{\beta_{max}}$).

In most cases the collector parallel distances go below the shading limit $\mathbf{c_{dp\,min}}$ due to area restrictions and decreasing tube-length between the parabolic troughs. Therefore a shading attenuation factor $\boldsymbol{\zeta_{shading}}$ has to be taken into account.

Up to which length **S** the collector width $\mathbf{c_w}$ is shaded by the preceding trough can be calculated by the following formula. Note, that in order to get valid results the collector distance $\mathbf{c_{dp}}$ and slope angle $\boldsymbol{\beta}$ have to allow shading. Apparently, the maximum shading length possible is equal to the collector width $\mathbf{c_w}$.

$$S = \frac{c_w}{2} - \left(c_{dp} - \frac{c_w}{2 \cdot \cos\beta} \right) \cdot \cos\beta$$

$$S = c_w - c_{dp} \cdot \cos\beta$$

Thus, if a collector field consists of **n** rows the shading attenuation factor $\boldsymbol{\zeta_{shading}}$ is given as follows:

$$\zeta_{shading} = 1 - \frac{(n-1) \cdot S}{n \cdot c_w}$$

A satisfying trade-off between shading losses and heat/pressure losses is a collector parallel distance $\mathbf{c_{dp}}$ that is three times the collector width $\mathbf{c_w}$. [Quaschning 2007]

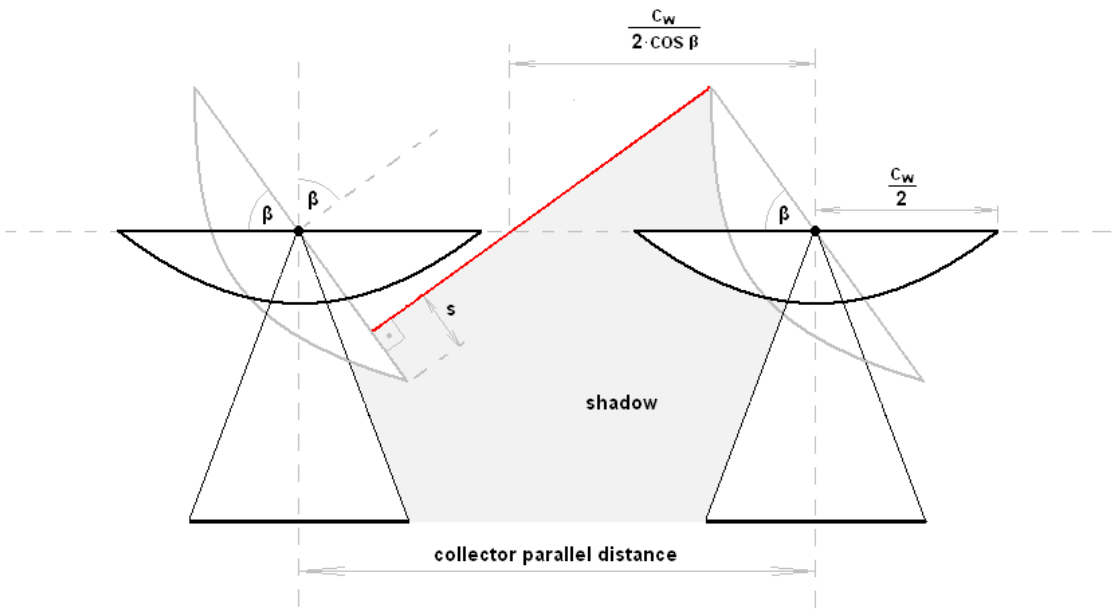

Figure 39: Parabolic Trough Shading Losses

5.3 The Collector-End Loss Attenuation Factor

As can be seen in the following figure 40, the reflected solar beam radiation does not reach the absorber tube at a certain length **x**, depending on the actual angle of incidence **Θ**. However, if several parabolic trough receivers are placed in a row with the distance $\mathbf{c_d}$ between them, the reflected radiation from the preceding one will reach the following absorber tube at a length **y**. Considering these facts, the collector-end-loss attenuation factor ζ_{end} can be defined as follows. $\mathbf{L_c}$ is the collector length, ***f*** the focal length and **n** the number of collectors placed in a row.

$$\zeta_{end} = 1 - \frac{(n-1) \cdot c_d + f \cdot \tan \Theta}{n \cdot L_c}$$

In most cases the collector-end losses can be neglected as today´s collector´s length is sufficiently large (EuroTrough collector length = 150 m). [Quaschning 2007]

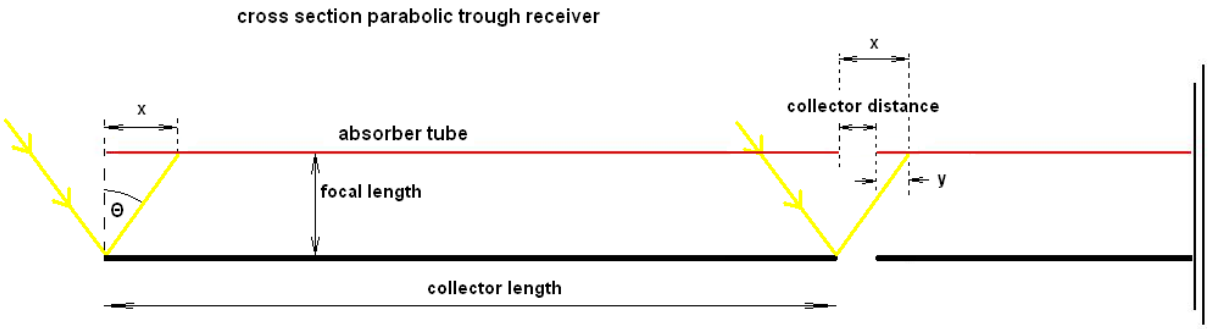

Figure 40: Parabolic Trough Receiver End-losses

With these attenuation factors taken into account, the solar radiation that can be received by parabolic trough collectors is calculated. This result (the effective solar radiation that reaches the parabolic trough receiver) is also called **IDR (incident direct radiation)**.

To get that amount of energy which finally reaches the heat transfer fluid in the tube, losses and efficiencies of parabolic trough collectors have to be taken into account. These are going to be explained in the following chapter.

5.4 Optical Losses and Optical Efficiency

Optical losses depend on the following 4 parameters:

The maximum possible amount of the effective incident radiation that can be reflected onto the receiver tube is defined by the **reflectivity** ρ_r. Values of ρ_r for clean silvered glass mirrors are around 0.93. As dirt accumulates on mirrors, their reflectivity decreases continuously until the next washing. Usually parabolic trough mirrors are washed, when the reflectivity reaches a value of about 0.9. [Goswami & Kreith 2008]

The **intercept factor** χ defines the fraction of the reflected solar radiation that does finally reach the absorber´s glass cover. A certain amount of the reflected radiation does not reach the tube due to either microscopic imperfections of the reflector or macroscopic shape errors in the parabolic trough concentrators. Thus, some rays are reflected in a wrong angle and therefore do not reach the absorber tube. A typical value for an intercept factor χ is 0.95. [Goswami & Kreith 2008]

Furthermore, if the radiation reaches the absorber, it is attenuated by the surrounding glass tube. In order to decrease thermal losses the steel absorber tube is placed inside an evacuated glass tube. The **transmissivity** τ_g defines the fraction of the remaining solar radiation that passes through the glass. A typical value for the transmissivity τ_g is 0.93. [Goswami & Kreith 2008]

The **absorptivity** α of the absorber tube coating defines the amount of radiation that is finally absorbed. For receiver pipes with cermet coating, a typical value for α is 0.95. It is slightly lower for pipes coated with nickel or chrome. [Goswami & Kreith 2008]

These four parameters multiplied give the **peak optical efficiency** $\eta_{opt,0°}$ of a parabolic trough receiver, when the angle of incidence Θ on the aperture plane is 0° (Thus, the cosine loss attenuation factor ζ_{cos} is 1). It is usually in the range of 0.70 – 0.76 for clean, good-quality parabolic trough collectors. [Goswami & Kreith 2008]

$$\eta_{opt,0°} = \rho_r \cdot \chi \cdot \tau_g \cdot \alpha \,|_{\Theta = 0°}$$

This peak optical efficiency $\eta_{opt,0°}$, is usually determined by measurements.

With increasing angle of incidence Θ the optical efficiency η_{opt} is reduced, due to aberrations.
As the angle of incidence Θ varies throughout the day and year, and therefore very seldom has the value zero, another attenuation factor has to be taken into account.
This attenuation factor for the peak optical efficiency $\eta_{opt,0°}$ is called **incidence angle modifier** ζ_{IAM}. [Quaschning 2007]

$$\eta_{opt} = \eta_{opt,0°} \cdot \zeta_{IAM}$$

An empirical equation for the incidence angle modifier ζ_{IAM} is given as follows. The two constants c_1 and c_2 have to be determined by measurements for different collectors, as the parameters for the optical efficiency depend on the type of collector. [Quaschning 2007]

$$\zeta_{IAM} = 1 - \frac{c_1 \cdot \Theta}{\cos\Theta} - \frac{c_2 \cdot \Theta^2}{\cos\Theta}$$

Test results at the SEGS plant in the USA have produced following values for the two constants c_1 and c_2 for a LS-2 collector: [Dudley et al. 1994]

These tests were made with concentric glass tube to attain an evacuated layer or a simple air layer around the absorber tube; and without concentric glass tube.
The equation for the incidence angle modifier ζ_{IAM} as mentioned above is valid from Θ = 0° up to Θ = 60° if constants of the following table are used.

Absorber tube casing	c_1	c_2
glass tube : air / vacuum	0.000884	0.00005369
bare tube	0.0003512	0.00003137

Table 5: Constants for the Incidence Angle Modifier IAM (SEGS LS-2) [Dudley et al. 1994]

With these relationships mentioned above the total power P_{total} received by the absorber tubes of a collector field with **n** rows and the total aperture area A_a (number of collectors times the collector´s aperture area) is

$$P_{total} = G_{cnb} \cdot \zeta_{cos} \cdot \zeta_{shading} \cdot \eta_{opt} \cdot A_a \quad .$$

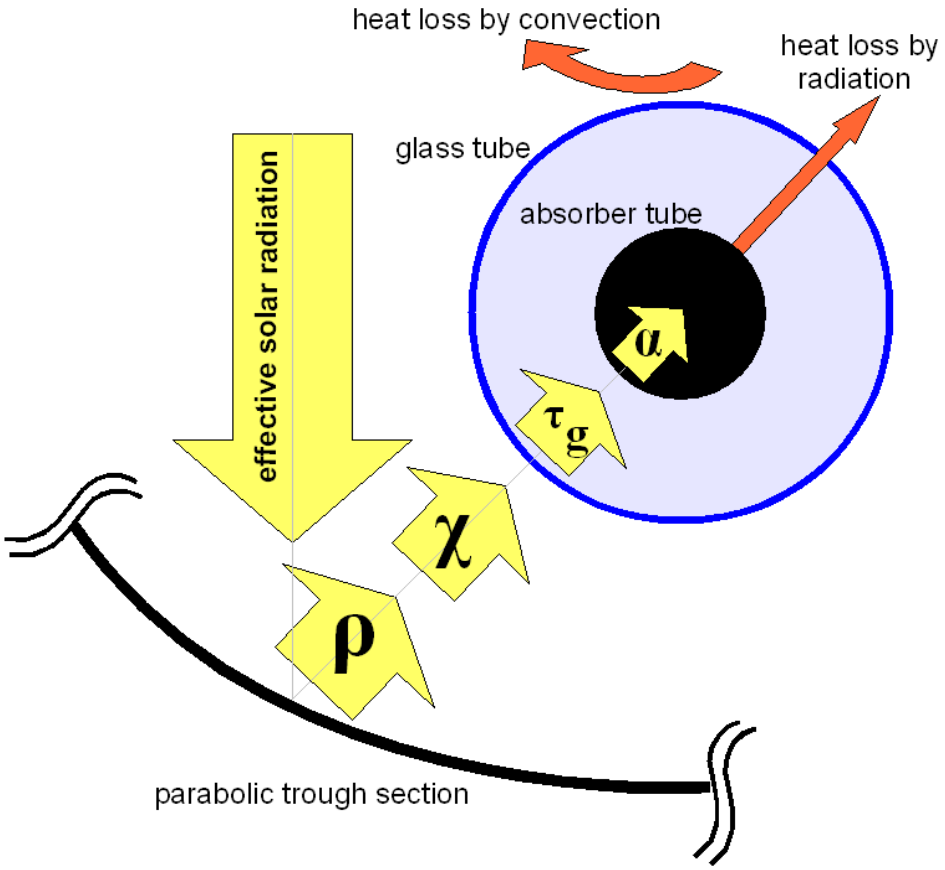

Figure 41: Optical and Thermal Losses - Parabolic Trough Receiver

5.5 Thermal Losses

As described in the previous chapter $\mathbf{P_{total}}$ is the power received by the absorber tubes. Unfortunately, it is not that amount of power that is responsible for the enthalpy raise of the heat transfer fluid. As a matter of principle, the absorber tube is no adiabatic system and thus, thermal losses will occur, due to the forcing temperature difference between the absorber tube and the environment.

These thermal losses can be divided into losses by convection $\mathbf{Q_C}$ and losses by radiation $\mathbf{Q_R}$.

However, the main thermal loss from the absorber tube to the concentric glass tube occurs by radiation. As the evacuated layer does not represent an ideal vacuum, also convective heat transfer happens in some extent, which can be neglected. Consequentially the glass tube loses heat by radiation and by convection (wind and/or natural convection). Additionally, the absorber tube loses heat via the vacuum bellows and supports. [Odeh et al. 1996]

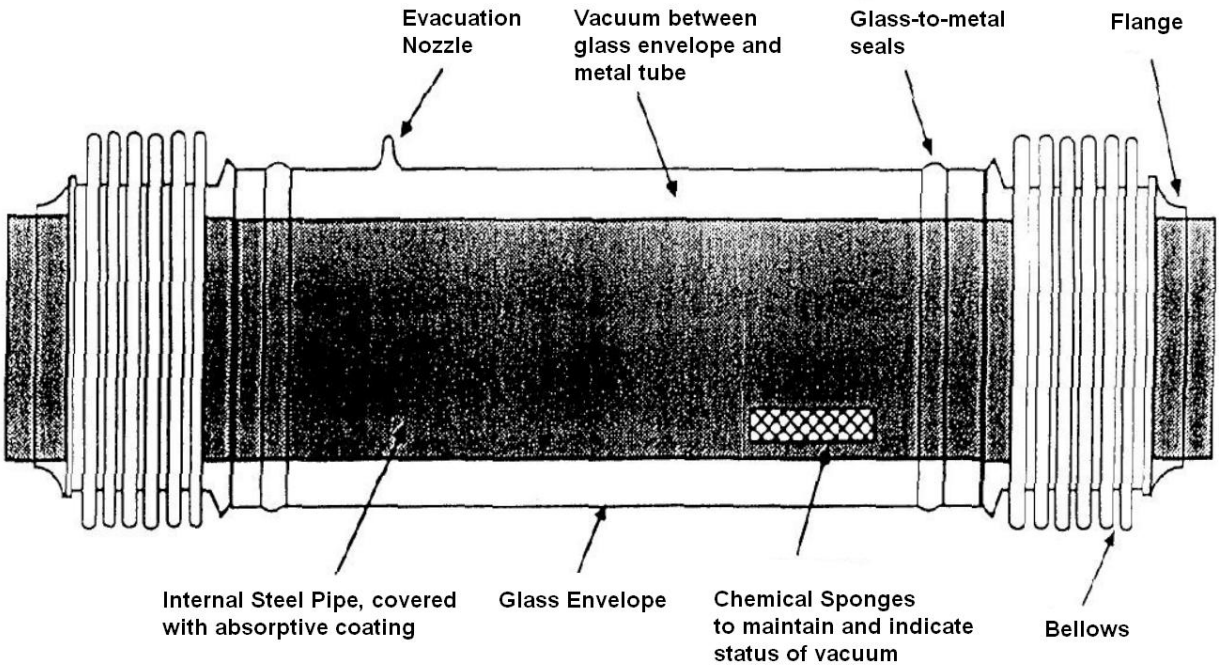

Figure 42: Absorber and Glass Tube, LS-2 Collector [Dudley et al. 1994]

The basic equations for the heat transfer via convection (starting from the outer glass surface) are: [Quaschning 2007]

$$Q_C = A_{tube} \cdot \alpha_C \cdot (T_{glass} - T_{ambient})$$

A_{tube} ….. surface of the surrounding glass tube
α_C …..... heat transfer coefficient (dependent on the wind-speed)
T_{glass} …. temperature of the surrounding glass tube

$T_{ambient}$... ambient temperature

The heat transfer coefficient α_c depends on the Reynolds number **Re** and the empirically established equation for the Nusselt number **Nu**: [Duffie & Beckman 2006]

$$Re = \frac{v_{wind} \cdot D}{\upsilon}$$

v_{wind}..... mean wind speed
D..... outer diameter of glass tube
υ..... kinematic viscosity of the ambient air

$$Nu = 0.40 + 0.54 \cdot Re^{0.52} \qquad \text{for } 0.1 < Re < 1000$$

$$Nu = 0.30 \cdot Re^{0.6} \qquad \text{for } 1000 < Re < 50000$$

$$Nu = \frac{\alpha_C \cdot D}{\lambda}$$

λ..... thermal conductivity of the ambient air

The basic equation for the heat transfer via radiation is: [Quaschning 2007]

$$Q_R = A_{absorber} \cdot \varepsilon \cdot \sigma \cdot \left[\left(\frac{T_{absorber}}{100} \right)^4 - \left(\frac{T_{ambient}}{100} \right)^4 \right]$$

The ambience is assumed as black body and the presence of the concentric glass tube is neglected.

$A_{absorber}$ .. surface of the absorber tube
ε ..... emittance of the absorber tube
σ ..... Stefan-Boltzmann constant $\qquad \sigma = 5.67 \frac{W}{m^2 K^4}$

$T_{absorber}$ ... absorber tube temperature in Kelvin
$T_{ambient}$ ... ambient temperature in Kelvin

With these equations for heat loss by convection and radiation the total absorber heat loss is the sum of the two components [Quaschning 2007]:

$$Q_{loss} = Q_C + Q_R$$

Although this absorber heat loss is governed by the well-known mechanisms of radiation, conduction and convection, it is a common practice to calculate thermal losses by semi-empirical equations developed from measurements.

5.5.1 Empirical Heat Loss Models

One model for the heat loss calculation of a parabolic trough receiver uses a single heat loss coefficient $\mathbf{U_{absorber}}$: [Romero-Alvarez et al. 2007]

$$Q_{loss} = U_{absorber} \cdot \pi \cdot d_o \cdot L_c \cdot \left(T_{absorber} - T_{ambient}\right) \qquad \text{[Watt]}$$

d_o..... outer diameter of the absorber tube
L_c..... absorber tube length (parabolic trough collector length)
$T_{absorber}$... outer absorber tube mean temperature
$T_{ambient}$... ambient temperature

The heat loss coefficient $\mathbf{U_{absorber}}$ depends on the absorber tube temperature and is found experimentally by performing specific thermal loss tests with the parabolic trough collector at several temperatures within its typical working temperature range. This variation of the heat loss coefficient $\mathbf{U_{absorber}}$ is described by the following equation, with the coefficients **a**, **b** and **c**:

$$U_{absorber} = a + b \cdot \left(T_{absorber} - T_{ambient}\right) + c \cdot \left(T_{absorber} - T_{ambient}\right)^2$$

As it is difficult to find values for **a**, **b** and **c** valid for a wide temperature range, different sets of values are given for certain temperature ranges. Following table gives the empirically established values for a LS-3 collector installed at SEGS VIII and IX:

$\mathbf{T_{absorber}}$	**a**	**b**	**c**
< 200	0.687257	0.001941	0.000026
> 200, < 300	1.433242	-0.005660	0.000046
> 300	2.895474	-0.016400	0.000065

Table 6: Coefficients a, b and c for the Heat Loss Coefficient $U_{absorber}$ [Romero-Alvarez et al. 2007]

The following equations show an empirical heat loss model which also takes into account the wind speed. **a**, **b** and **c** are collector specific factors. [Odeh et al. 1996]:

$$Q_{loss} = A_a \cdot \left(\left(a + c \cdot v_{wind}\right) \cdot \left(T_{absorber} - T_{ambient}\right) + \varepsilon \cdot b \cdot \left(T_{absorber}^4 - T_{sky}^4\right)\right)$$

$T_{absorber}$.. outer absorber tube temperature in Kelvin
$T_{ambient}$... ambient temperature in Kelvin
T_{sky}..... sky temperature in Kelvin
v_{wind}..... wind speed in [m/s]
ε ..... absorber emittance
A_a ..... aperture area of the collector

a [W/(K m²)]	b [W/(K^{-4} m²)]	c [J/(K m³)]
0.019182	0.00000000202	0.006612

Table 7: Empirical Factors a, b and c for the LS-3 Collector [Odeh et al. 1996]

The sky temperature $\mathbf{T_{sky}}$ in Kelvin can be calculated by the following formula:
[Duffie & Beckman 2006]

$$T_{sky} = T_{ambient} \cdot \left(0.711 + 0.0056 \cdot T_{dp} + 0.000073 \cdot T_{dp}^2 + 0.013 \cdot \cos(15 \cdot t)\right)^{\frac{1}{4}}$$

$T_{ambient}$... ambient temperature in Kelvin
T_{sky}..... sky temperature in Kelvin
T_{dp}..... dew point temperature in degrees Celcius
t..... hour from midnight

“The range of the difference between sky and air temperatures is from 5°C in a hot, moist climate to 30°C in a cold, dry climate.” [Duffie & Beckman 2006]
In practice the sky temperature is often neglected as it has a rather small effect on the collector`s efficiency; in the range of a few percent. In addition to this it would be quite costly to measure the sensitivity to sky temperature, as the collector tests had to be repeated on days with different sky temperature but everything else being the same (otherwise the effect of sky temperature would be masked by variations in air temperature, solar irradiation and wind speed). Collector test data is reported as a function of ambient temperature, which is equal to air temperature. For high-temperature collectors the effect of sky temperature is so small that one can safely set $\mathbf{T_{sky} = T_{air}}$, even when calculating the instantaneous efficiency. [Rabl 1985]

As can be seen in the 2 figures (43 and 44) below the results of the physical model and the model proposed by Odeh (1996) match quite well in temperature ranges above 290°C, that are typical for parabolic trough collectors. As the model proposed by Romero-Alvarez et al. (2007) does not take the wind-speed into account, a reasonable difference occurs (figure 44).

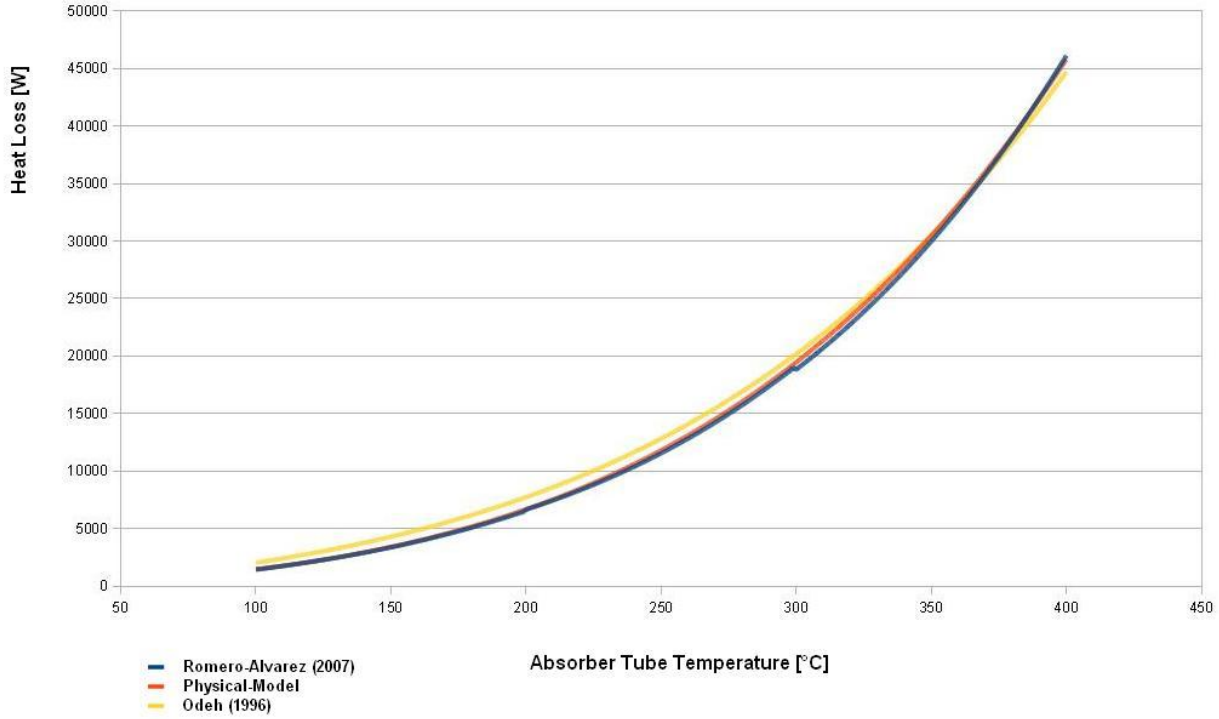

Figure 43: Comparison of the 3 Heat Loss Models at a Windspeed of 0 m/s

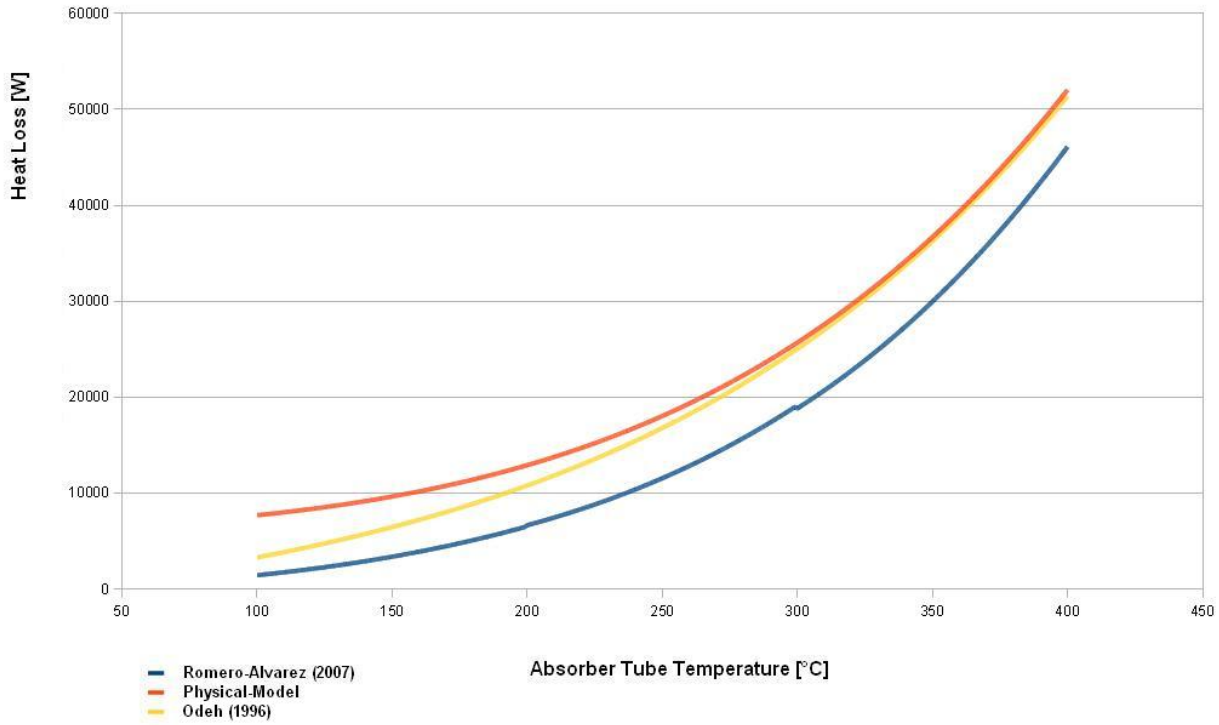

Figure 44: Comparison of the 3 Heat Loss Models at a Windspeed of 5 m/s

5.5.2 Selective Coating of Absorber Tubes

In thermal solar energy conversion, a critical part of the solar collector is the absorber surface, which should absorb a maximum amount of solar radiation and at the same time re-radiate a minimum amount of energy in the thermal infrared range. Thus the reflectivity of the absorber´s surface has to be minimized in the solar spectrum (high absorptivity) and maximized in the infrared spectrum (low emittance). [Farooq & Raja 2008]

As the radiation is received from the sun, absorber surfaces must have a high absorptivity for the solar energy spectrum, of which 98% are below a wavelength of 3 µm. Due to Wien´s displacement law which states that a higher body-surface-temperature leads to a lower wavelength of the emission´s peak, the range of wavelength in which the thermal losses via radiation happen is for the most part above 3 µm. Thus the wavelength range of the emitted radiation (heat loss of the absorber) overlaps only slightly the solar spectrum. Under these circumstances, it is possible to reduce the thermal losses via radiation in developing surfaces that have a high solar absorptivity, but a low long-wave emittance; that is, selective surfaces. [Duffie & Beckman 2006]
Steel absorber tubes of parabolic troughs have an absorptivity greater than 90% in the solar spectrum and a low emittance (less than 30%) in the infra-red range. [Goswami & Kreith 2008]
For a cermet absorber tube coating a practical value for the emittance is 0.16. [Trieb et al. 2004]

Furthermore the emittance ε varies dependent on the actual absorber tube temperature. In fact, the higher the temperature the higher the emittance, which is an additional reason for increasing heat losses at higher absorber tube temperatures. [Odeh et al. 1996]

Equations for the variation of the emittance ε can be given as follows:

LS-3 collector $\varepsilon = 0.00042 \cdot T_{absorber} - 0.0995$ [Odeh et al. 1996]

$\mathbf{T_{absorber}}$... absorber wall temperature in Kelvin

ET-100 collector $\varepsilon = 0.04795 + 0.0002331 \cdot T_{absorber}$ [Montes et al. 2009]

$\mathbf{T_{absorber}}$... absorber wall temperature in °Celcius

5.5.2.1 Mechanisms of Selectivity

Selective coatings consist of a layer of material with a high solar absorptivity that is applied to substrates with low emittance. Thus the coating absorbs solar energy, and the substrate is the poor emitter of long-wave radiation.
For the most part, the layers with high solar absorptivity consist of metal oxides whereas the substrates are metals. [Duffie & Beckman 2006]

High absorptivity layer	***Substrate***
copper oxide	aluminium
copper oxide	copper
nickel-zinc sulfide	galvanized iron
black chrome	nickel plating on a steel or copper base

Table 8: Examples of Selective Coatings Used in Solar Engineering [Duffie & Beckman 2006]

Black chrome selective surfaces with nickel plating, on a steel or copper base, as substrate, have been widely adopted for solar collectors. These coatings are formed by electroplating in a bath of chromic acid and other agents. However, these surfaces are replaced by cermet coatings that achieve better performances.

Cermet is the most attractive selective coating for receiver tubes, operating at medium-high temperatures, in terms of high photo-thermal efficiency and stability. Cermets consist of metallic nano-particles embedded in a ceramic matrix. [Esposito et al. 2009]
Sputtering processes are used to produce cermet selective surfaces on the receiver tubes of concentrating collectors, which operate at temperatures between 300 and 400°C. Four layers are deposited on the receiver´s steel pipe: “an anti-diffusing oxide layer to prevent diffusion of molecules of the steel substrate into the coatings, an infrared reflective layer (to provide low emittance), the cermet absorbing layer, and an anti-reflective oxide layer.” [Duffie & Beckman 2006]

Luz-solar-collectors (LS-3, LS-2) use Mo-Al_2O_3 cermet materials as solar absorber, due to good thermal stability at high operating temperatures in vacuum. These collector tubes sputtered with Mo-Al_2O_3 cermet materials have been mass-produced.
Single cermet layers with an isotropic metal volume fraction, deposited on a metal infrared reflector, such as Cu, and topped by an anti-reflection layer, show a solar absorptivity value of 0.8. However, for solar collectors, a higher absorptivity (> 0.9) is priority. In order to achieve higher absorptivity, graded cermet layers are used, where the metal volume fraction is gradually increased to reduce the reflectivity.
Furthermore, fundamental analysis led to the use of double cermet layer structure (a low metal volume fraction layer LMVF on a high metal volume fraction layer HMVF), that replaced graded cermet layers. [Zhang 2000]
“On examination of multilayer structures it is found that multilayer composites improve the solar absorptivity due to destructive interference effects within the coating.” [Farooq & Hutchins 2002]

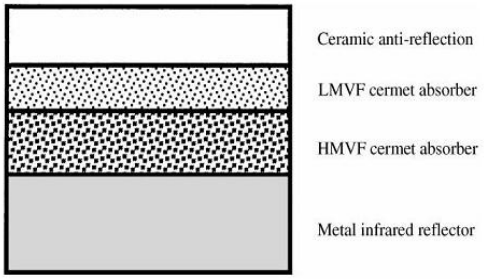

Figure 45: Structure of a Double Layer Cermet Coating [Zhang 2000]

Layer	***Material***	***Absorptivity α / Emittance ε***
anti-reflection	Al_2O_3	$\alpha = 0.96$ $\varepsilon = 0.11$ @ 350°C
LMVF cermet	Mo - Al_2O_3	
HMVF cermet	Mo - Al_2O_3	
infrared reflection	Mo	

Table 9: Example for a Selective Double Cermet Layer Structure with Mo-Al_2O_3 as Cermet [Zhang 2000]

As the rise of the solar field´s working temperature from 390°C to above 450°C will improve performance and reduce costs of power plants, more efficient selective coatings have to be developed. Thermal stability above 450°C, solar absorptivity values higher than 0.96 and thermal emittance values lower than 0.07 are aspired. [Kennedy & Price 2004]

As a single homogeneous cermet film is not able to give high absorptivity values, a more complex structure is necessary. Good values can be achieved by using two homogeneous cermet layers. A low metal volume fraction (LMVF) cermet is deposited on a high metal volume fraction (HMVF) cermet. The HMVF-cermet is deposited on the infrared reflector layer. In addition to high solar performances, this method requires a quite simple fabrication procedure. [Esposito et al. 2009]

This double layer approach enables high efficiency and stability up to 580°C, which is the maximum temperature foreseen for solar coatings at parabolic trough solar power plants. Materials that can be used are: molybdenum as metallic infrared reflector, silica-molybdenum composites as cermet layers and silica as anti-reflection layer. [Esposito et al. 2009]

Emittance values ε that can be reached are 0.072 at 400°C and 0.118 at 580°C, while maintaining a solar absorptivity value α of 0.94. [Esposito et al. 2009]

Layer	***Material***	***Thickness [nm]***	***Absorptivity α / Emittance ε***
anti-reflection	SiO_2	50	$\alpha = 0.94$ $\varepsilon = 0.072$ @ 400°C $\varepsilon = 0.118$ @ 580°C
LMVF cermet	Mo - SiO_2	30	
HMVF cermet	Mo - SiO_2	35	
infrared reflection	Mo	500	

Table 10: Layer Thickness and Materials of a Double Layer Cermet Selective Coating [Esposito et al. 2009]

5.6 The Energy Balance of the Absorber Tube

In the following, the general equations of heat transfer for a cylindrical tube are discussed, in order to calculate the enthalpy rise of the fluid within the absorber tube. The basic equations are valid for all kinds of parabolic trough collectors. Only concerning the correlations for the heat transfer coefficient α_{tube}, a distinction has to be made between two phase flow (DSG) or single phase flow.

In this work the whole IPSEpro collector unit is taken as one element of discretization. The fluid data is determined for the fluid mean temperature. Also the heat-flow equations are based on fluid and absorber tube mean temperatures. Thus, fluid and tube temperatures are higher at the collector end; and smaller at the collector start, respectively. The whole energy balance of each collector is then solved with these assumptions based on collector mean temperatures. As the heat loss of the absorber tube depends on the outer absorber tube temperature it is not possible to model an arbitrary length of collectors just with one IPSEpro collector unit. The accuracy of the calculation results depend on the used collector unit length (length of discretization), suitable values will be proposed later on. Therefore, the real length of one single parabolic trough collector (for instance, the length of one LS-3 collector is 99 meters) does not correspond with the length of the collector unit in IPSEpro. The length of one IPSEpro collector unit is defined by the parameter "element_length". Thus, if one wants to simulate the enthalpy raise of one real collector (100 meters long), there have to be connected two IPSEpro collector units in series, if the suitable element length is 50 meters.

The thermal power that hits the absorber tube is the direct normal irradiance **DNI** multiplied by all the attenuation factors already mentioned before. Due to thermal losses only a certain fraction of that energy flux is finally able to heat the fluid within the absorber tube.

The following definitions are made:

P_{total}..... total radiative power incident on the absorber´s surface (chapter 5.4)
Q_{trans}..... energy flux that finally heats the fluid
Q_{loss}..... heat loss due to radiation and convection

The energy flux that heats the fluid within the absorber tube is the total radiative power incident on the absorber´s surface minus the heat loss due to radiation and convection.

$$Q_{trans} = P_{total} - Q_{loss}$$

The heat loss $\mathbf{Q_{loss}}$ is calculated by one of the before mentioned correlations. Therefore the outer absorber tube temperature, besides ambient temperature and wind speed is needed. The ambient temperature and wind speed are parameters, which have to be set by the user.

The outer absorber tube temperature is a result of the energy balance at steady-state conditions.

$\mathbf{Q_{trans}}$ is defined by the heat transfer equation through a cylindrical tube with a certain thermal conductivity and the equation for heat transfer between the inner tube wall and the fluid. These two equations are

$$Q_{trans} = \alpha_{tube} \cdot \pi \cdot d_i \cdot L_c \cdot \left(T_{inner} - T_{mean} \right)$$ [Baehr & Stephan 1998]

and $$Q_{trans} = \frac{\left(T_{absorber} - T_{inner} \right) \cdot 2 \cdot \pi \cdot L_c \cdot \lambda_{absorber}}{\ln\left(\frac{d_o}{d_i} \right)}$$ [Baehr & Stephan 1998]

T_{mean} ..... heat transfer fluid mean temperature
T_{inner} ..... inner absorber tube mean temperature
$T_{absorber}$ ..... outer absorber tube mean temperature
L_c ..... absorber tube length
$\lambda_{absorber}$ ..... heat conductivity of the absorber tube
d_o ..... outer absorber tube diameter
d_i ..... inner absorber tube diameter
α_{tube} ..... heat transfer coefficient between the fluid and the inner absorber tube wall

Finally, correlations for the calculation of the heat transfer coefficient α_{tube} are necessary. Unlike the other equations mentioned so far in this chapter, these correlations depend on the fluid flowing within the absorber tubes. Thus, one has to distinguish between parabolic trough collectors for oil and those for direct steam generation. Furthermore, the direct steam generation concept requires correlations for preheating, evaporation and super-heating. Suitable correlations will be described in chapter 6.1 , 7.3, 7.5 and 7.6.

In order to solve this energy balance numerically in IPSEpro, reasonable starting values have to be provided (especially for the expected temperature level, dynamic viscosity, kinematic viscosity, heat capacity and thermal conductivity of the heat transfer fluid).

The following figure number 46 shows the difference between long and short elements. A too long element length leads to wrong calculation results, whereas too short elements might increase the computing time unnecessarily. Suitable values for the element length will be discussed in the chapters 6.3.1 (page 89) and 7.8.1 (page 120). In figure 46 a total collector length of 200 meters is assumed. In the upper part there is furthermore an element length of 20 meters assumed, thus separating the absorber tube into 10 sections of discretization. For each section the fluid exit temperature is a calculation result, according to the absorber tube´s energy balance, which takes into account the before mentioned equations and heat loss models. The absorber tube mean temperatures of each section are used to determine the heat loss. The fluid´s exit temperature at the last section is one of the final and wanted results, besides pressure level and enthalpy.
When considering the lower part of figure 46, only one element with the length of 200 meters is used. Therefore, only one value of the absorber tube mean temperature defines the heat loss, which limits the calculation accuracy.

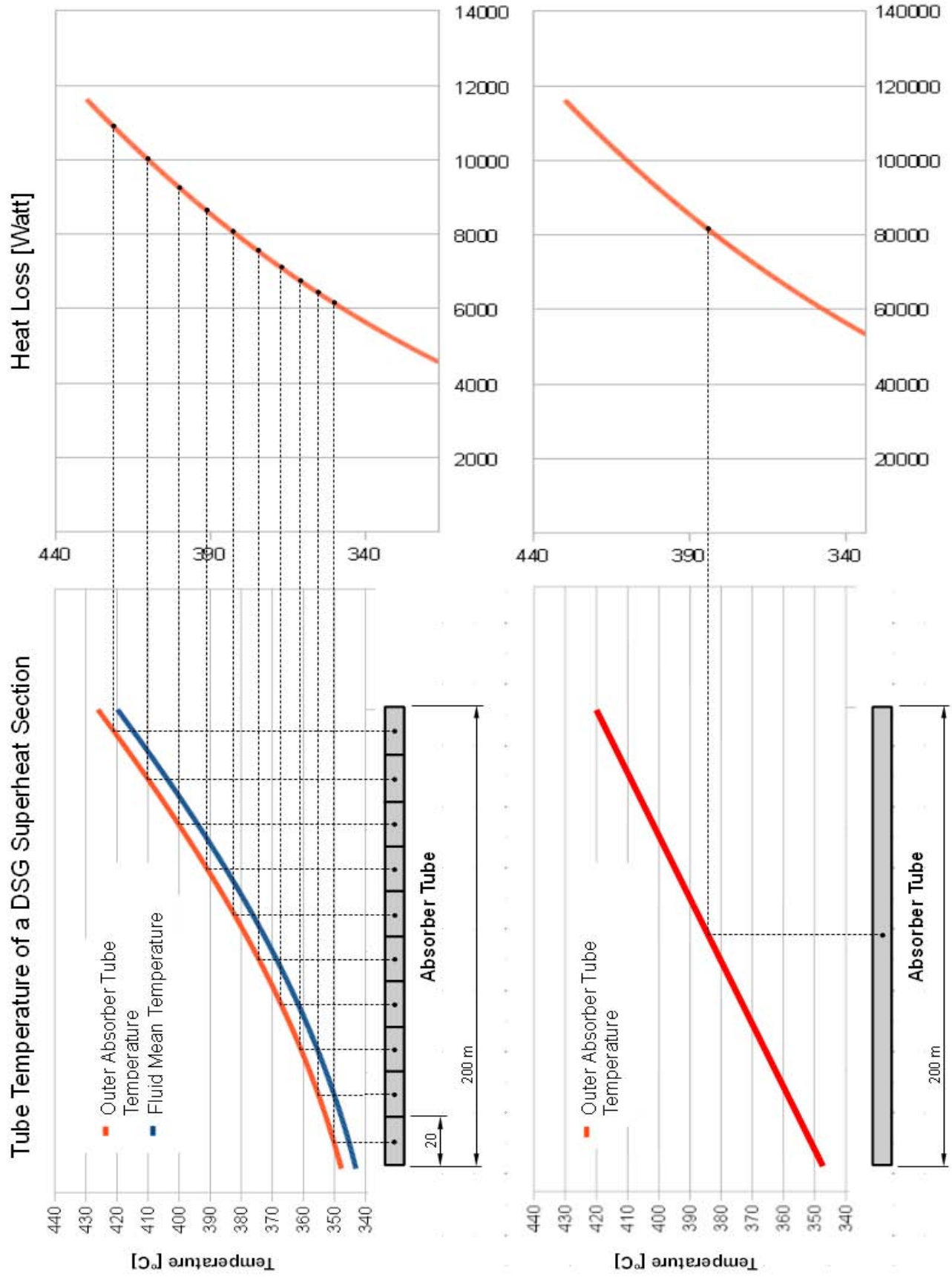

Figure 46: Discretization of the Absorber Tube

5.7 The Implementation in IPSEpro

The properties of heat transfer within the absorber tube depend on the fluid used. Therefore two different solar collector models have been created. There are two different units available in the IPSEpro icon bar. The “T_Solar_collector” unit is suitable for oil as heat transfer fluid, and the “W_Solar_collector” unit for water and steam.

As the correlations for losses and attenuation factors mentioned so far are valid for both collector units (“T_Solar_collector” for Oil and “W_Solar_collector” for DSG), they were inserted in the programme code in the same way.

The following figure show the upper part of the collector unit´s dialogue window. It is the same for both collector types.

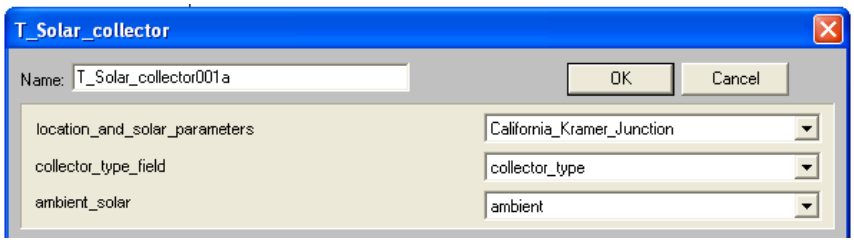

Figure 47: IPSEpro Dialogue Window of the Collector Unit

Besides the global “location_and_solar_parameters” two more globals are necessary to define a collector unit for oil or DSG.

These two globals are “collector_type_field” and “ambient_solar.”

5.7.1 The Global “collector_type_field”

Within the global “collector_type_field” the collector design can be selected. Available are the LS-1, LS-2 and LS-3 collector built by Luz International Limited and the ET-100 collector, developed by the EuroTrough Consortium (Geyer et al. 2002).

The following tables show the collector data implemented.
Note: All values except those for the collector length are automatically assigned to the units if a certain collector type has been selected. The collector length has to be determined by the user via the parameter “element_length”, which defines the level of discretization.

Type	*Width [m]*	*Length [m]*	*Aperture area [m²]*	*Reflectivity*
LS 1	2.5	50	128	0.94
LS 2	5	48	235	0.94
LS 3	5.76	99	545	0.94
ET 100	5.76	98.5	548.35	0.92

Table 11: Collector Data 1 [Romero-Alvarez 2007, Quaschning 2007, Elsaket 2007, Montes et al. 2009, Odeh et al. 1998, Dudley et al. 1994]

Type	*Intercept factor*	*Transmissivity*	*Absorptivity*	*Tube outer diameter [m]*
LS 1	0.87	0.94	0.94	0.0424
LS 2	0.89	0.95	0.95	0.07
LS 3	0.93	0.95	0.96	0.07
ET 100	0.92	0.945	0.94	0.07

Table 12: Collector Data 2 [Romero-Alvarez 2007, Quaschning 2007, Elsaket 2007, Montes et al. 2009, Odeh et al. 1998, Dudley et al. 1994]

Type	*Tube inner diameter [m]*	*Emittance of the outer absorber tube wall*
LS 1	0.032 *	0.39 @ 300°C
LS 2	0.059 *	0.24 @ 300°C (black chrome selective surface) 0.14 @ 350°C (cermet selective surface)
LS 3	0.059	$0.00042 * T_K - 0.0995$
ET 100	0.055	$0.04795 + 0.0002331 * T_{°C}$

*Table 13: Collector Data 3 [Romero-Alvarez 2007, Quaschning 2007, Elsaket 2007, Montes et al. 2009, Odeh et al. 1996, Dudley et al. 1994] * same tube wall thickness assumed*

Type	*Operating temperature [°C]*	
LS 1	307	
LS 2	349 / 390	
LS 3	390	
ET 100	400/500	

Table 14: Collector Data 4 [Romero-Alvarez 2007, Quaschning 2007, Elsaket 2007, Montes et al. 2009, Odeh et al. 1996, Dudley et al. 1994, Geyer et al. 2002]

In the figure below (figure 48) the IPSEpro dialogue window of the global “collector_type_field” is shown.

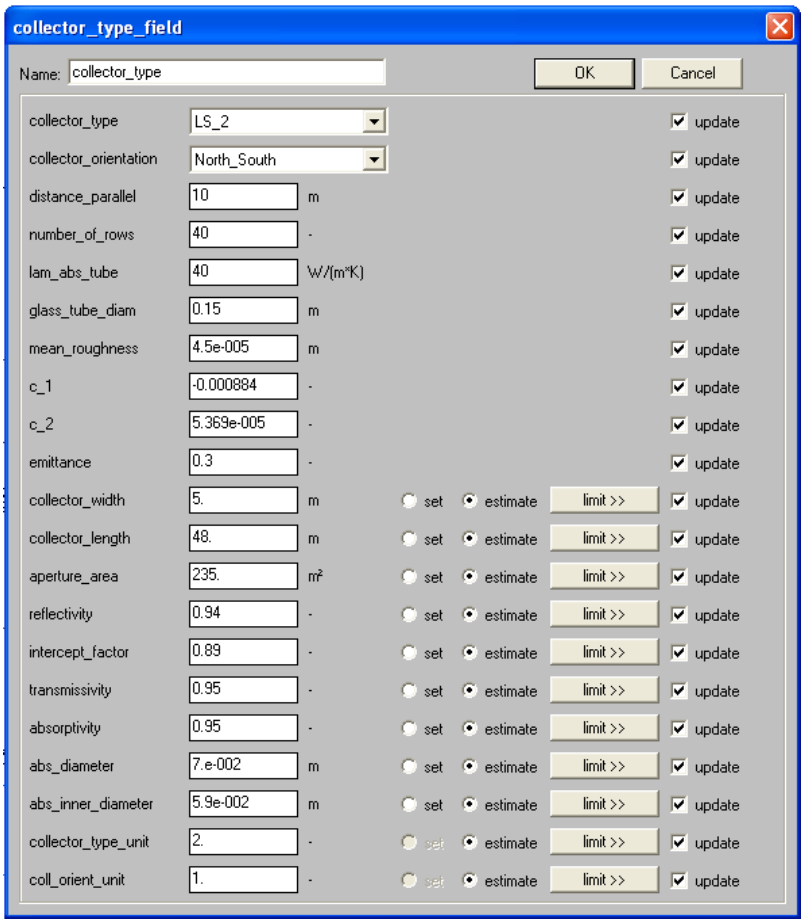

Figure 48: IPSEpro Dialogue Window of the Global "collector_type_field"

Next the orientation of the parabolic trough collector has to be selected via the switch “collector_orientation”. Available is either “North_South” or “East_West”.

The parameters “distance_parallel” (meter) and “number_of_rows” determine the distance between two rows of a collector field and the total number of rows.
These two parameters have an important influence on the shading attenuation factor.

The thermal conductivity (W/mK) of the absorber tube is set by the parameter “lam_abs_tube”.

The outer diameter of the evacuated glass tube is set by the parameter “glass_tube_diam” (meter), which is needed for the physical heat loss model.

The parameter “mean_roughness” is the mean height of the inner absorber tube´s roughness in meters, which is needed to determine the friction factor.

The two parameters “c_1” and “c_2” are only needed if the collector type “user_defined” is selected. These parameters define the incidence angle modifier.
For all the other collector types the constants, originally proposed for the LS-2 collector, are used.

Also the emittance of the absorber tube has only to be set for the collector type “user_defined”.

The same is valid for the remaining variables (“collector_width” until “abs_inner_diameter”). They are calculated automatically for all collector types, except the type “user_defined”. If that is the case they have to be set by the user.

The final two variables “collector_type_unit” and “coll_orient_unit” are just used within the programme code. They cannot be set by the user.

5.7.2 The Global “ambient_solar”

Via the global “ambient_solar” the ambient conditions are defined. The figure below shows the dialogue window with the required parameters.

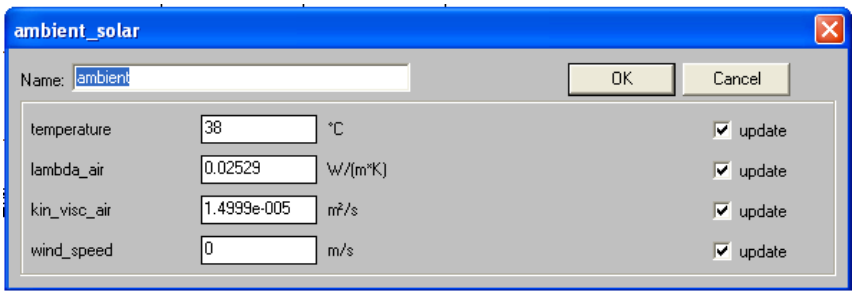

Figure 49: IPSEpro Dialogue Window for the Global "ambient_solar"

In order to define this global the air´s temperature, thermal conductivity “lambda_air” and kinematic viscosity “kin_visc_air” have to be set. Furthermore, the actual wind speed is required.

5.7.3 The Heat Loss Models Available

In the solar collector unit (oil or DSG) three heat loss models can be selected.
This is done by the switch “heat_loss_model”, which can be seen in the following figure.

Either the model “empirical_LS_3”, which corresponds to the model proposed by Romero-Alvarez et al. (2007), the model “empirical_LS_3_wind”, which corresponds to the model proposed by Odeh (1996), or the “physical_model” can be selected. These models correspond to those discussed in chapter 5.5.

Note: The influence of wind speed on the heat loss cannot be considered in the “empirical_LS_3” model.

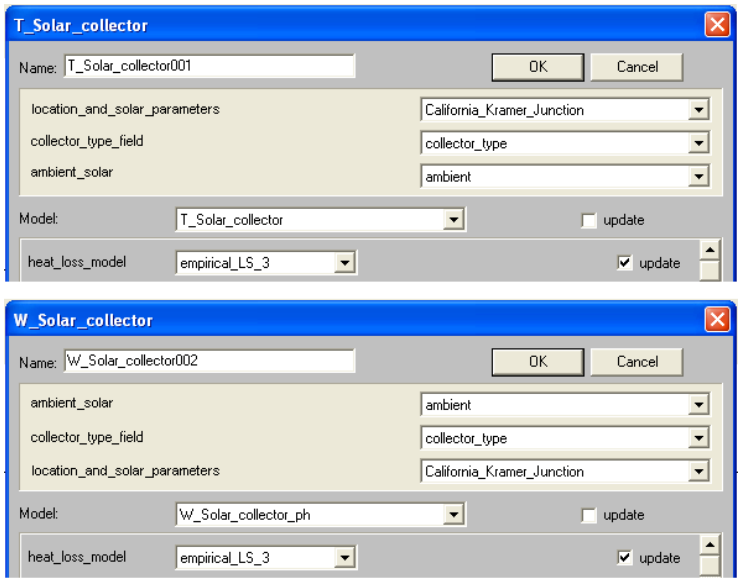

Figure 50: The Upper Parts of the IPSEpro Dialogue Windows for the 2 Solar Collector Units

Having defined all the parameters above, the attenuation factors and the heat loss can be calculated within the programme code.

Concerning the remaining part of the solar collector unit´s dialogue window there has to be distinguished between the unit for oil “T_Solar_collector” and the unit for DSG “W_Solar_collector”. Therefore, this dialogue window will be described in the following chapters, regarding to the corresponding collector type.

The rest of the dialogue window for the “T_Solar_collector” will be described in chapter 6.3.

The rest of the dialogue window for the “W_Solar_collector” will be described in chapter 7.8.

6 The Parabolic Trough Collector Model for Oil as Heat Transfer Fluid

As mentioned in the introduction of chapter 5, it has to be distinguished between the parabolic troughs using oil as heat transfer fluid and those for direct steam generation (DSG).

Within this chapter the unit for oil as heat transfer fluid “T_Solar_collector” will be described in detail.
Correlations for the heat transfer coefficient and the pressure loss are proposed.
The IPSEpro dialogue window will be described.
Furthermore, one chapter deals with the optimum element length for the collector unit, as it is a discrete calculation model.

Figure 51: Parabolic Trough Unit “T_Solar_collector” for Oil as Heat Transfer Fluid in IPSEpro-PSE

6.1 The Heat Transfer Coefficient

As the Nusselt number is defined as $Nu = \frac{\alpha_{tube} \cdot d_i}{\lambda_{fluid}}$, the heat transfer coefficient α_{tube} between the fluid and the inner absorber tube is: $\alpha_{tube} = \frac{Nu \cdot \lambda_{fluid}}{d_i}$

In the following, Nusselt correlations, that can be used for single phase liquid flow are given.

For laminar flow (Re < 2300) and constant heat transfer: $Nu = \frac{48}{11}$ [Marek & Nitsche 2007]

For turbulent flow (Re > 10 000), Dittus & Boelter equation : $Nu = 0.023 \cdot Re^{0.8} \cdot Pr^{0.4}$
[Steiner 2008]

"Nusselt number relations above are fairly simple, but they may give errors as large as 25%. This error can be reduced considerably to less than 10% by using more complex but accurate relations such as the second Petukhov equation (valid for: 0.5 < Pr < 2000, 10^4 < Re < 5 x 10^6):

$$Nu = \frac{(f/8)\cdot Re\cdot Pr}{1.07 + 12.7\cdot(f/8)^{0.5}\cdot(Pr^{(2/3)} - 1)} \quad .$$

The accuracy of this relation at lower Reynolds numbers is improved by modifying it as (valid for: 0.5 < Pr < 2000, 3 x10^3 < Re < 5 x 10^6)

$$Nu = \frac{(f/8)\cdot(Re - 1000)\cdot Pr}{1 + 12.7\cdot(f/8)^{0.5}\cdot(Pr^{(2/3)} - 1)}$$ [Gnielinski 1976],

where the friction factor f can be determined from an appropriate relation such as the first Petukhov equation." [Cengel 2003]

The friction factor f can be determined as follows (first Petukhov equation):

$$f = (0.79\cdot\ln Re - 1.64)^{-2}$$ [Cengel 2003]

Note: Due to very low Prandtl numbers the correlations mentioned above do not apply to liquid metals. [Cengel 2003]

6.2 Pressure Loss

In case of non-disturbed flow in the absorber tube the pressure loss **Δp** can be calculated by the following relation (Darcy & Weisbach equation) [Truckenbrodt 1996]:

$$\Delta p = \frac{f\cdot L_c\cdot\rho}{d_i\cdot 2}\cdot v^2$$

v …..... mean velocity of the heat transfer fluid
ρ …..... density of the heat transfer fluid
f …..... friction factor
L_c ..... length of the absorber tube
d_i ..... inner absorber tube diameter

With constant friction factor, the pressure loss increases with increasing tube length and decreasing tube diameter.
In laminar flow (Re < 2320) the friction factor f only depends on the Reynolds number and can be calculated as follows:

$$f = \frac{64}{Re}$$ [Truckenbrodt 1996]

The friction factor f in fully developed turbulent flow depends on the Reynolds number and the relative roughness ε_r/d_i. The relative roughness is the ratio of the mean roughness height ε_r of the

pipe to the pipe diameter $\mathbf{d_i}$.
This relationship cannot be obtained from a theoretical analysis. Only experiments using artificially roughened surfaces can give equations for the friction factor.

With following correlation, known as the **Colebrook equation**, the friction factor can be calculated for transitional and turbulent flow:

$$\frac{1}{\sqrt{f}} = -2 \cdot \log\left(\frac{2.51}{Re \cdot \sqrt{f}} + \frac{0.27 \cdot \varepsilon_r}{d_i} \right) \quad \text{[Truckenbrodt 1996]}$$

As this equation is implicit in f the determination of the friction factor requires some iteration unless a suitable equation solver is used.

The pressure loss in the IPSEpro unit is calculated by the equations mentioned above. As only turbulent flow occurs, the friction factor is calculated by the Colebrook equation.

6.3 The Collector Unit for Oil in IPSEpro

The describing equations were included in the solar collector unit using the IPSEpro Model Developing Kit (MDK). In this chapter, the basic setup of the unit “T_Solar_collector” is going to be explained.

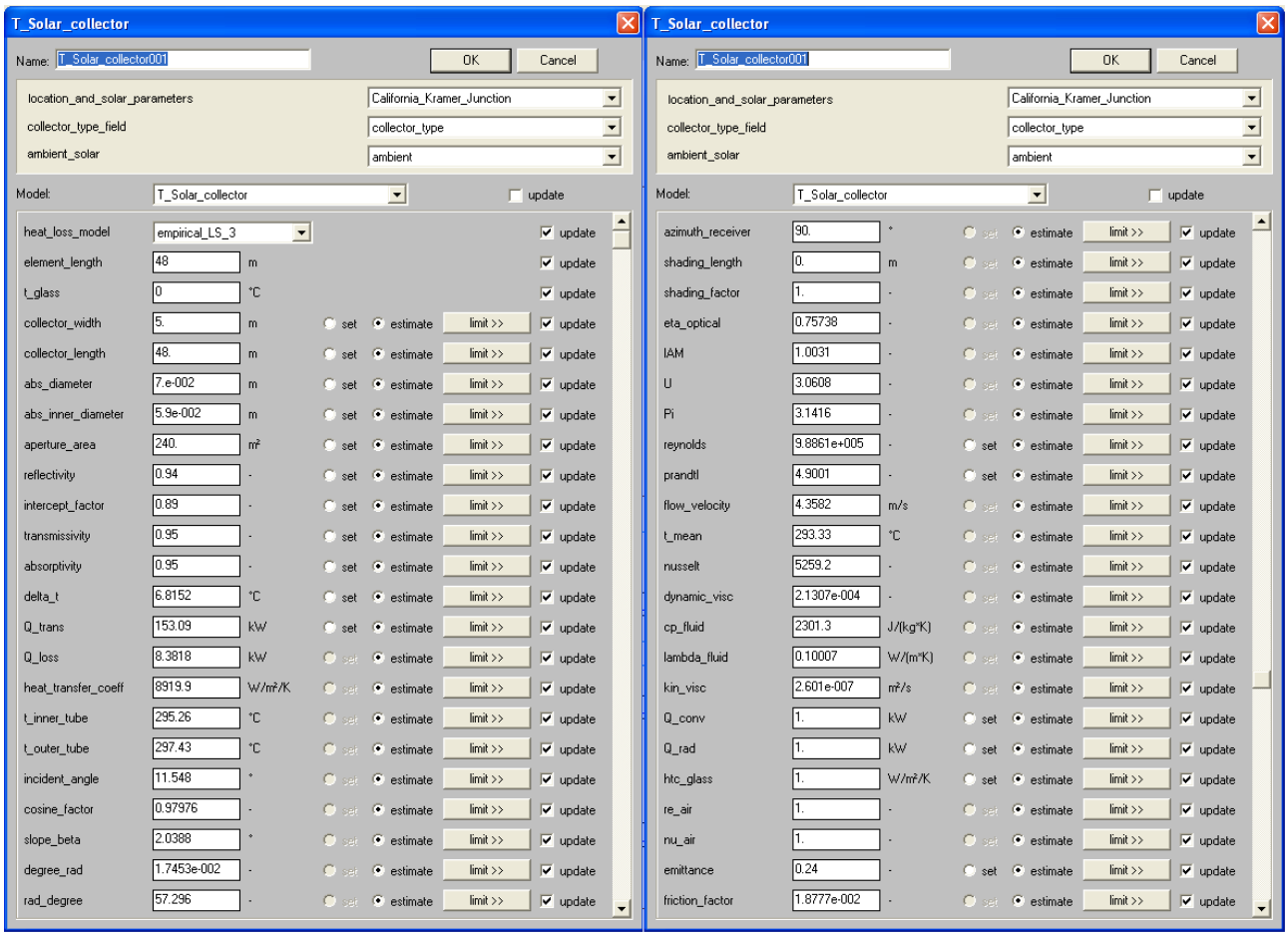

Figure 52: IPSEpro Dialogue Window for the Unit "T_Solar_collector"

After having fitted a new solar collector unit “T_Solar_collector” in a PSE project file, several settings have to be made.

At first 3 globals have to be selected. The first one is of the type “location_and_solar_parameters”, the second one is of the type “collector_type_field” and the third one is an “ambient_solar” global.

No special selection has to be made at the next line. There is only one single model available for the “T_Solar_collector”.

Next, the heat loss model has to be chosen. The models available have already been described in chapter 5.7.3.

The parameter “element_length” defines the absorber tube length for each unit within the IPSEpro project. With this parameter the level of discretization is determined. Suitable values are discussed in chapter 6.3.1.
In order to reach the total absorber tube length required, several collector units have to be connected in series. Of course for each of them the same globals and heat transfer models have to be selected.

The parameter “t_glass” is only necessary for the physical heat loss model. It has to be determined by measurements. Therefore, if another heat loss model is used it can be set to zero.

The remaining part of the dialogue window shows variables that are needed for the calculation and should not be set by the user. They are explained in detail within the appendix.

In order to avoid possible convergence problems, the default values of the used variables should be loaded before starting the first calculation.
When setting the feed pressure, the feed temperature and the mass flow to fixed values the unit is fully defined and ready for the solving process. However, if the default values loaded do not correspond to the actual settings, there might occur errors while running the solver. Therefore it is sometimes better to set the Reynolds number at a fixed value first (instead of the mass flow), run the calculation to get appropriate estimates, import the estimates and approach the intended settings by several calculation steps then. As soon as the correct estimates are imported, calculation will converge.

6.3.1 Suitable Element Length for the Absorber Tube´s Discretization

The maximum length of the element that keeps the inaccuracy within suitable limits is discussed in this chapter.

In order to determine the element length necessary, the following calculations have been made within an IPSEpro-PSE project.

The total collector length assumed for this example is 400m.
As a start, one IPSEpro collector unit is used to simulate the 400 meters of parabolic troughs. Thus, for given start values (pressure, temperature and mass flow are set) and a fixed solar irradiation the outlet conditions (pressure, temperature) are calculated.

Then, step by step, the element´s length is reduced to 200m (2 elements), 100m (4 elements) and finally to 40 m (10 elements).
The data of each element (heat loss, heat transferred, pressure drop, absorber tube temperature) is displayed in a data frame and then copied in an OpenOfficeCalc spreadsheet. Next, the total pressure drop, the total heat transferred and the total heat loss is plotted versus the element length. At the optimum element length the curve´s slope approaches the value zero or its tangent becomes horizontal.

As it can be seen in the figure 53 below, this is the case for an element length of 50 meters. Considering the small variations in total heat loss (about 3%), it should be accurate enough if an element length of 50 meters is used. Since the total variation in pressure drop is even smaller (only 0.2%), it can be neglected that the graph of the pressure drop converges at an element length of

about 25 meters.

The IPSEpro-PSE project files used for this example are shown in the appendix chapter B.

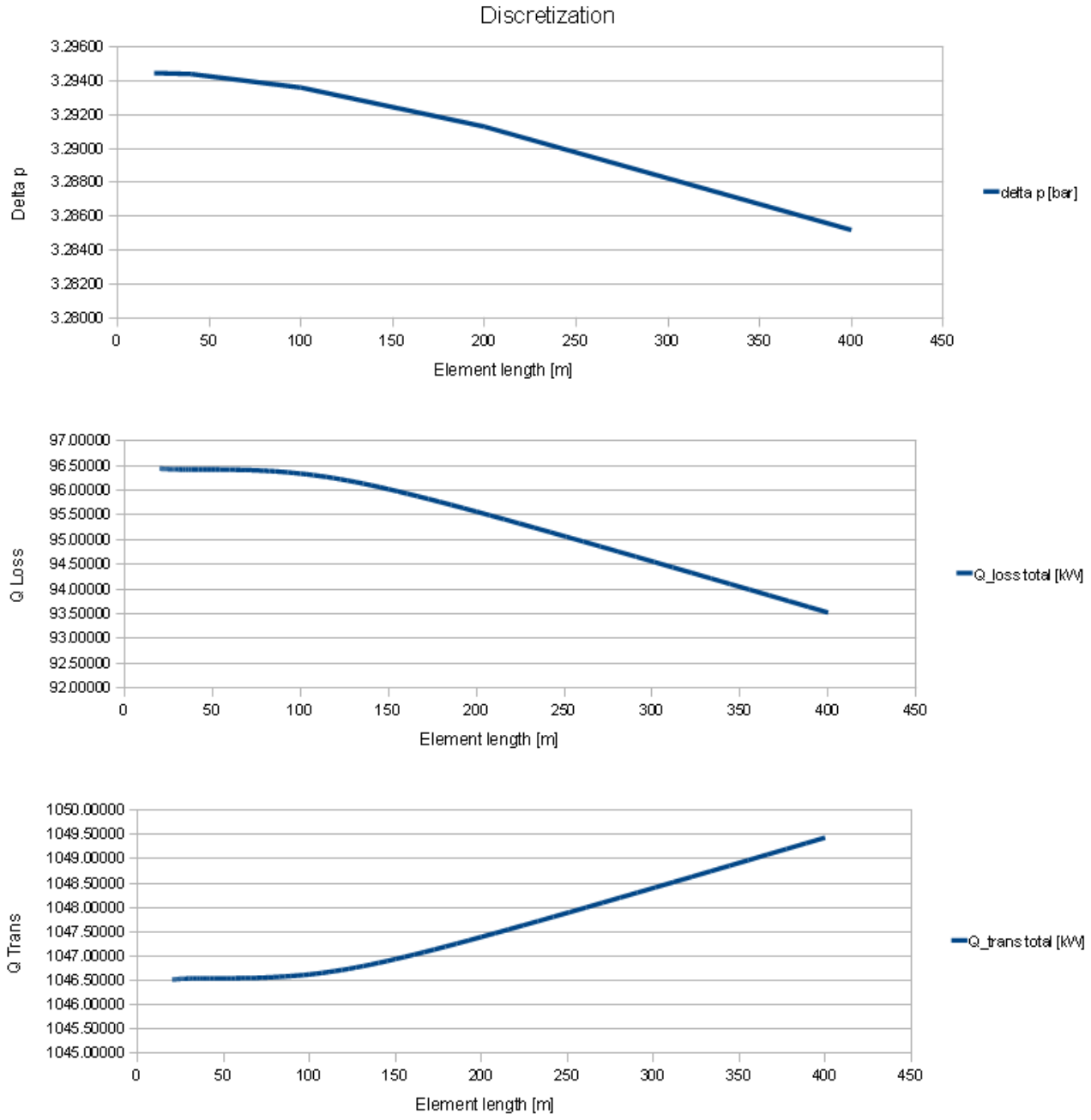

Figure 53: Element Length for the Oil Collector Unit

7 The Parabolic Trough Collector Model for Direct-Steam Generation (DSG)

Within this chapter the unit for DSG “W_Solar_collector” will be described in detail.
Correlations for the heat transfer coefficient and the pressure loss are proposed, depending on whether the preheating section, the evaporating section or the superheating section is modelled.

The IPSEpro dialogue window will be described.

Furthermore, one chapter deals with the optimum element length for the collector unit, as it is a discrete calculation model.

In order to understand heat transfer and pressure loss correlations suitable for the water-steam two-phase flow, which is by far more complicated than the single phase flow, some theoretical aspects have to be discussed.
The direct steam generation collector models have to be suitable for the preheating section (single phase flow water), for the evaporating section (two phase flow) and for the superheating section (single phase flow steam). Therefore, for each section, correlations for the heat transfer coefficient and for the pressure loss have to be found.

Before I actually start proposing specific correlations, I would like to begin with a general overview. I will describe what two-phase flow actually is, how it can be defined and classified.

Then I discuss all possible types of boiling within a tube, as heat transfer coefficients strongly depend on them.

Finally a convenient correlation for the heat transfer (concerning the recirculation concept) and pressure loss is found and implemented.

Unfortunately, in two-phase flow certain flow instabilities occur, that make the controllability more difficult. Therefore an important instability (Ledinegg instability) is described.

7.1 Two-Phase Flow in a Horizontal Pipe

“The main characterizing feature of two-phase flows is the fact that an interface exists between the two phases and, in gas-liquid flows, this interface takes a wide variety of forms. There is an almost infinite range of possibilities, but, in general, the surface tension effects tend to create curved interfaces leading to spherical shapes (e.g. droplets or bubbles). The bigger the occlusion of the discontinuous in the continuous phase, the bigger the departure from a spherical shape. Thus, small droplets tend to be spherical whereas bigger ones are often deformed in the gas flow, and likewise with bubbles.” [Butterworth & Hewitt 1977]

The description can be simplified by classifying types of interfacial distribution and calling these “flow patterns”. [Butterworth & Hewitt 1977]

There are the following main flow patterns possible: bubbly, intermittent, stratified, annular and spray or mist flow. The wavy flow, as mentioned in figure number 54, can be considered as a special case of the stratified flow. However, a clear distinction between these patterns cannot be made, as there are transition zones between them.

Dangerous temperature gradients between the lower and the upper side of the pipe can be avoided in bubbly and intermittent flow, as the steel absorber pipe´s inner wall is well-wetted. There is a good heat transfer coefficient all the way around the pipe, because the liquid phase is not stratified.

In the spray or mist flow, there is an equal distributed heat transfer coefficient too, thus avoiding a dangerous temperature gradient.

In the stratified flow the steam stays above the water´s surface and therefore the heat transfer coefficient is unequally distributed over the tube´s surface. The heat transfer coefficient in the steam section of the pipe can be very low and temperature differences larger than 100°C may occur between the lower and the upper side of the pipe, when it is heated from one side. The resulting thermal stress and bending may destroy the pipe.

Whether the absorber pipe is heated from the side or from underneath can be explained as follows:
As the collector is tracking the sun, it is horizontal at solar noon and tilted in the morning or afternoon (north-south orientation). The pipe is heated from the side (surface of the water in the tube stays horizontally) in the tilted positions, causing high temperature gradients.
In the horizontal position, the concentrated solar radiation hits the absorber tube from underneath, mainly in that section where the water is flowing and thus a good heat transfer coefficient prevails.

In the annular flow there is a thin film of water wetting the upper part of the pipe, too, that causes good heat transfer coefficients all way around the pipe. Therefore no dangerous temperature gradients occur.

Nevertheless, the problems due to two-phase flow can be avoided using suitable direct steam generation concepts.

[Romero-Alvarez et al. 2007]

It is important to estimate the prevailing flow pattern though, as the heat transfer coefficients in non-wetted areas of the pipe are 10 to 20 times smaller (depending on the flow velocity of the

steam) than in areas covered by the liquid phase. [Goebel 1998]
Once the prevailing flow pattern is known, the heat transfer coefficients can be determined. [Odeh et al. 1998]

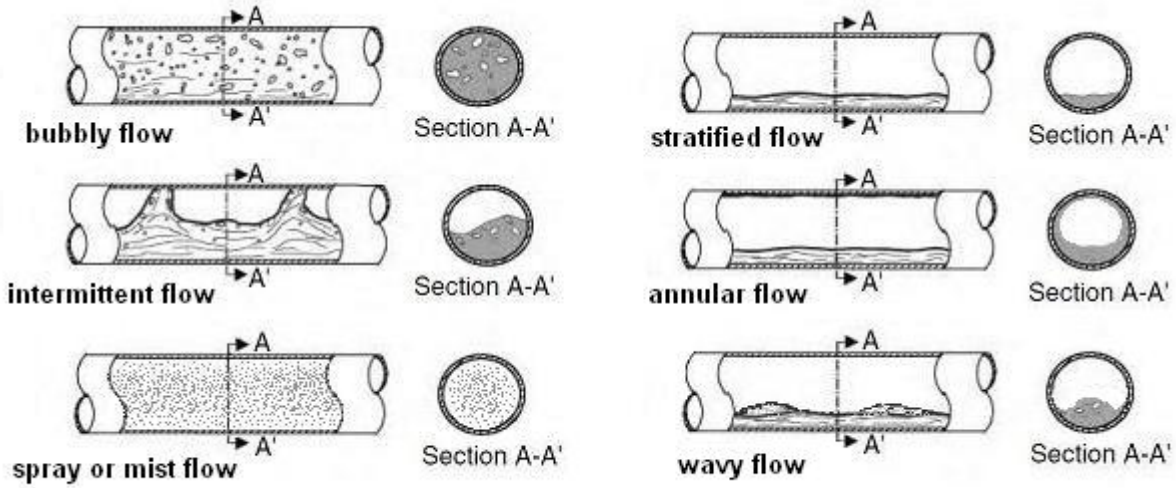

Figure 54: Two-Phase Flow Patterns

7.1.1 Flow Pattern Maps

For the design of systems where two-phase flow occurs, flow pattern maps may be helpful to get a first estimate of the prevailing flow conditions. As an example the flow pattern map created by Mandhane et al. (1974) is shown in the following figure.

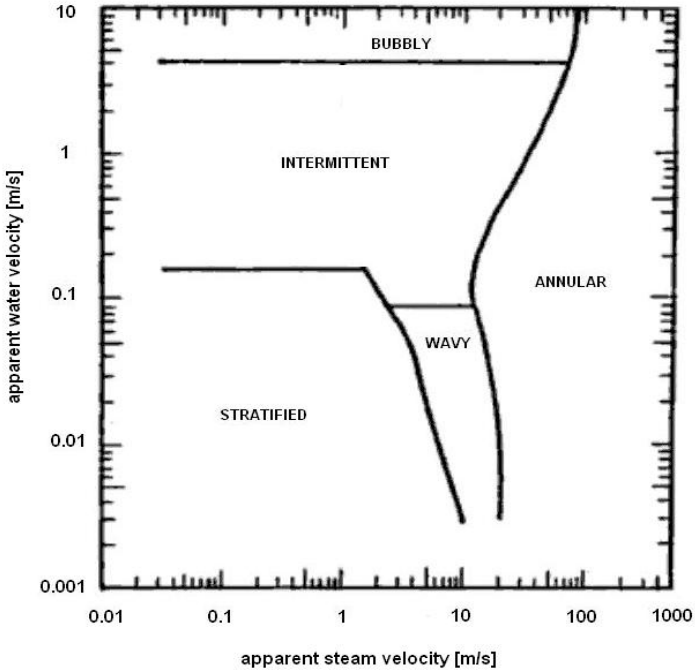

Figure 55: Flow Pattern Map [Mandhane et al. 1974, as cited by Goebel 1998]

In dependence on the apparent velocity (or superficial velocity) of the gas or steam phase $\mathbf{w_{St}}$ and the apparent velocity of the liquid phase $\mathbf{w_L}$, the different flow patterns are plotted. The apparent velocity of a phase is the velocity it would have if it had the whole cross section for itself. [Goebel 1998]

$$w_{St} = \frac{\dot{m}_{St}}{\rho_{St} \cdot A_c} \qquad w_L = \frac{\dot{m}_L}{\rho_L \cdot A_c}$$

ρ_{St}..... density of the gas or steam phase [kg/m³]
ρ_L..... density of the liquid phase [kg/m³]
w_{St}..... apparent velocity of the gas or steam phase [m/s]
w_L..... apparent velocity of the liquid phase [m/s]
$\dot{m}_{St}$ ... mass flow of steam phase [kg/s]
$\dot{m}_L$ ... mass flow of liquid phase [kg/s]
A_c..... cross sectional area of the pipe [m²]

This diagram was developed by using the results of about 6000 experiments and plotting each flow pattern in dependence on $\mathbf{w_{St}}$ and $\mathbf{w_L}$. The lines shown in the diagram, separating the different flow patterns, have to be taken more as transition regions than strict boundaries. Thus, the diagram is absolute empirical and depends on the governing pressure. [Goebel 1998]

A flow pattern map (figure 56) based on analytic models that does not depend on the pressure is described as follows [Taitel & Dukler 1976, as cited by Mayinger 1982]:

On the abscissae the Lockhart-Martinelli parameter **X** is plotted, which represents the ratio of frictional pressure drop of the liquid phase to that of the gas phase.

$$X = \left(\frac{\rho_{St}}{\rho_L}\right)^{0.5} \cdot \left(\frac{\eta_L}{\eta_{St}}\right)^{0.1} \cdot \left(\frac{1-\dot{x}}{\dot{x}}\right)^{0.9}$$ [Mayinger 1982]

ρ_{St}..... density of the gas or steam phase
ρ_L..... density of the liquid phase
η_{St}..... dynamic viscosity of the gas or steam phase
η_L..... dynamic viscosity of the liquid phase
$\dot{x}$ ..... steam mass fraction of the flow

There are two ordinates. On the left-hand side the parameter $\mathbf{F_2}$ is plotted, and on the right-hand side the parameters $\mathbf{F_1}$ and $\mathbf{F_3}$.

To determine whether there is stratified or wavy flow inside the tube (line c), the parameters $\mathbf{F_2}$ and **X** have to be evaluated and mapped.

$$F_2 = \frac{\rho_{St} \cdot w_{St}^2 \cdot w_L}{(\rho_L - \rho_{St}) \cdot g \cdot \upsilon_L \cdot \cos\beta_{tilt}}$$ [Mayinger 1982]

w_{St}..... apparent velocity of the gas or steam phase
w_L..... apparent velocity of the liquid phase
ρ_{St}..... density of the gas or steam phase
ρ_L..... density of the liquid phase
g…..... acceleration due to gravity
υ_L..... kinematic viscosity of the liquid phase
β_{tilt}..... tilt angle of the pipe (usually zero, as the absorber tubes are horizontal); positive value for tilt downstream

If the result is stratified flow it is definite.

But if the result is wavy flow, one has to evaluate the parameter $\mathbf{F_1}$, too, in order to check whether it really is wavy flow because annular or intermittent flow are also possible (line a and b).

$$F_1 = \left(\frac{\rho_{St}}{\rho_L - \rho_{St}}\right)^{0.5} \frac{w_{St}}{(d_i \cdot g \cdot \cos\beta_{tilt})^{0.5}}$$ [Mayinger 1982]

ρ_{St}..... density of the gas or steam phase
ρ_L..... density of the liquid phase
w_{St}..... apparent velocity of the gas or steam phase
g…..... acceleration due to gravity

β_{tilt}..... tilt angle of the pipe (usually zero, as the absorber tubes are horizontal); positive value for tilt downstream
d_i ..... inner absorber tube diameter

In the case that F_1 indicates wavy or annular flow, it is definite.

If the evaluation of parameter F_1 indicates intermittent flow, one has to check parameter F_3, because bubbly flow is possible, too (line d).

$$F_3 = \left[\frac{|dp/dz|_{liquid}}{(\rho_L - \rho_{St}) \cdot g \cdot \cos \beta_{tilt}} \right]^{0.5}$$ [Mayinger 1982]

ρ_{St}..... density of the gas or steam phase
ρ_L..... density of the liquid phase
g..... acceleration due to gravity
β_{tilt}..... tilt angle of the pipe (usually zero, as the absorber tubes are horizontal); positive value for tilt downstream
$|dp/dz|_{liquid}$ ..... frictional pressure gradient assuming the liquid to flow alone in the pipe

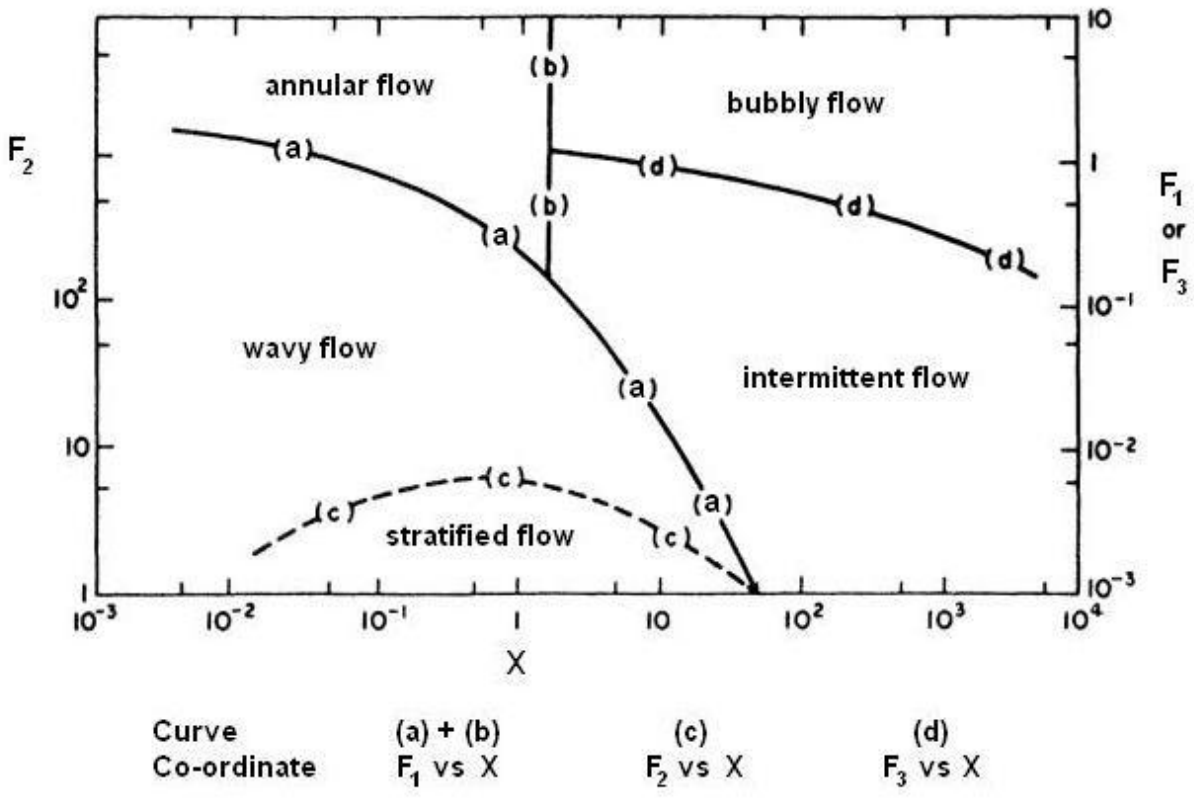

Figure 56: Flow Pattern Map for Horizontal Flow [Taitel & Dukler 1976, as cited by Collier & Thome 1996]

As it was mentioned concerning the flow pattern map by Mandhane, the lines shown in the diagram above, separating the different flow patterns, have to be taken more as transition regions

than strict boundaries.
For instance, as the flow in a parabolic trough receiver tube (direct steam generation) exceeds the line **(a)** between wavy and annular flow, it is obvious that there will occur a transitional flow, that is, the open annular flow. [Goebel 1998]

7.1.2 Fundamental Terms and Definitions of the Two - Phase Flow

In order to describe the boiling heat transfer several fundamental terms and definitions are necessary.

Let´s assume a pipe in which a certain two-phase flow pattern prevails. If a particular cross-section in that pipe is looked at, the total cross-sectional area $\mathbf{A_c}$ can be separated into two parts. That is, the cross-sectional area of the steam phase $\mathbf{A_{St}}$ and the cross-sectional area of the liquid phase $\mathbf{A_L}$. Thus, there can be defined the **void fraction** ε_v in the following way : [Stephan 1988]

In a sufficient small segment of the tube with the length $\mathbf{\Delta z}$ the areas $\mathbf{A_{St}}$ and $\mathbf{A_L}$ do not vary and

$$\varepsilon_v = \frac{A_{St} \cdot \Delta z}{A \cdot \Delta z} = \frac{V_{St}}{V_t} \quad \text{, respectively} \quad 1 - \varepsilon_v = \frac{V_L}{V_t} \quad .$$

V_t..... total volume [m³]
V_{St}..... volume of steam phase [m³]
V_L..... volume of liquid phase [m³]

This **void fraction (volumetric steam quality)** ε_v has to be distinguished from the **volumetric flow steam quality** $\dot{\varepsilon}_v$, which is determined by the volume flows as follows: [Stephan 1988]

$$\dot{\varepsilon}_v = \frac{\dot{V}_{St}}{\dot{V}_t}$$

$\dot{V}_{St}$ …volume flow of steam phase [m³/s]
$\dot{V}_t$ ….total volume flow (steam + liquid phase) [m³/s]

The ratio of the steam mass flow to the total mass flow in the tube is called the **flow steam mass fraction (flow steam quality)** $\dot{x}$: [Stephan 1988]

$$\dot{x} = \frac{\dot{m}_{St}}{\dot{m}} \quad \text{, respectively} \qquad 1 - \dot{x} = \frac{\dot{m}_L}{\dot{m}}$$

$\dot{m}_{St}$ .. mass flow of steam phase [kg/s]
$\dot{m}_L$ ... mass flow of liquid phase [kg/s]
$\dot{m}$ … total mass flow within the tube [kg/s]

Note: The **flow steam quality** $\dot{x}$ has to be distinguished from the **steam quality** x used in thermodynamic tables, which is defined as follows:

$$x = \frac{m''}{m' + m''}$$

m'' ... mass of the saturated steam [kg]
m' ... mass of the boiling liquid [kg]

With the steam mass flow $\dot{m}_{St}$ and the liquid mass flow $\dot{m}_L$, the velocities of the two phases can be calculated, flowing through the cross-sections $\mathbf{A_{St}}$, and $\mathbf{A_L}$ respectively: [Stephan 1988]

$$u_{St} = \frac{\dot{m}_{St}}{\rho_{St} \cdot A_{St}} = \frac{\dot{x} \cdot \dot{m}}{\rho_{St} \cdot \varepsilon_v \cdot A_c}$$

$$u_L = \frac{\dot{m}_L}{\rho_L \cdot A_L} = \frac{(1 - \dot{x}) \cdot \dot{m}}{\rho_L \cdot (1 - \varepsilon_v) \cdot A_c}$$

u_{St}..... velocity of the steam phase [m/s]
u_L..... velocity of the liquid phase [m/s]

The ratio of the two velocities mentioned above is called **slip s**: [Stephan 1988]

$$s = \frac{u_{St}}{u_L} = \frac{\dot{x} \cdot (1 - \varepsilon_v) \cdot \rho_L}{(1 - \dot{x}) \cdot \varepsilon_v \cdot \rho_{St}}$$

Note: If the slip **s** is equal to 1, that is $\mathbf{u_{St} = u_L}$, the volumetric steam quality ε_v is equal to the volumetric flow steam quality $\dot{\varepsilon}_v$ and the flow steam quality $\dot{x}$ is equal to the steam quality x . [Mayinger 1982]

$$\dot{\varepsilon}_v = \frac{\dot{V}_{St}}{\dot{V}} = \frac{u_{St} \cdot A_{St}}{u_{St} \cdot A_{St} + u_L \cdot A_L} = \frac{A_{St}}{A_c} = \varepsilon_v$$

As the density of the liquid and steam phase are determined by the thermodynamic state of the mixture, in a calculation model either the slip **s** or the local volumetric steam quality ε_v can be set. The second variable is given by the slip-equation mentioned above. [Mayinger 1982]

Forcing parameters for the slip are the pressure gradient in the tube and the buoyancy. The higher flow velocity of the steam phase is mainly reduced by the impulse exchange between the two phases, which increases with a growing extent of mixture. [Mayinger 1982]

Thus, the slip **s** increases

- with an increasing ratio of the liquid´s density to the steam´s density.
- decreasing viscosity of the liquid.
- when flow patterns prevail that keep the phases separated.
  [Mayinger 1982]

Practical values for the slip **s** are between 1 and 10. For higher pressures (from 30% to 90% of the critical pressure) the slip **s** varies between 1.7 and 1.1. [Mayinger 1982]

An useful correlation for the slip ratio **s** is given by Collier & Thome (1996):

$$s = \left[1 + \dot{x} \cdot \left(\frac{\rho_L}{\rho_{St}} - 1\right)\right]^{1/2}$$

$\dot{x}$ …. flow steam quality
ρ_L..... density of the liquid phase [kg/m³]
ρ_{St}..... density of the steam phase [kg/m³]

7.2 The Distinct Regions of Boiling Heat Transfer

As long as the tube wall temperature stays below the critical steam-bubble-formation temperature, the heat is transferred by single-phase forced flow (correlates with region **a** in figure 57), which can be described by equations that were already mentioned.

If the tube wall is superheated sufficiently, which means that the tube wall has reached a certain temperature above the saturation temperature $\mathbf{T_s}$ according to the prevailing pressure, steam bubbles form, although parts of the liquid are still sub-cooled (sub-cooled boiling region **b**). In this region the tube wall temperature is almost constant and its value is a little above saturation temperature.

When the mean temperature of the liquid has approached the saturation temperature $\mathbf{T_s}$, the initial point of the bulk boiling region **c** is reached. Within the bulk boiling region the heat transfer is for the most part determined by the formation of steam bubbles. The influence of convection is marginal. This region also includes plug flow and parts of the annular flow, as long as there are steam bubbles forming along the tube wall.

In the following region the liquid film´s thickness is reduced to a value where sufficient super-heating is suppressed and steam bubbles cannot form any more. For the most part the heat is conducted through the liquid film which vaporises at its surface. It is the region of forced convective heat transfer through liquid film (**d**).

Once the liquid film is completely evaporated, the tube wall´s temperature increases. This transition is called “dryout” and initiates the liquid deficient region **e**. Spray flow is prevailing.

When the liquid droplets are finally evaporated the region of convective heat transfer to vapour follows (**f**).

[Stephan 1988]

In the following figure these regions mentioned above are shown. A horizontal absorber tube that is heated from underneath is assumed. The tube wall temperature shown is that of the lower side.

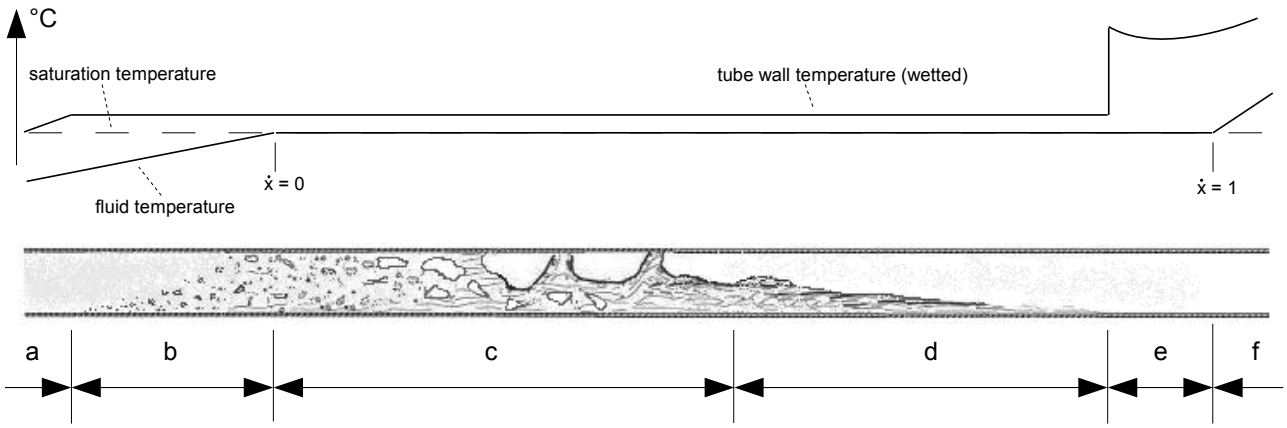

Figure 57: Example of Boiling Regions within an Horizontal Absorber Tube: (a) convection to single-phase liquid flow, (b) sub-cooled boiling, (c) bulk boiling, (d) forced convective heat transfer through liquid film, (e) liquid deficient region - dryout, (f) convective heat transfer to vapour

7.2.1 Sub-Cooled Boiling

If liquid enters a heated tube with less than saturation temperature, heat is transferred by single-phase forced flow as long as the tube wall is not sufficiently superheated. Thus, when this is the case, sub-cooled boiling begins and steam bubbles form. [Stephan 1988]

The heat transfer in a tube can be described in the following way:

$$q \cdot d_i \cdot \pi \cdot z = \dot{m} \cdot c_p \cdot (T_L - T_1) = \alpha_{tube} \cdot d_i \cdot \pi \cdot z \, (T_w - T_L) \qquad \text{[Stephan 1988]}$$

q..... heat flow per area [W/m²]
d_i..... inner tube diameter [m]
T_L..... liquid mean temperature at position z [°C]
T_1..... liquid mean temperature at the entry point [°C]
T_w..... tube wall temperature at the position z [°C]
z..... position measured from the entry point at which $t_L = t_1$ [m]
α_{tube}..... heat transfer coefficient between tube wall and liquid [W/m²K]
c_p..... specific heat capacity [J/kgK]
$\dot{m}$ …. mass flow [kg/s]

With some applied transformation of the equations above, the tube wall temperature $\mathbf{T_w}$ can be given as follows:

$$T_w = T_L + \frac{q}{\alpha_{tube}} = T_1 + q \cdot \left(\frac{d_i \cdot \pi \cdot z}{\dot{m} \, c_p} + \frac{1}{\alpha_{tube}} \right) \qquad \text{[Stephan 1988]}$$

Using the equation above, the coordinate **z** is given:

$$z = \left(\frac{T_w - T_1}{q} - \frac{1}{\alpha_{tube}} \right) \frac{\dot{m} \cdot c_p}{d_i \cdot \pi}$$

The difference $T_w - T_1$ can be substituted by the expression $\Delta T_{sub} + \Delta T$, where ΔT_{sub} is the difference between the entering liquid´s temperature and the saturation temperature, and ΔT is the temperature difference between saturation temperature and the superheated wall (tube wall superheating), when sub-cooled boiling begins. Thus, having substituted in this way, the initial position of sub-cooled boiling $\mathbf{z_1}$ is given as follows:

$$z_1 = \left(\frac{\Delta T_{sub} + \Delta T}{q} - \frac{1}{\alpha_{tube}} \right) \frac{\dot{m} \cdot c_p}{d_i \cdot \pi} \qquad \text{[Stephan 1988]}$$

The sub-cooled boiling region ends when the liquid mean temperature reaches the saturation temperature. This end position $\mathbf{z_2}$ is given in the following way, with $T_L - T_1$ substituted by ΔT_{sub} :

$$q \cdot d_i \cdot \pi \cdot z = \dot{m} \cdot c_p \cdot (T_L - T_1)$$

$$z = \frac{\dot{m} \cdot c_p}{q \cdot d_i \cdot \pi} (T_L - T_1)$$

$$z_2 = \frac{\dot{m} \cdot c_p}{q \cdot d_i \cdot \pi} \Delta T_{sub} \qquad \text{[Stephan 1988]}$$

In the region of sub-cooled boiling the heat transfer is noticeable better than in the region of single phase convection (**a**). On the one hand, the convection increases due to forming steam bubbles, and on the other hand steam bubbles condensate in the colder core flow, having transported internal energy. [Stephan 1988]

However, sub-cooled boiling does not occur when the liquid mean temperature has already reached the saturation temperature in the region of single phase convection (**a**). [Stephan 1988]

In order to calculate $\mathbf{z_1}$, the necessary tube wall super-heating $\mathbf{\Delta T}$ must be known. An empirical relationship, that is valid for pressures between 1 and 140 bar, can be given as follows:

$$\Delta T = \frac{5}{9} \left[\left(\frac{q}{1120} \right)^{0.463} \cdot p^{-0.535} \right]^{p^{0.0234}} \qquad \text{[VDI 2006]}$$

q..... heat flow per area [W/m²]

p..... pressure [bar]

Used with water as boiling liquid, this empirical relationship is independent on the tube wall´s characteristics. [VDI 2006]

The following figure shows the important parameters of sub-cooled boiling.

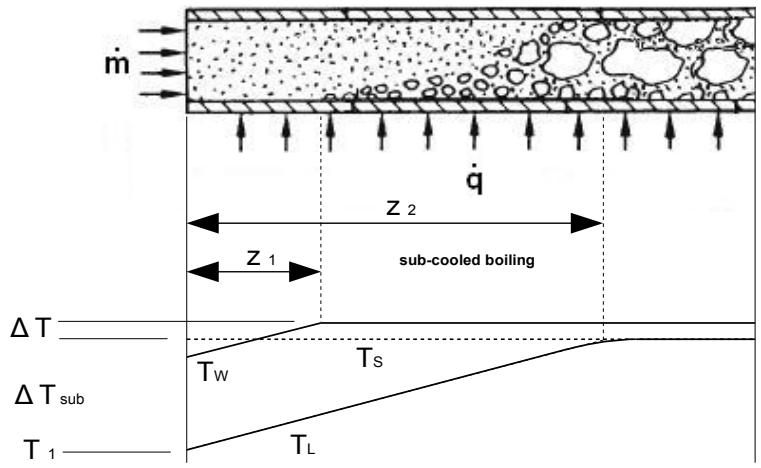

Figure 58: Sub-cooled Boiling [Stephan 1988]

Furthermore, the heat transfer coefficient between the tube wall and the water-steam-flow has to be determined.

In the sub-cooled boiling region, hence at the transition from single-phase convection to bulk boiling, both modes of heat transfer (heat transfer by convection and heat transfer by nucleate boiling) are important. [Butterworth 1977]

In order to include both modes of heat transfer, superposition models were developed. Such a model was proposed by Chen (1963), which is widely used nowadays. This model was originally developed for bulk boiling flow (saturated boiling) and was later extended by Butterworth (1979) to the sub-cooled flow regime, where it also produced results with acceptable accuracy.
[Steiner et al. 2005]

The heat flow in the sub-cooled region can be described by the following equations:
[Steiner et al. 2005]

$$q = q_{fc} \cdot F + q_{nb} \cdot S$$

q..... heat flow per area [W/m²]
q_{fc}..... forced convection heat flow [W/m²]
q_{nb}..... nucleate boiling heat flow [W/m²]
F ..... correction factor for the forced convective heat flow
S ..... correction factor for the nucleate boiling heat flow

$$q_{fc} = \alpha_{fc} \cdot (T_w - T_L)$$

α_{fc}..... heat transfer coefficient for forced convective heat flow [W/m²K]
T_w..... inner tube wall temperature

T_L..... liquid mean temperature

The heat transfer coefficient α_{fc} for forced convective heat flow is calculated using the Dittus & Boelter correlation, where the subscript "L" indicates the liquid phase.

$$\alpha_{fc} = 0.023 \cdot Re_L^{0.8} \cdot Pr_L^{0.4} \frac{\lambda_L}{d_i}$$

λ_L..... thermal conductivity of the liquid phase
d_i..... inner tube diameter

Reynolds and Prandtl number of the liquid phase:

$$Re_L = \frac{v_L \cdot d_i}{\upsilon_L} \qquad Pr_L = \frac{\eta_L \cdot c_{pL}}{\lambda_L}$$

η_L..... dynamic viscosity of the liquid phase
$c_{p\,L}$..... heat capacity of the liquid phase
v_L..... flow velocity of the liquid phase [m/s]
υ_L..... kinematic viscosity of the liquid phase [m²/s]

The nucleate boiling heat flow is obtained in the following way:

$$q_{nb} = \alpha_{nb} \cdot (T_w - T_s)$$

α_{nb}..... heat transfer coefficient for nucleate boiling heat flow [W/m²K]
T_w..... tube wall temperature
T_s..... saturation temperature according to the prevailing pressure

The heat transfer coefficient α_{nb} is calculated as follows:
[Steiner et al. 2005]

$$\alpha_{nb} = 0.00122 \frac{\lambda_L^{0.79} \cdot c_{pL}^{0.45} \cdot \rho_L^{0.49}}{\sigma_s^{0.5} \cdot \eta_L^{0.29} \cdot h_v^{0.24} \cdot \rho_{st}^{0.24}} \Delta T^{0.24} \cdot \Delta p_s^{0.75}$$

λ_L..... thermal conductivity [W/mK]
$c_{p\,L}$..... heat capacity of the liquid phase [J/kgK]
ρ_L..... density of the liquid phase [kg/m³]
σ_s..... surface tension [N/m]
η_L..... dynamic viscosity of the liquid phase [kg/ms]
h_v..... latent heat of evaporation – enthalpy of evaporation [J/kg]
ρ_{st}..... density of the steam phase [kg/m³]
ΔT..... tube wall superheating ($T_w - T_s$)
Δp_s..... saturation pressure difference; vapour pressure at superheated temperature T_w minus prevailing pressure (according to the saturation temperature T_s)

The surface tension σ_s between liquid phase and vapour phase of water can be calculated by the following equation, which is valid between the triple-point temperature T_t = 273.16 K and the critical-point temperature T_c = 647.096 K : [Wagner & Kruse 1998]

$$\frac{\sigma_s}{\sigma_{s0}} = 235.8 \cdot (1 - \Phi)^{1.256} \cdot [1 - 0.625 \cdot (1 - \Phi)]$$

$$\Phi = \frac{T}{T_c}$$

$$\sigma_{s0} = 1 \cdot 10^{-3} \frac{N}{m}$$

To finally calculate the heat flow in the sub-cooled boiling region the two correction factors for forced convective heat flow (**F**) and for nucleate boiling heat flow (**S**) have to be determined.

As the flow steam mass fraction in the sub-cooled boiling region is small, the correction factor **F** for the forced convective heat flow can be assumed to unity.

$$F = 1 \qquad \text{[Steiner et al. 2005]}$$

A correlation for the correction factor **S** is given as follows:
[Steiner et al. 2005]

$$S = \frac{1}{1 + 2.53 \cdot 10^{-6} \cdot (Re_L \cdot F^{1.25})^{1.17}}$$

For the sub-cooled boiling flow, where **F** can be assumed to unity, the factor **S** depends on the liquid-phase Reynolds number only.

7.2.2 Bulk Boiling Region

The heat transfer within the bulk boiling region depends on several parameters, such as mass flow, flow steam quality, properties of liquid and steam, tube-wall properties and pressure.
As a theory does not exist so far, it is not possible to calculate the heat transfer coefficient with the desired accuracy without using empirical or semi-empirical relationships. [VDI 2006]

Bulk boiling only occurs if the heat flow through the tube wall exceeds the amount of heat which can be carried by the two-phase flow without forming additional steam bubbles. Thus, bulk boiling begins if the heat flow **q** rises above a certain value, which is described by the following equation.

$$q \geqslant \frac{8 \cdot \sigma_s \cdot T_s}{\rho'' \cdot h_v \cdot \lambda_L} \alpha_{2\mathrm{Ph}}^2 \qquad \text{[Stephan 1988]}$$

σ_s..... surface tension [N/m]
T_s..... saturation temperature [K]
ρ''..... density of the dry saturated steam [kg/m³]

h_v..... enthalpy of evaporation [J/kg]
λ_L..... heat conductivity of the liquid phase [W/mK]
α_{2Ph}..... heat transfer coefficient of the two phase flow [W/m²K]

To ascertain whether the inequality mentioned above is valid, it is sufficient to determine the two-phase flow heat transfer coefficient $\boldsymbol{\alpha_{2Ph}}$ approximately, what can be done with the following relationship.

$$\frac{\alpha_{2\mathrm{Ph}}}{\alpha_{fc}} = 3.5 \cdot \left(\frac{1}{X}\right)^{0.5}$$ [Stephan 1988]

α_{fc}..... heat transfer coefficient for single-phase forced convective heat flow [W/m²K] (Dittus & Boelter correlation)
X..... Lockhart-Martinelli parameter

In order to determine the two-phase flow heat transfer coefficient $\boldsymbol{\alpha_{2Ph}}$ more accurately, following correlation uses a superposition model. [Stephan 1988]

$$\alpha_{2\mathrm{Ph}} = \alpha_B + \alpha_K$$

$\boldsymbol{\alpha_B}$ is the heat transfer coefficient of natural convective flow and is described by the following empirical correlation, valid for water at a pressure **p** between 0.0221 bar and 199 bar : [Stephan 1988]

$$\frac{\alpha_B}{\alpha_0} = \left[2.55 \cdot p_{star}^{0.27} + \left(9 + \frac{1}{1 - p_{star}^2}\right) \cdot p_{star}^2\right] \cdot \left[\frac{q}{q_0}\right]^{0.9 - 0.3 \cdot p_{star}^{0.15}}$$

$$p_{star} = \frac{p}{p_{cr}}$$

α_0..... base value for the heat transfer coefficient (= 3800 W/m²K)
q..... actual heat flow [W/m²]
q_0..... base value for the heat flow (= 20 000 W/m²)
p..... actual pressure [N/m²]
p_{cr}..... critical pressure (= 22.064 MPa)

Finally the heat transfer coefficient $\boldsymbol{\alpha_K}$ for forced convective flow is calculated by the Colburn-correlation, assuming that the liquid is the only phase: [Stephan 1988]

$$\alpha_K = 0.023 \cdot Re_L^{0.7} \cdot Pr_L^{1/3} \frac{\lambda_L}{d_i}$$

$$\mathrm{Re}_L = \frac{v_L \cdot d_i}{\upsilon_L} \qquad Pr_L = \frac{\eta_L \cdot c_{pL}}{\lambda_L}$$

η_L..... dynamic viscosity of the liquid phase

$c_{p\,L}$..... heat capacity of the liquid phase
v_L..... flow velocity of the liquid phase [m/s]
υ_L..... kinematic viscosity of the liquid phase [m²/s]
λ_L..... thermal conductivity of the liquid phase
d_i..... inner tube diameter

7.2.3 Region of Forced Convective Heat Transfer Through Liquid Film

The bulk boiling region is followed by the region of forced convective heat transfer through liquid film. The number of steam bubbles formed decreases and they disappear completely. The heat transfer is determined by the vaporization at the phase boundary between water and steam. Due to gravity the remaining liquid gathers for the most part at the bottom of the tube, leaving the top dry or less wetted. When loaded with a constant heat flow per area, the tube surface at the top reaches higher temperatures than the tube surface in lower, well wetted regions. Thus, the mean heat transfer coefficient for the entire tube surface depends amongst other things on the tube´s thermal conductivity. [Stephan 1988]

Using the evaluation results of experiments with water at pressures between 1 and 165 bar, Shah (1976 & 1982) has developed a correlation for the mean heat transfer coefficient. [Stephan 1988]

This correlation is valid as long as the Boiling number **Bo** exceeds the value 10^{-4}.

$$Bo = \frac{q}{\frac{\dot{m}}{A_c} \cdot h_v} \geqslant 10^{-4} \quad \text{[Stephan 1988]}$$

h_v..... enthalpy of evaporation [J/kg]
q..... heat flow per area [W/m²]
A_c..... cross-sectional area [m²]
$\dot{m}$ …. total mass flow [kg/s]

In order to calculate the heat transfer coefficient α_{2Ph}, one has to determine whether stratified flow or annular flow prevails.

If the Froude number **Fr** does not exceed the value 0.04, stratified flow pattern prevails.

$$Fr = \frac{\left(\frac{\dot{m}}{A_c}\right)^2}{\rho_L^2 \cdot g \cdot d_i} < 0.04 \quad \text{[Stephan 1988]}$$

$\dot{m}$ …. total mass flow[kg/s]
A_c..... cross-sectional area of the tube [m²]
ρ_L..... density of the liquid phase [kg/m³]
g..... acceleration due to gravity [m/s²]
d_i..... inner tube diameter [m]

For the stratified flow the mean heat transfer coefficient α_{2Ph} can be calculated as follows:

[Stephan 1988]

$$\frac{\alpha_{2Ph}}{\alpha_K} = 3.9 \cdot Fr^{0,24} \cdot \left(\frac{\dot{x}}{1-\dot{x}}\right)^{0.64} \cdot \left(\frac{\rho_L}{\rho_{St}}\right)^{0.4}$$

$$\alpha_K = \frac{\lambda_L}{d_i} \cdot 0.023 \cdot \left(\frac{\dot{m} \cdot (1-\dot{x}) \cdot d_i}{A_c \cdot \eta_L}\right)^{0.8} \cdot Pr_L^{0.4}$$

$$Pr_L = \frac{\eta_L \cdot c_{pL}}{\lambda_L}$$

α_K..... heat transfer coefficient of the single phase liquid flow [W/m²K]
$\dot{x}$ .... flow steam quality
ρ_L..... density of the liquid phase [kg/m³]
ρ_{St}..... density of the steam phase [kg/m³]
λ_L..... thermal conductivity of the liquid phase [W/mK]
d_i..... inner tube diameter [m]
$\dot{m}$ .... total mass flow [kg/s]
A_c..... cross-sectional area of the tube [m²]
η_L..... dynamic viscosity of the liquid phase [kg/ms]

If the Froude number **Fr** exceeds the value 0.04 the inner tube surface is completely wetted and annular flow pattern prevails. Now the mean heat transfer coefficient α_{2Ph} is calculated in the following way: [Stephan 1988]

If $$Fr = \frac{\left(\frac{\dot{m}}{A_c}\right)^2}{\rho_L^2 \cdot g \cdot d_i} \geqslant 0.04$$

then $$\frac{\alpha_{2Ph}}{\alpha_K} = 1.8 \cdot \left(\frac{\dot{x}}{1-\dot{x}}\right)^{0.64} \cdot \left(\frac{\rho_L}{\rho_{St}}\right)^{0.4}$$

7.2.4 A Heat Transfer Model Suitable for the Bulk Boiling Region and the Region of Forced Convective Heat Transfer Through Liquid Film in Horizontal Tubes

The following model was proposed by Shah (1976) as cited by Collier & Thome (1996):

In this model the heat transfer coefficient is determined by evaluation of 5 parameters C_0, **Bo** (Boiling number), **Fr** (Froude number), **N** and **F**. These parameters correlate with each other as follows:

$$C_0 = \left(\frac{1-\dot{x}}{\dot{x}}\right)^{0.8} \cdot \left(\frac{\rho_{St}}{\rho_L}\right)^{0.5}$$

$\dot{x}$ …. flow steam quality
ρ_L..... density of the liquid phase [kg/m³]
ρ_{St}..... density of the steam phase [kg/m³]

Two different mechanisms are considered, namely nucleate boiling and convective boiling. The larger one of these two coefficients (nucleate coefficient α_{nb} or convective coefficient α_{fc}) is used.

For horizontal tubes the Froude number **Fr** has to be evaluated.

$$Fr = \frac{\left(\frac{\dot{m}}{A_c}\right)^2}{\rho_L^2 \cdot g \cdot d_i}$$

$\dot{m}$ …. total mass flow [kg/s]
A_c..... cross-sectional area of the tube [m²]
ρ_L..... density of the liquid phase [kg/m³]
g..... acceleration due to gravity [m/s²]
d_i..... inner tube diameter [m]

If the Froude number **Fr** is larger than 0.04, then the parameter **N** is equal to C_0.

$$Fr \geqslant 0.04 \quad \rightarrow \quad N = C_0$$

If the Froude number **Fr** is smaller than 0.04, then **N** is given as follows:

$$Fr < 0.04 \quad \rightarrow \quad N = 0.38 \cdot Fr^{-0.3} \cdot C_0$$

Then for **N** is larger than 1.0, the following expressions for α_{nb} and α_{fc} are valid.
Note: The larger value of these two parameters has to be taken for the two-phase flow mean heat transfer coefficient α_{2Ph}.

$$N > 1.0 \rightarrow$$

$$Bo \geqslant 0.0003 \quad \rightarrow \quad \frac{\alpha_{nb}}{\alpha_{DB}} = 230 \cdot Bo^{0.5}$$

$$Bo < 0.0003 \quad \rightarrow \quad \frac{\alpha_{nb}}{\alpha_{DB}} = 1 + 46 \cdot Bo^{0.5}$$

$$\frac{\alpha_{fc}}{\alpha_{DB}} = \frac{1.8}{N^{0.8}}$$

α_{DB} ..... Dittus-Boelter heat transfer coefficient for properties of the liquid phase

$$\alpha_{DB} = 0.023 \cdot Re_L^{0.8} \cdot Pr_L^{0.4} \frac{\lambda_L}{d_i}$$

For N between 1 and 0.1, the correlation for α_{fc} stays the same. α_{nb} is defined as follows:
Note: The larger value of these two parameters has to be taken for the two-phase flow mean heat transfer coefficient α_{2Ph}.

$$1.0 > N > 0.1 \rightarrow$$

$$\frac{\alpha_{nb}}{\alpha_{DB}} = F \cdot Bo^{0.5} \cdot \exp(2.74 \cdot N^{-0.1})$$

$$\frac{\alpha_{fc}}{\alpha_{DB}} = \frac{1.8}{N^{0.8}}$$

For N smaller than 0.1, the correlation for α_{fc} again stays the same. α_{nb} is defined as follows:
Note: The larger value of these two parameters has to be taken for the two-phase flow mean heat transfer coefficient α_{2Ph}.

$$N < 0.1 \rightarrow$$

$$\frac{\alpha_{nb}}{\alpha_{DB}} = F \cdot Bo^{0.5} \cdot \exp(2.47 \cdot N^{-0.15})$$

$$\frac{\alpha_{fc}}{\alpha_{DB}} = \frac{1.8}{N^{0.8}}$$

The constant F is determined in the following way:

$$Bo \geqslant 0.0011 \quad \rightarrow \quad F = 14.7$$

$$Bo < 0.0011 \quad \rightarrow \quad F = 15.43$$

7.2.5 Critical Heat Flow

When natural convection at low pressures is considered, the temperature of a wall that is loaded with the critical heat flow per area $\mathbf{q}_{critical}$ changes according to the line A – B, as shown in the figure 59. Unfortunately in most cases, the wall materials used cannot withstand the temperatures reached at point B. Thus, this phenomenon is usually called “burnout”. At high pressures and forced convection this curve continues far smoother beyond the critical heat flow. Thus, the temperature raise is not that large. [Mayinger 1982]

Basically the low thermal conductivity of the steam phase leads on the one hand to a decreasing heat flow per area for a constant wall temperature, or on the other hand to a wall temperature rise for a given heat flow. Thus, the smaller the void fraction (volumetric steam quality), the higher is the critical heat flow $\mathbf{q}_{critical}$. [Stephan 1988]

Bertoletti et al. (1965) as cited by Mayinger (1982), provided a correlation for determining the flow steam quality $\dot{x}$ where the critical heat flow is most likely reached:

$$\dot{x}_{critical} = 10 \cdot \frac{1 - \frac{p}{p_c}}{\sqrt[3]{\frac{\dot{m}}{A_c}}} - 0.7944 \cdot \frac{q \cdot \left(\frac{p_c}{p} - 1\right)^{0.4} \cdot d_i^{0.4}}{h_v}$$

d_i..... inner tube diameter [m]
$\dot{m}$ …. total mass flow [kg/s]
A_c..... cross-sectional area of the tube [m²]
q..... heat flow per area note: unit in [kW/m²]
h_v..... enthalpy of evaporation note: unit in [kJ/kg]
p_c..... critical pressure [bar] for water: 220.64 bar
p..... pressure [bar]

This equation for the critical flow steam quality is implemented in the IPSEpro model, in order to check if the critical heat flow may be reached.

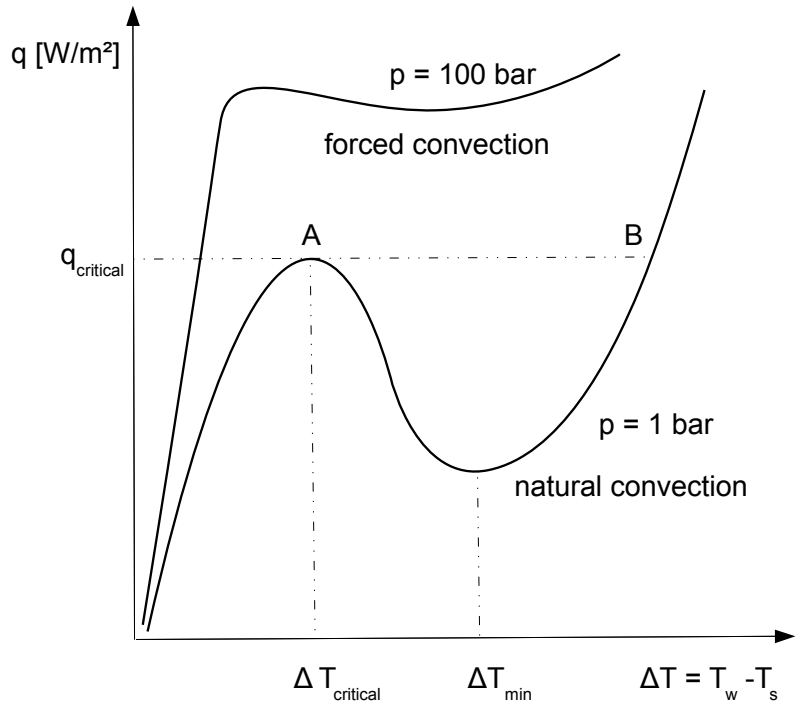

Figure 59: Heat Flow vs. Wall Super-heating for Forced and Natural Convection [Mayinger 1982]

7.3 The Two-Phase Flow Heat Transfer Correlation Implemented (Evaporating Section)

As it is rather difficult to distinguish between the diverse regions of two-phase flow within the absorber tube, heat transfer models that are qualified for more than one regions are preferred, even if several case differentiations are required. Furthermore, I limit myself to only delineate models of direct steam recirculation concepts, as the steam mass fraction within the evaporation section never exceeds a certain limit. With a recirculation-rate between 3 and 5, as it was proposed by Goebel (1998), the steam mass fraction would range between 0.25 and 0.16. Hence, the liquid deficient region or dryout is never reached.
Thus, for the evaporation section the heat transfer model by Shah (1976) of chapter 7.2.4 is used. The calculated α_{2Ph} is equal to α_{tube} then.
Note: In the calculations implemented, the definition of the steam mass fraction is based on the assumption of homogeneous flow. This simplification was proposed by Eck & Hirsch (2007) or Odeh et al. (1998).

$$\dot{x} = x = \frac{h - h'}{h'' - h'}$$

7.4 Pressure Loss in the Two-Phase Flow Region

According to Eck et al. (2003), a useful empirical correlation, that correlates best with measured results, was proposed by Friedel (1974).

It is based on at least 25 000 measured values and is valid for horizontal flow. [Mayinger 1982]

The basic relationship of this model is described by the pressure loss ratio $\mathbf{R_p}$, that is the ratio of the two-phase pressure drop to the pressure drop that would occur if the whole mass flow streamed as liquid phase only. [Mayinger 1982]

$$R_p = \frac{(\Delta p / \Delta L_c)_{2Ph}}{(\Delta p / \Delta L_c)_{1Ph}} \quad \text{[Mayinger 1982]}$$

p..... pressure [Pascal]
L_c..... collector length [m]

The pressure drop of the fictive single phase flow is described by the well established Darcy & Weisbach equation:

$$\frac{\Delta p}{\Delta L_c} = \frac{f \cdot \rho_L}{d_i \cdot 2} \cdot v_f^2 \quad \text{[Mayinger 1982]}$$

f..... friction factor
ρ_L..... density of the liquid phase [kg/m³]
d_i..... absorber tube inner diameter [m]
v_f..... velocity of the fictive single phase flow [m/s]

The fictive single phase velocity $\mathbf{v_f}$ is the total mass flow $\dot{m}$ divided by the single phase`s density $\boldsymbol{\rho_L}$ and the cross-sectional area $\mathbf{A_c}$ of the tube. [Mayinger 1982]

$$v_f = \frac{\dot{m}}{\rho_L \cdot A_c}$$

$$f = (0.79 \cdot \ln Re - 1.64)^{-2}$$

Friedel (1974) developed the following equation for the pressure drop ratio $\mathbf{R_p}$: [Mayinger 1982]

$$R_p = a + 3.43 \cdot \dot{x}^{0.685} \cdot (1 - \dot{x})^{0.24} \cdot \left(\frac{\rho_L}{\rho_{St}}\right)^{0.8} \cdot \left(\frac{\eta_{St}}{\eta_L}\right)^{0.22} \cdot \left(1 - \frac{\eta_{St}}{\eta_L}\right)^{0.89} \cdot Fr_L^{-0.047} \cdot We_L^{-0.0334}$$

$$a = (1 - \dot{x})^2 + \dot{x}^2 \cdot \left(\frac{\rho_L \cdot f_{St}}{\rho_{St} \cdot f_L}\right) \qquad Fr_L = \frac{\left(\frac{\dot{m}}{A_c}\right)^2}{\rho_L^2 \cdot g \cdot d_i}$$

$$We_L = \left(\frac{\dot{m}}{A_c}\right)^2 \cdot \frac{d_i}{\rho_L \cdot \sigma_s} \qquad Re_L = \frac{v_L \cdot d_i}{\upsilon_L} \qquad Re_{St} = \frac{v_{St} \cdot d_i}{\upsilon_{St}}$$

$$f_j = \left[0.86859 \cdot \ln \frac{Re_j}{1.964 \cdot \ln Re_j - 3.8215}\right]^{-2} \quad \text{for } Re_j > 1055 \text{ and } j = L(\text{Liquid}), St(\text{Steam})$$

$\dot{x}$ …. flow steam quality
ρ_L..... density of the liquid phase [kg/m³]
ρ_{St}..... density of the steam phase [kg/m³]
η_{St}..... dynamic viscosity of the steam phase [kg/ms]
η_L..... dynamic viscosity of the liquid phase [kg/ms]
Fr..... Froude number
We..... Weber number
Re..... Reynolds number
f..... friction factor
$\dot{m}$ …. total mass flow [kg/s]
A_c..... cross-sectional area of the pipe [m²]
d_i..... inner diameter of the absorber tube [m]
υ_{St}..... kinematic viscosity of the steam phase [m²/s]
υ_L..... kinematic viscosity of the liquid phase [m²/s]
v_{St}..... velocity of the steam phase [m/s]
v_L..... velocity of the liquid phase [m/s]
σ_s..... surface tension [N/m]
g..... acceleration due to gravity [m/s²]

7.4.1 Two-Phase Flow Instabilities

In this chapter I want to give an idea of how two-phase flow instabilities can influence the controllability of a real plant. As it is very difficult to model these dynamic phenomena within steady state simulations, I do not consider it in my models.

Flow boiling instabilities and its effects have been well documented and researched since the early 1960s. These instabilities may be the reason for structural vibrations, acoustic noise and most importantly may lead to the initiation of critical heat flow. For heat flow controlled systems, elevated surface temperatures and even “burnout” may occur. A well acknowledged and important static instability is the flow excursion or Ledinegg instability. [Zhang et al. 2009]

The Ledinegg instability occurs in boiler tubes through which the flow is forced either by an imposed pressure difference or a pump. [Brennen 2005]

There are two curves that are important for the description of this phenomenon. The **internal characteristic curve** and the **external characteristic curve** of a steam generator´s tube. [Kakac & Bon 2008]

The internal characteristic curve is the pressure drop along a tube Δp plotted versus the mass flow $\dot{m}$. This curve is shown in figure 60 below. Assuming that the heat flow through the tube is independent on the flow rate, there will be a pure liquid flow at high flow rates as the heat flow is not enough to evaporate the fluid. On the other hand, at low flow rates the vapor phase will prevail. The rough forms of the two hypothetical characteristics for all-vapor and all-liquid flow are drawn as dashed lines below. The all-vapor line lies above the all-liquid line due to the difference in density.
However the actual characteristic curve must make a transition from the all-vapor line towards the all-liquid line which leads to the non-monotonic form as shown below. [Brennen 2005]

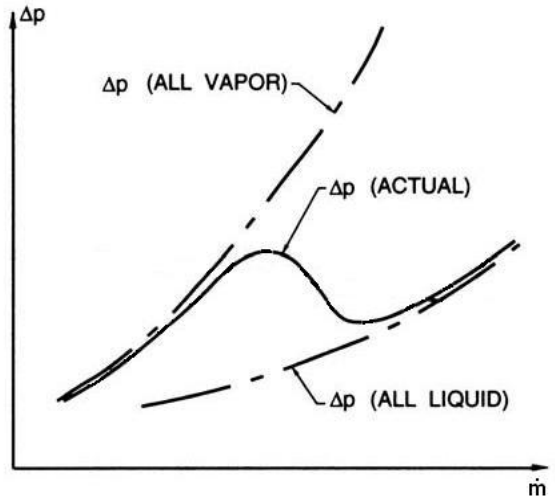

Figure 60: Internal Characteristic Curve [Brennen 2005]

The external characteristic curve is the pressure raise -Δp of the pump plotted versus the mass

flow $\dot{m}$. The possible operating point is then given by the intersection of these two characteristic curves. For instance, single phase pipeline characteristics are usually simple quadratic curves, whereas pump characteristics can be far more complex than shown in figure 61 below. [Brennen 2005]

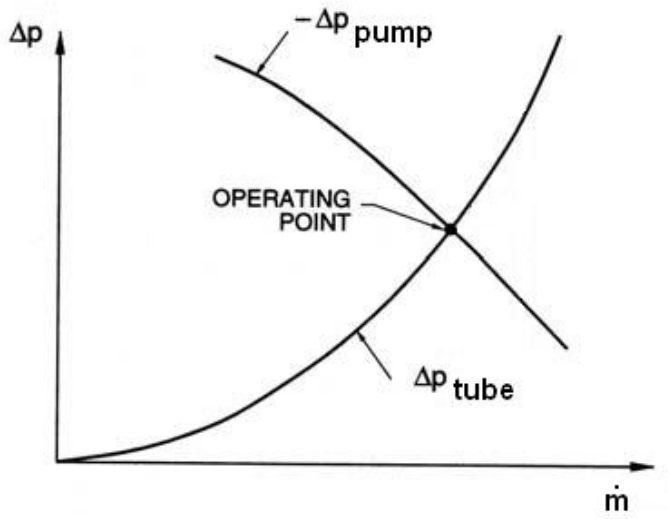

Figure 61: Intersection of Characteristic Curves [Brennen 2005]

In order to analyse the stability of that operating point given above, one has to ascertain what would happen if the system mass flow rate increased. Analysing the figure above, an increase in mass flow rate would lead to a higher pressure loss than the pump is able to compensate. Thus, the flow rate would decline again, reaching its equilibrium at the operation point. Hence, this system can be qualified as stable. [Brennen 2005]

Instability occurs if the gradients of the two characteristics are inverted. Thus a raise in mass flow rate would lead to a pump pressure exceeding the pressure drop in the tube. [Brennen 2005]

When the gradient of the demand pressure drop (internal characteristic curve) becomes smaller than the loop supply pressure drop (external characteristic curve), instabilities occur. Expressed as a mathematical relationship this fact can be written as follows:

$$\left.\frac{\partial(\Delta p)}{\partial \dot{m}}\right|_{channel\ demand} \leqslant \left.\frac{\partial(\Delta p)}{\partial \dot{m}}\right|_{pump\ supply}$$ [Zhang et al. 2009]

Ledinegg observed that the internal characteristic curve had a negative slope region in addition to two positive slope regions, thus making the pressure-drop a multi-valued function of the flow rate. [Kakac & Bon 2008]

The Ledinegg instability´s mechanism is shown in figure 62 below.

In case of an external characteristic curve **A** which has a gradient at point **P** that exceeds that one of the internal characteristic curve **B**, a stable operation is not possible at this intersection. As a small change in flow rate would lead either to operation point **P'** or **P''**. A slight decrease in flow rate causes a spontaneous shift to Point **P''**, whereas an increase in flow rate leads to Point **P'**. Usually the stabilisation at Point **P''** corresponds to such a low flow rate that burn-out occurs, which must be avoided. [Kakac & Bon 2008]

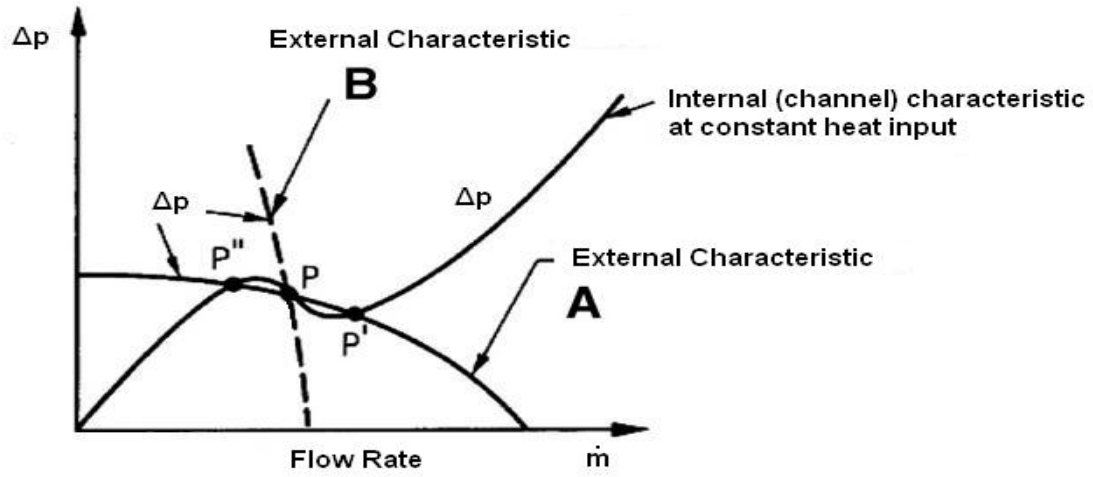

Figure 62: Ledinegg Instability [Kakac & Bon 2008]

A standard way to avoid the Ledinegg instability is making the internal characteristic curve´s gradient bigger than that of the external characteristic curve (**B**). [Kakac & Bon 2008]

To maintain system stability, the pump supply curve (external characteristic curve) needs to be considered. A stable system can be achieved by installing a constant displacement pump, which has an almost negative infinite gradient (the flow rate is constant, regardless of the pressure drop). [Zhang et al. 2009]

Also installing an orifice at the inlet of the tube can improve the stability of the system. As the orifice causes an additional pressure drop it moderates the negative gradient of the demand curve. This effect is shown in figure 63 below. In order to draw the total system´s internal characteristic curve **C**, the pressure drop curve **A** of the orifice and the tube´s demand curve **B** have to be added. As a result the negative gradient at point **a** is transformed into a positive gradient at point **b**. Thus the Ledinegg instability can be avoided at the same mass flow rate. However, the increased pressure drop requires more pumping power to provide the same mass flow rate.
[Zhang et al. 2009]

Another issue of the Ledinegg instability is the fact that it limits the number of parallel tubes between common header pipes. Even with the use of a constant displacement pump the supply curve (external characteristic curve) of an individual tube gradually loses its ability to withstand a Ledinegg instability with an increasing number of parallel tubes. [Zhang et al. 2009]

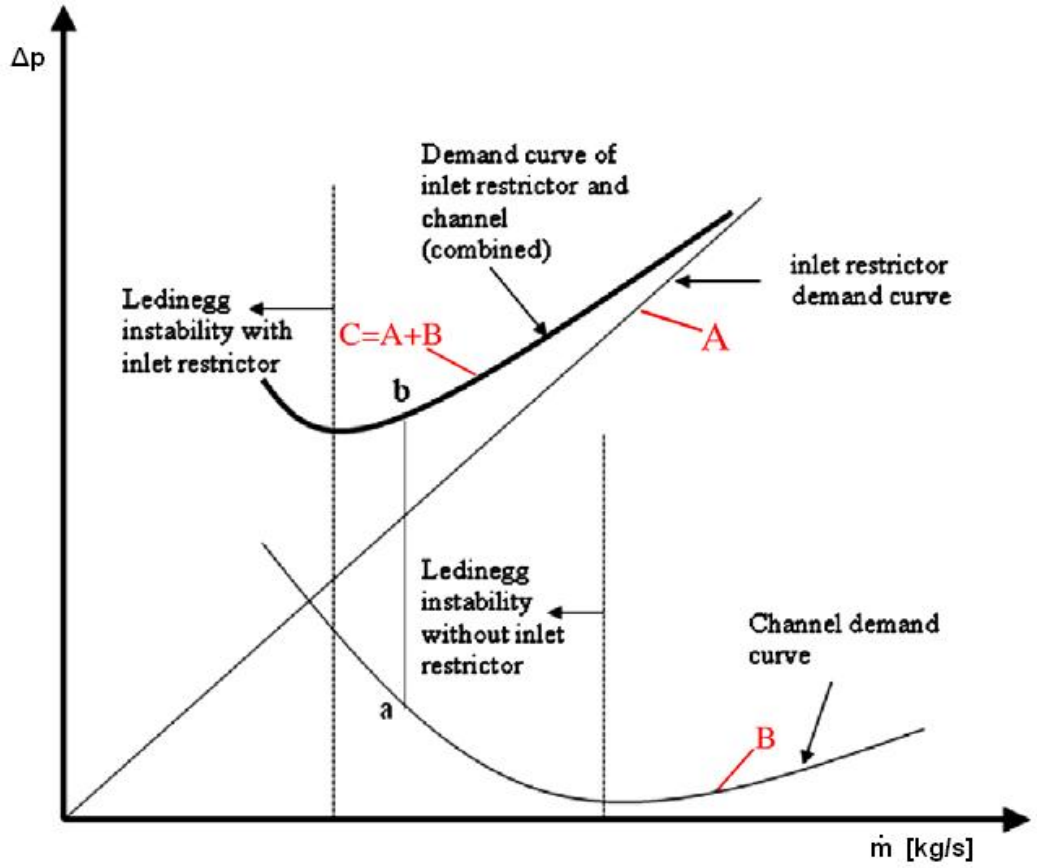

Figure 63: Improvement of Stability Using an Orifice [Zhang et al. 2009]

7.5 Region of Convective Heat Transfer to Vapour (Superheating Section)

When the liquid film on the tube´s surface is completely evaporated, thus after "dryout", there are still liquid droplets remaining in the flow. After the last liquid droplet has been evaporated, the flow steam mass fraction or flow steam quality $\dot{x}$ reaches the value 1 and the region of convective heat transfer to vapour begins. Within this region the single phase heat transfer correlations can be used again.

The following, already mentioned Dittus & Boelter correlation for single phase turbulent flow is appropriate again (Re > 10 000): [Butterfield 1992]

$$Nu = 0.023 \cdot Re_{St}^{0.8} \cdot Pr_{St}^{0.4}$$

$$Re_{St} = \frac{v_{St} \cdot d_i}{\upsilon_{St}} \qquad Pr_{St} = \frac{\eta_{St} \cdot c_{pSt}}{\lambda_{St}}$$

η_{St}..... dynamic viscosity of the steam phase [kg/ms]
$c_{p\ St}$..... heat capacity of the steam phase [J/kgK]

v_{St}..... flow velocity of the steam phase [m/s]
υ_{St}..... kinematic viscosity of the steam phase [m²/s]
λ_{St}..... thermal conductivity of the steam phase [W/mK]
d_i..... inner tube diameter [m]

Another possibility for single phase turbulent flow is again the empirical correlation proposed by Gnielinski (1976); (valid for: 0.5 < Pr < 2000, 3 x10^3 < Re < 5 x 10^6):

$$Nu = \frac{(f/8)\cdot(Re_{St} - 1000)\cdot Pr_{St}}{1 + 12.7\cdot(f/8)^{0.5}\cdot(Pr_{St}^{(2/3)} - 1)}$$ [Stephan 1988]

The friction factor f can be determined as follows:

$$f = (0.79\cdot\ln Re_{St} - 1.64)^{-2}$$ [Cengel 2003]

7.6 Region of Convective Heat Transfer to Water (Preheating Section)

The same equations as mentioned in the previous chapter 7.5 can be used. Only properties for water have to be inserted, instead of those for steam.

The heat transfer coefficient for fully developed single phase flow (water or dry steam) can be calculated with the Dittus-Boelter correlation. [Odeh et al. 1998]

7.7 Pressure Loss in the Single Phase Flow Regions

Single phase flow occurs in the preheating and in the super-heating section. Therefore, correlations used for oil as heat transfer fluid, are valid here as well (properties of superheated steam or water have to be inserted). [Pye et al. 2006]

7.8 The Collector Unit for DSG in IPSEpro

The before mentioned equations were included in the solar collector unit using the IPSEpro Model Developing Kit (MDK).
In this chapter, the basic setup of the unit “W_Solar_collector” is going to be explained.

An important fact that has to be mentioned, is, that these DSG models developed are only suitable for the DSG recirculation concept.

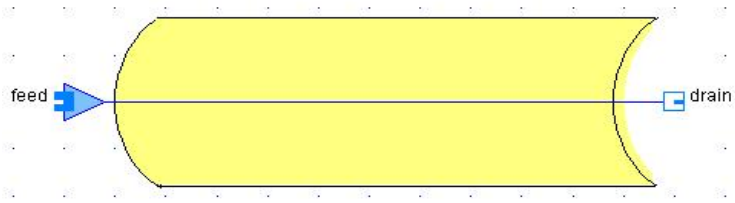

Figure 64: Parabolic Trough Collector Unit "W_Solar_collector" for DSG in IPSEpro-PSE

All equations regarding the solar radiation reaching the absorber tube correspond to the correlations used in the unit “T_Solar_collector” for oil as heat transfer fluid. Also the heat loss models that can be selected are the same. The big difference is that the correlations for the heat transfer coefficient in the two phase region are by far more complicated.

Again, after having fitted a DSG unit in a PSE project file, the following settings have to be made:

The 3 globals have to be selected. The first one is of the type “ambient_solar” , the second one is of the type “collector_type_field” and the third one is an “location_and_solar_parameters” global.

In order to distinguish between single and two-phase flow, there are 3 different models available.
The model “W_Solar_collector_ph” contains the equations for the preheating section.
The model “W_Solar_collector_evap” is used for the evaporation section (two-phase flow).
And finally the model “W_Solar_collector_sh” contains equations for the single phase superheating section.

Next, the heat loss model has to be chosen. The models available have already been described in chapter 5.7.3.

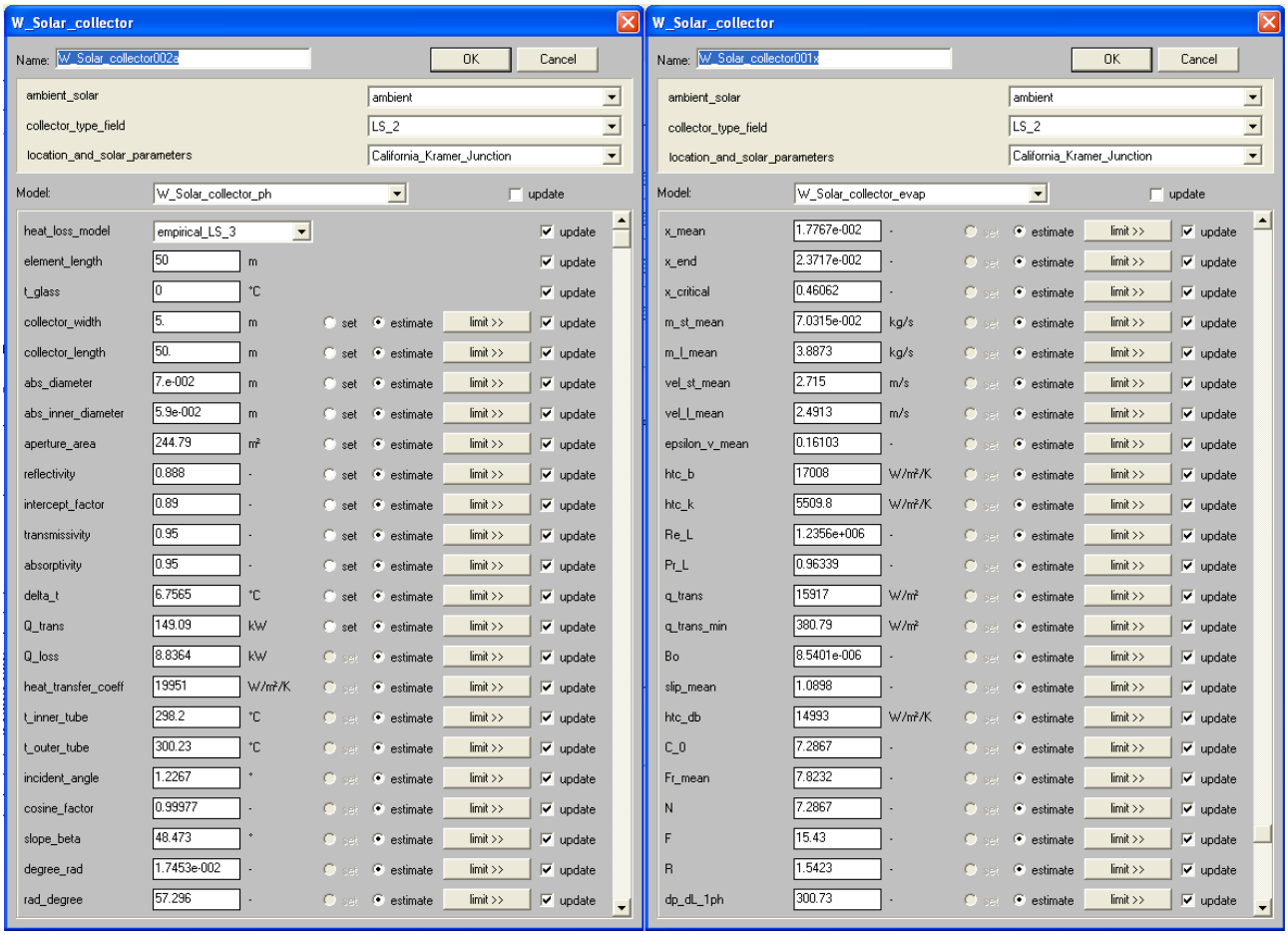

Figure 65: IPSEpro Dialogue Windows for the Unit "W_Solar_collector"

The parameter “element_length” defines the absorber tube length for each unit within the IPSEpro project. With this parameter the level of discretization is determined. Suitable values are discussed in chapter 7.8.1. In order to reach the total absorber tube length required, several collector units have to be connected in series. Of course for each of them the same globals and heat transfer models have to be selected.

The parameter “t_glass” (mean temperature of the surrounding glass tube) is only necessary for the physical heat loss model. It has to be determined by measurements. Therefore, if another heat loss model is used, this parameter can be set to zero.

The following specific collector data (up to the variable “absorptivity”), has to be set if the collector type “user_defined” has been selected.

The remaining part of the dialogue window shows variables that are needed for the calculation and should not be set by the user. They are explained in detail within the appendix.

In order to avoid possible convergence issues the default values of the used variables should be loaded before starting the first calculation.

When setting the feed pressure, the feed temperature and the mass flow to fixed values the unit is fully defined and ready for the solving process.

7.8.1 Suitable Element Length for Single Phase and Evaporating Units

The maximum length of the element that keeps the inaccuracy within suitable limits is discussed in this chapter.

In order to determine the element length necessary, the following calculations have been made within an IPSEpro-PSE project. These files are shown in the appendix chapter B.

There has been distinguished between the 3 collector unit models (preheating model, evaporating model, superheating model).

Concerning the **preheating model** the following calculations have been done:

The total collector length is assumed to be 200 meters.
As a start, one IPSEpro collector unit is used to simulate the 200 meters of parabolic troughs. Thus, for given start values (pressure, temperature and mass flow are set) and a fixed solar irradiation the outlet conditions (pressure, temperature) are calculated.

Then, step by step, the element´s length is reduced to 100 m (2 elements), 50 m (4 elements) and finally to 20 m (10 elements).
The data of each element (heat loss, heat transferred, pressure drop, absorber tube temperature) is displayed in a data frame and then copied in an OpenOfficeCalc spreadsheet. Next, the total pressure drop, the total heat transferred and the total heat loss is plotted versus the element length. At the optimum element length the curve´s slope approaches the value zero or its tangent becomes horizontal.

As it can be seen in figure 66 below, this is the case for an element length of about 50 meters. Considering the small variations in total heat loss (about 5%), it should be accurate enough if an element length of 50 meters is used.
When considering the pressure drop plot, the curve´s tangent approaches the horizontal at an element length of 50 m, but does not seem to converge. However, taking into account the rather small total variation of about 1%, an element length of 50 meters should be accurate enough.

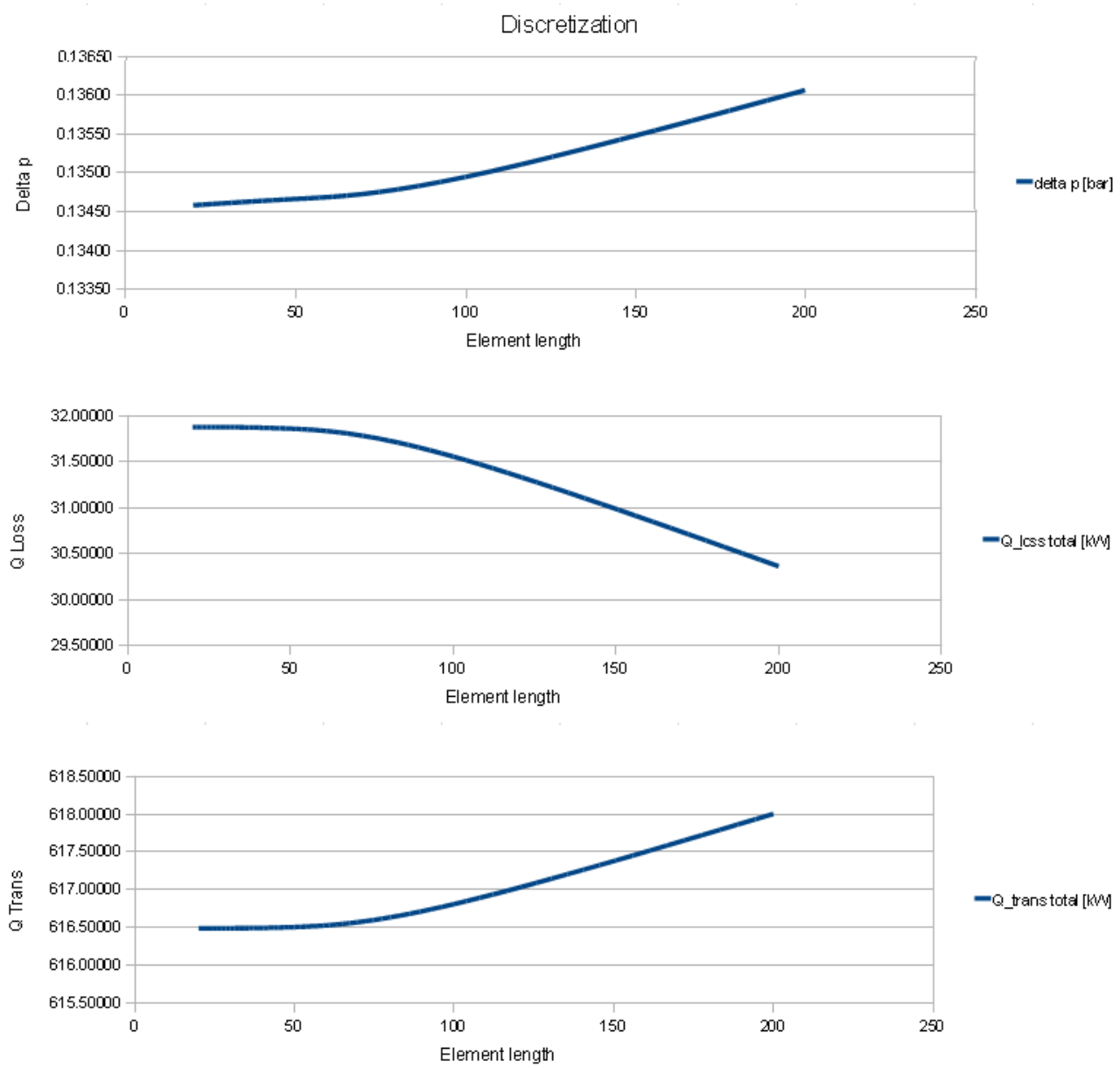

Figure 66: Element Length Preheating Section

Concerning the **evaporating model** the following calculations have been done:

The total collector length is assumed to be 200 meters.
As a start, one IPSEpro collector unit is used to simulate the 200 meters of parabolic troughs. Thus, for given start values (pressure, temperature and mass flow are set) and a fixed solar irradiation the outlet conditions (pressure, temperature) are calculated.

Then, step by step, the element´s length is reduced to 100 m (2 elements), 50 m (4 elements), 20 m (10 elements) and finally to 10 m (20 elements).
The data of each element (heat loss, heat transferred, pressure drop, absorber tube temperature) is displayed in a data frame and then copied in an OpenOfficeCalc spreadsheet. Next, the total pressure drop, the total heat transferred and the total heat loss is plotted versus the element

length. At the optimum element length the curve´s slope approaches the value zero or its tangent becomes horizontal.

As it can be seen in figure 67 below, this is the case at an element length of about 50 meters for the pressure drop. Considering the small variations in total pressure drop (about 0.3%), it should be accurate enough if an element length of 50 meters is used. Depending on the needed accuracy, even larger elements could be chosen.
Due to the constant temperature during phase change, the total variation in heat loss and heat transferred are very small. Thus, the accuracy of the evaporation section depends on the pressure drop only.

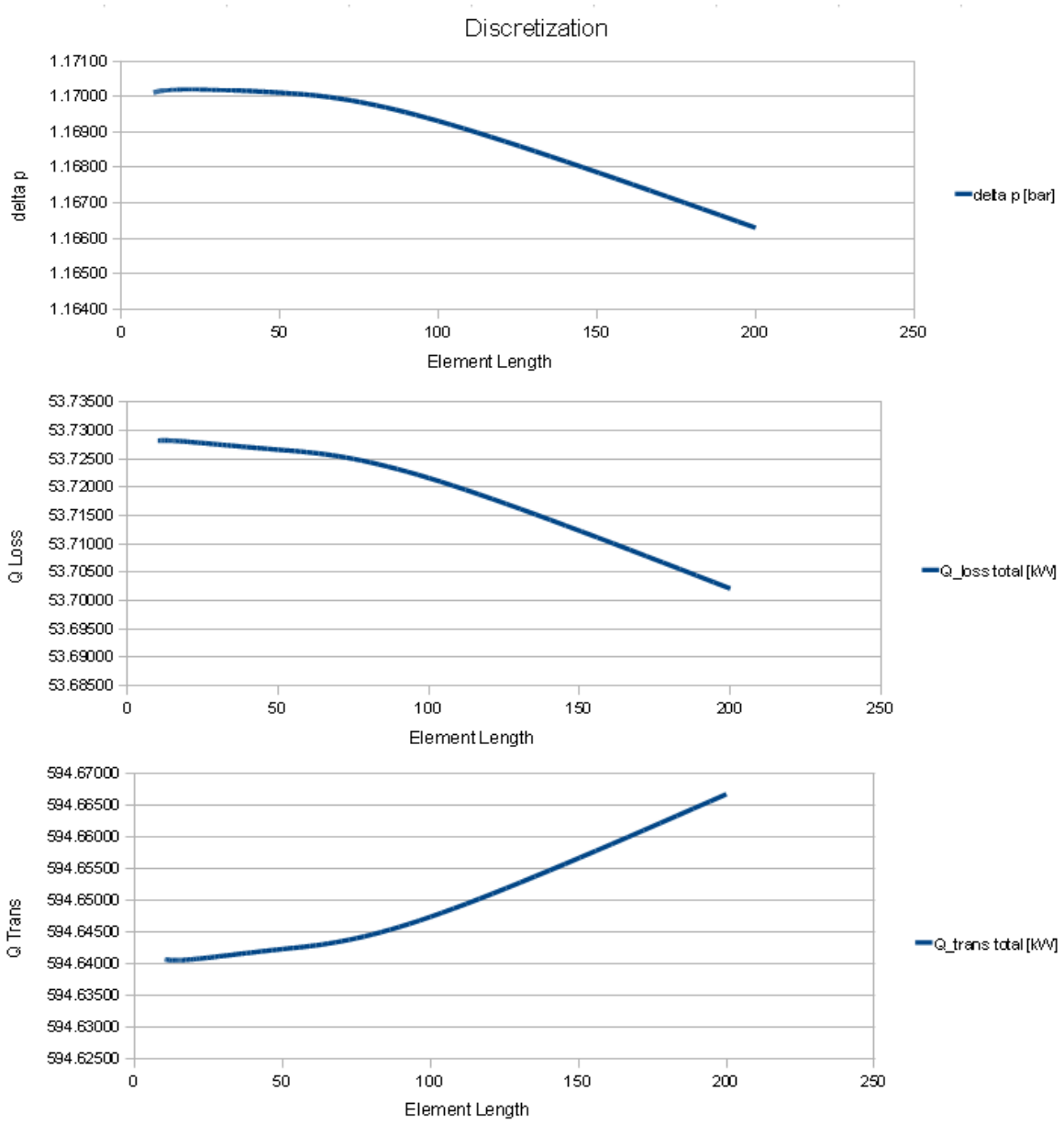

Figure 67: Element Length Evaporating Section

Concerning the **superheating model**, the same calculations have been done as already mentioned for the evaporate model.

As it can be seen in figure 68 below, the curves for the heat transferred and heat loss approach the horizontal at an element length of about 20 meters. However, the total variation in heat loss is about 2%. Thus, depending on the needed accuracy, an element length between 50 and 20 meters should be adequate.
There is no big variation in pressure drop. The total variation in this calculation is only 0.3%. Thus, the element length for the superheat section depends on the heat loss only.

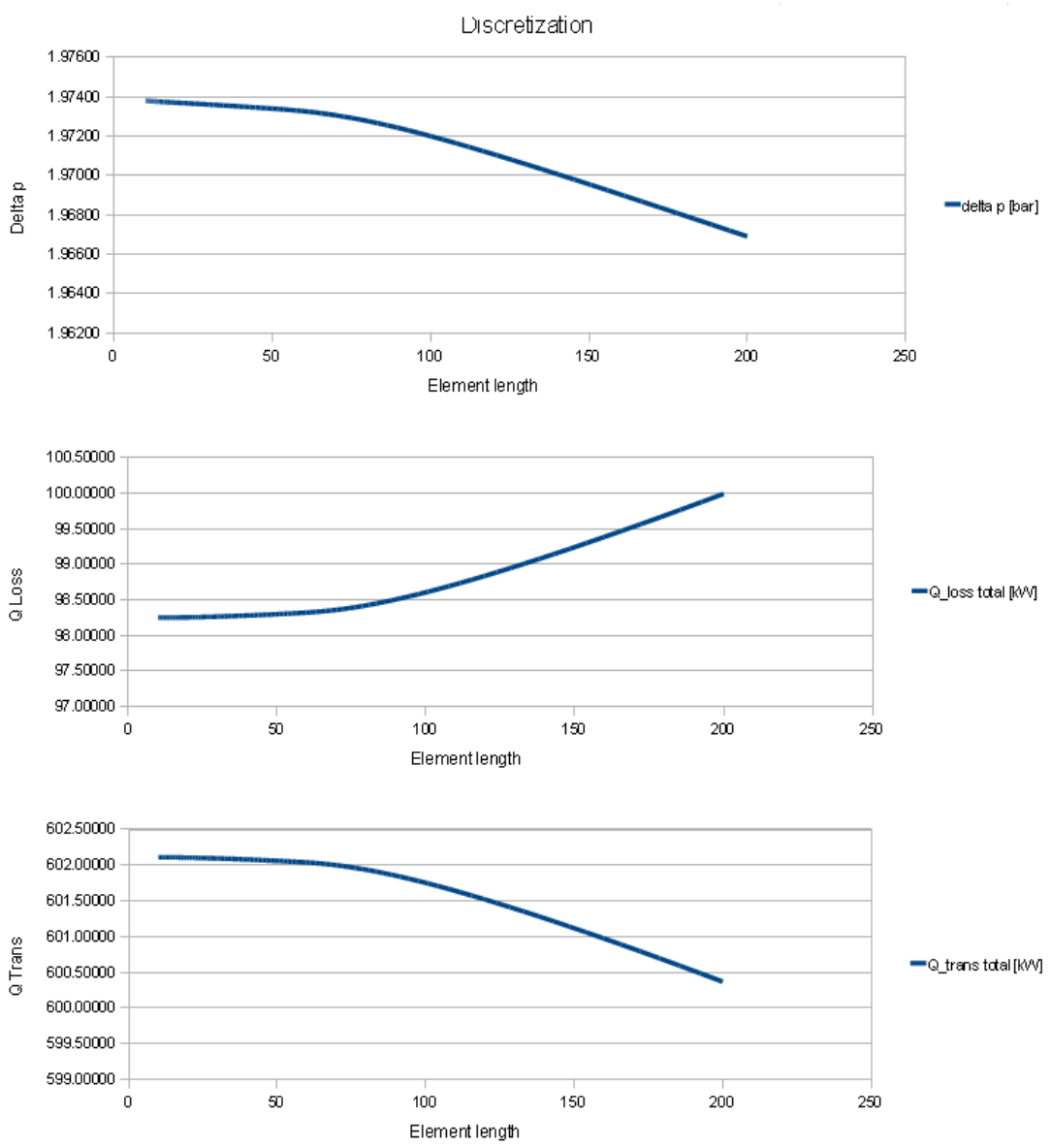

Figure 68: Element Length Superheating Section

8 Power Plant Models

In this chapter I describe two parabolic trough collector plants that I modelled in IPSEpro using the developed parabolic trough collector units. I would like to give an idea how these two units can be used in IPSEpro power plant steady-state simulation and up to which extent the transferred heat rate correlates with measurements.

In order to show the application of the collector unit for oil, I modelled the SEGS VI solar thermal power plant that is operated in California. The therefore needed plant data is provided by Patnode (2006). The SEGS VI IPSEpro power plant model and calculation results are described in chapter 8.1.

In chapter 8.2 I describe the modelling of a parabolic trough DSG plant. As the developed evaporation units are only valid for the recirculation mode, it is also applied in this model.
Since the direct steam generation concept has certain advantages regarding the power plant total efficiency, I would like to compare the results with those of the power plant for oil. Therefore I chose the same location, the same parabolic trough collector types and the same total aperture area. Also the steam cycle has the same basic configuration, but with different live steam and stage conditions, respectively. Furthermore, there is no steam reheat in contrast to the first plant. More detailed information will be given in the corresponding chapter.

Since the SEGS VI power plant uses evaporative (wet) condenser cooling, both IPSEpro power plant models use this concept, too. Note: The evaporative cooling tower is not modelled within the IPSEpro-PSE flow sheet. Only the source, the sink and the pump of the condenser cooling water are displayed.

8.1 An IPSEpro Model for the Parabolic Trough Power Plant SEGS VI

The solar thermal parabolic trough power plant SEGS VI started its operation in 1988 and is located at Kramer Junction in the Mojave Desert, California, USA. Figure 69 shows a simplified diagram of the SEGS VI power plant. This solar thermal power plant uses synthetic oil as heat transfer fluid. The parabolic trough collectors capture and concentrate sunlight in order to heat the synthetic oil flowing inside the absorber tubes. Then the hot oil is used to generate steam. Therefore an oil/water heat exchanger is necessary to connect the steam cycle with the oil circuit. Then the generated steam expands in a turbine which drives a generator to produce electricity. After the turbine the steam condensates in the condenser and is then recirculated to the steam generator. The cooling tower rejects the heat from the circulating condenser cooling water by evaporative heat and mass transfer to the ambient air. In order to provide electric power also on cloudy days, the plant has a supplementary natural gas boiler.

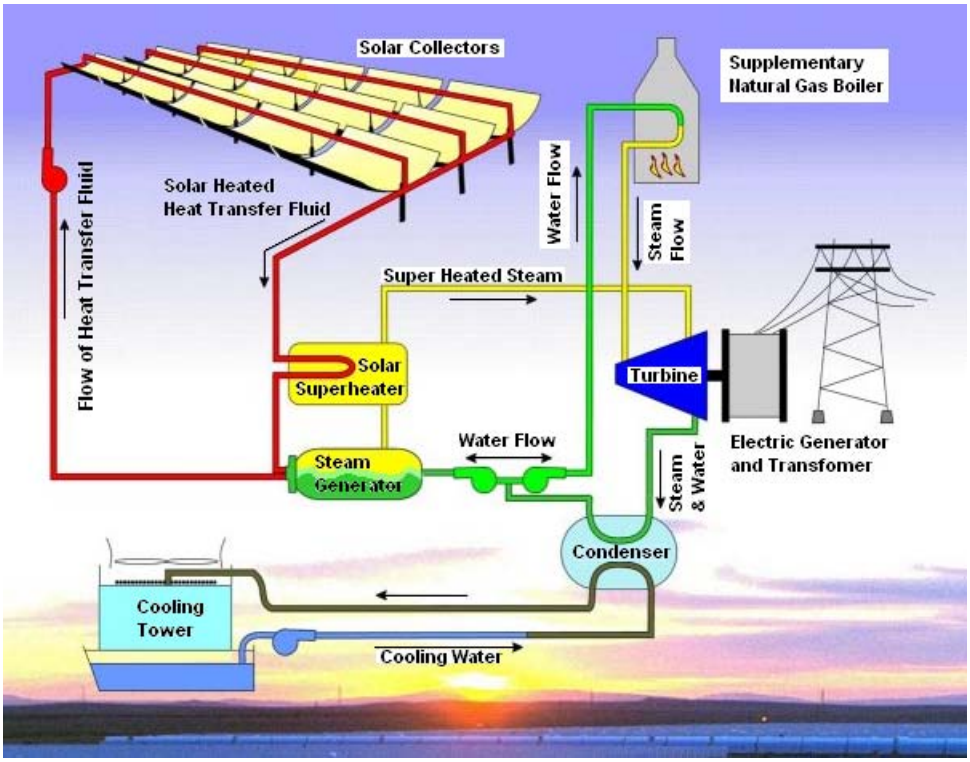

Figure 69: SEGS Principle Diagram [Nextera Energy Resources 2010]

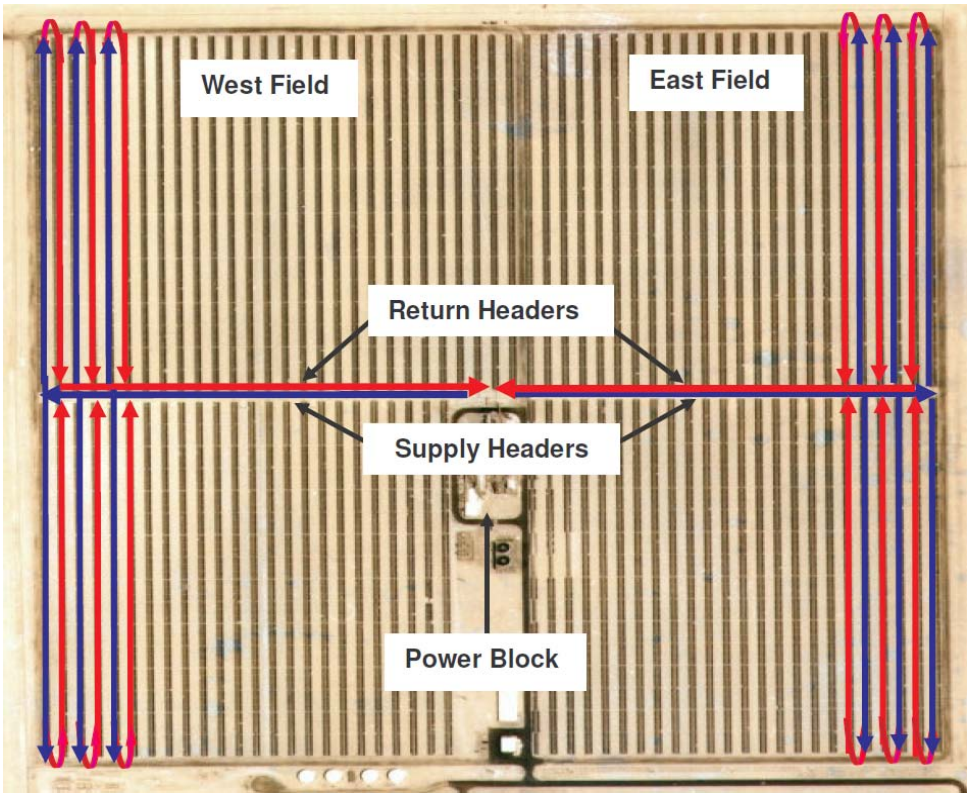

Figure 70: SEGS VI Solar Field Layout [Patnode 2006]

The solar field (figure 70) consists of 50 parallel loops of solar collectors which are connected by header pipes (centre-feed concept). Each parallel loop is an assembly of 16 LS-2 parabolic trough solar collectors, arranged in two parallel rows of 8 collectors. The heat transfer fluid leaves the cold header, enters the collector loop (where it is heated up) and is then pumped back to the steam generator via the hot header pipe. During peak summer periods the temperature rise across the solar field is about 100°C, from an inlet temperature of around 293°C to an outlet temperature of about 390°C. For constant flow rate the solar field outlet temperature will be lower at cloudy periods or during winter. [Patnode 2006]

In the IPSEpro power plant model one of the 50 collector loops is reproduced and a mass flow gain unit (the gain units “T_Header_mix” or “T_Header_split” are described in the appendix) is used after and before the collector loop in order to get the power provided by 50 parallel loops. With this simplification only one loop has to be solved. It is assumed that the sky is cloudless. Therefore the possible partial shading of the solar collector field does not have to be taken into account. Since the whole solar model is only valid for clear days without any clouds anyway, the solar collector field can be replaced by only one loop. However, the correct number of collector rows and the distance between them has to be taken into account, in order to calculate the shading attenuation factor in the early hours of the morning and late hours of the afternoon. This is considered within the global “collector_type_field”.

The distance between the single collector rows amounts to 13 meters. [Stuetzle 2002]

The power cycle used in the SEGS plant is a conventional Rankine steam cycle. The steam generator consists of two parallel heat exchanger trains, that are arrangements of superheater, evaporator and feedwater preheater in series, as well as a reheater in parallel with the other three heat exchangers. [Patnode 2006]

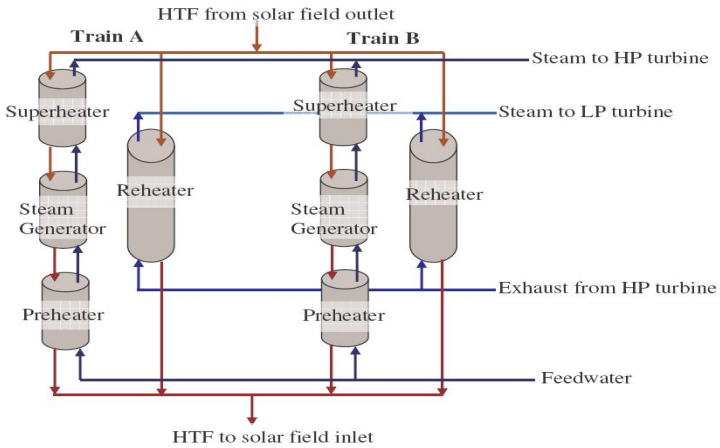

Figure 71: Steam Generator SEGS VI [Patnode 2006]

In the IPSE-Pro model these two trains are modelled as one single train.

The rated electric gross output power of the SEGS VI plant is 35 MW with 100% solar operation. The thermodynamic state of the plant at this rated power is referred as the reference-state.
At rated power conditions the steam generator produces dry steam at a temperature and pressure of 371°C and 100 bar. [Patnode 2006]

The turbine of the SEGS VI plant consists of two high pressure stages and five low pressure stages, with reheat after the last high pressure stage. The temperature after reheat is again

approximately 371°C at a pressure level of 17.5 bar (at rated power conditions). Steam for the feedwater heaters is taken after each stage. The first turbine stage, an impulse stage, is followed by 6 reaction stages. [Patnode 2006]

Turbine stage	Inlet pressure [bar]	Exit pressure [bar]	Isentropic Efficiency
1	100.00	33.61	0.8376
2	33.61	18.58	0.8463
3	17.10	7.98	0.8623
4	7.98	2.73	0.9170
5	2.73	0.96	0.9352
6	0.96	0.29	0.8800
7	0.29	0.08	0.6445

Table 15: Reference Efficiency and Pressures for Turbine Sections [Patnode 2006]

The efficiency of the stages vary at partial load. The relation between the mass flow ratio (mass flow to rated mass flow) and the isentropic efficiency is mentioned by Patnode (2006).

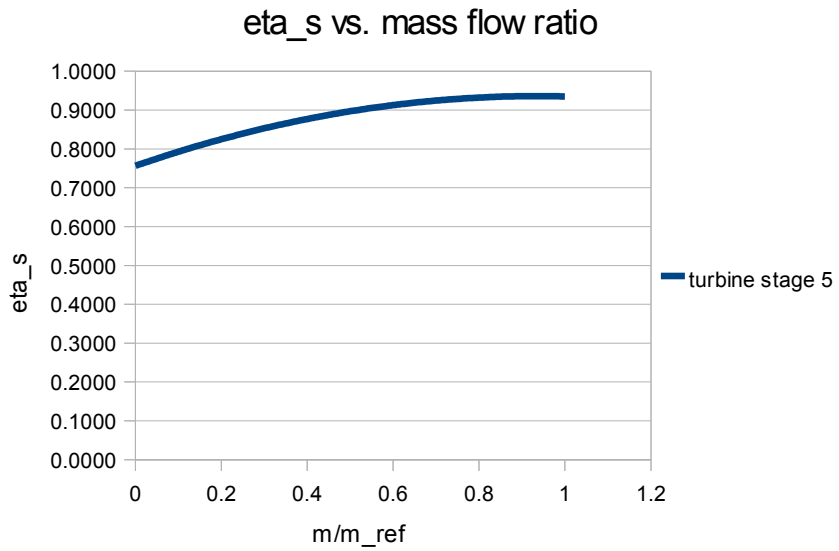

Figure 72: Isentropic Efficiency vs. Mass Flow Rate of Stage 5 [Patnode 2006]

Following Stodola´s elliptic law for steam turbines, the pressure drop over a group of turbine stages varies with the mass flow. This relationship between turbine entry pressure, entry temperature, mass flow rate and outlet pressure at reference conditions and partial load can be described as follows.

$$\sqrt{\frac{p_{\alpha}^2 - p_{\omega}^2}{T_{\alpha}}} = \frac{\dot{m}}{\dot{m}_0} \cdot \sqrt{\frac{p_{\alpha 0}^2 - p_{\omega 0}^2}{T_{\alpha 0}}}$$ [Jericha 1985]

p_α.....pressure at turbine entry [bar]
p_ω..... pressure at turbine outlet [bar]
T_α..... temperature at turbine entry [K]
$p_{\alpha 0}$.... pressure at turbine entry at reference conditions [bar]
$p_{\omega 0}$.... pressure at turbine outlet at reference conditions [bar]
$T_{\alpha 0}$.... temperature at turbine entry at reference conditions [K]
$\dot{m}$ .. mass flow [kg/s]
$\dot{m}_0$. mass flow at reference conditions [kg/s]

Note: In this work the elliptic law is applied for each reaction stage, although in the strict sense, it is only valid for a group of turbine stages.

During partial load, the steam mass flow is determined by the steam generator (power provided by the solar field) and the outlet pressure of the turbine is set equal to the condensing pressure. Thus, the inlet pressure of the 6 reaction stages is calculated by Stodola´s elliptic law.

After having modelled the SEGS VI power plant at rated conditions, also the partial load behaviour was considered. IPSEpro turbine partial load models of the standard model library have been taken and set according to the data provided by Patnode (2006).

The IPSEpro SEGS VI plant model is only run in 100% solar mode (the auxiliary natural gas boiler is not taken into account).

The SEGS VI power plant uses evaporative (wet) condenser cooling. Therefore, the cooling tower rejects heat from the circulating cooling water by evaporative heat and mass transfer to the ambient air. After leaving the condenser the cooling water is pumped to the top of the tower, is distributed and cascades down the fill media to the well at the bottom. In addition, two fans located at the top of the tower propel the warm, moist air upward in the atmosphere. Simultaneously, fresh ambient air is drawn through the bottom of the tower and across the fill media. Approximately 1 – 2% of the cooling water is lost due to evaporation. In order to keep the cooling water flow constant, fresh water has to be added after the collection in the sump at the bottom of the tower. During the design of the plant the water consumption for makeup feedwater, cooling water and other site services was estimated at 555 066 m³ per year. [Patnode 2006]
The rated parasitic power consumption of the cooling tower is listed at 0.91 MW, at a reference cooling water flow rate of 1393.3 kg/s. Patnode (2006) assumes that this power includes the cooling water pumping power and the power needed for the twin two-speed air fans. The cooling tower fans are listed at 0.116 MW each at the higher operating speed of 106 rpm. On summer days and spring/fall days the cooling tower fans are assumed to run at the higher operation speed, whereas during days in winter both fans operate at the lower speed of 53 rpm. [Patnode 2006]

In this work the cooling tower fans are assumed to run at full speed during the whole day and the pumping power for the cooling water is calculated for each operating point. Patnode (2006) provides cooling water temperature measurements at the inlet and outlet of the steam condenser on June 20th, 1998. Based on these measurements I set the inlet temperature to 24°C and the outlet temperature to 34°C. In order to calculate the required pumping power for the condenser cooling water I assumed the pressure rise at the pump to 2 bar. Furthermore, the two cooling tower fans are assumed to run at full speed (0.116 MW each). This constant additional power consumption is needed for the calculation of the total solar-to-electric efficiency.

The total solar-to-electric efficiency (total plant efficiency) is the net power plant output (MW_e) divided by the power provided by the sun (MW). The power provided by the sun is the direct normal irradiance DNI, reaching the surface of the earth, times the total aperture area of the

parabolic trough collectors. The net power plant output is the generator output minus all parasitic consumptions (pumping power for the feedwater, pumping power for the cooling water, power for the cooling tower fans and pumping power for the heat transfer oil).

In the following figure 73 the IPSEpro-PSE project file of the modelled SEGS VI plant is shown. The orange piping represents the heat transfer oil circuit. Let's start with the collector loop at the top of the figure. The heat transfer oil enters the loop at a temperature of about 280°C, flows through the 16 solar collector units and leaves the collector loop at a temperature of 390°C. After the collector loop the mass flow of the heat transfer oil is multiplied by the real number of collector loops in order to get the power of the whole solar field. Then the hot oil flow is separated into two parallel streams. One leads to the steam superheater, evaporator and preheater, that are connected in series. The second oil stream reheats the steam coming from the high pressure turbine. Thereafter, the two parallel streams merge and the cold heat transfer oil is pumped back to the solar field. Of course the total oil mass flow has to be divided again by the real number of collector loops, in order to get the required mass flow for the single collector loop representing the whole solar field. In the model I set the collector loop exit temperature to 390°C and the oil mass flow is a calculation result. In the steam cycle the live steam conditions are set to 100 bar and 371°C. Thus the live steam mass flow is a result of the energy balance within the steam generator. After the high pressure turbine the steam reheat temperature is set to 371°C again. The condensing pressure is set to 0.08 bar and the pressure level of each reaction stage is a calculation result according to the elliptic law (Note: It is assumed that the elliptic law is valid for one single stage). At every operating point calculated, the exit temperature of the solar field is set to 390°C. Also the live steam conditions (371°C at 100 bar) are constant during the day. As already mentioned before, the cooling water exit and inlet temperature of the condenser were set to the levels provided by Patnode (2006) (inlet at 24°C, outlet at 34°C). In order to take the power consumption of the two cooling tower fans into account, they are assumed to run at the high speed (106 rpm) consuming 0.116 MW each. Note: The cooling tower is not shown in figure 73. The power of the two fans is taken into account within the data frame. Only the source, the sink and the pump for the condenser cooling water are shown.

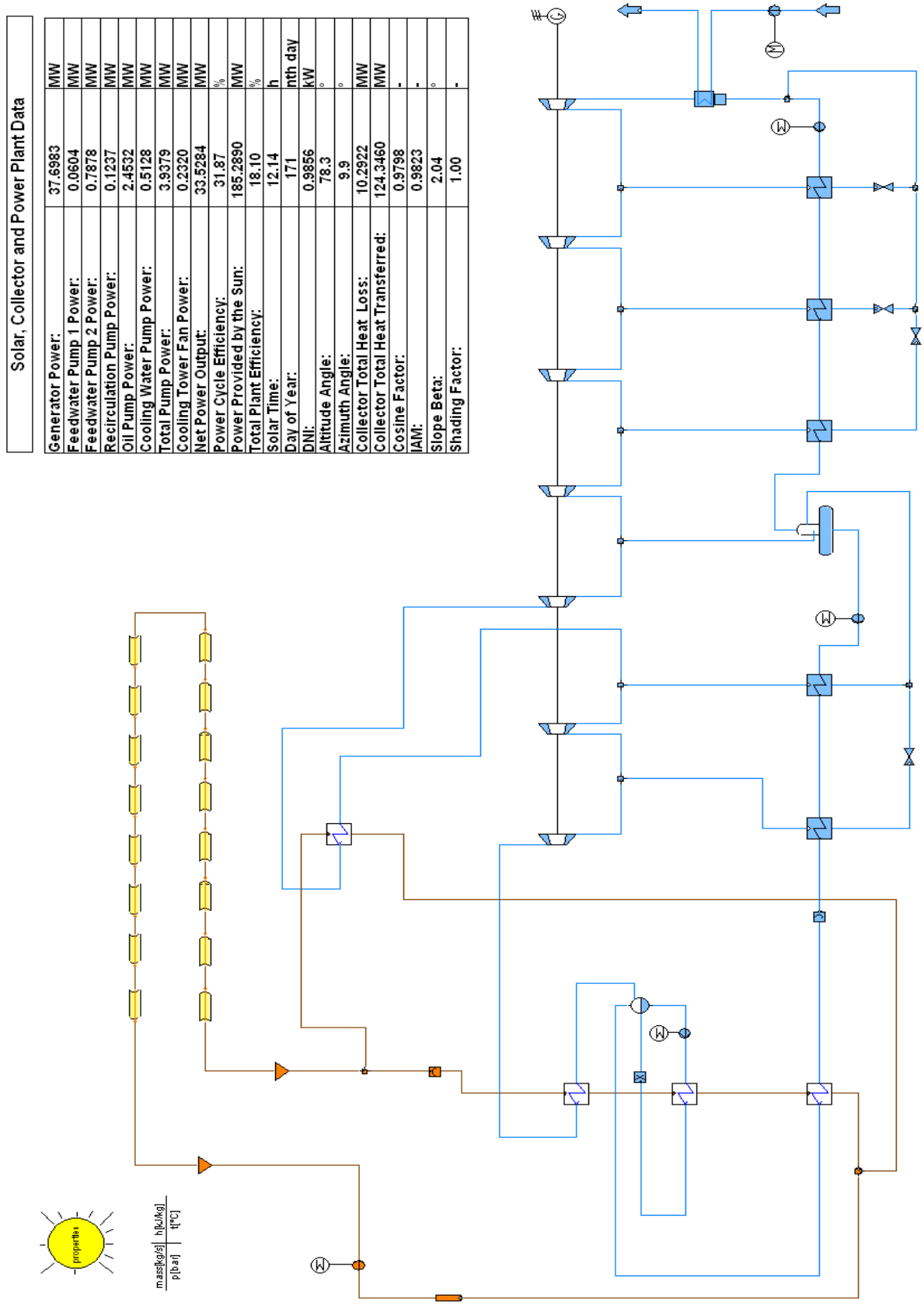

Figure 73: IPSEpro SEGS VI Model; Data Table from the 20th of June at 12:00

For certain days, Patnode (2006) provided direct normal irradiance measurements as well as heat rate data of absorbed and transferred heat per square meter of the total collector aperture area. The absorbed heat is the fraction of the incident solar radiation that finally hits the absorber tube. The heat transferred is the fraction of the incident solar radiation, that heats up the oil within the absorber tube. Therefore, the heat transferred is the absorbed heat reduced by the thermal losses.

In order to validate my collector models, I calculated on two specific days the direct normal irradiance, the total absorbed heat (per m² of aperture area) and the total heat transferred (per m² of aperture area) with the IPSEpro SEGS VI model. I calculated a typical day in summer (20th of June) and a typical day in spring (12th of March).

In the following figures 74 and 75, the data provided by Patnode (2006) (continuous lines and the circular symbols for the DNI) and the corresponding IPSEpro calculation results (dashed lines) are shown.

As can be seen in figure 74, the direct normal irradiance (DNI) values calculated match well with the measured ones. Also the lines for the total absorbed heat per square meter of aperture area (blue continuous line and blue dashed line) match quite well in the morning and in the afternoon. Between 11:00 am and 3:00 pm there is a small difference, that might be the consequence of a reduced intercept factor due to wind loads. The assumption of possible wind loads is reconfirmed by the lines for the retained heat (red continuous line and red dashed line). Since there is no wind taken into account in the used IPSEpro heat loss model, the calculated heat loss is smaller than the real one.

Figure 75 shows the results for a day in spring. Due to the collector north-south orientation and the sun´s low altitude angle the angle of incidence on the aperture plane is larger at noon than in the morning or afternoon. These circumstances lead to the characteristic shape of the lines for retained and absorbed heat during the colder seasons. As can be seen in figure 75, the values for the transferred heat are lower at noon than they are during hours in the morning and hours in the afternoon. The main reason for this characteristic shape is the variation of the cosine loss during a day as discussed in chapter 5.1. Basically, the sun´s current position (defined by the altitude and azimuth angle) and the corresponding collector tilt angle (slope β) determine the angle of incidence on the parabolic trough´s aperture plane. This angle of incidence defines the cosine loss attenuation factor which is the reason for the characteristic shape of the line for absorbed and transferred heat. In addition, the location of the power plant influences the cosine loss attenuation factor. Let´s consider the northern hemisphere. The further north the power plant is located, the smaller is the sun´s altitude angle at solar noon, thus causing a large angle of incidence on the now horizontal aperture plane of the parabolic trough (north-south orientation). On the other hand, the further south the location of the power plant, the larger is the sun´s altitude angle at solar noon. Thus, causing a small angle of incidence and a small cosine loss. The extreme case would be reached, if the sun was at the zenith at solar noon. There the incoming solar radiation would be perpendicular to the parabolic trough´s aperture plane, causing no cosine attenuation at all. Finally, the values for the absorbed and transferred heat are higher during hours in the morning and during hours in the afternoon, because the way of the sun starts in the eastern part of the sky and ends in the western part. Therefore, due to the north-south orientation of the parabolic trough collector, the angle of incidence reaches small values in the morning and in the afternoon as the parabolic trough collector´s aperture plane can be tilted towards the sun (big slope β). Only the mutual shading limits the maximum slope angle β (chapter 5.2). The shading losses and the atmospheric attenuation are the reasons for the steep ascent and descent of the lines for the absorbed and transferred heat during the early hours in the morning and the late hours in the afternoon (figure 75).

Considering now the lines for calculated and measured data, shown in figure 75, the calculation results match quite well the measured values, except in the afternoon after 1:00 pm. There the measured DNI slightly exceeds the calculated values, which might be the result of a change in the atmosphere´s attenuation. Thus, also the measured values for the absorbed heat are higher than the calculated ones.

Also piping loss measurements are shown in figures 74 and 75. As these are rather small when compared to the absorber heat loss I did not model them in detail. Piping heat losses and additional pressure losses can be taken into account in my models when setting the corresponding parameters within the unit “T_pipe” (is located before the oil pump in the heat transfer fluid circuit; figure 73).

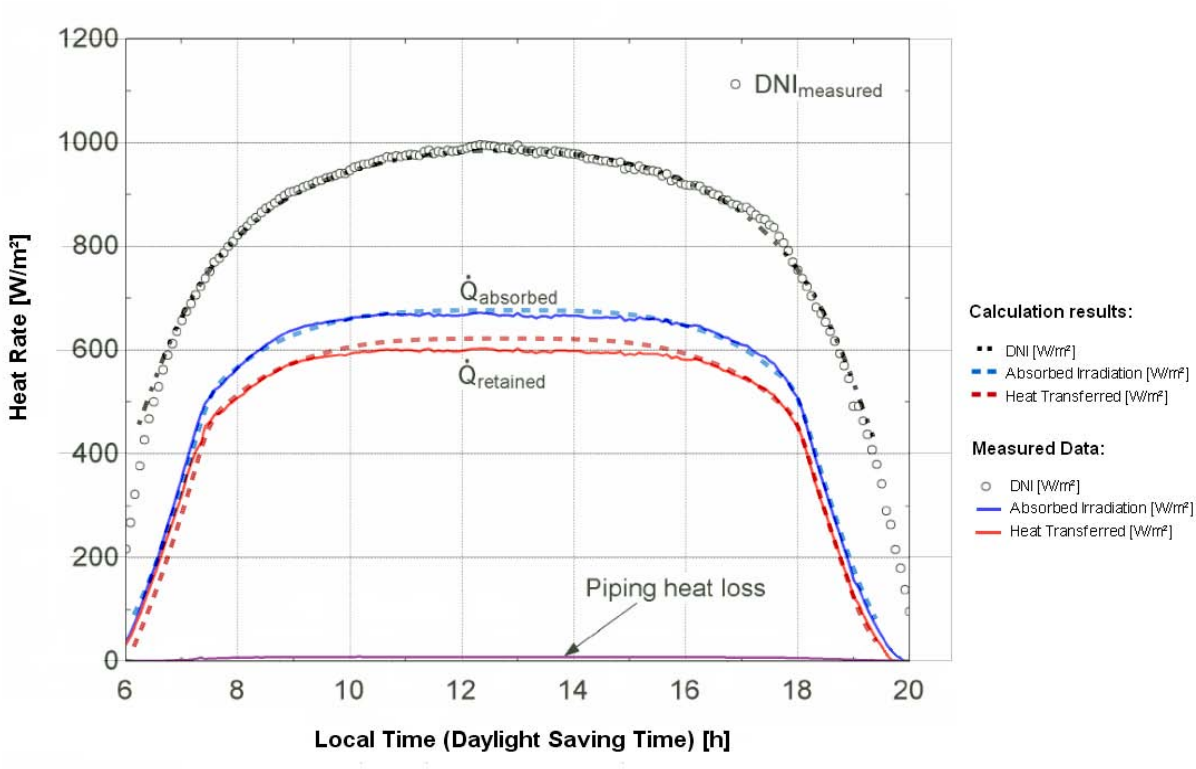

Figure 74: Measured [Patnode 2006] and Calculated Data, 20th of June

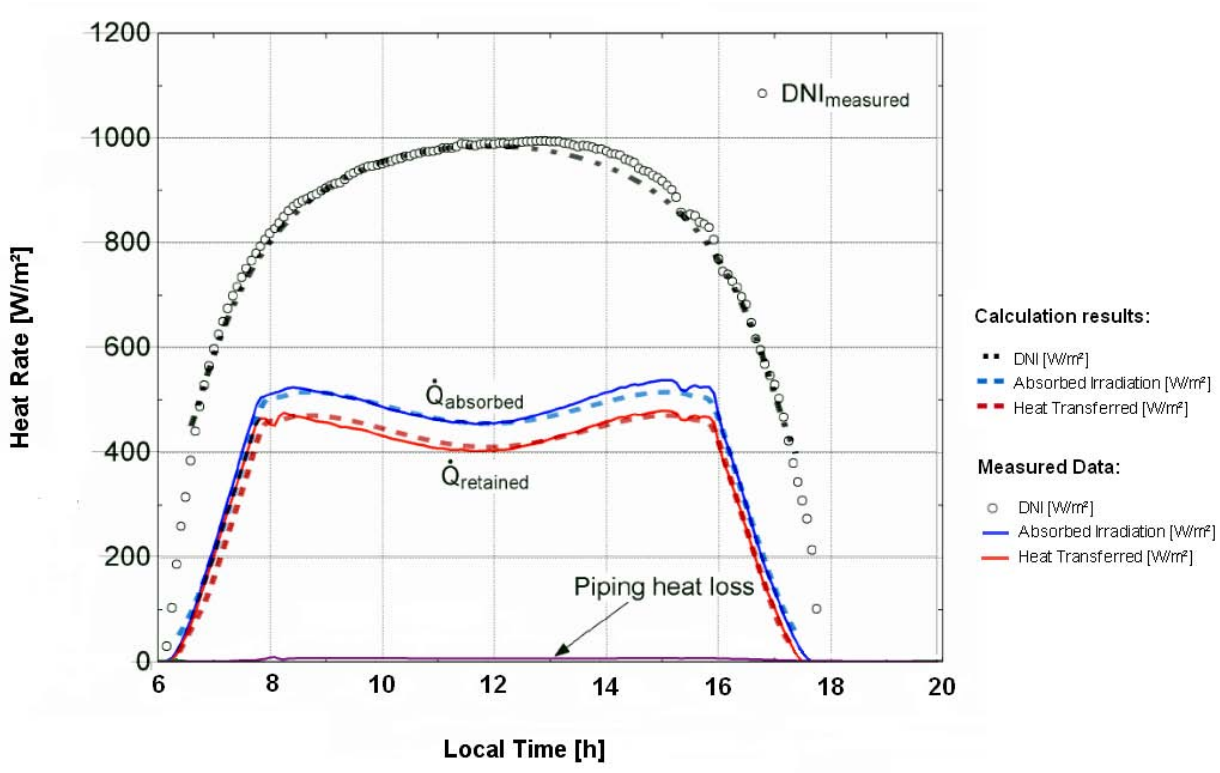

Figure 75: Measured [Patnode 2006] and Calculated Data, 12th of March

In order to give an idea of the possible power plant output and the total solar-to-electric efficiency on these specific days the following figures 76 and 77 are shown. These figures show calculation results for the IPSEpro SEGS VI model. The figures are based on the calculation results provided in appendix C on the pages C1 and C2 (the results correspond to the data table in figure 73).

In figure 76 the power output follows the corresponding results for the heat retained. The big difference between June and March also shows the importance of a good part load behaviour of the plant´s power cycle.

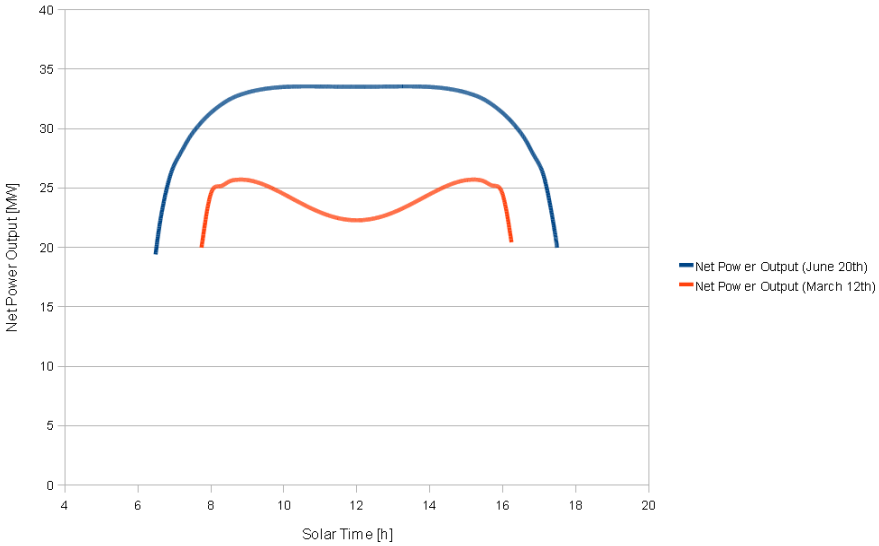

Figure 76: IPSEpro Model SEGS VI Net Power Output

In figure 77 the calculated total solar-to-electric efficiencies are shown. The low values for the month March at noon are the consequence of a quite large angle of incidence. The cosine loss attenuation factor is the major cause of this decrease in efficiency.

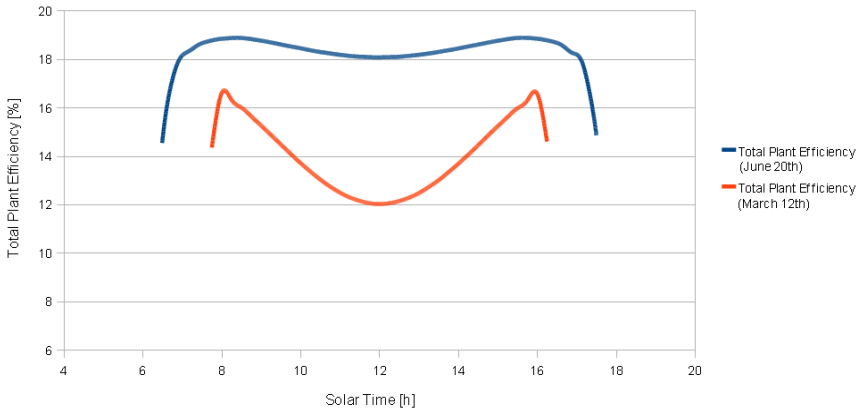

Figure 77: IPSEpro Model SEGS VI Total Plant Efficiency

An interesting fact that can be seen in the figures above is that the total plant efficiency on the 12th of March has a peak value around 8 am and 4 pm, whereas the line of the net power output has a by far more smooth shape. Since the net power output is the direct normal irradiance (DNI) multiplied by the total aperture area and the total plant efficiency, the shape of the net power output line is also determined by the DNI values. As the gradient of the DNI curve is quite large around 8 am and 4 pm, the smooth shape of the net power output line can be explained.

As already mentioned in chapter 5.1 the angle of incidence defines the cosine loss attenuation factor. For the north-south collector orientation, the small altitude angle of the sun at noon limits the efficiency in the colder seasons. The following figures show the altitude angle of the sun plotted versus the azimuth angle (figure 78) and the cosine attenuation factor plotted versus the solar time (figure 79). The values are shown for the 20th of June and the 12th of March at the location of the SEGS VI power plant (Kramer Junction, California, USA). Also these values are included in the calculation data tables in appendix C on the pages C1 and C2.

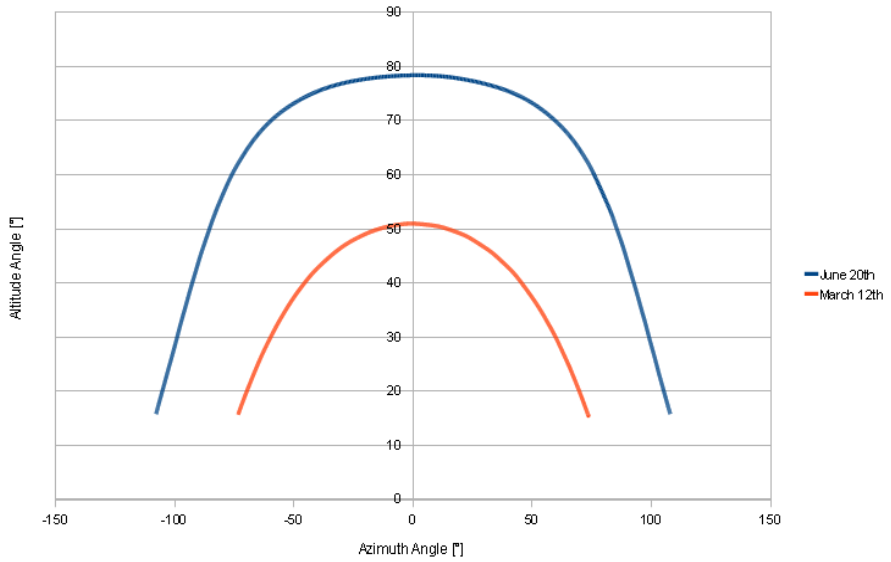

Figure 78: Altitude and Azimuth Angle at Kramer Junction, California, USA; June 20th and March 12th

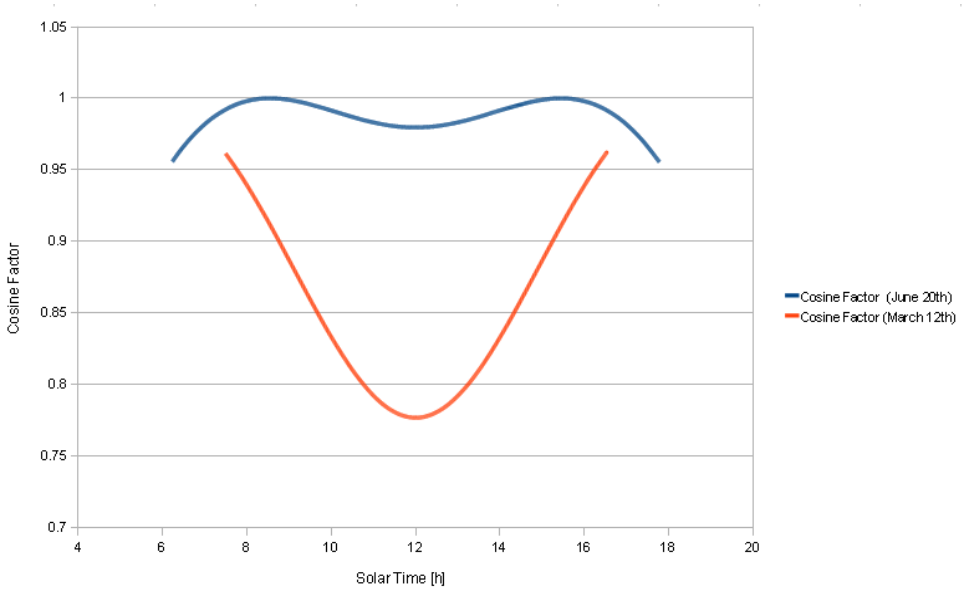

Figure 79: Cosine Attenuation Factor on June 20th and March 12th

The altitude angle of the sun amounts to 78° on the 20th of June at solar noon, but only slightly exceeds 50° on the 12th of March.

The tables in appendix C (page C1 and C2) show the IPSEpro calculation results of these two day-simulations. The data shown are steady state calculation results in time steps of 15 minutes. The results correspond to the data frame shown in figure 73.

In summary, the following can be said: The solar-to-electric efficiency and performance of solar thermal power plants, using parabolic trough collectors, largely depend on the time of year, on the current solar time and on the location.

8.2 An IPSEpro Model for a DSG Parabolic Trough Power Plant

Since there are no commercial DSG parabolic trough power plants in operation so far, I simulated a plant using reasonable data and compared its performance to that of the SEGS VI simulation. Therefore I modelled a recirculation-mode DSG plant using the same collector type, the same total aperture area and the same location. The live steam conditions and the steam cycle are different, as there is no steam reheat possible. Higher steam temperatures can be reached due to the absence of oil as heat transfer fluid.

Basically, the solar field consists again of 50 collector loops, which are fed by the cold header pipe (feed water) and drain into the hot header pipe (superheated steam). Each collector loop has a total collector length of 768 meters (defined by the SEGS VI simulation: 16 times 48 m is 768 m). The length of the preheating, evaporating and superheating section is then defined by the live steam temperature, the steam quality at the end of the evaporating section and the feed water temperature entering the solar field. For a given steam mass flow the length of the superheating section defines the live steam temperature and the length of the evaporating section defines the steam quality reached at the water/steam separator. Furthermore, the length of the preheating section defines the temperature of the feed water entering the solar field. In this simulation 22% of the collector loop length is used for preheating, 48% for evaporating and 30% for superheating. The data of the LS-2 collector type is used in this simulation again. Furthermore, the same heat loss model as in the SEGS VI simulation is used.
The live steam conditions are assumed to 500°C and 100 bar. These conditions were proposed by Montes et al. (2009) and Zarza et al. (2001).

For the part load behaviour, I used the same assumptions as for the SEGS VI simulation. In general, the steam cycle is the same, except with higher live steam temperature and without reheat.

In figure 80 the IPSEpro-PSE model of the DSG power plant is shown. Again, only one collector loop is modelled. In order to simulate the whole solar field, a mass flow gain and split unit is used (blue triangle shaped units; “W_Header_mix” and “W_Header_split” are included in the appendix). After leaving the last feed water preheater of the power cycle the total mass flow is reduced by the “W_Header_split” unit, adjusting the mass flow to a suitable value for one collector loop. According to Montes et al. (2009) the mass flow per loop should be in the range of 1 – 2 kg/s in order to keep the pressure drop within a reasonable range. Then the feed water is mixed with the recirculation mass flow coming from the water/steam separator, which is located after the evaporation section. Thereafter, the feed water enters the collector preheating section and reaches the saturation temperature at the end of this section. In the “W_Xprescription” unit (blue square with an x inside) at the beginning of the evaporating section, the steam quality is set to 0. In the following three “W_Xprescription” units no settings are made. They are only required for the display of the steam quality. After the evaporating section the steam/water separator separates the two phases. Then the saturated steam enters the superheating section. After the “W_Header_mix” unit, where the mass flow is adjusted to the total mass flow, the superheated steam expands in the turbine. According to Eck et al. (2003), the water at saturation temperature that leaves the water/steam separator is mixed with the feed water flow before the collector preheating section. Another possibility would be to pump the water, that leaves the separator, directly back to the evaporating part. But this would require a separate preheating section and thus a more complex tube assembly [Goebel 1998].
Furthermore, the same cooling tower configuration that was described for the SEGS VI plant is used again. The cooling tower fan power is assumed to be constant during the day (0.116 MW each).

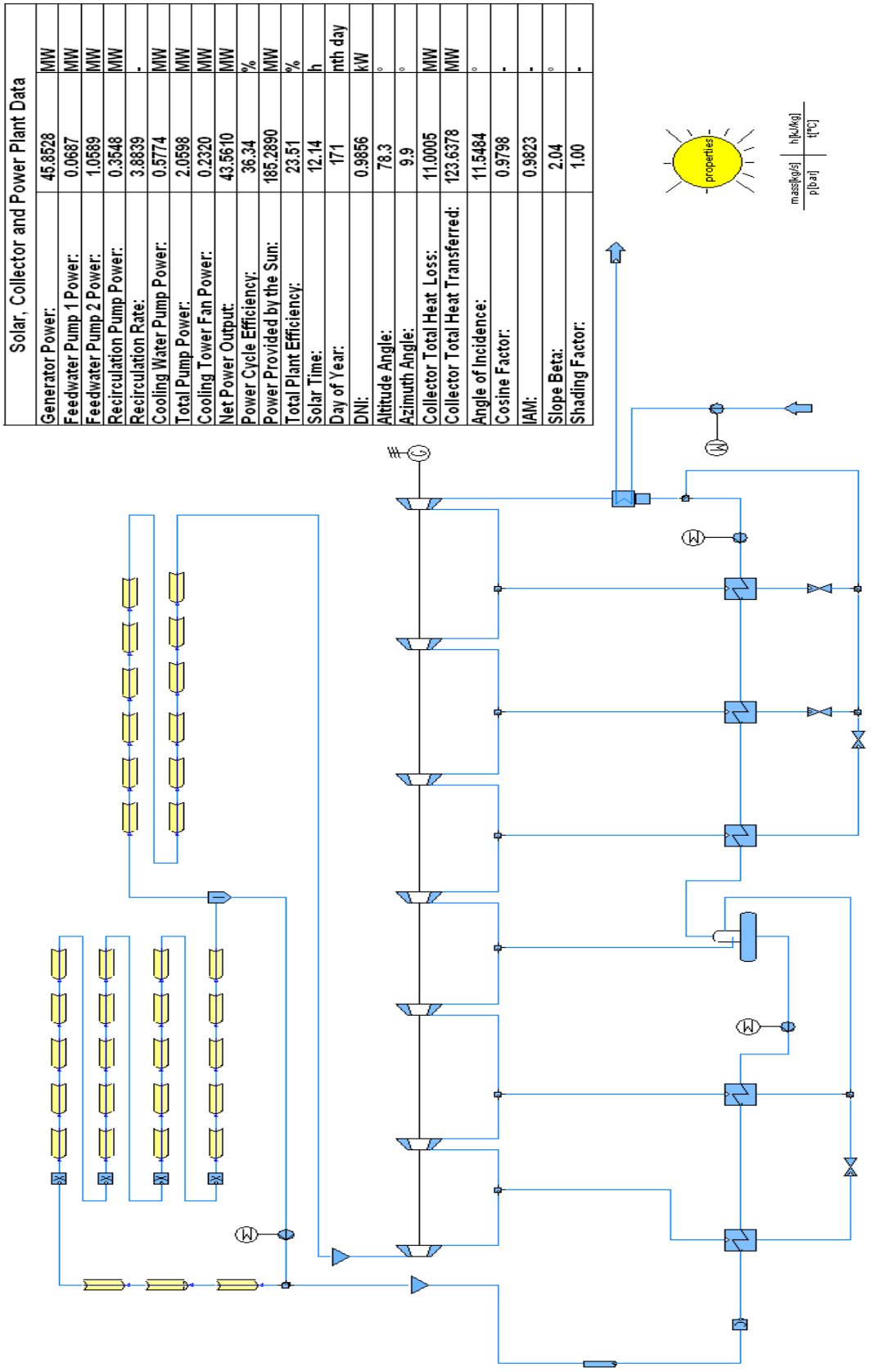

Figure 80: IPSEpro DSG Model; Data Table from the 20th of June at 12:00

After having modelled the DSG parabolic trough solar power plant, I calculated the steady-state results for certain operating points throughout a day. They were calculated in time steps of 15 minutes, starting at 6:30 am until 5:15 pm. The solar irradiation data is again from the 20th of June at Kramer Junction, California, USA. All the results are shown in appendix C (page C4).

In the following I compare the results of the IPSEpro DSG simulation with those of the IPSEpro SEGS VI simulation:

The first interesting aspect is a comparison of the thermal performance of the collector field. Since the absorber tube temperatures of the two concepts are different, there might be a difference in total heat loss. For the DSG concept, the evaporating section has an almost constant temperature of around 318°C and the tube temperatures of the superheating section (live steam temperature is 500°C) exceed those of the SEGS VI plant. At the collectors using oil as heat transfer fluid the temperature rises continuously to an end temperature of about 390°C, starting at around 280°C. In figure 81, I show the ratio of the total heat transferred to the power provided by the sun. It shows, which fraction of the incident solar power is finally able to heat the fluid within the absorber tube. However, the thermal performance of these two different collector fields is rather the same. The performance of the collector field using oil as heat transfer fluid is slightly better than that of the DSG field. This is due to a slightly smaller absorber tube mean temperature. Thus, the expected higher efficiency of the DSG concept cannot be confirmed by the thermal performance of the solar field.

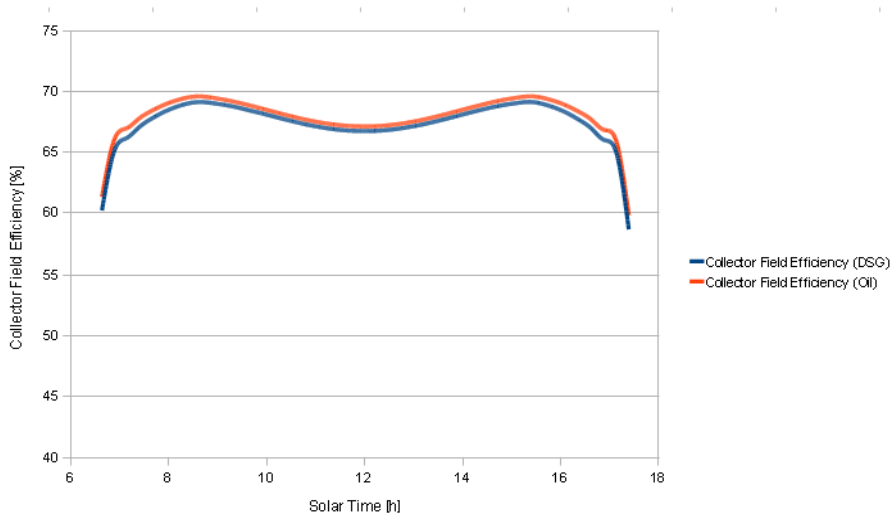

Figure 81: Thermal Performance of the Solar Field (DSG vs.Oil)

But if the total plant efficiencies of these two concepts are compared (figure 82), the higher efficiency of the DSG concept can be seen clearly. With the assumptions mentioned, a maximum solar-to-electric efficiency of about 24% may be reached, compared to 19% for the oil concept. Therefore, the absence of the oil-water heat exchanger, the higher live steam temperature and the lower pumping power for the solar field are crucial factors for increasing the power plant efficiency.

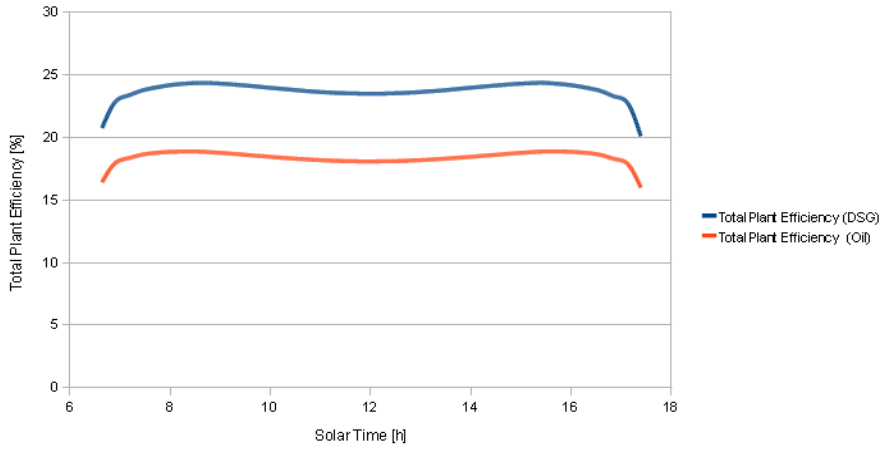

Figure 82: Total Plant Efficiency on June 20th (DSG vs. Oil)

When using the same total collector aperture area the higher efficiency of the plant leads to a higher net power output. This can be seen in figure 83. The DSG plant achieves a maximum net power output of about 44 MW, whereas the SEGS VI plant reaches values up to about 34 MW.

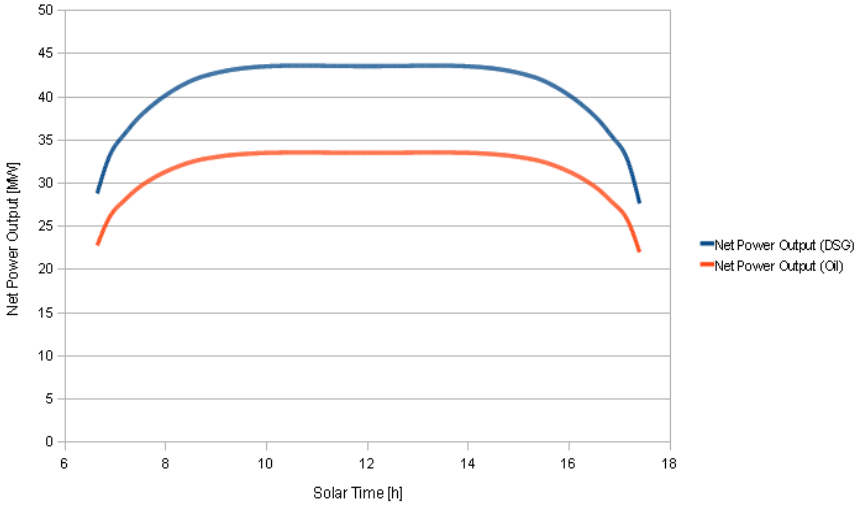

Figure 83: Net Power Output on the 20th of June (DSG vs. Oil)

In summary, the following can be said: Although the direct steam generation concept promises higher efficiencies, stable and practically feasible control concepts have to be developed in order to cope with dynamic instabilities (for instance the Ledinegg instability). Also the issue of high temperature gradients across the absorber tube at higher flow steam qualities (stratified flow) has to be addressed. Once these problems are solved, the parabolic trough direct steam generation concept might play a major role in the field of solar thermal power plants.

9 Conclusion and Outlook

The first aim of this work was to describe possible solar thermal power plant configurations in order to give an overview of the actual state of the art. Then, the second and main part was the enlargement of an already partially existing IPSEpro solar model library. Therefore the today´s most used collector concept, the parabolic trough collector, was chosen for a detailed modelling. Thereafter, power plant configurations were simulated within IPSEpro-PSE, using the developed solar modules.

Before I actually started with the modelling of the collector units, I had to determine the solar radiation that is available on the earth´s surface. I described equations that are able to determine the actual position of the sun for a certain location on earth. Having calculated this position, equations are shown which enable the calculation of that fraction of radiation that can be finally received by a certain aperture area.

When considering the parabolic trough collector, two concepts are possible. The first and today´s most established one is the parabolic trough collector using oil as heat transfer fluid. Thus, an additional heat exchanger between the oil circuit and the steam cycle is necessary. The second concept generates steam directly within the absorber tubes of the solar collector field. This concept is called direct steam generation (DSG) and promises higher solar-to-electric efficiencies. In this work I started the modelling of the parabolic trough collectors in general, regardless of the used fluid within the absorber tube. Since the attenuation of the incident solar radiation is the same for collectors with heat transfer fluid or DSG, at first both concepts can be treated in the same way. The distinction has to be made, when calculating the heat loss and the heat transfer. Since the absorber tube inner wall temperature is determined by the heat transfer coefficient, that differs for different phases or fluids, different collector models had to be created. I created one IPSEpro unit for oil as heat transfer fluid (“T_Solar_collector”) and one IPSEpro unit for DSG (“W_Solar_collector”). Concerning the DSG unit, the model for preheating, evaporating and superheating had to be distinguished. For each case different equations for the heat transfer coefficient are valid. The same distinctions had to be made concerning the pressure loss (pumping power) within the absorber tubes. For each application I described suitable correlations.

Since in this work the whole IPSEpro collector unit “T_Solar_collector” or “W_Solar_collector” is taken as one element of discretization, I proposed suitable values for the collector element length.

Then, I created IPSEpro-PSE flow-sheets in order to calculate two power plant concepts.
The first solar thermal power plant model is based on the SEGS VI (Solar Electric Generation Station) that is operated at Kramer Junction in California, USA, since 1988. This plant uses oil as heat transfer fluid and the solar field outlet temperature of 390°C enables live steam conditions of 371°C at 100 bar. After having modelled this power plant, the thermal performance of the IPSEpro collector field has been compared to measurements that are provided by Patnode (2006). The comparison showed that the calculated values of the transferred heat correlate well with the measured values.
Finally, I wanted to compare the performance of the SEGS VI plant with a direct steam generation (DSG) plant. Therefore I modelled a recirculation-mode DSG plant using the same collector type, the same total aperture area and the same location. However, the live steam conditions and the steam cycle are different, as there is no steam reheat possible.
The performance of these two solar power plants was calculated throughout one day. The steady-state results for a certain number of operating points were calculated. I compared the results for the net power output and the solar-to-electric efficiency. As expected, the DSG concept enables higher solar-to-electric efficiencies, due to the higher live steam temperature, the absence of the

oil/water heat exchanger and the lower parasitic losses.

For future continuative work the following recommendations are given:

As the equations for the DSG unit are quite complex and can lead to convergence problems, it might be suitable to derive simpler models based on the detailed ones.

Also different condenser cooling concepts are of interest. In the two plant models mentioned in chapter 8.1 and 8.2, I assumed water-cooled condensers, as they are used in the SEGS VI plant. In case that there is not enough water available for cooling, an air cooling concept would have to be used. Due to the usually high ambient temperatures at solar thermal power plant sites, high air mass flow rates and condenser pressure levels would be necessary. All these factors may lead to a major decrease in solar-to-electric efficiencies and to longer investment payback times.

Concerning the intention of developing a comprehensive solar thermal power plant model library for IPSEpro, there is still work left for other concentrated solar power (CSP) concepts. The detailed modelling of the parabolic trough collectors itself was complex enough to fill this work´s scope. In order to offer a comprehensive CSP library, all the other concepts that were basically explained at the beginning of this work would have to be modelled and verified with real measurement data.
As a next step the linear Fresnel single tube concept should be modelled, as it is quite similar to the parabolic trough collector concept. However, a major modification of the heat loss models would be necessary, as well as a different description for the DNI attenuation.
Concerning the solar power tower concepts, the most difficult part would be the modelling of the solar field´s performance. For instance, shading losses are by far more complicated than those of the parabolic trough concepts.
Also the modelling of heat storage concepts should be considered, as they enable power supply even after sunset, increasing the possible plant operating time per day.

10 References

Abengoa Solar 2008: Official Web Site, <http://www.abengoasolar.com>, (08.02.2010)

Badescu V. 2008: Modeling Solar Radiation at the Earth´s Surface, Springer Verlag, Berlin, Heidelberg

Baehr H.D., Stephan K. 1998: Wärme- und Stoffübertragung, 3. Auflage, Springer Verlag, Berlin, Heidelberg, Germany

Bertoletti S. et al. 1965:A General Correlation for Predicting the Heat Transfer Crisis with Steam Water Mixtures, Energia Nucleare 12(3)

Birnbaum J., Eck M., Fichtner M.; Hirsch T., Lehmann D., Zimmermann G. 2008: A Direct Steam Generation Solar Power Plant with Integrated Thermal Storage, Proceedings of the 14th SolarPACES Symposium, Las Vegas, USA

Bockamp S., Griestop T., Fruth M., Ewert M., Lerchenmüller H., Mertins M., Morin G., Häberle A., Dersch J. 2003: Solar Thermal Power Generation, PowerGen Europe, Düsseldorf, Germany

Brennen C.E. 2005: Fundamentals of Multiphase Flows, California Institute of Technology, Cambridge University Press

Butterfield M.H. 1992: Dynamics and Control in Nuclear Power Plants, British Nuclear Energy Society, Thomas Telford, London

Butterworth D. & Hewitt G. F. 1977: Two-Phase Flow and Heat Transfer, Oxford University Press, Walton Street, Oxford

Cengel Y.A. 2003: Heat Transfer – A Practical Approach, Second Edition, McGraw-Hill Higher Education, New York

Chen J.C. 1963: A Correlation for Boiling Heat Transfer to Saturated Fluids in Convective Flow, ASME preprint 63HT34, presented at the 6th National Heat Transfer Conference, Boston

Collier J. G. & Thome J. R. 1996: Convective Boiling and Condensation, 3rd Edition, Oxford University Press, Oxford

Crastan V. 2009: Elektrische Energieversorgung 2, Energie- und Elektrizitätswirtschaft, Kraftwerktechnik, alternative Stromerzeugung, Dynamik, Regelung und Stabilität, Betriebsplanung und Führung, 2. bearbeitete Auflage, Springer Verlag, Berlin, Heidelberg

Dittus F.W. & Boelter L.M.K. 1930: Publications on Engineering 2, University of California

Dudley V.E., Kolb G.J., Mahoney A.R., Mancini T.B., Matthews C.W., Sloan M., Kearney D. 1994: Test Results SEGS LS-2 Solar Collector, Sandia National Laboratories, Sandia Corporation, USA

Duffie J.A.& Beckman W.A. 2006: Solar Engineering of Thermal Processes, 3rd edition, John Wiley & Sons, Inc., Hoboken, New Jersey

Eck M., Steinmann W.D. 2001: Direct Steam Generation in Parabolic Troughs: First Results of the DISS Project, Solar Energy Forum 2001: The Power to Choose, Washington, D.C., USA

Eck M., Zarza E., Eickhoff M., Rheinländer J., Valenzuela L. 2003: Applied Research Concerning the Direct Steam Generation in Parabolic Troughs, Solar Energy 74, Elsevier Ltd.

Eck M. & Hirsch T. 2007: Dynamics and Control of Parabolic Trough Collector Loops with Direct Steam Generation, Solar Energy 81, Elsevier Ltd.

Elsaket G.M. 2007: Simulating the Integrated Solar Combined Cycle for Power Plants Application

in Libya, Master of Science Thesis, School of Engineering, Cranfield University

Esposito S., Antonaia A., Addonizio M.L., Aprea S. 2009: Fabrication and Optimisation of Highly Efficient Cermet-based Spectrally Selective Coatings for High Operating Temperature, Thin Solid Films 517, Elsevier B.V.

Falcone P.K. 1986: A Handbook for Solar Central Receiver Design, SAND86-8009, Sandia National Laboratories, Livermore, CA, USA

Farooq M. & Hutchins M.G. 2002: A Novel Design in Composities of Various Materials for Solar Selective Coatings, Solar Energy Materials & Solar Cells 71, Elsevier Science B.V.

Farooq M. & Raja I.A. 2008: Optimisation of Metal Sputtered and Electroplated Substrates for Solar Selective Coatings, Renewable Energy 33, Elsevier Ltd.

Fernandez D.V.: PS10 – a 11 MWe Solar Tower Power Plant with Saturated Steam Receiver, <http://www.upcomillas.es/catedras/crm/report05/Comunicaciones/Mesa%20IV/D.%20Valerio%20Fern%C3%A1ndez%20-%20Solucar%202.pdf> (24.03.2010)

Friedel L. 1974: Modellgesetze für den Reibungsdruckabfall in der Zweiphasenströmung, Dissertation, Technische Universität Hannover

Geyer M., Lüpfert E., Osuna R., Esteban A., Schiel W., Schweitzer A., Zarza E., Nava P., Langenkamp J., Mandelberg E. 2002: EuroTrough – Parabolic Trough Collector Developed for Cost Efficient Solar Power Generation, Proceedings of 11th Solar-PACES International Symposium on Concentrated Solar Power and Chemical Energy Technologies, Zurich, Switzerland

Gnielinski V. 1976: New Equations for Heat and Mass Transfer in Turbulent Pipe and Channel Flow, International Chemical Engineering 16

Goebel O. 1998: Wärmeübergang in Absorberrohren von Parabolrinnen-Solarkraftwerken, Fortschr.-Ber. VDI Reihe 6 Nr. 402, VDI Verlag GmbH, Düsseldorf

Goswami D. Y. & Kreith F. 2008: Energy Conversion, CRC Press, Taylor & Francis Group, Boca Raton, USA

Häberle A., Zahler C., Lerchenmüller H., Mertins M., Wittwer C., Trieb F., Dersch J. 2002: The Solarmundo Line Focussing Collector – Optical and Thermal Performance and Cost Calculations, Proceedings of 11th Solar-PACES International Symposium on Concentrated Solar Power and Chemical Energy Technologies, Zurich, Switzerland

Hottel H. C. 1976: A Simple Model for Estimating the Transmittance of Direct Solar Radiation Through Clear Atmosphere, Solar Energy, Vol. 18, USA

Jericha H. 1985: Thermische Turbomaschinen, Vorlesungsskriptum, Institut für Thermische Turbomaschinen und Maschinendynamik, Technische Universität Graz

Johansson T., Kelly H., Reddy A., Williams R. 1992: Renewable Energy, Sources for Fuels and Electricity, Islandpress, Washington DC

Kakac S., Bon B. 2008: A Review of Two-Phase Flow Dynamic Instabilities in Tube Boiling Systems, International Journal of Heat and Mass Transfer 51, Elsevier Ltd.

Kaltschmitt M., Streicher W., Wiese A. 2007: Renewable Energy – Technology, Economics and Environment, Springer Verlag, Berlin, Heidelberg, Germany

Kearney D.W. 2007: Parabolic Trough Collector Overview – notes on a bit of history-development after Luz-and a recent surge in trough collector technology offerings, Parabolic Trough Workshop at the National Renewable Energy Laboratory, Golden CO, <http://www.nrel.gov/csp/troughnet/pdfs/2007/kearney_collector_technology.pdf> (26.03.2010)

Kelly B & Kearney D. 2006: Parabolic Trough Solar System Piping Model, Subcontract Report

NREL/SR-550-40165, NREL National Renewable Energy Laboratory

Kennedy C., Price H. 2004: Development and Testing of High-Temperature Solar Selective Coatings, Conference Paper NREL/CP-520-36581, NREL National Renewable Energy Laboratory

Laing D., Schiel W., Heller P. 2002: Dish-Sterling-Systeme - Eine Technologie zur dezentralen solaren Stromerzeugung, FVS Themen 2002, Jahrestagung des Forschungs-Verbunds Sonnenenergie, Stuttgart, Germany

Lüpfert E., Geyer M., Schiel W., Esteban A., Osuna R., Zarza E., Nava P 2001: Eurotrough Design Issues and Prototype Testing at PSA, Proceedings of the ASME International Solar Energy Conference, Solar Energy: The Power to Choose, Washington, DC, USA

Malayeri M.R., Zunft S., Eck M. 2004: Compact Field Separators for the Direct Steam Generation in Parabolic Trough Collectors: An Investigation of Models, Energy 29, Elsevier Ltd.

Mandhane J.M., Gregory G.A., Aziz K. 1974: A Flow Pattern Map for Gas Liquid Flow in Horizontal Pipes, International Journal of Multiphase Flow, Vol. 1

Marek R. & Nitsche K. 2007: Praxis der Wärmeübertragung – Grundlagen – Anwendungen – Übungsaufgaben, Hanser Verlag, München

Mayinger F. 1982: Strömung und Wärmeübergang in Gas-Flüssigkeits-Gemischen, Springer-Verlag, Vienna, Austria

Mills D.R.. & Morrison G.L. 2000: Compact Linear Fresnel Reflector Solar Thermal Power Plants, Solar Energy Vol. 68, Elsevier Science Ltd.

Montes M.J., Abanades A., Martinez-Val J.M. 2009: Performance of a Direct Steam Generation Solar Thermal Power Plant for Electricity Production as a Function of the Solar Multiple, Solar Energy 83, Elsevier Ltd.

Morin G., Platzer W., Eck M., Uhlig R., Häberle A., Berger M., Zarza E. 2006: Road Map Towards the Demonstration of a Linear Fresnel Collector Using a Single Tube Receiver, Solar-PACES,13th International Symposium on Concentrated Solar Power and Chemical Energy Technologies , Seville, Spain

Nextera Energy Resources 2010: Official Web Site, <http://www.nexteraenergyresources.com/content/where/portfolio/solar/solar_plant.shtml>, (31.03.2010)

Odeh S.D., Morrison G.L., Behnia M. 1996: Thermal Analysis of Parabolic Trough Solar Collectors for Electric Power Generation, School of Mechanical and Manufacturing Engineering, University of New South Wales, Sydney, Australia

Odeh S.D, Morrison G.L., Behnia M. 1998: Modelling of Parabolic Trough Direct Steam Generation Solar Collectors, Solar Energy Vol. 62, Elsevier Science Ltd.

Odeh S.D., Morrison G.L., Behnia M. 1998a: Performance of Horizontal and Inclined Direct Steam Generation Trough Solar Collectors, School of Mechanical and Manufacturing Engineering, University of New South Wales, Sydney, Australia

Palz W. & Greif J. 1996: European Solar Radiation Atlas, Springer Verlag, Berlin

Patnode A.M. 2006: Diploma Thesis – Simulation and Performance Evaluation of Parabolic Trough Solar Power Plants, University of Wisconsin-Madison, USA

Perz E.W. & Bergmann S. 2006: A Simulation Environment for the Techno-economic Performance Prediction of Water and Power Cogeneration Systems Using Renewable and Fossil Energy Sources, EUROMED 2006: Conference on Desalination Strategies in South Mediterranean Countries, Montpellier, France

Petukhov B.S. 1970: Heat Transfer and Friction in Turbulent Pipe Flow with Variable Physical

Properties, Advances in Heat Transfer (ed. Irvine T.F. & Hartnett J.P.), Vol. 6, Academic Press, New York

Platzer W. 2009: Solarthermische Kraftwerke mit Fresnelkollektoren, Energy 2.0 - Kompendium, Photovoltaik & Solarthermie Fachbericht, Publish-Industry Verlag GmbH

PSA 2010: Official Website of the Plataforma Solar de Almeria, <http://www.psa.es/webeng/instalaciones/parabolicos.php>, (01.04.2010)

PS 10 Report 2006: 10 MW Solar Thermal Power Plant for Southern Spain, Final Technical Progress Report, <http://ec.europa.eu/energy/res/sectors/doc/csp/ps10_final_report.pdf> (25.01.2010)

Pye J., Morrison G., Behnia M. 2006: Pressure Drops for Direct Steam Generation in Line-Focus Solar Thermal Systems, Australian and New Zealand Solar Energy Society (ANZSES) Conference – Clean Energy? Can Do!, Sydney, Australia

Quaschning V. 2007: Regenerative Energiesysteme - Technologie-Berechnung-Simulation, 5. aktualisierte Auflage, Hanser Verlag, München

Rabl A. 1985: Active Solar Collectors and their Applications, Oxford University Press, Inc., New York, USA

Radecki A.K. 2007: Picture of the Solar Electric Generation Stations III-VII at Mojave Desert – California, <http://commons.wikimedia.org/wiki/File:Solarplant-050406-04.jpg>, (01.04.2010)

Reynolds D.J., Behnia M., Morrison G.L. 2002: A Hydrodynamic Model for a Line-Focus Direct Steam Generation Solar Collector, School of Mechanical and Manufacturing Engineering, University of New South Wales, Sydney, Australia

Richter C., Teske S., Short R. 2009: Concentrating Solar Power – Global Outlook 09 – Why Renewable Energy is Hot, Greenpeace International - Netherlands, Solar PACES - Spain, ESTELA European Solar Thermal Electricity - Brussels

Romero-Alvarez M., Zarza E., Kreith F., Goswami D.Y. 2007: Handbook of Energy Efficiency and Renewable Energy, CRC Press Taylor & Francis Group, Boca Raton, USA

Sen Z. 2008: Solar Energy Fundamentals and Modeling Techniques – Atmosphere – Environment - Climate Change and Renewable Energy, Springer-Verlag London Limited

Sener 2007: Solar Tres – First Commercial Molten Salt Central Receiver Plant 17 MW - 15 hours Storage - 6500 hrs/yr, NREL CSP Technology Workshop, Sener Ingenieria y Sistemas S.A., <http://www.nrel.gov/csp/troughnet/pdfs/2007/martin_solar_tres.pdf> (02.03.2010)

Silva M.E.V., Araujo A.S., Medeiros M.R.Q. 2002: Adjustment of the Clear Sky Coefficients for the Transmission of Solar Radiation under the Ambient Conditions in Fortaleza, Universidade Federal do Ceara, Laboratorio de Energia Solar Aplicada, Fortaleza,Brazil

SimTech 2002: IPSEpro - The Design Suite, Company Pamphlet, SimTech GmbH, Riesstrasse 120, 8010 Graz, Austria

Solar Millennium AG 2008: The Parabolic Trough Power Plants Andasol 1 to 3 – The Largest Solar Power Plants in the World – Technology Premiere in Europe, Company Pamphlet, Solar Millennium AG, Erlangen, Germany, <http://www.solarmillennium.de/upload/Download/Technologie/eng/Anda sol1-3engl.pdf> (02.03.2010)

Steiner H., Kobor A., Gebhard L. 2005: A Wall Heat Transfer Model for Subcooled Boiling Flow, International Journal of Heat and Mass Transfer 48, Elsevier Ltd.

Steiner H. 2008: Höhere Strömungslehre und Wärmeübertragung, Vorlesungsskriptum, Institut für Strömungslehre und Wärmeübertragung, Technische Universität Graz

Steinmann W. D. & Eck M. 2006: Buffer Storage for Direct Steam Generation, Solar Energy 80, Elsevier Ltd.

Stephan K. 1988: Wärmeübergang beim Kondensieren und beim Sieden, Springer-Verlag, Berlin, Heidelberg, Germany

Stine W. & Diver R.B. 1994: A Compendium of Solar Dish/Sterling Technology, Report SAND93-7026 UC-236, Sandia National Laboratories, Sandia Corporation, Albuquerque, New Mexico

Stuetzle T.A. 2002: Diploma Thesis – Automatic Control of the 30 MWe SEGS VI Parabolic Trough Plant, University of Wisconsin-Madison, USA

Taitel Y. & Dukler A.E. 1976: A Model for Predicting Flow Regime Transitions in Horizontal and Near Horizontal Gas-Liquid Flow, AIChE J. 22

Trieb F., Kronshage S., Quaschning V., Dersch J., Lerchenmüller H., Morin G., Häberle A. 2004: Solarthermische Kraftwerkstechnologie für den Schutz des Erdklimas, Projektbericht Sokrates-Projekt, DLR Stuttgart, Frauenhofer Institut Freiburg, PSE Freiburg, <http://www.dlr.de/tt/Portaldata/41/Resources/dokumente/institut/system/projects/AP_2_1_Modellbildung.pdf> (02.03.2010)

Truckenbrodt E. 1996: Fluidmechanik – Band 1 – Grundlagen und elementare Strömungsvorgänge dichtebeständiger Fluide, 4. ergänzte Auflage, Springer - Verlag, Berlin Heidelberg

VDI (Verein Deutscher Ingenieure) 2006: VDI-Wärmeatlas, 10. bearbeitete Auflage, VDI-Gesellschaft Verfahrenstechnik und Chemieingenieurwesen, Springer-Verlag, Berlin Heidelberg

Wagner W. & Kruse A. 1998: Properties of Water and Steam - The Industrial Standard IAPWS-IF97 for the Thermodynamic Properties and Supplementary Equations for Properties - Tables based on these Equations, Springer-Verlag, Berlin Heidelberg, New York

Winston R., Minano J.C., Benitez P. 2005: Nonimaging Optics, Elsevier Academic Press Inc., London

Winter C.J., Sizmann R.L., Vant-Hull L.L. 1991: Solar Power Plants – Fundamentals-Technology-Systems-Economics, Springer Verlag, Berlin, Heidelberg

Zarza E., Weyers H.D., Eck M., Hennecke K. 2001: The DISS Project - Direct Steam Generation in Parabolic Troughs – Operation and Maintenance Experience – Update on Project Status, Proceedings of Solar Forum, Solar Energy – The Power to Choose, Washington DC, USA

Zarza E. 2007: Overview on Direct Steam Generation (DSG) and Experience at the Plataforma Solar de Almeria (PSA), Parabolic Trough 2007 Workshop, Denver, USA, <http://www.nrel.gov/csp/troughnet/pdfs/2007/zarza_dsg_overview.pdf> (02.03.2010)

Zhang T., Tong T., Chang J., Peles Y., Prasher R., Jensen M.K., Wen J.T., Phelan P. 2009: Ledinegg Instability in Microchannels, International Journal of Heat and Mass Transfer 52, Elsevier Ltd.

Zhang Q. 2000: Recent Progress in High-Temperature Solar Selective Coatings, Solar Energy Materials & Solar Cells 62, Elsevier Science B.V.

Appendix

Appendix A: IPSEpro-MDK Parameters, Variables and Switches

Appendix B: IPSEpro-PSE Project Files for the Estimation of the Suitable Element Length

Appendix C: IPSEpro-PSE Calculation Results of Chapter 8

A IPSEpro-MDK Parameters, Variables and Switches

location_and_solar_parameters

Parameters

longitude	longitude of the location in question in degrees east of Greenwich
latitude	latitude north or south. zero at the equator. north positive. south negative.
time_zone_meridian	The meridian in degrees east on which the local standard time is based. For instance, for "Central European Time" the standard meridian in degrees east is 15.
day_of_month	15 for the 15th of June for instance
local_time_hour	For the local standard time 10:30, the local time hour is 10. Note: If daylight saving time is valid one hour has to be subtracted. The local time hour would be 9 then. The time format is 24 hours, beginning with hour 0 up to hour 23
local_time_minute	For the local standard time 10:30, the local time minute is 30. Values range from 0 up to 59 minutes.
altitude	The site´s elevation above sea level.
r_0_user_defined	correction factor for user-defined climate type 1 if not applicable
r_1_user_defined	correction factor for user-defined climate type 1 if not applicable
r_k_user_defined	correction factor for user-defined climate type 1 if not applicable
surface_azimuth_angle	northern hemisphere: The surface azimuth angle is the angle between the projection of the plane´s normal on the horizontal plane and the direction southward. Displacements east of south are negative and west of south are positive. southern hemisphere: The surface azimuth angle is the angle between the projection of the plane´s normal on the horizontal plane and the direction northward. Displacements east of north are negative and west of north are positive.
slope_angle	The slope is the angle between the plane of the surface in question and the horizontal. If that angle exceeds 90° the surface has a downward-facing component.

Variables

angle_of_incidence	The angle of incidence is the angle between the beam radiation on a surface and the normal to that surface.
B	variable necessary for the equation of time
E	result of the equation of time, which takes into account the earth´s real motion around the sun
n	number of days spent since January the 1st
local_time	The local time is the standard time in hours. The time 10:30 corresponds with

	10.5 hours.
solar_time	solar time in hours
omega	Omega is called the "hour angle". The hour angle is the angular displacement of the sun east or west of the local meridian due to rotation of the earth on its axis at 15° per hour.
degree_rad	converts degree into radian
declination	Within a year the latitude where the sun reaches the zenith at solar noon varies between 23°27' north, the tropic of Cancer, and 23°27' south, the tropic of Capricorn.
altitude_angle	is the angle between the horizontal and the line to the sun. It is the complement of the zenith angle.
azimuth_angle	It is the angle between the projection of beam radiation on the horizontal plane and the direction southward. Displacements east of south are negative and west of south are positive (northern hemisphere). The solar azimuth angle in southern hemisphere is the angle between the projection of beam radiation on the horizontal plane and the direction northward. Displacements east of north are negative and west of north are positive.
rad_degree	converts radian into degree
air_mass	The air mass is the ratio of the mass of the atmosphere through which radiation passes to the mass it would pass if the sun was at the zenith.
zenith_angle	The zenith angle is the angle between the vertical and the line to the sun. It is the complement of the altitude angle.
G	extraterrestrial radiation incident on the plane normal to radiation
a_0_star	a_0* is a constant, necessary for clear sky transmittance (hottel 1976)
a_1_star	a_1* is a constant, necessary for clear sky transmittance (hottel 1976)
k_star	k* is a constant, necessary for clear sky transmittance (hottel 1976)
r_0	correction factor for climate type (hottel 1976)
r_1	correction factor for climate type (hottel 1976)
r_k	correction factor for climate type (hottel 1976)
a_0	a_0 is a constant, necessary for clear sky transmittance (hottel 1976)
a_1	a_1 is a constant, necessary for clear sky transmittance (hottel 1976)
k	k is a constant, necessary for clear sky transmittance (hottel 1976)
transmittance_b	atmospheric transmittance for beam radiation only
DNI	direct normal irradiance DNI received on the earth´s surface. Also known as clear-sky normal beam radiation.
transmittance_d	atmospheric transmittance for diffuse radiation only.
diffuse_radiation	clear sky diffuse radiation incident on a horzontal plane on the earth´s surface
total_radiation	clear-sky total radiation (clear-sky global radiation) received on a horizontal plane on the earth´s surface

Switches

hemisphere (northern, southern) select hemisphere in which the power plant is located

month (April, August, December, February, January, July, June, March, May, November, October, September) the month has to be selected

climate_type (mid_latitude_summer, mid_latitude_winter, subarctic_summer, tropical, user_defined)
tropical: latitude < 30°
mid-latitude: 30° < latitude < 60°
subarctic: 60° < latitude

collector_type_field

Parameters

distance_parallel	collectors are usually placed in parallel rows in a large field. the distance_parallel is the distance between these rows, measured from one collector´s plane of symmetry (along its axis) to the next.
number_of_rows	number of parallel rows of a certain collector field. important for the shading attenuation factor.
lam_abs_tube	thermal conductivity of the steel absorber pipe
glass_tube_diam	glass tube outer diameter
mean_roughness	mean hight of roughness of the inner absorber tube in meters
c_1	constant for incidence angle modifier. has to be determined by measurements.
c_2	constant for incidence angle modifier. has to be determined by measurements.
emittance	emittance of the absorber tube. has to be set if the collector type is userdefined.

Variables

collector_width	width of a single parabolic trough collector unit
collector_length	length of a single parabolic trough collector unit
aperture_area	aperture area, as that area does not necessarily mate with the product collector_width times collector_length.
reflectivity	The maximum possible amount of the effective incident radiation that can be reflected onto the receiver tube is defined by the reflectivity. For clean silvered glass mirrors the reflectivity is around 0.93. As dirt accumulates on mirrors, their reflectivity decreases until the next washing. Usually parabolic trough mirrors are washed, when the reflectivity reaches a value of about 0.9.
intercept_factor	The intercept factor defines the fraction of the reflected solar radiation that does finally reach the absorber´s glass cover. A certain amount of the reflected radiation does not reach the tube due to either microscopic imperfections of the reflector or macroscopic shape errors in the parabolic trough concentrators. Thus, some rays are reflected in a wrong angle and therefore do not reach the absorber tube. A typical value for an intercept factor is 0.95.
transmissivity	The transmissivity defines the fraction of the remaining solar radiation that passes through the glass tube. A typical value for the transmissivity is 0.93.
absorptivity	The absorptivity of the absorber tube coating defines the amount of radiation that is finally absorbed. For receiver pipes with cermet coating, a typical value for the absorptivity is 0.95.
abs_diameter	absorber tube outer diameter
abs_inner_diameter	inner absorber tube diameter
collector_type_unit	allows to call the collector type in the unit as the switch value cannot be loaded.
coll_orient_unit	makes the collector_orientation switch value accessable in the unit. north_south = 1, east_west = 0

Switches

collector_type (ET_100, LS_1, LS_2, LS_3, user_defined)	the suitable type of collector has to be chosen. if the required type is not available, a custom one can be defined by the

	user	
collector_orientation	(East_West, North_South)	parabolic trough receivers are placed horizontally, but differ in their orientation. They are either placed with their axis North-South or East-West.

ambient_solar

Parameters

temperature	temperature of the ambient air
lambda_air	thermal conductivity of the ambient air
kin_visc_air	kinemtaic viscosity of the ambient air
wind_speed	windspeed in meters per second

T_Solar_collector

Parameters

element_length	The parameter "element_length" defines the absorber tube length for each unit within the IPSEpro project. With this parameter the level of discretization is determined.
t_glass	temperature of the glass tube´s surface

Variables

collector_width	width of a single parabolic trough collector unit
collector_length	length of a single parabolic trough collector unit
abs_diameter	absorber tube outer diameter
abs_inner_diameter	inner absorber tube diameter
aperture_area	aperture area, as that area does not necessarily mate with the product collector_width times collector_length.
reflectivity	The maximum possible amount of the effective incident radiation that can be reflected onto the receiver tube is defined by the reflectivity. For clean silvered glass mirrors the reflectivity is around 0.93. As dirt accumulates on mirrors, their reflectivity decreases until the next washing. Usually parabolic trough mirrors are washed, when the reflectivity reaches a value of about 0.9.
intercept_factor	The intercept factor defines the fraction of the reflected solar radiation that does finally reach the absorber´s glass cover. A certain amount of the reflected radiation does not reach the tube due to either microscopic imperfections of the reflector or macroscopic shape errors in the parabolic trough concentrators. Thus, some rays are reflected in a wrong angle and therefore do not reach the absorber tube. A typical value for an intercept factor is 0.95.
transmissivity	The transmissivity defines the fraction of the remaining solar radiation that passes through the glass tube. A typical value for the transmissivity is 0.93.
absorptivity	The absorptivity of the absorber tube coating defines the amount of radiation that is finally absorbed. For receiver pipes with cermet coating, a typical value for the absorptivity is 0.95.
delta_t	temperature difference between feed and drain mass flow
Q_trans	heat that can be used for the enthalpy raise of the heat transfer fluid
Q_loss	heat loss absorber
heat_transfer_coeff	heat transfer coefficient between thermooil and steel absorber tube. depends on Reynolds and Prandtl number determined by the flow.
t_inner_tube	inner absorber tube wall temperature
t_outer_tube	outer absorber tube wall temperature
incident_angle	As parabolic trough collectors are placed horizontally either along the north-south axis or east-west axis and can only rotate about that axis, there is always a certain angle of incidence T remaining (exceptions: north-south orientation:

	sun is at the zenith or near the horizon; east-west orientation: at solar noon) that is the cause for cosine losses.
cosine_factor	the cosine factor is the cosine of the remaining incident-angle
slope_beta	The slope ß of the receiver in question is determined by the solar altitude and azimuth angle.
degree_rad	transfrorms degree into radian
rad_degree	transforms radian into degree
azimuth_receiver	the receiver´s azimuth angle
shading_length	indicates the length of the collector-with, that is shaded
shading_factor	it is the shading attenuation factor, by which the DNI is multiplied, to take shading losses into account
eta_optical	optical peak efficiency times the incidence angle modifier
IAM	incidence angle modifier: With increasing angle of incidence the optical efficiency is reduced, due to aberrations. This attenuation factor for the peak optical efficiency is called incidence angle modifier.
U	heat loss coefficient U of the absorber
Pi	Pi = 3.14159.....
reynolds	reynolds number of the flow in the absorber tube
prandtl	prandtl number of the flow in the absorber tube
flow_velocity	mean flow velocity of the heat transfer fluid inside the absorber tube
t_mean	mean temperature of fluid
nusselt	nusselt number of the flow inside the absorber tube
dynamic_visc	dynamic viscosity of the heat transfer fluid
cp_fluid	heat capacity of heat transfer fluid
lambda_fluid	thermal conductivity of the heat transfer fluid
kin_visc	kinematic viscosity of the heat transfer fluid
Q_conv	convective heat loss
Q_rad	radiative heat loss: the ambience is assumed as black body and the presence of the concentric glass tube is neglected.
htc_glass	heat transfer coefficient between ambient air and the glass tube
re_air	Reynolds number of the ambient air flow. provided relationships between reynolds number and nusselt number are valid for reynolds numbers up to 50000.
nu_air	Nusselt number of the ambient air flow
emittance	emittance of the absorber tube surface. this variable has to be set, if the collector type is userdefined.
friction_factor	friction factor of the absorber tube
delta_p	pressure loss in the absorber tube
distance_parallel	distance between parallel collector rows. measured from one collector´s plane of symmetry to the next collector´s plane of symmetry.
number_of_rows	number of parallel rows within one collector field
lam_abs_tube	thermal conductivity of the absorber tube
glass_tube_diam	outer diamter of the glass tube, surrounding the absorber tube
mean_roughness	mean roughness of the inner absorber tube

temperature_ambient	ambient temperature
lambda_air	thermal conductivity of the ambient air
kin_visc_air	kinematic viscosity of the ambient air
v_wind	wind speed in meters per second
spec_vol	specific volume of the heat transfer fluid

Switches

heat_loss_model (empirical_LS_3, empirical_LS_3_wind, physical_model)
empirical_LS_3 model [Romero-Alvarez et al. 2007]
note: the empirical_LS_3 model does not take wind speed into account
empirical_LS_3_wind [Odeh et al. 1996]

W_Solar_collector

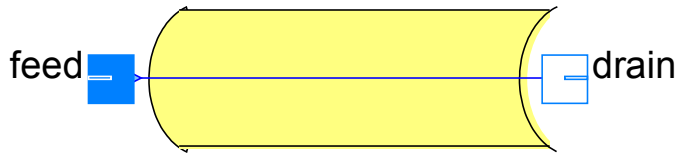

W_Solar_collector_ph

Parameters

element_length	The parameter "element_length" defines the absorber tube length for each unit within the IPSEpro project. With this parameter the level of discretization is determined.
t_glass	temperature of the glass tube´s outer surface

Variables

collector_width	width of a single parabolic trough collector unit
collector_length	length of a single parabolic trough collector unit
abs_diameter	absorber tube outer diameter
abs_inner_diameter	inner absorber tube diameter
aperture_area	aperture area, as that area does not necessarily mate with the product collector_width times collector_length.
reflectivity	The maximum possible amount of the effective incident radiation that can be reflected onto the receiver tube is defined by the reflectivity. For clean silvered glass mirrors the reflectivity is around 0.93. As dirt accumulates on mirrors, their reflectivity decreases until the next washing. Usually parabolic trough mirrors are washed, when the reflectivity reaches a value of about 0.9.
intercept_factor	The intercept factor defines the fraction of the reflected solar radiation that does finally reach the absorber´s glass cover. A certain amount of the reflected radiation does not reach the tube due to either microscopic imperfections of the

	reflector or macroscopic shape errors in the parabolic trough concentrators. Thus, some rays are reflected in a wrong angle and therefore do not reach the absorber tube. A typical value for an intercept factor is 0.95.
transmissivity	The transmissivity defines the fraction of the remaining solar radiation that passes through the glass tube. A typical value for the transmissivity is 0.93.
absorptivity	The absorptivity of the absorber tube coating defines the amount of radiation that is finally absorbed. For receiver pipes with cermet coating, a typical value for the absorptivity is 0.95.
delta_t	temperature difference between feed and drain mass flow
Q_trans	heat that can be used for the enthalpy raise of the heat transfer fluid
Q_loss	heat loss absorber
heat_transfer_coeff	heat transfer coefficient between thermooil and steel absorber tube. depends on Reynolds and Prandtl number determined by the flow.
t_inner_tube	inner absorber tube wall temperature
t_outer_tube	outer absorber tube wall temperature
incident_angle	As parabolic trough collectors are placed horizontally either along the north-south axis or east-west axis and can only rotate about that axis, there is always a certain angle of incidence T remaining (exceptions: north-south orientation: sun is at the zenith or near the horizon; east-west orientation: at solar noon) that is the cause for cosine losses.
cosine_factor	the cosine factor is the cosine of the remaining incident-angle
slope_beta	The slope ß of the receiver in question is determined by the solar altitude and azimuth angle.
degree_rad	transfrorms degree into radian
rad_degree	transforms radian into degree
azimuth_receiver	the receiver´s azimuth angle
shading_length	indicates the length of the collector-with, that is shaded
shading_factor	it is the shading attenuation factor, by which the DNI is multiplied, to take shading losses into account
eta_optical	optical peak efficiency times the incidence angle modifier
IAM	incidence angle modifier: With increasing angle of incidence the optical efficiency is reduced, due to aberrations. This attenuation factor for the peak optical efficiency is called incidence angle modifier.
U	heat loss coefficient U of the absorber
Pi	Pi = 3.14159...
reynolds	reynolds number of the flow in the absorber tube
prandtl	prandtl number of the flow in the absorber tube
flow_velocity	mean flow velocity of the heat transfer fluid inside the absorber tube
t_mean	mean temperature of fluid
nusselt	nusselt number of the flow inside the absorber tube
dynamic_visc	dynamic viscosity of the heat transfer fluid
cp_fluid	heat capacity of heat transfer fluid
lambda_fluid	thermal conductivity of the heat transfer fluid
kin_visc	kinematic viscosity of the heat transfer fluid
Q_conv	convective heat loss

Q_rad	radiative heat loss: the ambience is assumed as black body and the presence of the concentric glass tube is neglected.
htc_glass	heat transfer coefficient between ambient air and the glass tube
re_air	Reynolds number of the ambient air flow. provided relationships between reynolds number and nusselt number are valid for reynolds numbers up to 50000.
nu_air	Nusselt number of the ambient air flow
emittance	emittance of the absorber tube surface. this variable has to be set, if the collector type is userdefined.
friction_factor	friction factor of the absorber tube
delta_p	pressure loss in the absorber tube
distance_parallel	distance between parallel collector rows. measured from one collector´s plane of symmetry to the next collector´s plane of symmetry.
number_of_rows	number of parallel rows within one collector field
lam_abs_tube	heat conductivity of the absorber tube
glass_tube_diam	diameter of the glass tube, surrounding the absorber tube
mean_roughness	mean roughness of the inner absorber tube
temperature_ambient	temperature of the ambient air
lambda_air	thermal conductivity of the ambient air
kin_visc_air	kinematic viscosity of the ambient air
v_wind	wind speed in meters per second
p_mean	mean pressure in the absorber tube
v_mean	mean specific volume of the water

Switches

heat_loss_model (empirical_LS_3, empirical_LS_3_wind, physical_model)	empirical_LS_3 model [Romero-Alvarez et al. 2007] note: the empirical_LS_3 model does not take windspeed into account empirical_LS_3_wind [Odeh et al. 1998]

W_Solar_collector_evap

Parameters

element_length	The parameter "element_length" defines the absorber tube length for each unit within the IPSEpro project. With this parameter the level of discretization is determined.
t_glass	temperature of the glass tube´s outer surface

Variables

collector_width	width of a single parabolic trough collector unit
collector_length	length of a single parabolic trough collector unit
abs_diameter	absorber tube outer diameter

abs_inner_diameter	inner absorber tube diameter
aperture_area	aperture area, as that area does not necessarily mate with the product collector_width times collector_length.
reflectivity	The maximum possible amount of the effective incident radiation that can be reflected onto the receiver tube is defined by the reflectivity. For clean silvered glass mirrors the reflectivity is around 0.93. As dirt accumulates on mirrors, their reflectivity decreases until the next washing. Usually parabolic trough mirrors are washed, when the reflectivity reaches a value of about 0.9.
intercept_factor	The intercept factor defines the fraction of the reflected solar radiation that does finally reach the absorber´s glass cover. A certain amount of the reflected radiation does not reach the tube due to either microscopic imperfections of the reflector or macroscopic shape errors in the parabolic trough concentrators. Thus, some rays are reflected in a wrong angle and therefore do not reach the absorber tube. A typical value for an intercept factor is 0.95.
transmissivity	The transmissivity defines the fraction of the remaining solar radiation that passes through the glass tube. A typical value for the transmissivity is 0.93.
absorptivity	The absorptivity of the absorber tube coating defines the amount of radiation that is finally absorbed. For receiver pipes with cermet coating, a typical value for the absorptivity is 0.95.
delta_t	temperature difference between feed and drain mass flow
Q_trans	heat that can be used for the enthalpy raise of the heat transfer fluid
Q_loss	heat loss absorber
heat_transfer_coeff	heat transfer coefficient between thermooil and steel absorber tube. depends on Reynolds and Prandtl number determined by the flow.
t_inner_tube	inner absorber tube wall temperature
t_outer_tube	outer absorber tube wall temperature
incident_angle	As parabolic trough collectors are placed horizontally either along the north-south axis or east-west axis and can only rotate about that axis, there is always a certain angle of incidence T remaining (exceptions: north-south orientation: sun is at the zenith or near the horizon; east-west orientation: at solar noon) that is the cause for cosine losses.
cosine_factor	the cosine factor is the cosine of the remaining incident-angle
slope_beta	The slope ß of the receiver in question is determined by the solar altitude and azimuth angle.
degree_rad	transfrorms degree into radian
rad_degree	transforms radian into degree
azimuth_receiver	the receiver´s azimuth angle
shading_length	indicates the length of the collector-with, that is shaded
shading_factor	it is the shading attenuation factor, by which the DNI is multiplied, to take shading losses into account
eta_optical	optical peak efficiency times the incidence angle modifier
IAM	incidence angle modifier: With increasing angle of incidence the optical efficiency is reduced, due to aberrations. This attenuation factor for the peak optical efficiency is called incidence angle modifier.
U	heat loss coefficient U of the absorber
Pi	Pi = 3.14159....
t_mean	mean temperature of fluid

dynamic_visc	dynamic viscosity of the heat transfer fluid
cp_fluid	heat capacity of heat transfer fluid
lambda_fluid	thermal conductivity of the heat transfer fluid
kin_visc	kinematic viscosity of the heat transfer fluid
Q_conv	convective heat loss
Q_rad	radiative heat loss: the ambience is assumed as black body and the presence of the concentric glass tube is neglected.
htc_glass	heat transfer coefficient between ambient air and the glass tube
re_air	Reynolds number of the ambient air flow. provided relationships between reynolds number and nusselt number are valid for reynolds numbers up to 50000.
nu_air	Nusselt number of the ambient air flow
emittance	emittance of the absorber tube surface. this variable has to be set, if the collector type is userdefined.
delta_p	pressure loss in the absorber tube
distance_parallel	distance between parallel collector rows. measured from one collector´s plane of symmetry to the next collector´s plane of symmetry.
number_of_rows	number of parallel rows within one collector field
lam_abs_tube	thermal conductivity of the absorber tube
glass_tube_diam	outer diameter of the glass tube, surrounding the absorber tube
mean_roughness	mean roughness of the inner absorber tube
temperature_ambient	ambient air temperature
lambda_air	thermal conductivity of the ambient air
kin_visc_air	kinematic viscosity of the ambient air
v_wind	wind speed in meters per second
p_mean	mean pressure in the absorber tube
h_mean	mean enthalpy of the fluid within the absorber tube
x_start	flow steam quality at entry
x_mean	mean flow steam quality
x_end	flow steam quality at the end
x_critical	estimate of the flow steam quality at which the critical heat flow might be reached
m_st_mean	mean steam mass flow
m_l_mean	mean liquid phase mass flow
vel_st_mean	mean steam phase velocity
vel_l_mean	mean liquid phase velocity
epsilon_v_mean	mean volumetric steam quality
htc_b	nucleate boiling coefficient for the Shah (1976) model
htc_k	convective boiling coefficient for the Shah (1976) model
Re_L	Reynolds number of the liquid phase
Pr_L	Prandtl number of the liquid phase
q_trans	specific heat flow through absorber tube
q_trans_min	minimum specific heat flow through absorber tube to allow bulk boiling
Bo	Boiling number
slip_mean	mean slip. the slip is the ratio of the two phase velocities for steam and liquid

htc_db	Dittus-Boelter heat transfer coefficient for the Shah (1976) model
C_0	variable necessary for the Shah (1976) model
Fr_mean	mean Froude number
N	variable necessary for the Shah (1976) model
F	variable necessary for the Shah (1976) model
R	pressure loss ratio for the Friedel (1974) model
dp_dL_1ph	single phase pressure drop [pascal/m]
f	friction factor single phase
We	Weber number
Re_St	Reynolds number of steam phase
f_L	friction factor liquid phase for Friedel (1974) model
f_St	friction factor steam phase for the Friedel (1974) model

Switches

heat_loss_model (empirical_LS_3, empirical_LS_3_wind, physical_model) empirical_LS_3 model [Romero-Alvarez et al. 2007]
note: the empirical_LS_3 model does not take windspeed into account
empirical_LS_3_wind [Odeh et al. 1998]

W_Solar_collector_sh

Parameters

element_length	The parameter "element_length" defines the absorber tube length for each unit within the IPSEpro project. With this parameter the level of discretization is determined.
t_glass	temperature of the glass tube´s outer surface

Variables

collector_width	width of a single parabolic trough collector unit
collector_length	length of a single parabolic trough collector unit
abs_diameter	absorber tube outer diameter
abs_inner_diameter	inner absorber tube diameter
aperture_area	aperture area, as that area does not necessarily mate with the product collector_width times collector_length.
reflectivity	The maximum possible amount of the effective incident radiation that can be reflected onto the receiver tube is defined by the reflectivity. For clean silvered glass mirrors the reflectivity is around 0.93. As dirt accumulates on mirrors, their reflectivity decreases until the next washing. Usually parabolic trough mirrors are washed, when the reflectivity reaches a value of about 0.9.
intercept_factor	The intercept factor defines the fraction of the reflected solar radiation that does finally reach the absorber´s glass cover. A certain amount of the reflected radiation does not reach the tube due to either microscopic imperfections of the reflector or macroscopic shape errors in the parabolic trough concentrators.

	Thus, some rays are reflected in a wrong angle and therefore do not reach the absorber tube. A typical value for an intercept factor is 0.95.
transmissivity	The transmissivity defines the fraction of the remaining solar radiation that passes through the glass tube. A typical value for the transmissivity is 0.93.
absorptivity	The absorptivity of the absorber tube coating defines the amount of radiation that is finally absorbed. For receiver pipes with cermet coating, a typical value for the absorptivity is 0.95.
delta_t	temperature difference between feed and drain mass flow
Q_trans	heat that can be used for the enthalpy raise of the heat transfer fluid
Q_loss	heat loss absorber
heat_transfer_coeff	heat transfer coefficient between single phase and steel absorber tube. depends on Reynolds and Prandtl number determined by the flow.
t_inner_tube	inner absorber tube wall temperature
t_outer_tube	outer absorber tube wall temperature
incident_angle	As parabolic trough collectors are placed horizontally either along the north-south axis or east-west axis and can only rotate about that axis, there is always a certain angle of incidence T remaining (exceptions: north-south orientation: sun is at the zenith or near the horizon; east-west orientation: at solar noon) that is the cause for cosine losses.
cosine_factor	the cosine factor is the cosine of the remaining incident-angle
slope_beta	The slope ß of the receiver in question is determined by the solar altitude and azimuth angle.
degree_rad	transfrorms degree into radian
rad_degree	transforms radian into degree
azimuth_receiver	the receiver´s azimuth angle
shading_length	indicates the length of the collector-with, that is shaded
shading_factor	it is the shading attenuation factor, by which the DNI is multiplied, to take shading losses into account
eta_optical	optical peak efficiency times the incidence angle modifier
IAM	incidence angle modifier: With increasing angle of incidence the optical efficiency is reduced, due to aberrations. This attenuation factor for the peak optical efficiency is called incidence angle modifier.
U	heat loss coefficient U of the absorber
Pi	Pi = 3.14159....
reynolds	reynolds number of the flow in the absorber tube
prandtl	prandtl number of the flow in the absorber tube
flow_velocity	mean flow velocity of the heat transfer fluid inside the absorber tube
t_mean	mean temperature of fluid
nusselt	nusselt number of the flow inside the absorber tube
dynamic_visc	dynamic viscosity of the heat transfer fluid
cp_fluid	heat capacity of heat transfer fluid
lambda_fluid	thermal conductivity of the heat transfer fluid
kin_visc	kinematic viscosity of the heat transfer fluid
Q_conv	convective heat loss
Q_rad	radiative heat loss: the ambience is assumed as black body and the presence

	of the concentric glass tube is neglected.
htc_glass	heat transfer coefficient between ambient air and the glass tube
re_air	Reynolds number of the ambient air flow. provided relationships between reynolds number and nusselt number are valid for reynolds numbers up to 50000.
nu_air	Nusselt number of the ambient air flow
emittance	emittance of the absorber tube surface. this variable has to be set, if the collector type is userdefined.
friction_factor	friction factor of the absorber tube
delta_p	pressure loss in the absorber tube
distance_parallel	distance between parallel collector rows. measured from one collector´s plane of symmetry to the next collector´s plane of symmetry.
number_of_rows	number of parallel rows within one collector field
lam_abs_tube	thermal conductivity of the absorber tube
glass_tube_diam	diameter of the glass tube, surrounding the absorber tube
mean_roughness	mean roughness of the inner absorber tube
temperature_ambient	temperature of the ambient air
lambda_air	thermal conductivity of the ambient air
kin_visc_air	kinematic viscosity of the ambient air
v_wind	wind speed in meters per second
p_mean	mean pressure in the absorber tube
v_mean	mean specific volume of the steam

Switches

heat_loss_model (empirical_LS_3, empirical_LS_3_wind, physical_model) empirical_LS_3 model
[Romero-Alvarez et al. 2007]
note: the empirical_LS_3 model does not take windspeed into account
empirical_LS_3_wind [Odeh et al. 1998]

T_Header_mix

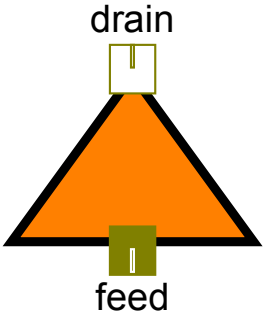

Parameters

collector_loops	number of collector loops connected to the header tube

T_Header_split

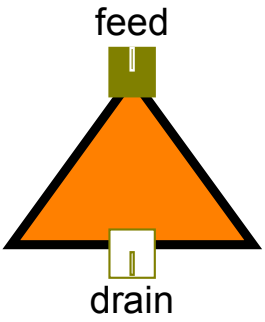

Parameters

collector_loops	number of collector loops connected to the header tube

W_Header_mix

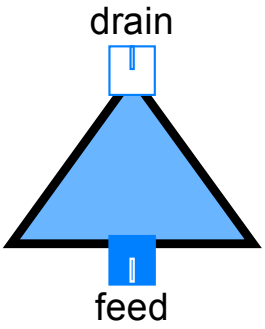

Parameters

collector_loops	number of collector loops connected to the header tube

W_Header_split

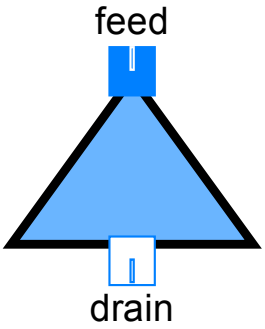

Parameters

collector_loops	number of collector loops connected to the header tube

B IPSEpro-PSE Project Files for the Estimation of the Suitable Element Length

This chapter contains all the data needed for the calculations described in the chapters 6.3.1 (on page 89) and 7.8.1 (on page 120). The data is shown in the following figures (84 - 90). In the upper part of each figure the used collector configuration is displayed. The total collector length is at first modelled with one IPSEpro collector unit, then with 2, 4, 10 and finally even with 20 units. The element length changes accordingly. The corresponding calculation results of each IPSEpro collector unit are shown in the tables below. In the small table on the left-hand side the temperature, pressure and enthalpy at the collector entry are shown. In the small tables on the right-hand side the temperature, pressure and enthalpy at the collector end are shown.

Figure 84 and 85 show the data for the “T_Solar_collector” unit for oil.

Figure 86 shows the data for the “W_Solar_collector” preheating model.

Figure 87 and 88 show the data for the “W_Solar_collector” evaporating model.

Figure 89 and 90 show the data for the “W_Solar_collector” superheating model.

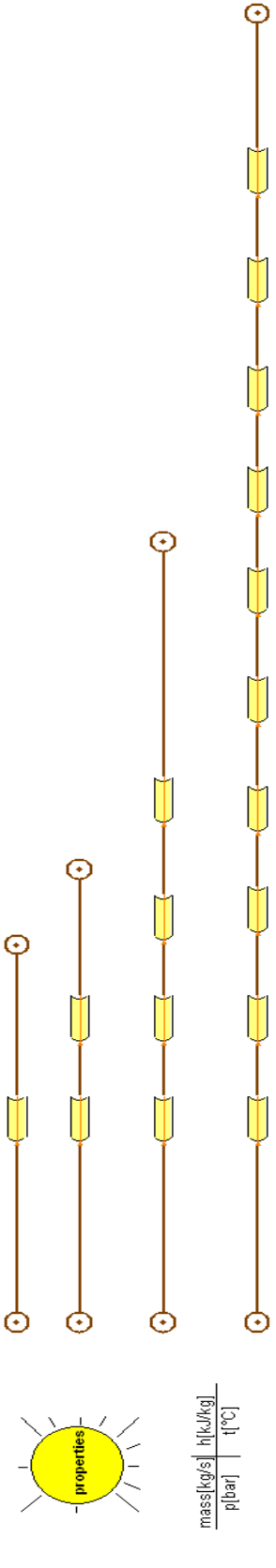

Start	
Pressure	26.0000
Temp	277.0000
Enthalpy	521.1066

Reynolds Number	625198.2928									
Friction Factor	0.0190									
Velocity	2.5384									
Delta p	3.285200									
Heat Transfer Coefficient	5355.4972									
Absorber Tube Temperature	321.7725									
Heat Loss	93.5241									
QTrans	1049.4341									
t mean	317.3449									

End	
Pressure	22.7148
Temp	357.6897
Enthalpy	711.9822

Reynolds Number	573695.0695	687116.5430								
Friction Factor	0.0190	0.0189								
Velocity	2.4698	2.6169								
Delta p	1.602374	1.688935								
Heat Transfer Coefficient	5145.9382	5593.7001								
Absorber Tube Temperature	302.5329	342.4347								
Heat Loss	39.0016	56.5681								
QTrans	532.4775	514.9110								
t mean	297.9306	338.2003								

End	
Pressure	22.7087
Temp	357.5393
Enthalpy	711.6101

Reynolds Number	537372.1557	602340.9238	657403.8493	720700.8859						
Friction Factor	0.0191	0.0190	0.0190	0.0189						
Velocity	2.4366	2.5067	2.5805	2.6556						
Delta p	0.792090	0.811950	0.833720	0.855870						
Heat Transfer Coefficient	4989.5673	5264.0647	5481.0258	5717.7440						
Absorber Tube Temperature	292.3684	313.0672	333.0070	352.1517						
Heat Loss	17.9715	21.5474	25.9478	30.8742						
QTrans	267.7681	264.1922	259.7918	254.8653						
t mean	287.6517	308.5625	328.6827	348.0132						

End	
Pressure	22.7064
Temp	357.4826
Enthalpy	711.4699

Reynolds Number	517168.8756	544791.5757	575053.3698	597441.0649	618309.2881	640325.9030	663581.9206	688177.8837	714225.1683	735660.7243
Friction Factor	0.0191	0.0191	0.0190	0.0190	0.0190	0.0190	0.0190	0.0189	0.0189	0.0189
Velocity	2.4165	2.4436	2.4710	2.4997	2.5290	2.5585	2.5883	2.6182	2.6483	2.6813
Delta p	0.314630	0.317610	0.320600	0.323950	0.327410	0.330900	0.334400	0.337940	0.341490	0.345480
Heat Transfer Coefficient	4900.1594	5021.9523	5151.6827	5244.1947	5328.1535	5414.9220	5504.6925	5597.6725	5694.0858	5768.8574
Absorber Tube Temperature	286.0982	294.5539	302.8878	311.1141	319.2168	327.1908	335.0370	342.7563	350.3494	357.8274
Heat Loss	6.7599	7.3430	7.8267	8.4616	9.1316	9.8361	10.5746	11.3467	12.1518	12.9903
QTrans	107.5360	106.9529	106.4691	105.8343	105.1642	104.4598	103.7212	102.9491	102.1440	101.3055
t mean	281.3095	289.8627	298.2898	306.5923	314.7663	322.8125	330.7318	338.5250	346.1929	353.7361

End	
Pressure	22.7056
Temp	357.4766
Enthalpy	711.4551

Figure 84: Data for the Estimation of the Element Length (Oil)

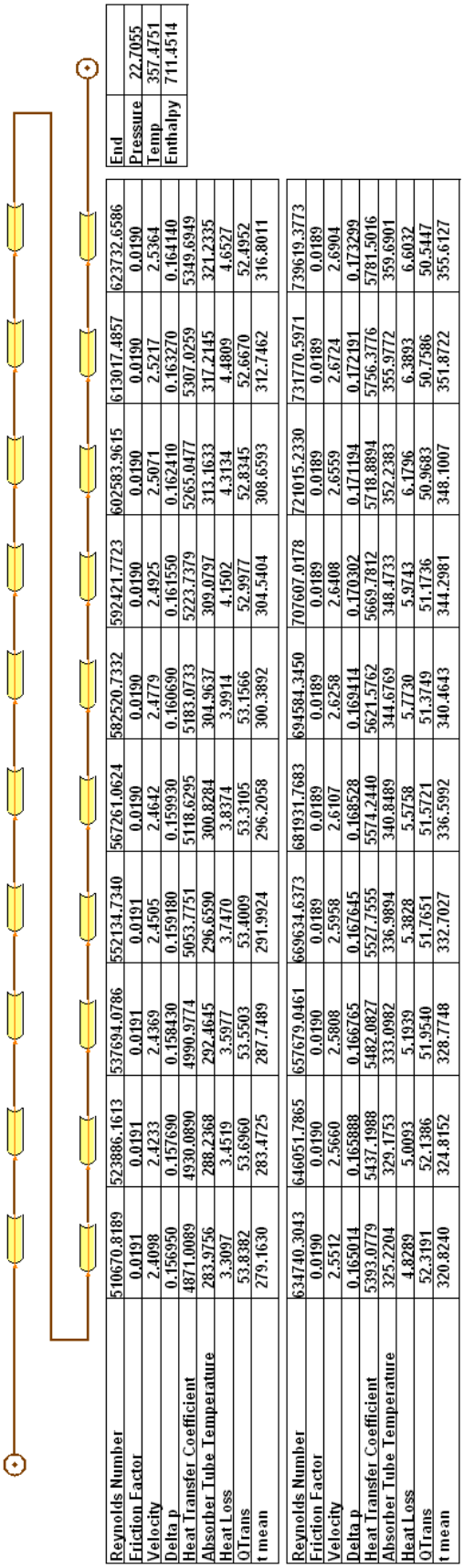

End	
Pressure	22.7055
Temp	357.4751
Enthalpy	711.4514

Reynolds Number	510670.8189	523886.1613	537694.0786	552134.7340	567261.0624	582520.7332	592421.7723	602583.9615	613017.4857	623732.6586
Friction Factor	0.0191	0.0191	0.0191	0.0191	0.0190	0.0190	0.0190	0.0190	0.0190	0.0190
Velocity	2.4098	2.4233	2.4369	2.4505	2.4642	2.4779	2.4925	2.5071	2.5217	2.5364
Delta p	0.156950	0.157690	0.158430	0.159180	0.159930	0.160690	0.161550	0.162410	0.163270	0.164140
Heat Transfer Coefficient	4871.0089	4930.0890	4990.9774	5053.7751	5118.6295	5183.0733	5223.7379	5265.0477	5307.0259	5349.6949
Absorber Tube Temperature	283.9756	288.2368	292.4645	296.6590	300.8284	304.9637	309.0797	313.1633	317.2145	321.2335
Heat Loss	3.3097	3.4519	3.5977	3.7470	3.8374	3.9914	4.1502	4.3134	4.4809	4.6527
QTrans	53.8382	53.6960	53.5503	53.4009	53.3105	53.1566	52.9977	52.8345	52.6670	52.4952
t mean	279.1630	283.4725	287.7489	291.9924	296.2058	300.3892	304.5404	308.6593	312.7462	316.8011

Reynolds Number	634740.3043	646051.7865	657679.0461	669634.6373	681931.7683	694584.3450	707607.0178	721015.2330	731770.5971	739619.3773
Friction Factor	0.0190	0.0190	0.0190	0.0189	0.0189	0.0189	0.0189	0.0189	0.0189	0.0189
Velocity	2.5512	2.5660	2.5808	2.5958	2.6107	2.6258	2.6408	2.6559	2.6724	2.6904
Delta p	0.165014	0.165888	0.166765	0.167645	0.168528	0.169414	0.170302	0.171194	0.172191	0.173299
Heat Transfer Coefficient	5393.0779	5437.1988	5482.0827	5527.7555	5574.2440	5621.5762	5669.7812	5718.8894	5756.3776	5781.5016
Absorber Tube Temperature	325.2204	329.1753	333.0982	336.9894	340.8489	344.6769	348.4733	352.2383	355.9772	359.6901
Heat Loss	4.8289	5.0093	5.1939	5.3828	5.5758	5.7730	5.9743	6.1796	6.3893	6.6032
QTrans	52.3191	52.1386	51.9540	51.7651	51.5721	51.3749	51.1736	50.9683	50.7586	50.5447
t mean	320.8240	324.8152	328.7748	332.7027	336.5992	340.4643	344.2981	348.1007	351.8722	355.6127

Figure 85: Data for the Estimation of the Element Length (Oil)

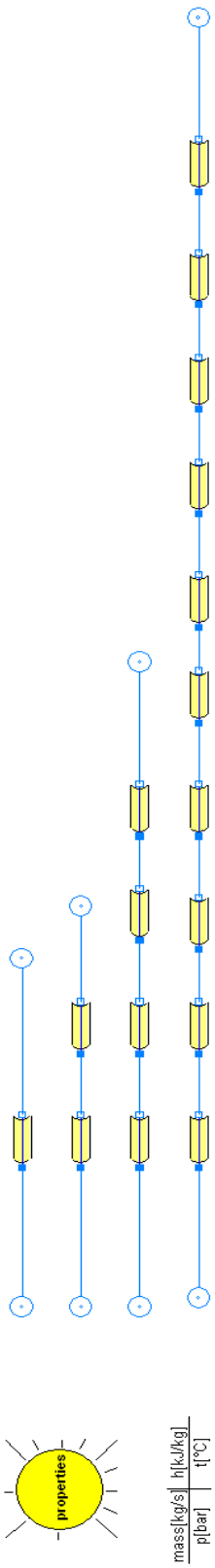

Start	
Pressure	170.0000
Temp	200.0000
Enthalpy	859.0181

Reynolds Number	274325.123075																	End	
Friction Factor	0.019905																	Pressure	169.8639
Velocity	0.687115																	Temp	299.6390
Delta p	0.136065																	Enthalpy	1334.4054
Heat Transfer Coefficient	6964.913519																		
Absorber Tube Temperature	255.352168																		
Heat Loss	30.362513																		
QTrans	618.003446																		
t mean	249.819514																		

Reynolds Number	247581.499727	305857.204460																End	
Friction Factor	0.020020	0.019792																Pressure	169.8651
Velocity	0.650470	0.712703																Temp	299.4691
Delta p	0.064777	0.070169																Enthalpy	1333.4887
Heat Transfer Coefficient	6666.848172	7333.480782																	
Absorber Tube Temperature	232.075295	281.429261																	
Heat Loss	11.940153	19.614012																	
QTrans	312.242826	304.568967																	
t mean	226.368610	276.103168																	

Reynolds Number	233079.167128	262855.770172	292041.574577	321530.163503														End	
Friction Factor	0.020092	0.019951	0.019839	0.019744														Pressure	169.8653
Velocity	0.636545	0.662296	0.692720	0.729159														Temp	299.4259
Delta p	0.031810	0.032865	0.034181	0.035807														Enthalpy	1333.7555
Heat Transfer Coefficient	6505.219034	6836.460600	7168.128765	7532.592554															
Absorber Tube Temperature	219.284717	245.447723	270.266621	293.426473															
Heat Loss	5.208779	6.862230	8.803184	10.983141															
QTrans	156.882711	155.229259	153.288305	151.108348															
t mean	213.482529	239.840513	264.849608	288.204559															

Reynolds Number	224064.533555	236235.099252	248224.100716	260067.948471	271805.380967	283484.490756	295162.665880	306907.027487	318795.476710	330925.345295								End	
Friction Factor	0.020141	0.020076	0.020017	0.019963	0.019915	0.019870	0.019828	0.019789	0.019752	0.019717								Pressure	169.8654
Velocity	0.629218	0.638536	0.648464	0.659051	0.670359	0.682455	0.695421	0.709354	0.724371	0.740622								Temp	299.4235
Delta p	0.012608	0.012753	0.012914	0.013089	0.013281	0.013491	0.013718	0.013965	0.014235	0.014528								Enthalpy	1333.2429
Heat Transfer Coefficient	6403.506677	6540.551739	6673.979582	6805.440013	6936.544205	7069.021418	7204.837578	7346.382456	7496.740800	7660.157526									
Absorber Tube Temperature	211.322875	222.071615	232.640679	243.019475	253.190064	263.133531	272.829724	282.256910	291.391347	300.217558									
Heat Loss	1.910992	2.146927	2.402303	2.677040	2.970613	3.282165	3.610476	3.953941	4.310526	4.608752									
QTrans	62.925604	62.689669	62.434293	62.159556	61.865982	61.554431	61.226120	60.882655	60.526069	60.227844									
t mean	205.460276	216.290355	226.938194	237.394145	247.641021	257.660556	267.433185	276.937758	286.151166	295.052792									

Figure 86: Data for the Estimation of the Element Length (DSG Preheating)

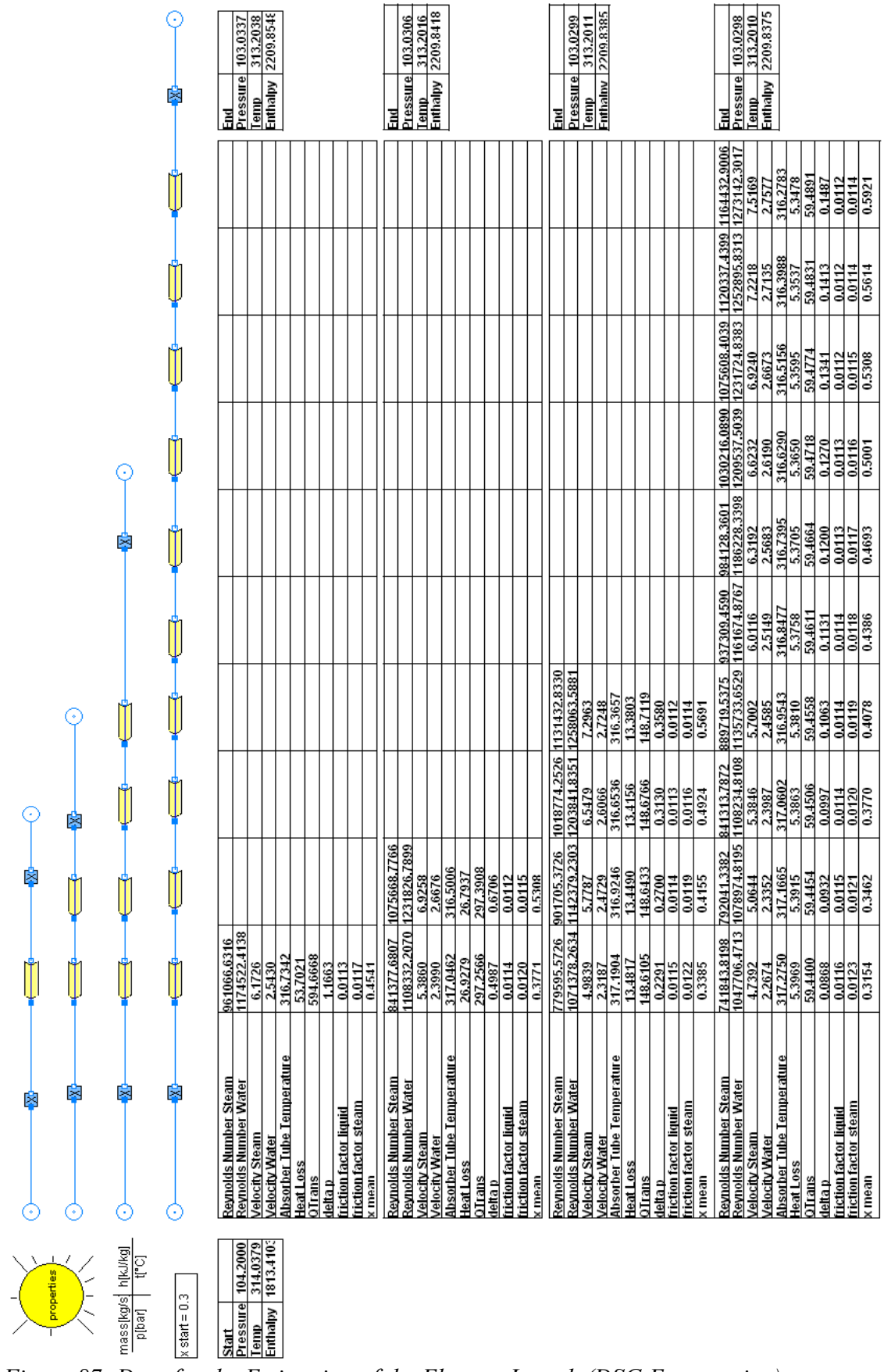

Start	
Pressure	104.2000
Temp	314.0379
Enthalpy	1813.4103

Reynolds Number Steam	961066.6316														
Reynolds Number Water	1174522.4138														
Velocity Steam	6.1726														
Velocity Water	2.5430														
Absorber Tube Temperature	316.7342														
Heat Loss	53.7021														
QTrans	594.6668														
delta p	1.1663														
friction factor liquid	0.0113														
friction factor steam	0.0117														
x mean	0.4541														
Reynolds Number Steam	841377.6807	1075668.7766													
Reynolds Number Water	1108332.2070	1231826.7899													
Velocity Steam	5.3860	6.9258													
Velocity Water	2.3990	2.6676													
Absorber Tube Temperature	317.0462	316.5006													
Heat Loss	26.9279	26.7937													
QTrans	297.2566	297.3908													
delta p	0.4987	0.6706													
friction factor liquid	0.0114	0.0112													
friction factor steam	0.0120	0.0115													
x mean	0.3771	0.5308													
Reynolds Number Steam	779595.5726	901705.3726	1018774.2526	1131432.8330											
Reynolds Number Water	1071378.2634	1142379.2303	1203841.8351	1258063.5881											
Velocity Steam	4.9839	5.7787	6.5479	7.2963											
Velocity Water	2.3187	2.4729	2.6066	2.7248											
Absorber Tube Temperature	317.1904	316.9246	316.6536	316.3657											
Heat Loss	13.4817	13.4490	13.4156	13.3803											
QTrans	148.6105	148.6433	148.6766	148.7119											
delta p	0.2291	0.2700	0.3130	0.3580											
friction factor liquid	0.0115	0.0114	0.0113	0.0112											
friction factor steam	0.0122	0.0119	0.0116	0.0114											
x mean	0.3385	0.4155	0.4924	0.5691											
Reynolds Number Steam	741843.8198	792041.3382	841313.7872	889719.5375	937309.4590	984128.3601	1030216.0890	1075608.4039	1120337.4399	1164432.9066					
Reynolds Number Water	1047706.4713	1078974.8195	1108234.8108	1135733.6529	1161674.8767	1186228.3398	1209537.5039	1231724.8383	1252895.8313	1273142.3017					
Velocity Steam	4.7392	5.0644	5.3846	5.7002	6.0116	6.3192	6.6232	6.9240	7.2218	7.5169					
Velocity Water	2.2674	2.3352	2.3987	2.4585	2.5149	2.5683	2.6190	2.6673	2.7135	2.7577					
Absorber Tube Temperature	317.2750	317.1665	317.0602	316.9543	316.8477	316.7395	316.6290	316.5156	316.3988	316.2783					
Heat Loss	5.3969	5.3915	5.3863	5.3810	5.3758	5.3705	5.3650	5.3595	5.3537	5.3478					
QTrans	59.4400	59.4454	59.4506	59.4558	59.4611	59.4664	59.4718	59.4774	59.4831	59.4891					
delta p	0.0868	0.0932	0.0997	0.1063	0.1131	0.1200	0.1270	0.1341	0.1413	0.1487					
friction factor liquid	0.0116	0.0115	0.0114	0.0114	0.0114	0.0113	0.0113	0.0112	0.0112	0.0112					
friction factor steam	0.0123	0.0121	0.0120	0.0119	0.0118	0.0117	0.0116	0.0115	0.0114	0.0114					
x mean	0.3154	0.3462	0.3770	0.4078	0.4386	0.4693	0.5001	0.5308	0.5614	0.5921					

End	
Pressure	103.0337
Temp	313.2038
Enthalpy	2209.8545

End	
Pressure	103.0306
Temp	313.2016
Enthalpy	2209.8418

End	
Pressure	103.0299
Temp	313.2011
Enthalpy	2209.8385

End	
Pressure	103.0298
Temp	313.2010
Enthalpy	2209.8375

Figure 87: Data for the Estimation of the Element Length (DSG Evaporating)

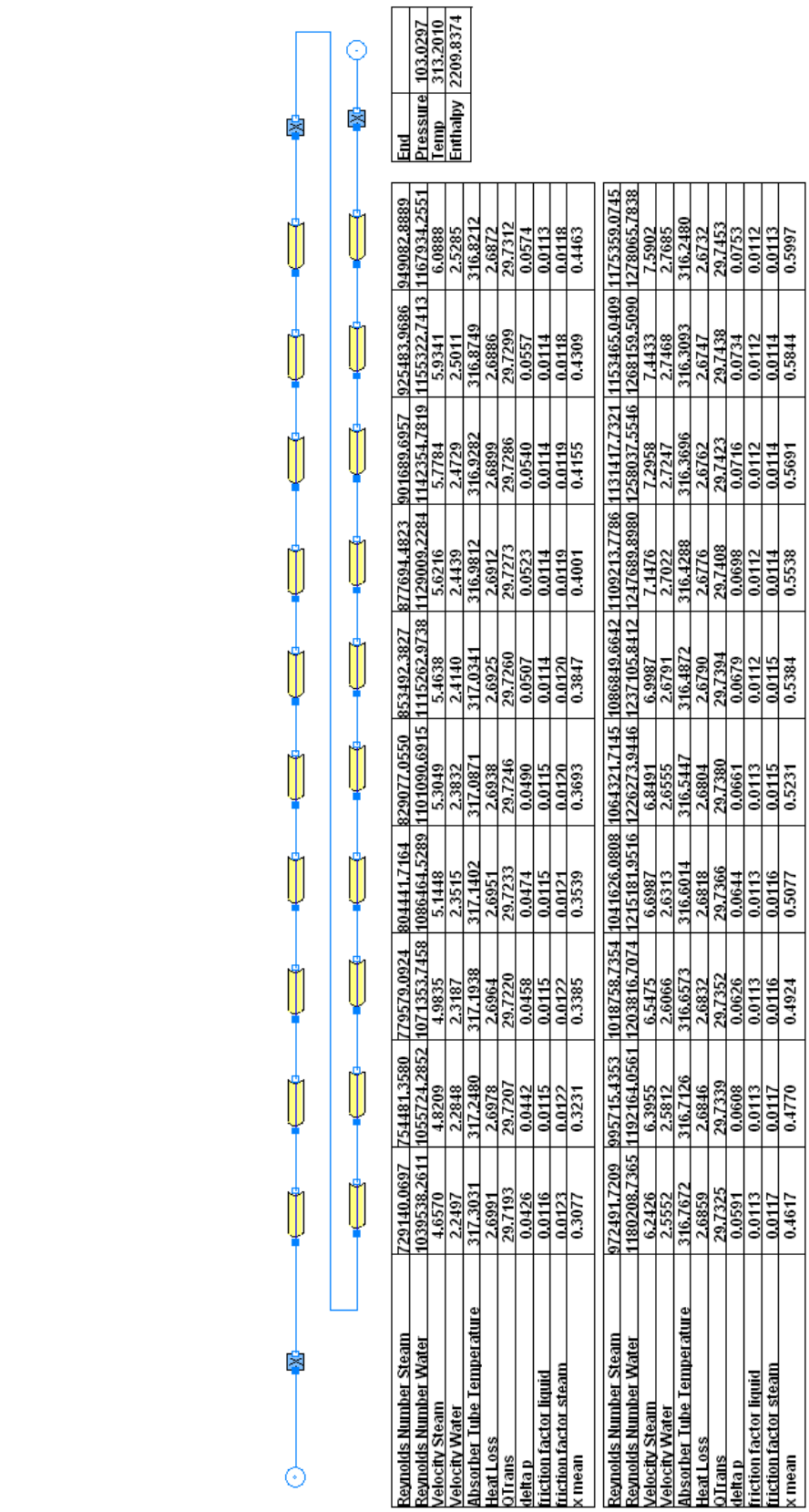

End	
Pressure	103.0297
Temp	313.2010
Enthalpy	2209.8374

Reynolds Number Steam	729140.0697	754481.3580	779579.0924	804441.7164	829077.0550	853492.3827	877694.4823	901689.6957	925483.9686	949082.8889
Reynolds Number Water	1039538.2611	1055724.2852	1071353.7458	1086464.5289	1101090.6915	1115262.9738	1129009.2284	1142354.7819	1155322.7413	1167934.2551
Velocity Steam	4.6570	4.8209	4.9835	5.1448	5.3049	5.4638	5.6216	5.7784	5.9341	6.0888
Velocity Water	2.2497	2.2848	2.3187	2.3515	2.3832	2.4140	2.4439	2.4729	2.5011	2.5285
Absorber Tube Temperature	317.3031	317.2480	317.1938	317.1402	317.0871	317.0341	316.9812	316.9282	316.8749	316.8212
Heat Loss	2.6991	2.6978	2.6964	2.6951	2.6938	2.6925	2.6912	2.6899	2.6886	2.6872
QTrans	29.7193	29.7207	29.7220	29.7233	29.7246	29.7260	29.7273	29.7286	29.7299	29.7312
delta p	0.0426	0.0442	0.0458	0.0474	0.0490	0.0507	0.0523	0.0540	0.0557	0.0574
friction factor liquid	0.0116	0.0115	0.0115	0.0115	0.0115	0.0114	0.0114	0.0114	0.0114	0.0113
friction factor steam	0.0123	0.0122	0.0122	0.0121	0.0120	0.0120	0.0119	0.0119	0.0118	0.0118
x mean	0.3077	0.3231	0.3385	0.3539	0.3693	0.3847	0.4001	0.4155	0.4309	0.4463

Reynolds Number Steam	972491.7209	995745.4353	1018758.7354	1041626.0808	1064321.7145	1086849.6642	1109213.7786	1131417.7321	1153465.0409	1175359.0745
Reynolds Number Water	1180208.7365	1192164.0561	1203816.7074	1215181.9516	1226273.9446	1237105.8412	1247689.8980	1258037.5546	1268159.5090	1278065.7838
Velocity Steam	6.2426	6.3955	6.5475	6.6987	6.8491	6.9987	7.1476	7.2958	7.4433	7.5902
Velocity Water	2.5552	2.5812	2.6066	2.6313	2.6555	2.6791	2.7022	2.7247	2.7468	2.7685
Absorber Tube Temperature	316.7672	316.7126	316.6573	316.6014	316.5447	316.4872	316.4288	316.3696	316.3093	316.2480
Heat Loss	2.6859	2.6846	2.6832	2.6818	2.6804	2.6790	2.6776	2.6762	2.6747	2.6732
QTrans	29.7325	29.7339	29.7352	29.7366	29.7380	29.7394	29.7408	29.7423	29.7438	29.7453
delta p	0.0591	0.0608	0.0626	0.0644	0.0661	0.0679	0.0698	0.0716	0.0734	0.0753
friction factor liquid	0.0113	0.0113	0.0113	0.0113	0.0113	0.0112	0.0112	0.0112	0.0112	0.0112
friction factor steam	0.0117	0.0117	0.0116	0.0116	0.0115	0.0115	0.0114	0.0114	0.0114	0.0113
x mean	0.4617	0.4770	0.4924	0.5077	0.5231	0.5384	0.5538	0.5691	0.5844	0.5997

Figure 88: Data for the Estimation of the Element Length (DSG Evaporating)

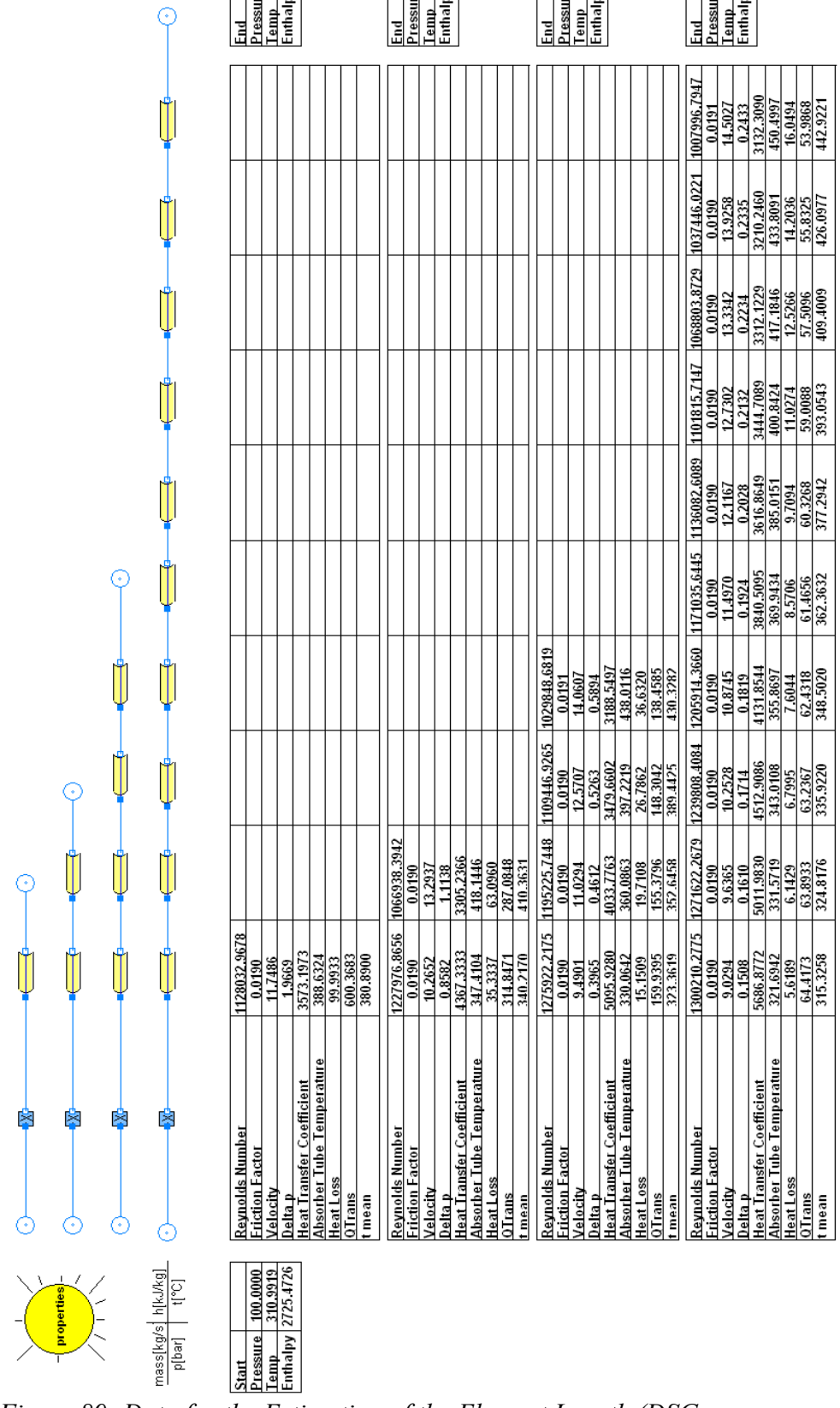

Start	
Pressure	100.0000
Temp	310.9919
Enthalpy	2725.4726

Reynolds Number	1128032.9678												
Friction Factor	0.0190												
Velocity	11.7486												
Delta p	1.9689												
Heat Transfer Coefficient	3573.1973												
Absorber Tube Temperature	388.6324												
Heat Loss	99.9933												
QTrans	600.3683												
t mean	380.8900												
Reynolds Number	1227976.8656	1066938.3942											
Friction Factor	0.0190	0.0190											
Velocity	10.2652	13.2937											
Delta p	0.8582	1.1138											
Heat Transfer Coefficient	4367.3333	3305.2366											
Absorber Tube Temperature	347.4104	418.1446											
Heat Loss	35.3337	63.0960											
QTrans	314.8471	287.0848											
t mean	340.2170	410.3631											
Reynolds Number	1275922.2175	1195225.7448	1109446.9265	1029848.6819									
Friction Factor	0.0190	0.0190	0.0190	0.0191									
Velocity	9.4901	11.0294	12.5707	14.0607									
Delta p	0.3965	0.4612	0.5263	0.5894									
Heat Transfer Coefficient	5095.9280	4033.7763	3479.6602	3188.5497									
Absorber Tube Temperature	330.0642	360.0863	397.2219	438.0116									
Heat Loss	15.1509	19.7108	26.7862	36.6320									
QTrans	159.9395	155.3796	148.3042	138.4585									
t mean	323.3619	352.6458	389.4425	430.3282									
Reynolds Number	1300210.2775	1271622.2679	1239808.4084	1205914.3660	1171035.6445	1136082.6089	1101815.7147	1068803.8729	1037446.0221	1007996.7947			
Friction Factor	0.0190	0.0190	0.0190	0.0190	0.0190	0.0190	0.0190	0.0190	0.0190	0.0191			
Velocity	9.0294	9.6365	10.2528	10.8745	11.4970	12.1167	12.7302	13.3342	13.9258	14.5027			
Delta p	0.1508	0.1610	0.1714	0.1819	0.1924	0.2028	0.2132	0.2234	0.2335	0.2433			
Heat Transfer Coefficient	5686.8772	5011.9830	4512.9086	4131.8544	3840.5095	3616.8649	3444.7089	3312.1229	3210.2460	3132.3090			
Absorber Tube Temperature	321.6942	331.5719	343.0108	355.8697	369.9434	385.0151	400.8424	417.1846	433.8091	450.4997			
Heat Loss	5.6189	6.1429	6.7995	7.6044	8.5706	9.7094	11.0274	12.5266	14.2036	16.0494			
QTrans	64.4173	63.8933	63.2367	62.4318	61.4656	60.3268	59.0088	57.5096	55.8325	53.9868			
t mean	315.3258	324.8176	335.9220	348.5020	362.3632	377.2942	393.0543	409.4009	426.0977	442.9221			

End	
Pressure	98.0331
Temp	450.7880
Enthalpy	3247.5320

End	
Pressure	98.0280
Temp	451.2840
Enthalpy	3248.8916

End	
Pressure	98.0267
Temp	451.3310
Enthalpy	3249.0219

End	
Pressure	98.0263
Temp	451.3395
Enthalpy	3249.0457

Figure 89: Data for the Estimation of the Element Length (DSG Superheating)

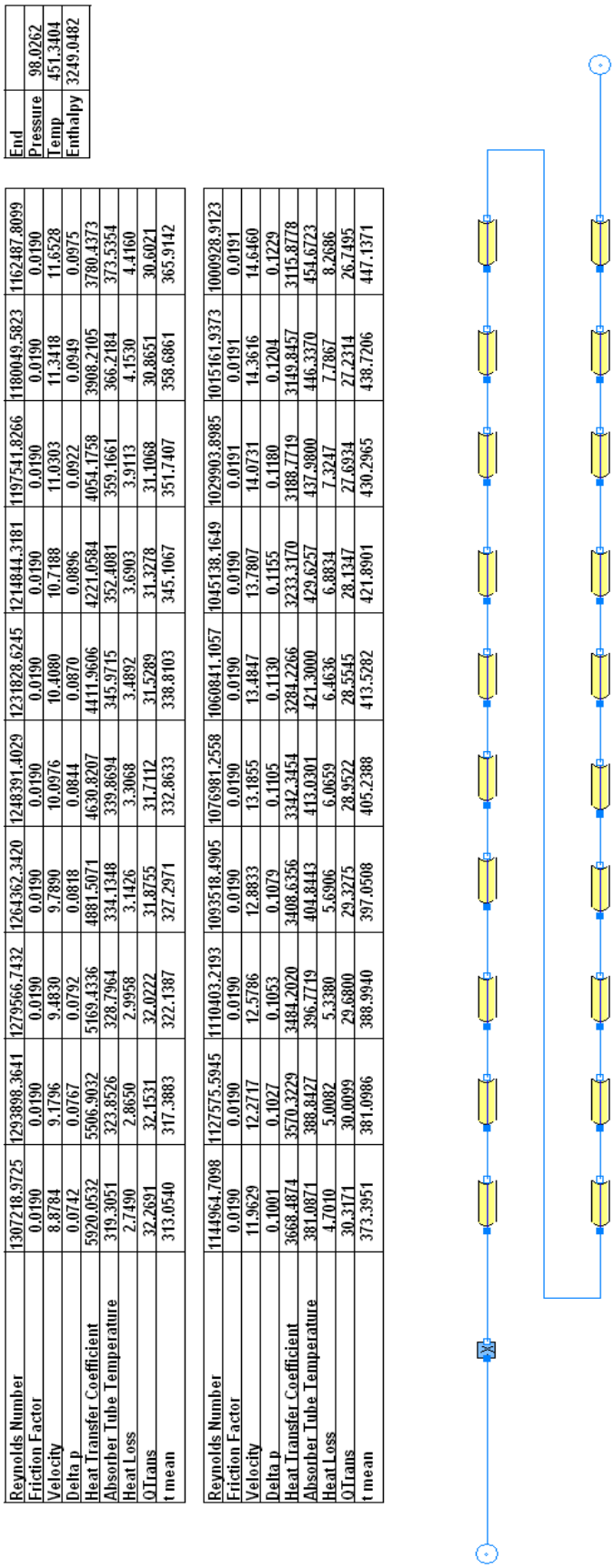

End	
Pressure	98.0262
Temp	451.3404
Enthalpy	3249.0482

Reynolds Number	1307218.9725	1293898.3641	1279566.7432	1264362.3420	1248391.4029	1231828.6245	1214844.3181	1197541.8266	1180049.5823	1162487.8099
Friction Factor	0.0190	0.0190	0.0190	0.0190	0.0190	0.0190	0.0190	0.0190	0.0190	0.0190
Velocity	8.8784	9.1796	9.4830	9.7890	10.0976	10.4080	10.7188	11.0303	11.3418	11.6528
Delta p	0.0742	0.0767	0.0792	0.0818	0.0844	0.0870	0.0896	0.0922	0.0949	0.0975
Heat Transfer Coefficient	5920.0532	5506.9032	5169.4336	4881.5071	4630.8207	4411.9606	4221.0584	4054.1758	3908.2105	3780.4373
Absorber Tube Temperature	319.3051	323.8526	328.7964	334.1348	339.8694	345.9715	352.4081	359.1661	366.2184	373.5354
Heat Loss	2.7490	2.8650	2.9958	3.1426	3.3068	3.4892	3.6903	3.9113	4.1530	4.4160
QTrans	32.2691	32.1531	32.0222	31.8755	31.7112	31.5289	31.3278	31.1068	30.8651	30.6021
t mean	313.0540	317.3883	322.1387	327.2971	332.8633	338.8103	345.1067	351.7407	358.6861	365.9142

Reynolds Number	1144964.7098	1127575.5945	1110403.2193	1093518.4905	1076981.2558	1060841.1057	1045138.1649	1029903.8985	1015161.9373	1000928.9123
Friction Factor	0.0190	0.0190	0.0190	0.0190	0.0190	0.0190	0.0190	0.0191	0.0191	0.0191
Velocity	11.9629	12.2717	12.5786	12.8833	13.1855	13.4847	13.7807	14.0731	14.3616	14.6460
Delta p	0.1001	0.1027	0.1053	0.1079	0.1105	0.1130	0.1155	0.1180	0.1204	0.1229
Heat Transfer Coefficient	3668.4874	3570.3229	3484.2020	3408.6356	3342.3454	3284.2266	3233.3170	3188.7719	3149.8457	3115.8778
Absorber Tube Temperature	381.0871	388.8427	396.7719	404.8443	413.0301	421.3000	429.6257	437.9800	446.3370	454.6723
Heat Loss	4.7010	5.0082	5.3380	5.6906	6.0659	6.4636	6.8834	7.3247	7.7867	8.2686
QTrans	30.3171	30.0099	29.6800	29.3275	28.9522	28.5545	28.1347	27.6934	27.2314	26.7495
t mean	373.3951	381.0986	388.9940	397.0508	405.2388	413.5282	421.8901	430.2965	438.7206	447.1371

Figure 90: Data for the Estimation of the Element Length (DSG Superheating)

C IPSEpro-PSE Calculation Results of Chapter 8

June 20th Time	06:15:00 AM	06:30:00 AM	06:45:00 AM	07:00:00 AM	07:15:00 AM	07:30:00 AM	07:45:00 AM	08:00:00 AM	08:15:00 AM	08:30:00 AM	08:45:00 AM	09:00:00 AM	09:15:00 AM	09:30:00 AM	09:45:00 AM	10:00:00 AM
Generator Power: [MW]	20.96	24.69	28.44	30.37	31.96	33.24	34.3	35.18	35.91	36.48	36.87	37.17	37.39	37.55	37.65	37.71
Feedwater Pump 1 Power: [MW]	0.02	0.03	0.04	0.04	0.05	0.05	0.05	0.05	0.06	0.06	0.06	0.06	0.06	0.06	0.06	0.06
Feedwater Pump 2 Power: [MW]	0.39	0.48	0.56	0.6	0.64	0.67	0.7	0.72	0.74	0.75	0.77	0.77	0.78	0.78	0.79	0.79
Recirculation Pump Power: [MW]	0.06	0.07	0.09	0.09	0.1	0.1	0.11	0.11	0.12	0.12	0.12	0.12	0.12	0.12	0.12	0.12
Oil Pump Power: [MW]	0.49	0.7	0.97	1.15	1.33	1.52	1.69	1.86	2.02	2.15	2.24	2.31	2.37	2.41	2.44	2.46
Cooling Water Pump Power: [MW]	0.33	0.37	0.42	0.43	0.45	0.46	0.48	0.49	0.49	0.5	0.5	0.51	0.51	0.51	0.51	0.51
Total Pump Power: [MW]	1.3	1.65	2.07	2.32	2.56	2.81	3.03	3.23	3.42	3.58	3.69	3.78	3.84	3.89	3.92	3.94
Cooling Tower Fan Power: [MW]	0.23	0.23	0.23	0.23	0.23	0.23	0.23	0.23	0.23	0.23	0.23	0.23	0.23	0.23	0.23	0.23
Net Power Output: [MW]	19.42	22.81	26.14	27.81	29.16	30.2	31.04	31.71	32.25	32.67	32.95	33.16	33.31	33.43	33.49	33.54
Power Cycle Efficiency: [%]	30.25	30.74	31.37	31.75	31.97	32.04	32.05	32.03	31.99	31.96	31.93	31.91	31.89	31.88	31.87	31.87
Power Provided bythe Sun: [MW]	133.4	138.8	145.82	151.74	156.76	161.06	164.75	167.93	170.68	173.08	175.16	176.97	178.54	179.98	181.07	182.08
Total Plant Efficiency: [%]	14.56	16.43	17.92	18.33	18.6	18.75	18.84	18.88	18.9	18.87	18.81	18.74	18.66	18.57	18.5	18.42
Solar Time: [h]	6.48	6.64	6.89	7.14	7.39	7.64	7.89	8.14	8.39	8.64	8.89	9.14	9.39	9.66	9.89	10.14
Dayof Year: [n‴ day]	171	171	171	171	171	171	171	171	171	171	171	171	171	171	171	171
DNI: [kW]	0.71	0.74	0.78	0.81	0.83	0.86	0.88	0.89	0.91	0.92	0.93	0.94	0.95	0.96	0.96	0.97
Altitude Angle: [°]	18.8	20.8	23.7	26.7	29.8	32.8	35.9	38.9	42	45.1	48.1	51.2	54.2	57.5	60.3	63.2
Azimuth Angle: [°]	-105.9	-104.7	-102.9	-101	-99.1	-97.3	-95.3	-93.4	-91.3	-89.2	-86.9	-84.5	-81.9	-78.7	-75.7	-71.9
Collector Total Heat Loss: [MW]	9.18	9.38	9.6	9.72	9.84	9.93	10.01	10.09	10.15	10.19	10.22	10.25	10.27	10.28	10.29	10.29
Collector Total Heat Transferred: [MW]	73.18	85.1	96.23	101.58	106.17	110.09	113.42	116.23	118.59	120.41	121.67	122.63	123.34	123.88	124.18	124.38
Cosine Factor: [-]	0.97	0.97	0.98	0.99	0.99	0.99	1	1	1	1	1	1	1	0.99	0.99	0.99
IAM: [-]	0.97	0.98	0.98	0.99	0.99	0.99	1	1	1	1	1	1	0.99	0.99	0.99	0.99
Slope Beta: [°]	70.52	68.6	65.71	62.82	59.91	56.98	54.02	51.02	48	44.93	41.82	38.67	35.48	32.02	28.96	25.63
Shading Factor: [-]	0.87	0.95	1	1	1	1	1	1	1	1	1	1	1	1	1	1
Time	**10:15:00 AM**	**10:30:00 AM**	**10:45:00 AM**	**11:00:00 AM**	**11:15:00 AM**	**11:30:00 AM**	**11:45:00 AM**	**12:00:00 PM**	**12:15:00 PM**	**12:30:00 PM**	**12:45:00 PM**	**01:00:00 PM**	**01:15:00 PM**	**01:30:00 PM**	**01:45:00 PM**	**02:00:00 PM**
Generator Power: [MW]	37.74	37.75	37.74	37.73	37.72	37.7	37.7	37.7	37.71	37.72	37.73	37.74	37.75	37.74	37.7	37.63
Feedwater Pump 1 Power: [MW]	0.06	0.06	0.06	0.06	0.06	0.06	0.06	0.06	0.06	0.06	0.06	0.06	0.06	0.06	0.06	0.06
Feedwater Pump 2 Power: [MW]	0.79	0.79	0.79	0.79	0.79	0.79	0.79	0.79	0.79	0.79	0.79	0.79	0.79	0.79	0.79	0.79
Recirculation Pump Power: [MW]	0.12	0.12	0.12	0.12	0.12	0.12	0.12	0.12	0.12	0.12	0.12	0.12	0.12	0.12	0.12	0.12
Oil Pump Power: [MW]	2.46	2.47	2.47	2.46	2.46	2.45	2.45	2.45	2.46	2.46	2.46	2.47	2.47	2.46	2.45	2.44
Cooling Water Pump Power: [MW]	0.51	0.51	0.51	0.51	0.51	0.51	0.51	0.51	0.51	0.51	0.51	0.51	0.51	0.51	0.51	0.51
Total Pump Power: [MW]	3.95	3.95	3.95	3.95	3.94	3.94	3.94	3.94	3.94	3.94	3.95	3.95	3.95	3.95	3.94	3.92
Cooling Tower Fan Power: [MW]	0.23	0.23	0.23	0.23	0.23	0.23	0.23	0.23	0.23	0.23	0.23	0.23	0.23	0.23	0.23	0.23
Net Power Output: [MW]	33.56	33.56	33.56	33.55	33.54	33.53	33.53	33.53	33.53	33.54	33.55	33.56	33.56	33.55	33.53	33.48
Power Cycle Efficiency: [%]	31.86	31.86	31.86	31.86	31.87	31.87	31.87	31.87	31.87	31.87	31.86	31.86	31.86	31.86	31.87	31.87
Power Provided bythe Sun: [MW]	182.92	183.63	184.2	184.65	184.98	185.2	185.3	185.29	185.17	184.94	184.59	184.12	183.53	182.8	181.93	180.9
Total Plant Efficiency: [%]	18.34	18.28	18.22	18.17	18.13	18.11	18.09	18.1	18.11	18.14	18.18	18.23	18.29	18.36	18.43	18.51
Solar Time: [h]	10.39	10.64	10.89	11.14	11.39	11.64	11.89	12.14	12.39	12.64	12.89	13.14	13.39	13.64	13.89	14.14
Dayof Year: [n‴ day]	171	171	171	171	171	171	171	171	171	171	171	171	171	171	171	171
DNI: [kW]	0.97	0.98	0.98	0.98	0.98	0.99	0.99	0.99	0.98	0.98	0.98	0.98	0.98	0.97	0.97	0.96
Altitude Angle: [°]	66.1	68.9	71.5	73.9	76	77.5	78.3	78.3	77.3	75.7	73.6	71.1	68.5	65.7	62.8	59.8
Azimuth Angle: [°]	-67.5	-62.2	-55.7	-47.4	-36.8	-23.3	-7.3	9.9	25.6	38.6	48.8	56.8	63.1	68.3	72.6	76.2
Collector Total Heat Loss: [MW]	10.3	10.3	10.3	10.29	10.29	10.29	10.29	10.29	10.29	10.29	10.3	10.3	10.3	10.3	10.29	10.29
Collector Total Heat Transferred: [MW]	124.48	124.51	124.49	124.45	124.4	124.36	124.35	124.35	124.37	124.41	124.46	124.49	124.51	124.47	124.36	124.14
Cosine Factor: [-]	0.99	0.99	0.98	0.98	0.98	0.98	0.98	0.98	0.98	0.98	0.98	0.98	0.99	0.99	0.99	0.99
IAM: [-]	0.99	0.99	0.99	0.98	0.98	0.98	0.98	0.98	0.98	0.98	0.98	0.99	0.99	0.99	0.99	0.99
Slope Beta: [°]	22.27	18.87	15.43	11.97	8.49	4.99	1.49	2.04	5.54	9.04	12.52	15.97	19.4	22.8	26.15	29.47
Shading Factor: [-]	1	1	1	1	1	1	1	1	1	1	1	1	1	1	1	1

June 20th

Time	02:15:00 PM	02:30:00 PM	02:45:00 PM	03:00:00 PM	03:15:00 PM	03:30:00 PM	03:45:00 PM	04:00:00 PM	04:15:00 PM	04:30:00 PM	04:45:00 PM	05:00:00 PM	05:15:00 PM	05:30:00 PM
Generator Power: [MW]	37.52	37.36	37.12	36.81	36.4	35.8	35.05	34.15	33.06	31.73	30.08	28.11	23.81	21.57
Feedwater Pump 1 Power: [MW]	0.06	0.06	0.06	0.06	0.06	0.06	0.05	0.05	0.05	0.04	0.04	0.04	0.03	0.02
Feedwater Pump 2 Power: [MW]	0.78	0.78	0.77	0.76	0.75	0.74	0.72	0.69	0.66	0.63	0.6	0.55	0.46	0.41
Recirculation Pump Power: [MW]	0.12	0.12	0.12	0.12	0.12	0.12	0.11	0.11	0.1	0.1	0.09	0.09	0.07	0.06
Oil Pump Power: [MW]	2.41	2.36	2.3	2.23	2.13	1.99	1.84	1.67	1.49	1.3	1.12	0.94	0.64	0.52
Cooling Water Pump Power: [MW]	0.51	0.51	0.51	0.5	0.5	0.49	0.48	0.47	0.46	0.45	0.43	0.41	0.36	0.34
Total Pump Power: [MW]	3.88	3.83	3.76	3.67	3.56	3.39	3.21	2.99	2.76	2.53	2.28	2.03	1.56	1.35
Cooling Tower Fan Power: [MW]	0.23	0.23	0.23	0.23	0.23	0.23	0.23	0.23	0.23	0.23	0.23	0.23	0.23	0.23
Net Power Output: [MW]	33.41	33.29	33.13	32.91	32.62	32.18	31.61	30.92	30.06	28.97	27.57	25.85	22.02	19.99
Power Cycle Efficiency: [%]	31.88	31.9	31.91	31.94	31.96	32	32.03	32.05	32.04	31.95	31.7	31.31	30.65	30.33
Power Provided bythe Sun: [MW]	179.7	178.31	176.7	174.85	172.73	170.28	167.46	164.2	160.43	156.03	150.87	144.8	137.59	134.34
Total Plant Efficiency: [%]	18.59	18.67	18.75	18.82	18.88	18.9	18.88	18.83	18.74	18.57	18.27	17.85	16.01	14.88
Solar Time: [h]	14.39	14.64	14.89	15.14	15.39	15.64	15.89	16.14	16.39	16.64	16.89	17.14	17.39	17.49
Dayof Year: [n''' day]	171	171	171	171	171	171	171	171	171	171	171	171	171	171
DNI: [kW]	0.96	0.95	0.94	0.93	0.92	0.91	0.89	0.87	0.85	0.83	0.8	0.77	0.73	0.71
Altitude Angle: [°]	56.8	53.8	50.7	47.7	44.6	41.5	38.4	35.4	32.3	29.3	26.3	23.3	20.3	19.1
Azimuth Angle: [°]	79.4	82.3	84.9	87.3	89.5	91.6	93.7	95.6	97.6	99.4	101.3	103.1	105	105.7
Collector Total Heat Loss: [MW]	10.28	10.26	10.24	10.22	10.19	10.14	10.08	10	9.91	9.82	9.71	9.58	9.34	9.21
Collector Total Heat Transferred: [MW]	123.78	123.25	122.5	121.49	120.18	118.25	115.82	112.94	109.52	105.49	100.79	95.31	82.28	75.15
Cosine Factor: [-]	0.99	1	1	1	1	1	1	1	0.99	0.99	0.98	0.98	0.97	0.97
IAM: [-]	0.99	0.99	1	1	1	1	1	0.99	0.99	0.99	0.99	0.98	0.98	0.97
Slope Beta: [°]	32.75	35.98	39.17	42.31	45.41	48.47	51.49	54.48	57.44	60.37	63.27	66.17	69.05	70.2
Shading Factor: [-]	1	1	1	1	1	1	1	1	1	1	1	1	0.93	0.88

March 12th

Time	07:45:00 AM	08:00:00 AM	08:15:00 AM	08:30:00 AM	08:45:00 AM	09:00:00 AM	09:15:00 AM	09:30:00 AM	09:45:00 AM	10:00:00 AM	10:15:00 AM	10:30:00 AM	10:45:00 AM	11:00:00 AM	11:15:00 AM	11:30:00 AM
Generator Power: [MW]	21.58	26.55	27.32	27.77	27.96	27.93	27.74	27.43	27.04	26.6	26.13	25.68	25.25	24.87	24.55	24.32
Feedwater Pump 1 Power: [MW]	0.02	0.03	0.04	0.04	0.04	0.04	0.04	0.04	0.03	0.03	0.03	0.03	0.03	0.03	0.03	0.03
Feedwater Pump 2 Power: [MW]	0.41	0.52	0.54	0.54	0.55	0.55	0.54	0.54	0.53	0.52	0.51	0.5	0.49	0.48	0.47	0.47
Recirculation Pump Power: [MW]	0.06	0.08	0.08	0.09	0.09	0.09	0.09	0.08	0.08	0.08	0.08	0.08	0.08	0.07	0.07	0.07
Oil Pump Power: [MW]	0.53	0.82	0.88	0.92	0.94	0.93	0.92	0.89	0.86	0.83	0.79	0.76	0.73	0.7	0.68	0.67
Cooling Water Pump Power: [MW]	0.33	0.39	0.4	0.41	0.41	0.41	0.41	0.4	0.4	0.39	0.39	0.38	0.38	0.37	0.37	0.37
Total Pump Power: [MW]	1.36	1.85	1.94	1.99	2.02	2.01	1.99	1.95	1.91	1.85	1.8	1.75	1.71	1.66	1.63	1.61
Cooling Tower Fan Power: [MW]	0.23	0.23	0.23	0.23	0.23	0.23	0.23	0.23	0.23	0.23	0.23	0.23	0.23	0.23	0.23	0.23
Net Power Output: [MW]	19.99	24.47	25.15	25.55	25.71	25.69	25.52	25.25	24.9	24.51	24.1	23.7	23.31	22.97	22.69	22.48
Power Cycle Efficiency: [%]	30.4	31.09	31.19	31.25	31.28	31.28	31.25	31.21	31.15	31.1	31.04	30.99	30.93	30.89	30.85	30.82
Power Provided bythe Sun: [MW]	139.09	147.22	153.92	159.48	164.14	168.05	171.36	174.15	176.51	178.51	180.18	181.56	182.7	183.59	184.28	184.76
Total Plant Efficiency: [%]	14.37	16.62	16.34	16.02	15.66	15.28	14.89	14.5	14.11	13.73	13.38	13.05	12.76	12.51	12.31	12.17
Solar Time: [h]	7.74	7.99	8.24	8.49	8.74	8.99	9.24	9.49	9.74	9.99	10.24	10.49	10.74	10.99	11.24	11.49
Dayof Year: [n''' day]	71	71	71	71	71	71	71	71	71	71	71	71	71	71	71	71
DNI: [kW]	0.74	0.78	0.82	0.85	0.87	0.89	0.91	0.93	0.94	0.95	0.96	0.97	0.97	0.98	0.98	0.98
Altitude Angle: [°]	18.6	21.5	24.3	27.1	29.8	32.4	34.9	37.3	39.6	41.8	43.7	45.5	47.1	48.4	49.5	50.3
Azimuth Angle: [°]	-71	-68.4	-65.8	-63	-60	-56.9	-53.6	-50.1	-46.3	-42.2	-37.9	-33.3	-28.4	-23.2	-17.7	-12
Collector Total Heat Loss: [MW]	9.23	9.49	9.54	9.57	9.58	9.58	9.57	9.55	9.52	9.5	9.47	9.44	9.42	9.4	9.38	9.37
Collector Total Heat Transferred: [MW]	75.06	90.6	92.97	94.34	94.89	94.81	94.24	93.3	92.1	90.74	89.31	87.89	86.54	85.35	84.36	83.61
Cosine Factor: [-]	0.95	0.94	0.93	0.91	0.9	0.89	0.87	0.86	0.85	0.83	0.82	0.81	0.8	0.79	0.79	0.78
IAM: [-]	0.97	0.96	0.95	0.94	0.94	0.93	0.92	0.91	0.9	0.89	0.88	0.88	0.87	0.86	0.86	0.85
Slope Beta: [°]	70.41	67.07	63.65	60.15	56.56	52.86	49.06	45.15	41.12	36.97	32.7	28.32	23.82	19.24	14.56	9.82
Shading Factor: [-]	0.87	1	1	1	1	1	1	1	1	1	1	1	1	1	1	1

March 12th

Time	11:45:00 AM	12:00:00 PM	12:15:00 PM	12:30:00 PM	12:45:00 PM	01:00:00 PM	01:15:00 PM	01:30:00 PM	01:45:00 PM	02:00:00 PM	02:15:00 PM	02:30:00 PM	02:45:00 PM	03:00:00 PM	03:15:00 PM	03:30:00 PM
Generator Power: [MW]	24.17	24.11	24.16	24.3	24.53	24.84	25.21	25.64	26.09	26.56	27	27.4	27.72	27.92	27.96	27.8
Feedwater Pump 1 Power: [MW]	0.03	0.03	0.03	0.03	0.03	0.03	0.03	0.03	0.03	0.03	0.03	0.04	0.04	0.04	0.04	0.04
Feedwater Pump 2 Power: [MW]	0.46	0.46	0.46	0.47	0.47	0.48	0.49	0.5	0.51	0.52	0.53	0.54	0.55	0.55	0.55	0.54
Recirculation Pump Power: [MW]	0.07	0.07	0.07	0.07	0.07	0.07	0.08	0.08	0.08	0.08	0.08	0.08	0.08	0.09	0.09	0.09
Oil Pump Power: [MW]	0.66	0.66	0.66	0.67	0.68	0.7	0.73	0.76	0.79	0.82	0.86	0.89	0.92	0.93	0.94	0.92
Cooling Water Pump Power: [MW]	0.37	0.37	0.37	0.37	0.37	0.37	0.38	0.38	0.39	0.39	0.4	0.4	0.41	0.41	0.41	0.41
Total Pump Power: [MW]	1.59	1.59	1.59	1.6	1.63	1.66	1.7	1.74	1.79	1.85	1.9	1.95	1.99	2.02	2.02	2
Cooling Tower Fan Power: [MW]	0.23	0.23	0.23	0.23	0.23	0.23	0.23	0.23	0.23	0.23	0.23	0.23	0.23	0.23	0.23	0.23
Net Power Output: [MW]	22.34	22.3	22.34	22.46	22.67	22.94	23.28	23.66	24.06	24.47	24.86	25.22	25.5	25.67	25.71	25.57
Power Cycle Efficiency: [%]	30.8	30.79	30.8	30.82	30.84	30.88	30.93	30.98	31.04	31.09	31.15	31.2	31.24	31.27	31.28	31.26
Power Provided bythe Sun: [MW]	185.05	185.15	185.07	184.8	184.33	183.67	182.79	181.68	180.32	178.67	176.71	174.38	171.63	168.38	164.52	159.95
Total Plant Efficiency: [%]	12.07	12.04	12.07	12.16	12.3	12.49	12.74	13.02	13.35	13.7	14.07	14.46	14.86	15.25	15.63	15.99
Solar Time: [h]	11.74	11.99	12.24	12.49	12.74	12.99	13.24	13.49	13.74	13.99	14.24	14.49	14.74	14.99	15.24	15.49
Dayof Year: [n``` day]	71	71	71	71	71	71	71	71	71	71	71	71	71	71	71	71
DNI: [kW]	0.98	0.98	0.98	0.98	0.98	0.98	0.97	0.97	0.96	0.95	0.94	0.93	0.91	0.9	0.88	0.85
Altitude Angle: [°]	50.8	51	50.8	50.4	49.6	48.6	47.2	45.7	43.9	42	39.8	37.5	35.1	32.6	30	27.3
Azimuth Angle: [°]	-6.2	-0.5	5.7	11.5	17.2	22.7	27.9	32.9	37.5	41.9	45.9	49.7	53.3	56.6	59.8	62.7
Collector Total Heat Loss: [MW]	9.36	9.36	9.36	9.37	9.38	9.4	9.42	9.44	9.47	9.49	9.52	9.55	9.57	9.58	9.58	9.57
Collector Total Heat Transferred: [MW]	83.14	82.97	83.11	83.56	84.28	85.25	86.43	87.76	89.18	90.62	91.98	93.2	94.17	94.78	94.91	94.42
Cosine Factor: [-]	0.78	0.78	0.78	0.78	0.79	0.79	0.8	0.81	0.82	0.83	0.85	0.86	0.87	0.89	0.9	0.91
IAM: [-]	0.85	0.85	0.85	0.85	0.86	0.86	0.87	0.88	0.88	0.89	0.9	0.91	0.92	0.93	0.93	0.94
Slope Beta: [°]	5.04	0.41	4.61	9.39	14.13	18.81	23.41	27.91	32.3	36.58	40.74	44.79	48.71	52.52	56.22	59.83
Shading Factor: [-]	1	1	1	1	1	1	1	1	1	1	1	1	1	1	1	1

Time	03:45:00 PM	04:00:00 PM	04:15:00 PM
Generator Power: [MW]	27.38	26.64	22.08
Feedwater Pump 1 Power: [MW]	0.04	0.03	0.03
Feedwater Pump 2 Power: [MW]	0.53	0.52	0.42
Recirculation Pump Power: [MW]	0.08	0.08	0.07
Oil Pump Power: [MW]	0.89	0.83	0.55
Cooling Water Pump Power: [MW]	0.4	0.4	0.34
Total Pump Power: [MW]	1.95	1.86	1.4
Cooling Tower Fan Power: [MW]	0.23	0.23	0.23
Net Power Output: [MW]	25.2	24.55	20.45
Power Cycle Efficiency: [%]	31.2	31.1	30.49
Power Provided bythe Sun: [MW]	154.47	147.89	139.91
Total Plant Efficiency: [%]	16.31	16.6	14.62
Solar Time: [h]	15.74	15.99	16.24
Dayof Year: [n``` day]	71	71	71
DNI: [kW]	0.82	0.79	0.74
Altitude Angle: [°]	24.6	21.7	18.9
Azimuth Angle: [°]	65.5	68.2	70.7
Collector Total Heat Loss: [MW]	9.55	9.5	9.25
Collector Total Heat Transferred: [MW]	93.14	90.87	76.61
Cosine Factor: [-]	0.93	0.94	0.95
IAM: [-]	0.95	0.96	0.96
Slope Beta: [°]	63.33	66.76	70.1
Shading Factor: [-]	1	1	0.89

June 20th DSG Time (Local Time – 1h)	06:30:00 AM	06:45:00 AM	07:00:00 AM	07:15:00 AM	07:30:00 AM	07:45:00 AM	08:00:00 AM	08:15:00 AM	08:30:00 AM	08:45:00 AM	09:00:00 AM	09:15:00 AM	09:30:00 AM	09:45:00 AM	10:00:00 AM	10:15:00 AM
Generator Power: [MW]	30.28	34.93	37.22	39.07	40.57	41.82	42.86	43.73	44.4	44.86	45.22	45.48	45.67	45.79	45.87	45.9
Feedwater Pump 1 Power: [MW]	0.03	0.04	0.05	0.05	0.06	0.06	0.06	0.06	0.06	0.07	0.07	0.07	0.07	0.07	0.07	0.07
Feedwater Pump 2 Power: [MW]	0.67	0.78	0.83	0.88	0.92	0.95	0.98	1	1.02	1.03	1.04	1.05	1.05	1.06	1.06	1.06
Recirculation Pump Power: [MW]	0.13	0.2	0.23	0.26	0.28	0.3	0.32	0.33	0.34	0.34	0.35	0.35	0.35	0.36	0.35	0.36
Recirculation Rate: [-]	4.21	4.29	4.25	4.19	4.14	4.08	4.03	3.99	3.96	3.93	3.92	3.9	3.89	3.89	3.88	3.88
Cooling Water Pump Power: [MW]	0.39	0.44	0.47	0.49	0.51	0.52	0.54	0.55	0.56	0.56	0.57	0.57	0.58	0.58	0.58	0.58
Total Pump Power: [MW]	1.23	1.47	1.58	1.68	1.76	1.83	1.89	1.94	1.98	2.01	2.03	2.04	2.05	2.06	2.06	2.06
Cooling Tower Fan Power: [MW]	0.23	0.23	0.23	0.23	0.23	0.23	0.23	0.23	0.23	0.23	0.23	0.23	0.23	0.23	0.23	0.23
Net Power Output: [MW]	28.82	33.23	35.41	37.16	38.58	39.75	40.73	41.55	42.19	42.63	42.96	43.21	43.39	43.5	43.57	43.61
Power Cycle Efficiency: [%]	35.44	36.04	36.33	36.44	36.45	36.43	36.41	36.39	36.37	36.36	36.35	36.35	36.34	36.34	36.34	36.34
Power Provided bythe Sun: [MW]	138.8	145.82	151.74	156.76	161.06	164.75	167.93	170.68	173.08	175.16	176.97	178.54	179.9	181.07	182.08	182.92
Total Plant Efficiency: [%]	20.77	22.79	23.34	23.71	23.95	24.13	24.26	24.34	24.37	24.34	24.28	24.2	24.12	24.02	23.93	23.84
Solar Time: [h]	6.64	6.89	7.14	7.39	7.64	7.89	8.14	8.39	8.64	8.89	9.14	9.39	9.64	9.89	10.14	10.39
Day of Year: [nth day]	171	171	171	171	171	171	171	171	171	171	171	171	171	171	171	171
DNI: [kW]	0.74	0.78	0.81	0.83	0.86	0.88	0.89	0.91	0.92	0.93	0.94	0.95	0.96	0.96	0.97	0.97
Altitude Angle: [°]	20.8	23.7	26.7	29.8	32.8	35.9	38.9	42	45.1	48.1	51.2	54.2	57.3	60.3	63.2	66.1
Azimuth Angle: [°]	-104.7	-102.9	-101	-99.1	-97.3	-95.3	-93.4	-91.3	-89.2	-86.9	-84.5	-81.9	-78.9	-75.7	-71.9	-67.5
Collector Total Heat Loss: [MW]	10.92	10.94	10.95	10.96	10.97	10.97	10.98	10.99	10.99	10.99	11	11	11	11	11	11
Collector Total Heat Transferred: [MW]	83.56	94.89	100.35	105.04	109.05	112.46	115.34	117.75	119.61	120.9	121.88	122.61	123.13	123.47	123.67	123.77
Angle of Incidence: [°]	13.73	11.75	9.81	7.93	6.09	4.32	2.61	0.98	0.58	2.06	3.45	4.75	5.95	7.04	8.03	8.9
Cosine Factor: [-]	0.97	0.98	0.99	0.99	0.99	1	1	1	1	1	1	1	0.99	0.99	0.99	0.99
IAM: [-]	0.98	0.98	0.99	0.99	0.99	1	1	1	1	1	1	0.99	0.99	0.99	0.99	0.99
Slope Beta: [°]	68.6	65.71	62.82	59.91	56.98	54.02	51.02	48	44.93	41.82	38.67	35.48	32.24	28.96	25.63	22.27
Shading Factor: [-]	0.95	1	1	1	1	1	1	1	1	1	1	1	1	1	1	1
Time (Local Time – 1h)	10:30:00 AM	10:45:00 AM	11:00:00 AM	11:15:00 AM	11:30:00 AM	11:45:00 AM	12:00:00 PM	12:15:00 PM	12:30:00 PM	12:45:00 PM	01:00:00 PM	01:15:00 PM	01:30:00 PM	01:45:00 PM	02:00:00 PM	02:15:00 PM
Generator Power: [MW]	45.91	45.91	45.89	45.87	45.86	45.85	45.85	45.86	45.88	45.89	45.91	45.91	45.9	45.86	45.78	45.64
Feedwater Pump 1 Power: [MW]	0.07	0.07	0.07	0.07	0.07	0.07	0.07	0.07	0.07	0.07	0.07	0.07	0.07	0.07	0.07	0.07
Feedwater Pump 2 Power: [MW]	1.06	1.06	1.06	1.06	1.06	1.06	1.06	1.06	1.06	1.06	1.06	1.06	1.06	1.06	1.06	1.05
Recirculation Pump Power: [MW]	0.36	0.36	0.36	0.36	0.35	0.35	0.35	0.35	0.36	0.36	0.36	0.36	0.36	0.35	0.36	0.35
Recirculation Rate: [-]	3.88	3.88	3.88	3.88	3.88	3.88	3.88	3.88	3.88	3.88	3.88	3.88	3.88	3.88	3.89	3.89
Cooling Water Pump Power: [MW]	0.58	0.58	0.58	0.58	0.58	0.58	0.58	0.58	0.58	0.58	0.58	0.58	0.58	0.58	0.58	0.57
Total Pump Power: [MW]	2.07	2.06	2.06	2.06	2.06	2.06	2.06	2.06	2.06	2.06	2.06	2.07	2.06	2.06	2.06	2.05
Cooling Tower Fan Power: [MW]	0.23	0.23	0.23	0.23	0.23	0.23	0.23	0.23	0.23	0.23	0.23	0.23	0.23	0.23	0.23	0.23
Net Power Output: [MW]	43.62	43.61	43.6	43.58	43.57	43.56	43.56	43.57	43.58	43.6	43.61	43.62	43.6	43.57	43.48	43.36
Power Cycle Efficiency: [%]	36.34	36.34	36.34	36.34	36.34	36.34	36.34	36.34	36.34	36.34	36.34	36.34	36.34	36.34	36.34	36.34
Power Provided bythe Sun: [MW]	183.63	184.2	184.65	184.98	185.2	185.3	185.29	185.17	184.94	184.59	184.12	183.53	182.8	181.93	180.9	179.7
Total Plant Efficiency: [%]	23.75	23.67	23.61	23.56	23.53	23.51	23.51	23.53	23.57	23.62	23.69	23.76	23.85	23.95	24.04	24.13
Solar Time: [h]	10.64	10.89	11.14	11.39	11.64	11.89	12.14	12.39	12.64	12.89	13.14	13.39	13.64	13.89	14.14	14.39
Day of Year: [nth day]	171	171	171	171	171	171	171	171	171	171	171	171	171	171	171	171
DNI: [kW]	0.98	0.98	0.98	0.98	0.99	0.99	0.99	0.98	0.98	0.98	0.98	0.98	0.97	0.97	0.96	0.96
Altitude Angle: [°]	68.9	71.5	73.9	76	77.5	78.3	78.3	77.3	75.7	73.6	71.1	68.5	65.7	62.8	59.8	56.8
Azimuth Angle: [°]	-62.2	-55.7	-47.4	-36.8	-23.3	-7.3	9.9	25.6	38.6	48.8	56.8	63.1	68.3	72.6	76.2	79.4
Collector Total Heat Loss: [MW]	11	11	11	11	11	11	11	11	11	11	11	11	11	11	11	11
Collector Total Heat Transferred: [MW]	123.8	123.78	123.74	123.69	123.66	123.64	123.64	123.66	123.7	123.75	123.79	123.8	123.76	123.65	123.43	123.06
Angle of Incidence: [°]	9.66	10.29	10.8	11.18	11.44	11.56	11.55	11.41	11.13	10.73	10.2	9.55	8.77	7.88	6.88	5.77
Cosine Factor: [-]	0.99	0.98	0.98	0.98	0.98	0.98	0.98	0.98	0.98	0.98	0.98	0.99	0.99	0.99	0.99	0.99
IAM: [-]	0.99	0.99	0.98	0.98	0.98	0.98	0.98	0.98	0.98	0.98	0.99	0.99	0.99	0.99	0.99	0.99
Slope Beta: [°]	18.87	15.43	11.97	8.49	4.99	1.49	2.04	5.54	9.04	12.52	15.97	19.4	22.8	26.15	29.47	32.75
Shading Factor: [-]	1	1	1	1	1	1	1	1	1	1	1	1	1	1	1	1

June 20th DSG Time (Local Time – 1h)	02:30:00 PM	02:45:00 PM	03:00:00 PM	03:15:00 PM	03:30:00 PM	03:45:00 PM	04:00:00 PM	04:15:00 PM	04:30:00 PM	04:45:00 PM	05:00:00 PM	05:15:00 PM
Generator Power: [MW]	45.45	45.17	44.8	44.31	43.6	42.71	41.64	40.36	38.81	36.89	34.53	29.08
Feedwater Pump 1 Power: [MW]	0.07	0.07	0.07	0.06	0.06	0.06	0.06	0.05	0.05	0.05	0.04	0.03
Feedwater Pump 2 Power: [MW]	1.05	1.04	1.03	1.02	1	0.97	0.94	0.91	0.87	0.82	0.77	0.64
Recirculation Pump Power: [MW]	0.35	0.35	0.34	0.34	0.33	0.31	0.3	0.28	0.26	0.23	0.19	0.11
Recirculation Rate: [-]	3.9	3.92	3.94	3.96	4	4.04	4.09	4.14	4.2	4.26	4.29	4.12
Cooling Water Pump Power: [MW]	0.57	0.57	0.56	0.56	0.55	0.54	0.52	0.51	0.49	0.46	0.44	0.38
Total Pump Power: [MW]	2.04	2.02	2	1.97	1.93	1.88	1.82	1.75	1.66	1.56	1.45	1.17
Cooling Tower Fan Power: [MW]	0.23	0.23	0.23	0.23	0.23	0.23	0.23	0.23	0.23	0.23	0.23	0.23
Net Power Output: [MW]	43.18	42.91	42.56	42.11	41.43	40.59	39.58	38.38	36.92	35.1	32.86	27.68
Power Cycle Efficiency: [%]	36.35	36.35	36.36	36.37	36.39	36.41	36.44	36.46	36.44	36.3	35.98	35.23
Power Provided bythe Sun: [MW]	178.31	176.7	174.85	172.73	170.28	167.46	164.2	160.43	156.03	150.87	144.8	137.59
Total Plant Efficiency: [%]	24.21	24.29	24.34	24.38	24.33	24.24	24.11	23.92	23.66	23.26	22.69	20.12
Solar Time: [h]	14.64	14.89	15.14	15.39	15.64	15.89	16.14	16.39	16.64	16.89	17.14	17.39
Dayof Year: [nth day]	171	171	171	171	171	171	171	171	171	171	171	171
DNI: [kW]	0.95	0.94	0.93	0.92	0.91	0.89	0.87	0.85	0.83	0.8	0.77	0.73
Altitude Angle: [°]	53.8	50.7	47.7	44.6	41.5	38.4	35.4	32.3	29.3	26.3	23.3	20.3
Azimuth Angle: [°]	82.3	84.9	87.3	89.5	91.6	93.7	95.6	97.6	99.4	101.3	103.1	105
Collector Total Heat Loss: [MW]	11	11	10.99	10.99	10.99	10.98	10.97	10.97	10.96	10.95	10.94	10.92
Collector Total Heat Transferred: [MW]	122.51	121.75	120.72	119.38	117.4	114.92	111.96	108.47	104.36	99.55	93.96	80.7
Angle of Incidence: [°]	4.55	3.24	1.84	0.35	1.23	2.87	4.59	6.38	8.22	10.11	12.06	14.05
Cosine Factor: [-]	1	1	1	1	1	1	1	0.99	0.99	0.98	0.98	0.97
IAM: [-]	0.99	1	1	1	1	1	0.99	0.99	0.99	0.99	0.98	0.98
Slope Beta: [°]	35.98	39.17	42.31	45.41	48.47	51.49	54.48	57.44	60.37	63.27	66.17	69.05
Shading Factor: [-]	1	1	1	1	1	1	1	1	1	1	1	0.93

List of Figures and Tables

Figure Index

Index of Tables